Acid Gas Removal from Natural Gas with Alkanolamines

A Modeling and Experimental Study

Sadegh, Negar

Publication date:
2013

Document Version
Publisher's PDF, also known as Version of record

Acid Gas Removal from Natural Gas with Alkanolamines:

A Modeling and Experimental Study

Negar Sadegh

Ph.D. Thesis

July 2012

Acid Gas Removal from Natural Gas with Alkanolamines: A Modeling and Experimental Study

Negar Sadegh

Ph.D. Thesis

Center for Energy Resources Engineering

Department of Chemical and Biochemical Engineering

Technical University of Denmark

DK-2800 Lyngby, Denmark

Acid Gas Removal from Natural Gas with Alkanolamines:

A Modeling and Experimental Study

by

Negar Sadegh

Dissertation

Presented to the Technical University of Denmark

in Partial Fulfillment

of the Requirements

for the Degree of

Doctor of Philosophy

Technical University of Denmark (DTU)
Department of Chemical and Biochemical Engineering
Center for Energy Process Engineering (CERE)
Soltofts Plads Building 229
DK-2800 Kongens Lyngby
Denmark

Phone: +45 4525 2800
Fax: +45 4588 2258
Contact: kt@kt.dtu.dk
http://www.kt.dtu.dk
http://www.cere.dtu.dk

Front cover: Asgard B Platform, Statoil Acid gas (CO_2 and H_2S) Removal Plant

Acknowledgments

This thesis is submitted as partial fulfillment of the requirement for the PhD degree at Technical University of Denmark (DTU). The work has been carried out at the department of Chemical and Biochemical Engineering of DTU and department of Gas Processing and LNG of Statoil research and development center from April 2009 to July 2012. The work has been done under supervision of associate professor Kaj Thomsen and Professor Erling Stenby from DTU. The experimental part of the project was done under the guidance of Doctor Eivind Johannessen and Doctor Even Solbraa from Statoil. The project was funded by Statoil ASA.

First of all, I would like to say my deepest thanks from all my heart to my parents, Mohammad Reza Sadegh and Soraya Payandeh, who have been a constant force in my life. Their understanding and their eternal love without any regret or complaint encouraged me to move forward during all my life. No words can explain how much I am thankful to them. I am always proud to be their daughter. I would like to say my sincerest gratitude to my brothers, Pirooz Sadegh and Parsa Sadegh, for always supporting me and being there with me. I owe them all the moments of my happy childhood. I would like to express my deepest thanks to my endless love, my husband, Hossein Alimadadi for his love that encouraged me to work hard during my Ph.D. studies. I was far from my family and my country, Iran, during my Ph.D. studies, his presence and his love never let me to feel far away from my beloved ones. I owe my achievements to him for making this hard period, happy and sweet for me. No words can express my eternal love to him.

I wish to express my sincere gratitude to associate professor Kaj Thomsen for his guidance and supervision throughout this work. I have benefited a lot from the data bank and programs. He always allowed me to solve problems with my own approach and at my own time. His attitude towards advising me allowed me to make many of my own mistakes and have many of my own successes. I am really thankful to him for his kind supervision during these years. It was always inspiring to work with him.

I would also like to give a special thanks to Professor Erling Stenby, my supervisor and the head of CERE and Chemistry department of DTU, for giving me the opportunity to join CERE, for his very kind leader ship. He is a great leader with brilliant innovative ideas that makes CERE such a pleasant place to study.

I have also been fortune enough to have been given the opportunity to travel to Norway to continue my research work in the Statoil research and development center under the supervision of Doctor Even Solbraa and Doctor Eivind Johannessen. I would like to thanks them for their kindness, encouragement and hospitality. I especially thank them for great supervising the experimental part of my project. I have learned a lot from them. Before I move to Statoil I had no experience to work in laboratory and it was their exceptional guidance that makes it possible to do this extensive experimental work. I would like to specifically thank Doctor Eivind Johannessen for his patience to many of my rising questions. I would also like to thank to Doctor Lars Henrik Gjertsen and Doctor Cecilie Gotaas Johnsen, the heads of the department and group for providing me such opportunity. My special thanks to Gunn Iren Rudolfsen and Ole Johan Berg, two expert technicians, that without them it was not possible to perform high pressure measurements. I Thank to Doctor Maria G. Lioliou to teach me how to do measurements with low pressure cell.

I would like to say me deep gratitude to Professor Dominique Richon for kindly reviewing the experimental part of the PhD dissertation. He was always too keen to answer my experimental questions.

I would like to thank Patricia Wagner and Anne Louise Biede for their great work in CERE administration. Special thanks to Patricia Wagner for always be kind to me. She made me feel like I am at home. Many thanks my the colleagues in CERE, Chemical engineering department of DTU and Statoil, Gas Process and LNG department for making such a nice atmosphere which makes me always enjoy being part of them.

And finally, financial support from the Statoil Company is greatly appreciated.

Negar Sadegh

Lyngby, Denmark

July 2012

Dedicated to my eternal loves, meanings of my life

My father, Mohammad Reza Sadegh

and

My Mother, Soraya Payandeh

Summary

Some 40 % of the world's remaining gas reserves are sour or acid, containing large quantities of CO_2 and H_2S and other sulfur compounds. Many large oil and gas fields have more than 10 mole % CO_2 and H_2S content. In the gas processing industry absorption with chemical solvents has been used commercially for the removal of acid gas impurities from natural gas. Alkanolamines, simple combinations of alcohols and ammonia, are the most commonly used category of chemical solvents for acid gas capture. This Ph.D. project is about thermodynamics of natural gas cleaning process with alkanolamines as solvent, modeling and experimental study. The project is collaboration between DTU and Statoil. Thermodynamic modeling is being done at DTU and experiments were performed at Statoil laboratories. In modeling part of the project, thermodynamic models were developed for CO_2-MDEA-H_2O, CO_2-MEA-H_2O, CO_2-MDEA-MEA-H_2O, H_2S-MDEA-H_2O, H_2S-CH_4-MDEA-H_2O systems and the constituent binary subsystems of the mentioned mixtures. The experimental part of the project includes vapor-liquid equilibrium measurements for CO_2-MDEA-H_2O and CO_2-MDEA-PZ-H_2O at atmospheric pressure, high pressure vapor-liquid equilibrium experiments for H_2S-CH_4-MDEA-H_2O, density measurements for aqueous MDEA and aqueous activated MDEA and piperazine solubility measurements in aqueous MDEA. Different commercial simulators together with the developed Extended UNIQUAC model were used to simulate the experimental data points. The effect of total pressure on acid gas solubility was also quantitatively investigated through both experimental and modeling approaches.

Resume på dansk

Ca. 40 % af verdens resterende gasreserver indeholder store mængder af de sure gasser CO_2 og H_2S og andre svovlforbindelser. Mange store olie og gasfelter har mere end 10 mol % CO_2 og H_2S indhold. De sure gasser fjernes industrielt ved absorption med kemiske opløsningsmidler. Vandige alkanolaminer, simple kombinationer af alkoholer og ammoniak, er den mest almindeligt anvendte gruppe af kemiske opløsningsmidler for absorption af sur gas. Dette ph.d.-projekt handler om termodynamisk modellering og eksperimentelle målinger vedrørende naturgas rensningsprocesser med anvendelse af alkanolaminer som opløsningsmiddel. Projektet er et samarbejde mellem DTU og Statoil. Den termodynamiske modellering blev udført på DTU og eksperimenter blev udført på Statoils laboratorier. I modelleringsdelen af projektet blev termodynamiske modeller tilpasset CO_2-MDEA-H_2O, CO_2-MEA-H_2O, CO_2-MDEA-MEA-H_2O, H_2S-MDEA-H_2O, H_2S-CH_4-MDEA-H_2O-systemer. Den eksperimentelle del af projektet omfatter damp-væske ligevægt målinger for CO_2-MDEA-H_2O og CO_2-MDEA-PZ-H_2O ved atmosfærisk tryk samt højtryks målinger af damp-væske ligevægt for H_2S-CH_4-MDEA-H_2O systemet. Desuden blev der udført densitet målinger for vandig MDEA og vandig MDEA tilsat piperazin. Piperazins opløselighed i vandig MDEA blev også bestemt eksperimentelt. Forskellige kommercielle simulatorer blev sammenlignet med den udviklede Extended UNIQUAC model til simulering af de eksperimentelle datapunkter. Virkningen af totaltryk på sur gas opløselighed blev også undersøgt kvantitativt med både eksperimentelle og modelbaserede metoder.

Nomenclature

List of Abbreviations:

VLE: Vapor-Liquid Equilibrium

SLE: Solid-Liquid Equilibrium

AARD: Average Absolute Relative Deviation

AAD: Average Absolute Deviation

MEA: Monoethanolamine

MDEA: Methyldiethanolamine

PZ: Piperazine

CO_2: Carbon dioxide

H_2S: Hydrogen sulfide

S^{2-}: Sulfide ion

H^+: Hydrogen ion

OH^-: Hydroxide ion

$MDEAH^+$: MDEA protonated ion

H_2CO_3: Carbonic acid

HCO_3^-: Bicarbonate ion

CO_3^{2-}: Carbonate ion

$MEACOO^-$: MEA carbonate ion

CH_4: Methane

$AgNO_3$: Silver Nitrate

NaOH: Sodium Hydroxide

Ag: Silver

Ag_2S: Silver sulfide

HCl: Hydrochloric acid

Na_2S: Sodium Sulfide

NRTL: Non-Random Two Liquid thermodynamic model

UNIQUAC: UNIversal QUAsi Chemical thermodynamic model

MSA: Mean Spherical Approximation

SRK: Soave-Redlich-Kwong thermodynamic model

e-NRTL: Electrolyte NRTL thermodynamic model

N: Number of data points

ppm: part per million

wt %: Weight percent

rpm: Round per minute

LNG: liquefied natural gas

pH: A measure of the activity of the (solvated) hydrogen ion

R: Gas constant

m : Molality (mole of solute per kg of solvent)

M: Molarity (mole of solute per liter of solution)

List of symbols:

H^E: Excess Enthalpy

C_p: Heat Capacity

H^{abs}: Heat of Absorption

C_p^0: Standard state heat capacity

H_f^0: Standard state enthalpy of formation

G_f^0: Standard state Gibbs free energy of formation

μ_i: Chemical potential

ρ : Density

α: Loading , mole acid gas per mole amine

P_{cr}: Critical pressure

T_{cr}: Critical temperature

ω : Acentric factor

V_i^∞ : Partial molar volume of component i at infinite dilution

γ_i : Activity coefficient of component i

$H_{i,w}$: Henry's constant of solute i in water

List of Contents

List of Tables

List of Figures

Chapter 1

Motivation and Scope of the Work

1 Motivation and Scope of the Work

1.1 Motivation

1.1.1 Background

A large part of the world's natural gas resources has high content of CO_2 and H_2S. CO_2 has to be removed from the natural gas because of transport requirements and sale gas specifications and H_2S need to be because of the toxicity limit. Aqueous alkanolamine solutions are the most widely used solvent in industry to absorb acid gases from natural gas. This research addresses the use of alkanolamine solutions to remove acid gases from natural gas. The aim of this work is to understand the thermodynamic behavior associated with this process by providing required acid gas solubility data and developing consistent thermodynamic models.

1.1.2 Knowledge Gap

A large number of different thermodynamic models have been developed for the simulation of acid gas solubility in alkanolamines. However it is known that many of the most used models can give large errors when extrapolated to high pressures, high amine concentrations, mixed solvents and mixed CO_2 and H_2S gases. Also most of the available thermodynamic models have difficulties to represent heat of the reaction which is one of the key parameters to calculate the energy cost of the plant. Regarding the experimental data, the available VLE data are very rare at high pressures, and there is data neither for amine concentrations higher than 75 wt %, nor for MDEA/PZ solvent with high MDEA concentration.

1.1.3 Objective of this work

- To develop a thermodynamic model which can describe thermodynamic and thermal properties of the acid gas-alkanolamine mixtures over extensive pressure, temperature and amine concentration range.

- Investigate the effect of total pressure on acid gas solubility.
- Obtain experimental data at conditions (mentioned above) that there is a gap in open literature.

This work has been a collaborative effort between Technical University of Denmark (DTU) at Lyngby, Denmark and Statoil Research and Development center (department of gas processing and LNG) in Trondheim, Norway. The modelling part of the work was done at center for energy resources engineering (CERE) at DTU Chemical Engineering and the experimental data were generated at department of Gas Processing and LNG, Statoil ASA Research and development laboratories.

1.2 Outline of the Dissertation

This work is divided into nine chapters. The work begins with outlining the scope and motivation of the work. Chapter 2 addresses background needed in natural gas treatment process. Chapter 3 provides background in chemical aqueous phase thermodynamics as well as describing information on the structure of the developed thermodynamic model. Chapter 4 discusses the developed thermodynamic model for CO_2-MDEA-H_2O, CO_2-MEA-H_2O, CO_2-MDEA-MEA-H_2O systems and the constituent subsystems as well as interpreting the results of the modeling. Chapter 5 shows the developed thermodynamic model for H_2S-MDEA-H_2O, H_2S-CH_4-MDEA-H_2O systems and the constituent subsystems as well as modeling the effect of total pressure on acid gas solubility. Chapter 6 addresses the issues of generating VLE data for CO_2-MDEA-H_2O and density data for MDEA-H_2O systems. In chapter 7, the effect of PZ is studied by acquiring VLE data for CO_2-MDEA-PZ-H_2O at two concentrations of PZ; in addition density data for MDEA-PZ-H_2O were measured. Chapter 8 presents the high pressure VLE data obtained for H_2S-CH_4-MDEA-H_2O systems. Chapter 9 attempts to summarize the work presented throughout this dissertation and to suggest recommendation for future continuation of this study. Appendix 11.3 presents preliminary results for piperazine solubility measurements in aqueous MDEA.

Chapter 2

Introduction to Natural Gas Treating Process, Acid Gas Removal from Natural Gas

2 Introduction to Natural Gas Treating Process, Acid Gas Removal from Natural Gas

2.1 Chapter Overview

The share of natural gas in the world energy panorama has been appreciably growing for the last years. This trend is expected to increase in the next few decades with the progressive replacement of fuel oil and coal by this relatively environment-friendly source of energy. However, this development will depend on the progress of gas processing technologies to give access to reserves now not exploitable. Many of the available gas fields are acid, containing large quantities of CO_2 and H_2S and other sulfur compounds. Gas that contains sulfur compounds impurities is called sour gas. Natural gas is usually considered sour if the hydrogen sulfide content is more than 5.7 milligrams of H_2S per cubic meter of natural gas (4 ppm[1] by volume) Processes that remove hydrogen sulfide and/or mercaptans (generally acid gases) are commonly referred as sweetening processes because they result in products that no longer have acid gases. This chapter gives an introduction on the process of acid gas removal from natural gas. The chapter addresses different issues of process including the reasons for acid gas removal, different common technologies and amine treating process which is the mostly applied technology in industry.

2.2 Reasons for Acid Gas Removal

Natural gas extracted from some wells contains significant amounts of sulfur and carbon dioxide. The composition of acid gases in natural gas varies widely depending on the gas field. Acid gas impurities, i.e. CO_2 and H_2S are detrimental to natural gas properties.

[1]ppm: part per million

For instance, in cryogenic conversion of natural gas to LNG[2], CO_2 transforms to solid state, hence, hinders the transportation of liquid in the pipes or the corrosive H_2S reduces service time of the transportation pipes. In addition H_2S is hazardous for human beings and CO_2 has no heating value. As a result the concentration of acid gas impurities in natural gas must be reduced to a specified level before further processing.

2.3 Acid gas Removal Technologies

The conventional acid gas removal technologies can be classified as:

- Chemical Absorption: In chemical absorption process, acid gases components react chemically with the solvent and formed dissolved chemical compounds. The solvent is regenerated in a stripper column by application of heat. Heat breaks the chemical bounds between acid gases and solvent and drives out the acid gases from the solution. The conventional chemical absorption process is amine process where alkanolamines used as a solvent.
- Physical Absorption: In physical absorption process, acid gases absorb in an organic solvent physically and without chemical reaction. Acid gases are absorbed in the solvent due to their high solubility. Since solubility rises with increasing pressure and decreasing temperature, physical absorption is mostly effective at high pressures and low temperatures. Therefore, compared to amine process, usually physical absorption capital and operating costs is higher attributed to high pressure equipment and refrigerating units required to achieve process operating high pressure and low temperature conditions. In addition, physical solvent is used for bulk removal of acid gases whereas application of chemical solvent is to achieve very low acid gas concentration. It should be noted that the choice between a physical and an amine based solvent has to be taken based on analysis of each case. Sometimes a physical solvent has lower operating and capital costs. However nowadays chemical absorption with amines dominates the market.
- Hybrid Process: In a hybrid process a physical and chemical solvent are applied simultaneously to benefit from the advantages of both processes.
- Membrane Separation Process: Membrane separation systems are mainly used for bulk removal of CO_2. This process is commonly applied at conditions with large flows or high CO_2 contents.

[2]LNG: Liquefied Natural Gas

2.4 Amine Process

In the gas processing industry absorption with chemical solvents has been used commercially for the removal of acid gas impurities from natural gas. The currently preferred chemical solvent technology for acid gas removal is chemical absorption of acid gases by amine-based absorbents. Alkanolamines, simple combinations of alcohols and ammonia, are the most commonly used category of amine chemical solvents used for acid gas removal. In addition to natural gas processing, chemical absorption of acid gases by alkanolamianes has been utilized in a various industries like petroleum refining, CO_2 capture from combustion and flue gases, removal of CO_2 from synthesis gas in ammonia or hydrogen plants.

2.4.1 Amine Type

Four types of amine are used commercially to remove acid gases: primary amines such as MEA[3], secondary amines such as DEA[4], tertiary amines such as MDEA[5] and cyclic amines such as PZ[6]. Figure 2-1 and Figure 2-2 shows chemical structure of the mentioned types of amines.

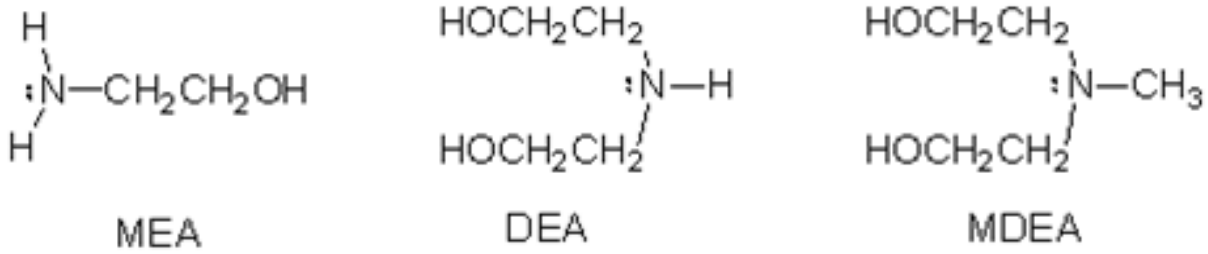

Figure 2-1. Chemical structure of primary, secondary and tertiary amines

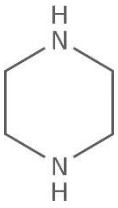

Figure 2-2. Chemical structure of PZ which is a cyclic amine

[3]MEA: Monoethanolamine (RNH_2: R is the alkyl group, $R = CH_2 - CH_2 - OH$)
[4]Diethanolamine (RNH_2: R is the alkyl group, $R = CH_2 - CH_2 - OH$)
[5]Methyldiethanolamine (R_2NCH_3: R is the alkyl group, $R = CH_2 - CH_2 - OH$)
[6]Piperazine (Cyclic amine with two secondary amine groups, $R_2N_2H_2$, R is the alkyl group, R= $CH_2 - CH_2$)

The reaction between H_2S and amines is almost instantaneous and happens due to the fast proton transfer between amine and hydrogen sulfide:

$$H_2S + Amine \leftrightarrow [Amine]H^+ + HS^- \quad (1\text{-}1)$$

Primary and secondary amines react with $CO_2$and create carbamate, for example the reaction for MEA (RNH_2) which is a primary amine can be written as:

$$CO_2 + H_2O + \mathrm{RNH_2} \leftrightarrow [\mathrm{RNH}]COO^- + H^+ + H_2O \quad (1\text{-}2)$$

Since three alkyl groups are connected to the nitrogen atom in MDEA chemical structure, the direct reaction between CO_2 and MDEA is hindered. Accordingly, CO_2 dissolves in water first, and form carbonic acid (H_2CO_3), and then carbonic acid reacts with the basic amine. The reaction between CO_2 and MDEA can be shown as:

$$CO_2 + H_2O + MDEA \leftrightarrow MDEAH^+ + HCO_3^- \quad (1\text{-}3)$$

The acid-base reaction between MDEA (more generally tertiary amine) and CO_2 is slower than MDEA reaction with H_2S. Hence, MDEA selectively removes H_2S. Unlike tertiary amines, in most cases primary and secondary amines react simultaneously with H_2S and CO_2, and that impedes selective removal of acid gases. To overcome slow rate of reaction of MDEA with CO_2, usually small amount of primary or secondary amines are mixed with MDEA. Reactions between amines and acid gases are exothermic (heat produced during the reaction). Based on the Le Chatelier's principle, by increasing acid gases concentration (increasing acid gas partial pressure) and/or decreasing temperature, the above reactions proceed to the right side. The selection of proper amine solution for optimized acid gas removal process depends on process conditions, acid gas partial pressures and purity of treated gases (NREL 2009). The advantages and disadvantages of the most commonly applied amines in industry are as follows. Nowadays aqueous solutions of MEA are only applied for treatment of gases containing low concentrations of CO_2 and H_2S, particularly when maximum removal of these impurities is intended (Anufrikov et al. 2007). The major advantages of MEA are: High reactivity, low cost, and low capacity for absorption of hydrocarbons (Anufrikov et al. 2007). The main disadvantages of MEA are: High corrosiveness of MEA which enhances by temperature, high heat of reaction with CO_2 and H_2S results in high energy requirements for solvent regeneration and consequently the total cost of the process increases, relatively high vapor pressure which brings about notable amine losses via vaporization.

Even though MDEA is more expensive than MEA and it has lower rate of reaction with CO_2 compared to primary and secondary amines, the following advantages makes it the most widely used amine in natural gas treatment industry.

Selective absorption of H_2S from its mixture with CO_2, low heat of reaction of acid gases with MDEA results in notably lower regeneration energy compared to MEA, significantly lower vapor pressure which reduces amine loss by evaporation, higher absorption capacity, very low corrosion rate, high thermal and chemical stability, lower corrosion rate and lower vapor pressure allows to use higher concentration of MDEA in the absorber column which results in lower circulation rate and consequently smaller plant size and lower plant cost, the low miscibility of MDEA with hydrocarbons result in negligible loss of the hydrocarbons.

Due to the mentioned advantages when only removal of H_2S is intended MDEA is solely used as the absorbent. For simultaneous removal of H_2S and CO_2 certain additives are used in MDEA based solution.

It is notable that since removal of CO_2 with MDEA is slow, additives such as piperazine are used to enhance the rate of reaction between CO_2 and MDEA. By adding the faster reacting amine in the exact required amount to MDEA, the desired CO_2 removal can be achieved without losing all the advantages that MDEA offers over other amines.

2.4.2 Flow Scheme

Figure 2-3 shows a typical amine process.

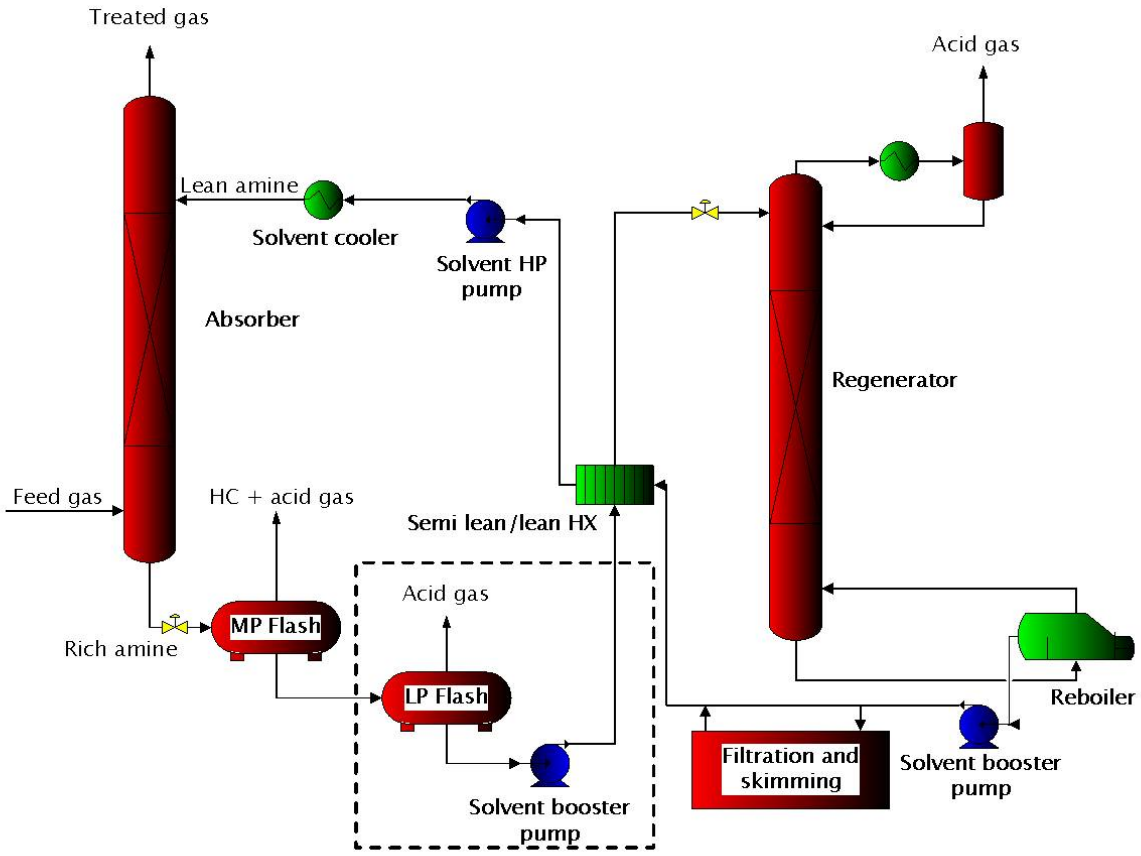

Figure 2-3. Typical Amine Flow Diagram

The inlet sour gas may contain CO_2, H_2S, mercaptans and other acid gases. The concentration of the acid gases is widely dependent on the reservoir of natural gas. Typically concentrations of CO_2 and/or H_2S in natural gas are between 0 to 50 % (molar basis). After the acid gas removal, the concentration of H_2S should be lower than about 4 ppm by volume and that of CO_2 is depending on the application. For sale purpose, the CO_2 content should be reduced down to 2.5 mole percent and for producing LNG that should be lowered down to 50 ppm. As it can be seen from the above figure, feed gas (natural gas) enters at the bottom of the absorber column while lean amine solution[7] (solvent) enters the column at the top. In the absorber, the lean amine solution is contacted counter currently with the gas stream. As the amine solution flows down the absorber column, it contacted with gas stream and acid gases react with the amine, hence amine solution becomes loaded with acid gases and leaves the bottom of the absorber as the rich amine[8]. The sweetened gas [9]stream

[7]Lean Amine: Unloaded aqueous amine solution
[8]Rich Amine: Aqueous amine solution loaded with acid gases
[9]Sweetened Gas: Gas that does not contain significant amounts of H_2S (generally acid gases)

exists at the top of the absorber where it goes for further processing. The rich amine solution leaves the bottom of the absorber and enters one or two flush drums where any dissolved hydrocarbons were removed. The recovered hydrocarbons are usually used as plant fuel. The rich amine solution is heated by exchanging heat with lean solvent stream in the heat exchanger and then fed to the top of the stripper column. As the rich amine solution flows down the stripper column to the reboiler, acid gases are driven out of the solution and the solution is regenerated. The reboiler at the bottom of the stripper column provides the heat required to strip acid gases from the solution. The lean amine solution which exits from the bottom of the stripper (reboiler) enters the filtering and skimming[10] unit to remove particles and heavy liquid hydrocarbons, then exchanges heat with the rich amine stream in the heat exchanger and is further cooled by the cooler before entering at the top of the absorber column. The stripped gas stream is cooled to recover the water and then is sent for further processing such as sulfur recovery units like Claus sulfur plant[11].

The absorber typically is a packed or a tray column. Absorption capacity, process kinetics and the ability to cool the lean amine stream using cooling water usually determine absorber temperature (Bishnoi 2000). In natural gas treatment process, absorber typically operates at 40 °C. Decrease in absorption capacity at higher temperatures and very slow rate of reaction at lower temperatures, makes the absorption unfeasible at temperatures far from 40 °C (Anufrikov et al. 2007). The absorber operating pressure is dependent on the studied process. In natural gas treatment process the absorber typically operate at about 70 bar (7000 kPa) or higher pressures (Bishnoi 2000). For the flue gas, the absorber pressure is around atmospheric pressure. Typical operating temperature of the stripper is around 120 °C. Increasing temperature of solvent inside the stripper removes acid gases from the solvent; recall that reaction between acid gases and aqueous amine is exothermic therefore increasing temperature moves the reaction to the reactant side and leads to produce molecular reactants (acid gases and amine in the molecular form). At higher temperatures there is a possibility of amine degradation and consequent equipment corrosion. The stripper pressure is around 1, 2 bar (100, 200 kPa). Notice that the mentioned numbers are typical operating conditions and the actual operating conditions may deviate a lot from these values.

In natural gas treatment process, typical amine concentration in the absorbent aqueous solution depends on the amine type and acid gases, for removal of both H_2S and CO_2, the MEA

[10] Skimming: Heavy hydrocarbons in the solvent create a liquid phase on top of the solvent. Removing the top layer of liquid is called skimming.

[11] Claus Process: Gas desulfurizing
process; recover elemental sulfur from the hydrogen sulfide gas.

concentration is between 20 to 30 mass % which is equivalent to 6 to 11 mole % (for aqueous MEA solvent) and MDEA concentration is in the range of 30 to 50 mass % which is equivalent to 6 to 13 mole % (for aqueous MDEA solvent). As it can be seen in mole percent scale typical MDEA and MEA concentration is similar.

Amine process economy is mainly dependent on the energy requirements for the solvent regeneration which is a function of the heat of reaction between acid gases and amine solution and the solution circulation rate which depends on solution capacity and (NREL 2009).

2.5 Role of Thermodynamics

The physical and chemical phenomena are both involved in acid gas treating, however absorption of acid gases into the aqueous alkanolamine solutions is governed by the mechanism of mass transfer with chemical reaction (Posey 1997). Equilibrium solubility is required to calculate the driving force for mass transfer. Therefore a thermodynamic model for predicting equilibrium solubility at all applicable conditions of temperature, amine concentration and acid gas loading[12] is highly demanded (Posey 1997). Thermodynamics is also needed for calculation of the free amine concentration (Bishnoi 2000). Chemical equilibrium calculations for all the species present in the liquid phase determine the amount of free amine for a specified overall acid gas concentration (Bishnoi 2000). The more available free amine, leads to faster rate of reaction between amine and acid gases (Bishnoi 2000).

[12]Loading = mole of absorbed acid gas per mole of amine.

Chapter 3

Background Thermodynamics, Modeling Structure

3 Background Thermodynamics, Modeling Structure

3.1 Chapter Overview

Acid gas removal from natural gas is typically performed by physical and chemical absorption into aqueous alkanolamine solutions. Thermodynamics has important role in the design of acid gas treating plants. Thermodynamic modeling of the behavior of these systems includes consideration of both phase and chemical equilibria. Thermodynamics quantifies the bulk phase concentration of acid gas and therefore a driving force for mass transfer, equilibrium compositions and thus outlet concentrations. A consistent thermodynamic model also quantifies amine volatility and thermal properties of the system. Speciation calculations are important for the design of gas treatment plants as the knowledge of the accurate composition of all species in the liquid phase is crucial for rate based models. Liquid phase concentrations will appear in the kinetic equations, and will influence the mass transfer calculations between liquid and gas phase. Amine partial pressure prediction will be used for calculating the amount of amine losses. Since the steam cost is over half of the total plant costs (Carson et al. 2000), prediction of heat of absorption is of great importance to increase cost efficiency.

This chapter addresses literature review over acid gas thermodynamic models, equilibrium thermodynamic of acid gas treatment process, and the relation between different types of data and model parameters. Equilibrium thermodynamics is broken into two parts in this chapter. The first part covers physical vapor-liquid equilibria (VLE) of molecular species. The second part addresses the chemical reactions occur in acid gas-alkanolamine-water systems.

3.2 Review of Previous Models

Thermodynamic models for acid gas absorption processes have been published for many years. Thermodynamic modeling of these multi component systems is very challenging. The reactions taking place in the solution give rise to a number of new ions and molecules.

Most of the available models can reproduce the CO_2 partial pressure of these solutions. Important properties such as amine partial pressure, speciation, and heat of reaction are reproduced with less accuracy. Thermodynamic models used for acid gas absorption process can be categorized in two groups: non-rigorous and rigorous models.

3.2.1 Non-rigorous models

Non-rigorous models are the simplest ones. This family of models is usually called "Kent and Eisenberg" models. They use simple mathematical relations for describing phase equilibrium and in most of them apparent equilibrium constants related to component concentrations instead of activity coefficients. Activity coefficients for all species are set to one. Apparent equilibrium constants are defined as function of ionic strength. Apparent equilibrium constants are fitted to experimental data. Most of the non-rigorous models are based on the apparent equilibrium assumption. This method provides a simple way for prediction of acid gas partial pressure, but it has two major disadvantages. First, the model shows inefficiency when extrapolated to conditions other than those equilibrium constants were tuned for. Second, using apparent equilibrium constant gives only an approximation of the species composition. Using this method, (Van Krevelen et al. 1949) suggested a method for calculating the partial pressures of CO_2, H_2S, and NH_3 into aqueous solutions. Later (DANCKWER.PV and MCNEIL 1967) used the procedure of Krevelen et al. for representing the phase behavior of amine-CO_2-water mixtures. The model of Dankwerts and McNeil used Henry law for acid gas partial pressure calculation and apparent equilibrium constants as function of ionic strength for speciation calculation. (Kent and Eisenberg 1976) modified Dankwerts and McNeil model for calculating CO_2 and H_2S partial pressure in MEA and DEA aqueous solutions. This model can well represent the CO_2 partial pressure although it is very simple. These capabilities make the model usable in commercial simulators like HYSYS. Even though this model shows good results for CO_2 partial pressure, it has two main insufficiencies. First it is only fair in concentration conditions range used for fitting equilibrium constant. Second it cannot predict the composition of species precisely. Accurate prediction of the composition requires precise activity coefficients. Gabrielsen (Gabrielsen et al. 2005) presented a correlation for describing the solubility of CO_2 in H_2O-MDEA solutions. Their model is based on Henry's law and apparent equilibrium constants that were tuned to experimental data.

3.2.2 Rigorous models

This category can be divided into two groups: excess Gibbs energy or activity coefficient models and equation of state models. In general, these models are comprised of two terms: a term for short range interactions (non-electrolyte activity coefficient models or equation of state), and a term for long range interactions (based on the electrostatic theories). Combining a classic, short range interaction model with an electrostatic term makes the model capable of representing the behavior of electrolyte systems.

Excess Gibbs Energy or Activity Coefficient Models

These models provide activity coefficients based on expressions for Excess Gibbs energy of the liquid phase. The speciation in the liquid phase is calculated from the activity coefficients. An equation of state is often used for determining fugacity coefficients of the vapor phase. Deshmukh and Mather (Deshmukh and Mather 1981) proposed a method based on the Guggenheim theory (Guggenheim and Turgeon 1955) for the H_2S/CO_2-MEA-H_2O system. In this model it is assumed that water behaves ideally and all the interaction parameters for water in the model are set to zero. Even though the model is simple, it shows good results for the CO_2 solubility. The model has problems with describing the phase behavior of the binary MEA-H_2O system. In 1975 Edwards et al. (Edwards et al. 1975) presented a molecular thermodynamic model for calculating vapor-liquid equilibria for dilute solutions of weak electrolytes. They used a Guggenheim-type equation for representation of activity coefficients. The model of Edwards is applicable to weak electrolytes, in dilute solutions; at concentrations below 2 m[13]. In 1978 Edwards et al. (Edwards et al. 1978) modified their original model by replacing the Guggenheim term with the Pitzer model. This model is valid at concentrations up to 20 m. Li and Mather (Li and Mather 1994) used the Pitzer and Simonson model (Pitzer and Simonson 1986), which is an extension of the Pitzer model, for modeling the CO_2-MEA-MDEA-H_2O system. Kuranov (Kuranov et al. 1996) used Pitzer model for representing the behavior of CO_2-MDEA-H_2O and H_2S-MDEA-H_2O systems. Perez-Salado Kamps (Kamps et al. 2001) and Ermatchkov (Ermatchkov et al. 2006a) used the Pitzer model for the MDEA-CO_2-H_2O mixture. Arcis (Arcis et al. 2009) applied the Pitzer model for representing VLE data and heat of absorption for the MDEA-CO_2-H_2O system.

Several authors applied a type of excess Gibbs Energy model that are local composition models. The Electrolyte NRTL model (e-NRTL) presented by Chen (Chen et al. 1982)and the Extended

[13] m: m refers to molality which is defined as mole of solute per kg of solvent.

UNIQUAC model presented by Thomsen and Rasmussen in 1999 (Thomsen and Rasmussen 1999) are the most commonly used local composition models applied for electrolyte systems. The e-NRTL model has been applied for modeling many alkanolamine-acid gas-water systems. Austgen (Austgen 1989), Posey (Posey and Rochelle 1997), Hilliard (Hilliard 2008), Le Bouhelec (le Bouhelec et al. 2007), Bishnoi and Rochelle (Bishnoi 2000) applied the e-NRTL model for their work. Hessen (Hessen et al. 2010) used the refined e-NRTL model for the CO_2-H_2O-MEA/MDEA system. Zhang (Zhang and Chen 2011) applied e-NRTL (e-NRTL in ASPEN PLUS) for modeling VLE, heat capacity and heat of absorption of CO_2-MDEA-H_2O system. Addicks (Addicks 2002) applied both Extended UNIQUAC and e-NRTL for VLE calculations in the CO_2-CH_4-MDEA-H_2O system. Faramarzi (Faramarzi et al. 2009) used the Extended UNIQUAC for modeling VLE of the CO_2-H_2O-MDEA/MEA system.

Equations of State

In the equation of state approach, an equation of state is used both for the liquid and the vapor phase. The model of Fürst and Renon (FURST and RENON 1993) is the most well-known electrolyte equation of state. The Fürst and Renon model is comprised of the SR (Schwartzentruber and Renon (1989)) EOS and a simplified MSA term. Several authors have applied the model of Fürst and Renon for acid gases-alkanolamine-H_2O systems. Vallee (Vallee et al. 1999) used this model for the CO_2/H_2S-DEA-H_2O system. (Li and Furst 2000) applied it for CO_2/H_2S-MDEA-H_2O mixtures. Solbraa (Solbraa 2002) implemented the Fürst and Renon model for the MDEA-CO_2-H_2O system. Huttenhuis (Huttenhuis et al. 2008) modified the Solbraa et al. model for the CO_2-CH_4-MDEA-H_2O system. Derks (Derks et al. 2010) used the Fürst and Renon model for the CO_2–PZ–MDEA–H_2O system. Button and Gubbins (Button and Gubbins 1999) applied the SAFT model for the CO_2-MEA/DEA-H_2O system.

3.3 Acid Gas Thermodynamics

This section discusses the typical problem in the acid gas thermodynamics.

3.3.1 Physical and Chemical Equilibria

Acid gas absorption or desorption can be simplified in two steps. In the first step gas phase species are dissolved into the aqueous phase, this step creates vapor-liquid equilibria. In the second step, chemical reactions occur in the aqueous phase and convert aqueous gas species into ions. This step accounts for chemical equilbria. Acid gas thermodynamics involve both physical and chemical

equilibria. Acid gases and alkanolamines are both weak electrolytes. They partially dissociate in the aqueous phase and form a complex mixture of nonvolatile or moderately volatile solvent species, highly volatile acid gas (molecular) species, and nonvolatile ionic species. Thermodynamics provides a framework for representing the physical and chemical equilibria of a weak electrolyte system.

3.3.2 Acid Gas Thermodynamics Problem

Acid gas thermodynamics usually used to solve the liquid phase speciation and partial pressure of each component present in the gas phase when system temperature, system pressure and total amine and acid gas concentration in the liquid phase are defined. The solution of this problem is explained in this section. It is worth to mention that in some cases, the problem is to calculate the liquid phase composition while gas phase composition is known, this inverse problem could also be solved with the illustrated algorithm (in this case liquid composition is adjusted until the gas composition is correct). Table 3-1 shows typical acid gas thermodynamics problem.

Table 3-1. Typical acid gas thermodynamics problem

Known	Unknown
System temperature	Mole fraction of all species present in the liquid phase
System pressure	Partial pressure of each molecular species present in the gas phase
Total amine concentration in the liquid phase	
Loading* (Total acid gas concentration in the liquid phase)	

**Loading (moles of total acid gas (reacted + not reacted)/moles of amine*

The solution of the problem is in essence analogous to bubble point calculations. In acid gas problem, liquid phase is specified (T, P, Total amount of acid gas, Total amount of amine, and Total amount of water) and the model will calculate liquid phase speciation and gas phase composition (partial pressure of gas phase components). The equations required to define the system and solve the problem will be shown in the remainder of this chapter.

3.4 Concentration Units

The experimental data available in literature are often presented in three concentration units: mole fractions, molarities and molalities. Most of the experimental data exist in the molality and loading (mole acid gas/mole amine) units, however thermodynamic models for electrolytes often used mole fraction unit. Molarity unit is also often used, but it is not a practical unit because it depends on

temperature and to a certain extent also on pressure. Density of amine solution is required to convert molarity units to molality units or mole fraction units. It is important to choose a concentration basis before start the modeling. In this work Extended UNIAQUAC model is developed based on mole fraction unit. Mole fraction unit is used for all equations and experimental data. As it mentioned some of the experimental data are presented in molarity unit and density is required to convert molarity to mole fraction. Therefore based on the literature data equations for density of MDEA-H_2O, MEA-H_2O and MDEA-MEA-H_2O at 25 °C were correlated. Density equations for MDEA-H_2O, MEA-H_2O systems were correlated based on density data of (Hawrylak et al. 2000). Density correlation for aqueous blends of MDEA and MEA was developed based on (Mandal et al. 2003) experimental data. The developed density equations represent density of aqueous amine solutions at 25 °C and as a function of amine composition. The next subsection will describe density correlations.

3.4.1 Density Correlations

Usually the temperature of making solvent (aqueous amine solution) is not mentioned in the literature. Hence, it is assumed that the aqueous amine solution is made at ambient temperature (25 °C), consequently density correlations were proposed at 25 °C.

Density of MDEA-H_2O mixture at 25 °C:

$$d = -0.6491x^4 + 1.6104x^3 - 1.4096x^2 + 0.4832x + 0.9985 \quad (3\text{-}1)$$

Density of MEA-H_2O mixture at 25 °C:

$$d = -0.2452x^5 + 0.6034x^4 - 0.4067x^3 - 0.0717x^2 + 0.1351x + 0.9967 \quad (3\text{-}2)$$

Density of MDEA-MEA-H_2O mixture at 25 °C:

$$d = -0.00002y^5 + 0.0002y^2 - 0.0013y + 1.0271 \quad (3\text{-}3)$$

In equations (3-1), (3-2) and (3-3) d is the solution density in $g.cm^{-3}$, x is the amine mole fraction and y represents ratio of MDEA mass percent to MEA mass percent. Equations (3-1) and (3-2) are correlated based on the experimental data from (Hawrylak et al. 2000) and equation (3-3) is proposed upon measurements of (Mandal et al. 2003).

3.5 Physical Equilibria, Vapor-Liquid Phase Equilibrium

In a closed system at constant temperature and pressure, physical equilibria determine the distribution of molecular species (including electrolytes) between the gas phase and the liquid phase. Gas phase species dissolve in the liquid phase, and liquid phase species have the possibility of vaporization.

3.5.1 Chemical Potential and Fugacity

Equilibrium between two phases, labeled α and β, is expressed by:

$$\mu_i^{\alpha} = \mu_i^{\beta} \tag{3-4}$$

The condition of phase equilibrium between the two phases is that the chemical potentials of each species in two phases are identical. The chemical potential does not have an immediate equivalent physical meaning, thus a way is needed to express the chemical potential in terms of an auxiliary function that might have more physical meaning. This useful auxiliary function is called fugacity.

Below equation relates μ_i to fugacity. Fugacity has the same unit of pressure.

$$\mu_i - \mu_i^0 = RTln\frac{f_i}{f_i^0} \tag{3-5}$$

In the above equation, μ_i^0 and f_i^0 are standard state chemical potential and standard state fugacity, respectively. Standard states are reference points. The temperature of the standard state must be the same as the state of interest. However the composition and pressure of the two states need not be the same. Keep in mind that in equation (3-5), the choice of standard state for either μ_i^0 or f_i^0 is arbitrary, but both may not be chosen independently; when one is chosen, the other one is fixed (Prausnitz et al. 1999). The ratio of f_i to f_i^0 is called activity:

$$a_i = \frac{f_i}{f_i^0} \tag{3-6}$$

By applying fugacity definition to equation (3-4), a new form of fundamental equation of phase equilibrium is obtained:

$$f_i^{\alpha} = f_i^{\beta} \tag{3-7}$$

3.5.2 Gas Phase Chemical Potential, Gas Phase Non-Idealities

The chemical potential of a component in an ideal gas mixture (mixture of ideal gases) at T and P is determined by:

$$\mu_i^{ig}(T,P) = \mu_i^{0,\mathrm{ig}}(\mathrm{T},\mathrm{P}) + RTlny_i \tag{3-8}$$

Where y_i is the mole fraction of component i in the ideal gas mixture and $\mu_i^{0,\mathrm{ig}}$ is the standard state chemical potential at system temperature T and some arbitrary pressure P. Standard state chemical potential is defined as chemical potential of the pure ideal gas (superscript 0 stands for pure and superscript "ig" indicates ideal gas). Notice that ideal gas standard state chemical potential is usually given at 1 bar (pressure of 1 bar is represented by P_0, P_0 = 1 bar). The chemical potentials of gases are highly dependent on pressure. Hence, standard state chemical potential at T and P is described by:

$$\mu_i^{0,ig}(T,P) = \mu_i^{0,\mathrm{ig}}(\mathrm{T},P_0) + RTln\frac{P}{P_0} \tag{3-9}$$

Replacing equation (3-9) in equation (3-8) yields to equation (3-10) for chemical potential of component i in an ideal gas mixture at pressure P:

$$\mu_i^{ig}(T,P) = \mu_i^{0,\mathrm{ig}}(\mathrm{T},P_0) + RTln\frac{Py_i}{P_0} \tag{3-10}$$

As it mentioned earlier, in acid gas thermodynamics gas phase is not ideal. The deviation of real mixture chemical potential from ideal gas mixture chemical potential at T and P is described by the residual term ($\mathrm{RTln}\widehat{\varphi_i}$). Thus, the chemical potential of component i in a real gas mixture is defined by sum of the chemical potential of component i in an ideal gas mixture and the residual term:

$$\mu_i^{g}(\mathrm{T},\mathrm{P}) = \mu_i^{0,\mathrm{ig}}(\mathrm{T},P_0) + RTln\frac{Py_i}{P_0} + \mathrm{RTln}\widehat{\varphi_i} \tag{3-11}$$

Where $\widehat{\varphi_i}$ is the fugacity coefficient of component i in the gas phase. Chemical potential of component i is related to the fugacity of component i in a gas phase is by equation (3-5), thus for a gas phase equation (3-5) is written as:

$$\mu_i^{g} - \mu_i^{0,g} = RTln\frac{f_i^g}{f_i^{0,g}} \tag{3-12}$$

Where,$f_i^{0,g}$ is the standard state fugacity. $f_i^{0,g}$ is defined as the fugacity of pure ideal gas at system temperature and an arbitrary pressure. The arbitrary pressure called P_0 chosen to be 1 bar, and because fugacity of pure ideal gas is equal to pressure, thus standard state fugacity for a component i in a gas phase ($f_i^{0,g}$) is set equal to 1 bar. Thus:

$$f_i^{0,g} = P_0 = 1\ bar$$

Substituting equation (3-11) in equation (3-12) yields to the equation for fugacity of component i in the vapor phase:

$$f_i^v = \hat{\varphi}_i P y_i \qquad (3\text{-}13)$$

In this study SRK equation of state is used to calculate the gas phase non-idealities.

3.5.3 Liquid Phase Chemical Potential, Liquid Phase Non-Idealities

The most difficult challenge in describing VLE in weak electrolyte systems is representing liquid phase behavior. Presence of ionic species in the liquid phase results in a highly non-ideal thermodynamic behavior. Liquid phase non-idealities deviations from ideal phase are usually expressed by activity coefficients.

The solution is defined as an ideal solution if the chemical potential of every species in the solution is described by:

$$\mu_i^{id}(T,P) = \mu_i^0(T,P) + \mathrm{RTln}x_i \qquad (3\text{-}14)$$

Where R is the gas constant, T is the absolute temperature in Kelvin, and x_i is the mole fraction of component i. μ_i^0 is known as the standard state or reference state chemical potential and is a function of temperature and pressure. For a real solution, the chemical potential is not a linear function of the logarithm of the mole fraction. The chemical potential of species i in a real solution is defined based on the definition for the ideal solution, chemical potential of species i in real solutions is calculated by the sum of two terms: an ideal term and an excess term ($\mu_i^{ex} = \mathrm{RTln}\gamma_i$). The excess term shows the deviation between chemical potential in a real mixture and chemical potential in an ideal mixture.

$$\mu_i^l(T,P) = \mu_i^{id}(T,P) + \mu_i^{ex}(T,P) = \mu_i^0(T,P) + \mathrm{RTln}x_i + \mathrm{RTln}\gamma_i = \mu_i^0(T,P) + \mathrm{RTln}(x_i\gamma_i) \qquad (3\text{-}15)$$

Where activity coefficient of component i (γ_i) is a function of temperature, pressure, and composition of the solution. Standard state chemical potential is usually given at 1 bar (pressure of 1 bar is represented by P_0, P_0 = 1 bar). Standard state chemical potential at pressure P is related to standard state chemical potential at pressure P_0 through equation (3-17).The standard state chemical potential of a species at a certain pressure can be calculated by integration of equation (3-14) from P_0 to P. The pressure dependence of the chemical potential of species i is given by:

$$\left[\frac{\partial \mu_i}{\partial P}\right]_T = V_i \tag{3-16}$$

V_i is the partial molar volume of component i. Assuming that the partial molar volume of the species is independent of pressure, integrating equation (3-14) results in:

$$\mu_i^{0,l}(T,P) = \mu_i^0(T,P_0) + V_i(P - P_0) \tag{3-17}$$

Replacing equation (3-17) in equation (3-15) yields to the following equation for chemical potential of component i in a real liquid mixture:

$$\mu_i^l(T,P) = \mu_i^0(T,P_0) + V_i\,(P - P_0) + RT\ln(x_i\gamma_i) \tag{3-18}$$

Chemical potential of component i in a liquid mixture is related to the fugacity of component i in a liquid phase by the general equation (3-5), thus for a liquid phase equation (3-5) is written as:

$$\mu_i^l - \mu_i^{0,l} = RT ln \frac{f_i^l}{f_i^{0,l}} \tag{3-19}$$

Where $f_i^{0,l}$ is the fugacity of i at some arbitrary condition known as the standard state.

Substituting equation (3-18) in equation (3-19) results in the following equation for the fugacity of component i in the liquid phase:

$$\frac{f_i^l}{f_i^{0,l}} = x_i\gamma_i \rightarrow f_i^l = x_i\gamma_i f_i^{0,l} \tag{3-20}$$

The definition of γ_i and $\mu_i^{0,l}$ is incomplete unless a standard state (reference state) is specified. "At any composition, the activity coefficient depends on the choice of standard state. Because the choice of standard state is arbitrary, it is convenient to choose $\mu_i^{0,l}$ $\left(or\ f_i^{0,l}\right)$ such that $\gamma_i$assumes values close to unity and when, for a range of conditions, γ_i is exactly equal to unity, the solution is

called ideal. However, because of the intimate relation between the activity coefficient and the standard state fugacity, the definition of solution ideality ($\gamma_i = 1$) is not complete unless the choice of standard state is clearly indicated (Prausnitz et al. 1999)." To specify the conditions at which the activity coefficient of component i becomes equal to unity, frequently two choices are used. Either of two choices leads to an ideal solution definition. One leads to an ideal solution in the sense of Raoult's law and the other leads to an ideal solution in the sense of Henry's law. The process of identifying standard states at which the activity coefficients of all species in a solution become unity is named as normalization. Next section will discuss standard states used in this modeling framework.

3.5.4 Standard States, Reference States

In this work water is considered as a solvent. The reference state for water is defined as the state of the pure component at the system temperature and pressure. Therefore, the chemical potential of water in an aqueous solution is calculated by the following equation:

$$\mu_w = \mu_w^0 + RTln(x_w\gamma_w) \tag{3-21}$$

In real mixture : $\gamma_w \to 1 \quad as \quad x_w \to 1$

μ_w^0 is the standard state chemical potential of water and equated to the molar Gibbs energy of pure liquid at system temperature and pressure. In the limit of $x_w \to 1$, γ_w becomes 1 and excess term vanishes. This standard state leads to the Raoult's law[14] definition for an ideal solution. Therefore, fugacity of water in aqueous solution is written as:

$$f_w = f_{pure,w}x_w\gamma_w \tag{3-22}$$

For a mixture of a nonvolatile solute dissolved in a solvent, equation (3-21) is used to define chemical potential of the solvent, here water, and the state of pure component is used as standard state for solvent. However, for a nonvolatile solute, for most cases, at normal temperatures and pressures, a pure nonvolatile solute cannot exist as liquid, thus for a nonvolatile solute, pure liquid at system temperature and pressure is often not a suitable standard state (Prausnitz et al. 1999). Thus, the chemical potential of all the dissolved solutes is written as:

$$\mu_i = \mu_i^* + RTlna_i = \mu_i^* + RT\ ln(x_i\gamma_i^*) \tag{3-23}$$

In real mixture : $\gamma_i^* \to 1 \quad as \quad x_i \to 0$

[14]Raoult's law: At any T, P and x : $f_i(T,P,x) = f_{pure\,i}(T,P,x)$, $x_i(x_i \to 1)$

Where μ_i^* is the standard state chemical potential of i, which is independent of composition, but is dependent on temperature, pressure and γ_i^* is the rational unsymmetrical activity coefficient. The standard state for the solute is defined by a hypothetical ideal solution of i in the solvent, at system temperature and pressure and at unit concentration, $x_i = 1$ (Prausnitz et al. 1999). In this ideal solution, $\gamma_i = 1$. In the real solution, $\gamma_i^* \rightarrow 1$ as $x_i \rightarrow 0$ (Prausnitz et al. 1999). Keep in mind that it is a very common to misunderstand the standard state for the solute as the solute at system temperature and pressure and at infinite dilution. That is not correct since at infinite dilution, the chemical potential of the solute is $-\infty$ (when $x_i = 0$ then ln(0)= $-\infty$ and from equation (3-23) $\mu_i = -\infty$) (Prausnitz et al. 1999). As mentioned earlier, the standard state chemical potential for the solute i must define at some fixed (non-zero) concentration, this concentration is unit concentration. Unit concentration is used because its logarithm is zero, therefore from equation (3-23) at unit concentration, $\mu_i = \mu_i^*$ (Prausnitz et al. 1999). This standard state definition leads to Henry's law[15] for an ideal solution. γ_i^* is the rational unsymmetrical activity coefficient and is defined by:

$$\gamma_i^* = \frac{\gamma_i}{\gamma_i^\infty} \tag{3-24}$$

Where γ_i^∞, is the infinite dilution activity coefficient of solute in water and it depends on temperature and pressure. According to this standard state definition, fugacity of the dissolved solute is defined by:

$$f_i = H_{i,solvent} x_i \gamma_i^* \tag{3-25}$$

3.5.5 Vapor-Liquid Equilibria Condition

Equation (3-4) shows the condition for vapor-liquid equilibria. For the systems studied in this work, vapor-liquid equilibrium is considered for water, amine (MDEA, MEA), acid gases (CO_2 and H_2S) and methane. Equations for chemical potential are already explained in the previous sections. For water, the condition for vapor-liquid equilibria is formulated by combining equations (3-11) and (3-21):

$$\frac{\mu_w^{0,l}(T,P_0) - \mu_w^{0,\mathrm{ig}}(T,P_0)}{RT} + \frac{V_w\,(P - P_0)}{RT} = \ln\left[\frac{P y_w \widehat{\varphi_w}}{x_w \gamma_w P_0}\right] \tag{3-26}$$

[15]Henry's law: At any T, P and x : $f_i(T,P,x) = H_{i,solvent}(T,P,solvent\ and\ solute\ nature)x_i \quad (x_i \rightarrow 0)$

In this work, activity coefficients are calculated from the Extended UNIQUAC model, the SRK equation of state is used for calculating fugacity coefficients in the vapor phase.

For amines, MDEA and MEA, and also for H_2S the condition for vapor-liquid equilibria is obtained by combining equations (3-11) and (3-23):

$$\frac{\mu_{i,aq}^{*}(T,P_0)-\mu_i^{0,ig}(T,P_0)}{RT}+\frac{V_i\,(P-P_0)}{RT}=\ln\left[\frac{Py_i\widehat{\varphi_i}}{x_i\gamma_i^{*}P_0}\right] \tag{3-27}$$

Methane is dissolved very little in water. It is common to use Henry's constant for sparingly soluble gases in liquid. Carbon dioxide is supercritical at system temperature, and it does not exist at system temperature as pure component, hence pure component standard state properties are not available for it. In such cases, the first term in the right hand side of equation (3-27) is substituted by Henry's constant:

$$\ln\left(\frac{H_i(T,P_{w,sat})}{P_0}\right)+\frac{V_i^{\infty}\,(P-P_{w,sat})}{RT}=\ln\left[\frac{Py_i\widehat{\varphi_i}}{x_i\gamma_i^{*}P_0}\right] \tag{3-28}$$

Equation (3-28) is known as Krichevski-Iliinskaya equation (Kritchevsky and Iliinskaya 1945) and is used at pressures above the boiling point pressure of the solvent. In this equation, P_0 is 1 bar, $P_{w,sat}$ is the vapor pressure of the solvent at the relevant temperature, P is the total pressure and V_i^{∞} is the partial molar volume of the solute at infinite dilution. In this study for both carbon dioxide and methane Henry's constant in pure water is used. For carbon dioxide a temperature dependent Henry's law correlation proposed by Rumpf and Maurer (RUMPF and MAURER 1993) is used.

$$\ln((H_{CO_{2,w}}^{*}M_w)=192.876-\frac{9624.4\,K}{T}+1.441\times10^{-2}K^{-1}T-28.749\ln(T) \tag{3-29}$$

$V_{CO_2}^{\infty}$ is calculated from the equation presented by Rumpf and Maurer (RUMPF and MAURER 1993). Henry's law correlation presented by Crovetto et al. (Crovetto et al. 1982) is used for methane. Notice that bubble point pressure of the studied electrolyte solutions can be found by simultaneously solving vapor-liquid equilibria equations. As explained earlier in this study SRK equation of state is used to calculate fugacity coefficients in the vapor phase (gas phase non-idealities). Classical mixing rule is utilized to calculate mixture properties. Notice that all binary interaction parameters were fixed to zero. Pure component properties that are applied in this study are summarized in Table 3-2.

Table 3-2. Pure component properties used in SRK EoS

Component	P_{cr}*, bar	T_{cr}**, K	ω***
H_2O	220.64	647.096	0.344
CO_2	73.773	304.1282	0.225
H_2S	89.63	373.5	0.094
MDEA	41.6	741.9	0.6253
MEA	71.24	678.2	0.4467
CH_4	45.99	190.6	0.012

P_{cr} : Critical pressure

**T_{cr} : Critical pressure*

***ω : Acenric factor*

3.6 Chemical Equilibria, Speciation Equilibria

The term speciation describes what happens when electrolytes are dissolved in water. Electrolytes dissociate partly or completely when dissolved in water. The composition of the created species in the solution at equilibrium is calculated by solving the equations for speciation equilibria. The condition for speciation equilibrium is that for each reaction the sum of the chemical potential of the reactants is equal to the sum of the chemical potentials of the products. Equations for chemical potential of water and dissolved solutes were already illustrated in section 3.5. Reactions that occur in each system will be explained in next chapter. The condition for chemical equilibrium for each reaction is commonly expressed by:

$$lnK = -\frac{\Delta G_j^0}{RT} = \sum_i \upsilon_{i,j} ln a_i \tag{3-30}$$

K is the equilibrium constant at the temperature T, ΔG_j^0 is the change of Gibbs energy of formation for the reaction j. a_i is the activity of component i and $\upsilon_{i,j}$ is the stoichiometric coefficient of component i involved in reaction j. Notice that in order to calculate the equilibrium composition of all the components present in the system, vapor-liquid equilibria equations and chemical equilibria equations have to be solved simultaneously.

3.6.1 Standard state properties

In this work, equilibrium constants are calculated from standard state chemical potentials (standard state chemical potential is equal to the molar Gibbs energy at standard state (G^0)). For most species, the values of standard state chemical potentials at 25 °C can be found in NIST tables (NIST). Standard state chemical potentials that are not available in these tables are regressed to experimental

data. Standard state chemical potentials are calculated from their values at 25 °C by integrating the Gibbs-Helmholtz equation using standard state enthalpies and standard state heat capacities:

$$-\frac{dlnK}{dT} = \frac{d(\frac{\Delta G^0}{RT})}{dT} = -\frac{\Delta H^0}{RT^2} \quad \text{(at constant Pressure)} \tag{3-31}$$

Integrating equation (3-31) form 298.15 K (25 °C) to the temperature of interest gives:

$$\ln K_T - \ln K_{298.15} = \int_{298.15}^{T} \frac{\Delta H^0}{RT^2} dT \tag{3-32}$$

The change in standard state enthalpy of formation with temperature is calculated from the corresponding heat capacities

$$\frac{d\Delta H^0}{dT} = \Delta C_P^0 \tag{3-33}$$

$C_{P,i}^0$ is the standard state heat capacity of component i and is correlated by the following equation for all solutes:

$$C_{P,i}^0 = a_i + b_i T + \frac{c_i}{T-200} \tag{3-34}$$

Inserting equation (3-34) in equation (3-33) and then in equation (3-32) gives the equilibrium constant as function of temperature:

$$R\ln K_T = R\ln K_{T_0} - \Delta H_{T_0}^0\left(\frac{1}{T}-\frac{1}{T_0}\right) + \Delta a\left(\ln\frac{T}{T_0}+\frac{T}{T_0}-1\right) + 0.5\Delta b\left(\frac{(T-T_0)^2}{T}\right) + \frac{\Delta C}{T_\Theta}\left(\frac{T-T_\Theta}{T}\ln\frac{T-T_\Theta}{T_0-T_\Theta} - \ln\frac{T}{T_0}\right) \tag{3-35}$$

With the value of the equilibrium constant at the temperature T, the composition of the solution can be calculated at the temperature T if the activity coefficients are known at this temperature. Keep in mind that in order to reproduce modeling predictions presented in this study it is of high importance to implement the developed model with the same fitted parameters and the same standard state properties presented in this work.

3.7 Extended UNIQUAC Model Structure

In this work, activity coefficients in the liquid phase are determined by the Extended UNIQUAC model presented by Thomsen and Rasmussen in 1999 (Thomsen and Rasmussen 1999). The

Extended UNIQUAC model is a combination of the original UNIQUAC model by Abrams and Prausnitz (ABRAMS and PRAUSNITZ 1975)with an extended Debye-Huckel term for long range interactions.

$$\frac{G^E}{RT} = \left(\frac{G^E}{RT}\right)_{\text{Combinatorial, UNIQUAC entropic}} + \left(\frac{G^E}{RT}\right)_{\text{Residual,UNIQUAC enthalpic}} + \left(\frac{G^E}{RT}\right)_{\text{Debye-Hückel}} \quad (3\text{-}36)$$

The combinatorial term is independent of temperature; it only depends on the relative size of the species:

$$\left(\frac{G^E}{RT}\right)_{UNIQUAC\ Entropic} = \sum_i x_i\, ln\left(\frac{\varphi_i}{x_i}\right) - \frac{z}{2}\sum_i x_i q_i\, ln\left(\frac{\varphi_i}{\theta_i}\right) \quad (3\text{-}37)$$

Z=10 is the coordination number, x_i is the composition, φ_i and are volume fraction and surface fraction of component i:

$$\varphi_i = \frac{x_i r_i}{\sum_j x_j r_j} \quad (3\text{-}38)$$

$$\theta_i = \frac{x_i q_i}{\sum_j x_j q_j} \quad (3\text{-}39)$$

The residual term represent interaction between different pairs and is dependent of temperature:

$$\left(\frac{G^E}{RT}\right)_{UNIQUAC\ Enthalpic} = -\sum_i x_i\, q_i ln\left(\sum_j x_j\, \psi_{ji}\right) \quad (3\text{-}40)$$

where ψ_{ji} is

$$\psi_{ji} = \exp\left(-\frac{u_{ji}-u_{ii}}{T}\right) \quad (3\text{-}41)$$

u_{ji}andu_{ii} are energy interaction parameters between species i and j . They are assumed symmetrical and temperature dependent.

$$u_{ji} = u_{ji}^0 + u_{ji}^T(T - 289.15) \quad (3\text{-}42)$$

The model parameters are r_i, q_i for species i and u_{ji}^0 and u_{ji}^T for interaction energy between species i and j.

The Debye-Huckel term is

$$\left(\frac{G^E}{RT}\right)_{Debye-Huckel} = -x_w M_w \frac{4A}{b^3}\left[\ln\left(1+b\sqrt{I}\right) - b\sqrt{I} + \frac{b^2 I}{2}\right] \quad (3\text{-}43)$$

x_w is water mole fraction, M_w ($kgmol^{-1}$) is water molar mass, b is considered to be a constant equal to 1.50 $(kg/mol)^{1/2}$and I is the ionic strength in mol (kg H_2O)$^{-1}$ which is defined by:

$$I = \frac{1}{2}\sum_i m_i z_i^2 \quad (3\text{-}44)$$

Where m_i and z_i are the molality (mole/kg H_2O) and the charge number of ionic species i, respectively.

In equation (3-43), A is the Debye-Hückel constant and is presented by:

$$A = \frac{F^3}{4\pi N_A}\left[\frac{d}{2(\varepsilon_0 DRT)^3}\right]^{\frac{1}{2}} \quad (3\text{-}45)$$

Where F($Cmol^{-1}$) is the Faraday's constant, N_A (mol^{-1}) is Avogadro's number, ε_0 ($C^2J^{-1}m^{-1}$) is the vacuum permittivity, R ($Jmol^{-1}K^{-1}$) is the gas constant, T (K) is the temperature, d (kgm^{-3}) is the density and D is the dielectric constant (relative permittivity). Notice that d and D parameters are temperature dependent. Based on the d and D values, Debye-Huckel constant can be presented by the following equation in the temperature range of $273.15 \le T \le 383.15$.

$$A = \left[1.131 + 1.335\times10^{-3}\times(T-273.15) + 1.164\times10^{-5}\times(T-273.15)^2\right] kg^{\frac{1}{2}} mol^{-\frac{1}{2}} \quad (3\text{-}46)$$

Keep in mind that there is no adjustable parameter in the Debye-Huckel term.

3.8 Types of Experimental Data

This section discusses how different types of experimental data are related to the model parameters.

3.8.1 Partial Pressure Data, Acid Gas Solubility Data

Data in the form of acid gas solubility (acid gas partial pressure over the mixture of aqueous amine), as a function of loading (mole acid gas/mole amine) and temperature have been used to adjust acid gas partial pressure through the simultaneous regression of model parameters. Equation (3-27) and (3-28) relate model parameters to partial pressure of H_2S and partial pressure of CO_2, respectively.

3.8.2 Total Pressure Data

Data in the form of total pressure of the solution as a function of temperature and concentration was used to adjust the activity coefficients through the simultaneous regression of UNIQUAC model parameters. Total pressure is the sum of partial pressure of all vapor phase constituents, equation (3-47). Through summation of partial pressures, model parameters are related to total pressure data. Determination of activity coefficients from total pressure measurements was proposed by Barker in1953 (BARKER 1953). Barker (BARKER 1953) showed that the accuracy of activity coefficients derived from total pressure data is comparable with those derived from partial pressure measurements. That is beneficial especially at conditions where partial pressure data are few or not available.

$$P_{Total} = \sum_{i=1}^{n} P_{i,partial\ pressure} \tag{3-47}$$

In the above equation, P_{Total} is the total pressure and is equal to sum of partial pressure of components present in the vapor phase. n is the number of components in the vapor phase and $P_{i,partial\ pressure}$ is the partial pressure of each component.

3.8.3 Pure Vapor Pressure Data

Pure vapor pressure data as a function of temperature were used to regress model parameters. Pure vapor pressure is beneficial to modeling because pure vapor pressure data are related to infinite dilution activity coefficients. Using pure vapor pressure data for regression provides more accurate estimation of infinite dilution activity coefficients. The following equation shows the condition for vapor-liquid equilibria for a pure component.

$$-\frac{\Delta G^0}{RT} = ln\frac{y_i\varphi_i P_i^{Vapor}}{x_i\gamma_i^* P^0} \tag{3-48}$$

In the above equation $P^0$is 1 bar,y_{H_2S} and x_{H_2S} are equal to 1 as both gas and liquid phases are pure. γ_i^* is the unsymmetrical activity coefficient for the dissolved and is defined by equation (3-24) ($\gamma_i^* = \frac{\gamma_i}{\gamma_i^\infty}$). According to the definitions for the standard state, for the pure dissolved solute:

$$\gamma_i \rightarrow 1 \qquad as \qquad x_i \rightarrow 1$$

Therefore above equation (3-48) is reduced to

$$-\frac{\Delta G^0}{RT} = ln\frac{\varphi_i \gamma^{\infty}_{H_2S} P_i^{Vapor}}{1} \quad (3\text{-}49)$$

Where γ_i^{∞} is the infinite dilution activity coefficient (activity coefficient of component i in the mixture of component i and water when mixture is very dilute with respect to component i) and is defined by:

$$ln\gamma_i^{\infty} = ln\gamma_i^{C\infty} + ln\gamma_i^{R\infty} \quad (3\text{-}50)$$

In this equation, C stands for the combinatorial term of the UNIQUAC equation and R indicates the enthalpy term of the UNIQUAC equation. $\gamma_i^{C\infty}$ and $\gamma_i^{R\infty}$ are described by the following equations:

$$ln\gamma_i^{C\infty} = ln\frac{r_i}{r_w} + 1 - \frac{r_i}{r_w} - \frac{Z}{2}q_i\left[ln\frac{r_i q_w}{r_w q_i} + 1 - \frac{r_i q_w}{r_w q_i}\right] \quad (3\text{-}51)$$

$$ln\gamma_i^{R\infty} = q_i[1 - ln\psi_{wi} - \psi_{iw}] \quad (3\text{-}52)$$

In this equation w and i denotes water and component i respectively. ψ_{wi} is the interaction parameter between water and component i. Z is the coordination number that is assumed to be fixed at 10.

3.8.4 Heat Capacity Data

As stated by equation (3-33) the liquid phase heat capacity of a mixture is calculated by taking the derivative of the enthalpy of the liquid phase at constant pressure. Data in the form of the heat capacity of mixture as a function of temperature and concentration were used to adjust activity coefficients through simultaneous regression of the model parameters by taking the derivative of the UNIQUC model. Notice that heat capacity data are useful to determine heat capacity parameters in equation (3-34); also they are efficient for determining the value of the surface area parameter q, because the UNIQUAC contribution to the excess enthalpy and excess heat capacity is proportional to the parameter q. An important advantage of the Extended UNIQUAC model compared to models like the Pitzer is that temperature dependence is built into the model. This enables the model to describe thermodynamic properties that are temperature derivatives of the excess Gibbs function, such as heat of mixing and heat capacity

3.8.5 Excess Enthalpy Data

In this work, excess enthalpy is defined identical to heat of mixing and is described as the isothermal enthalpy change per mole of solution when mixing two pure liquids without a chemical

reaction. Excess enthalpy data is favorable for the modeling, since this type of data is directly related to the temperature dependence of excess Gibbs energy. Equation (3-48) describes the relationship between the temperature dependence of the activity coefficient, excess Gibbs energy and the excess enthalpy data.

$$\left(\frac{\partial(\frac{G^E}{T})}{\partial T}\right)_{P,x} = -\frac{H^E}{T^2} = x_w\left(\frac{\partial ln\gamma_w}{\partial T}\right)_{P,x} + x_{alkanolamine}\left(\frac{\partial ln\gamma_{alkanolamine}}{\partial T}\right)_{P,x} \quad (3\text{-}53)$$

Regressing excess Gibbs energy to excess enthalpy data improves model temperature dependency.

3.8.6 Freezing Point Depression Data

Freezing point data were also used in the parameter estimation process. This kind of data is useful to get a better estimation for water activity. In the temperature range considered, ice is the only solid phase that is formed. The solid – liquid equilibrium criterion is:

$$\mu_w^S = \mu_w^l \quad (3\text{-}54)$$

The solid phase is pure water; therefore the chemical potential of water in the solid phase is equal to its standard chemical potential in the solid phase.

$$\mu_w^S = \mu_w^{0,S} \quad (3\text{-}55)$$

The chemical potential of water in the liquid phase is expressed by

$$\mu_w^l = \mu_w^{0,l} + RTlna_w \quad (3\text{-}56)$$

Combing equations (3-51) and (3-49) yields to:

$$-\frac{\Delta G^0}{RT} = lna_w \quad (3\text{-}57)$$

3.8.7 Heat of Absorption Data

In this work the heat involved when acid gas is absorbed in the liquid phase is calculated form the energy balance of the absorption process. The enthalpy balance for the absorption process thus is written as:

$$\Delta H_{abs} = \frac{n_{Final}H^L_{Final} - n_{Initial}H^L_{Initial} - \Delta n_{Acid\ Gas}H^g_{Acid\ Gas}}{\Delta n_{Acid\ Gas}} \quad (3\text{-}58)$$

In the above equation ΔH_{abs} is the heat of absorption which is usually given relative to the moles of acid gas absorbed, H^{L}_{Final} is the molar enthalpy of the final solution, $H^{L}_{Initial}$ is the molar enthalpy of the initial solution, $H^{g}_{Acid\ Gas}$ is the molar enthalpy of the gaseous acid gas absorbed in the liquid solution, n_{Final} is the number of moles of the final solution, $n_{Initial}$ is the number of moles of the initial solution and $\Delta n_{Acid\ Gas}$ is the number of moles of acid gas absorbed.

Heats of absorption data reported in the literature are classified into two types: I) integral heat of absorption, II) differential heat of absorption. The integral heat of absorption for a solution of amine-acid gas-water is the enthalpy change of the solution per mole of acid gas form loading zero to final acid gas loading. However, differential heat of absorption refers to the enthalpy change per mole of acid gas when very small amount of the acid gas is added to the loaded solution. H^{L}_{Final}, $H^{L}_{Initial}$ and $H^{g}_{Acid\ Gas}$ values are required to calculate both types of heat of absorption.

The total enthalpy of formation of an electrolyte solution at constant pressure and composition is calculated by:

$$nH = \widetilde{n_w} H_w + \sum_i \widetilde{n_i} H_i \tag{3-59}$$

Where H_w is the partial molar enthalpy of water and H_i is the partial molar enthalpy of solutes. $\widetilde{n_w}$ and $\widetilde{n_i}$ are the mole numbers of water and solutes at equilibrium, respectively. H_w and H_i are calculated from the derivatives of chemical potential with respect to temperature at constant pressure and composition.

Chemical potential of water is written by equation (3-21) ($\mu_w = \mu_w^0 + RTln(x_w\gamma_w)$), differentiation of equation (3-21) with respect to temperature at constant pressure and composition leads to:

$$\left[\frac{\partial\left(\frac{\mu_w}{RT}\right)}{\partial T}\right]_{P,x} = \left[\frac{\partial\left(\frac{\mu_w^0}{RT}\right)}{\partial T}\right]_{P,x} + \left[\frac{\partial ln x_w}{\partial T}\right]_{P,x} \tag{3-60}$$

$$\frac{H_w}{RT^2} = \frac{H_w^0}{RT^2} + \frac{H_w^{ex}}{RT^2} \tag{3-61}$$

Thus:

$$H_w = H_w^0 + H_w^{ex} \tag{3-62}$$

Therefore, partial molar enthalpy of water (H_w) is calculated by the sum of water molar enthalpy of formation in the standard state (H_w^0) and partial molar excess enthalpy of water (H_w^{ex}).

Chemical potential of dissolved solute is described by equation (3-23) ($\mu_i = \mu_i^* + RTlna_i = \mu_i^* + RT\ ln(x_i\gamma_i^*)$), differentiation of equation (3-23) with respect to temperature at constant pressure and composition yields:

$$\left[\frac{\partial\left(\frac{\mu_i}{RT}\right)}{\partial T}\right]_{P,x} = \left[\frac{\partial\left(\frac{\mu_i^*}{RT}\right)}{\partial T}\right]_{P,x} + \left[\frac{\partial ln\gamma_i^*}{\partial T}\right]_{P,x} \quad (3\text{-}63)$$

$$\frac{H_i}{RT^2} = \frac{H_i^0}{RT^2} + \frac{H_i^{ex}}{RT^2} \quad (3\text{-}64)$$

Partial molar enthalpy of solutes (H_i) is calculated by the sum of molar enthalpy of formation of solutes in the standard state (H_i^0) and partial molar excess enthalpy of solutes (H_i^{ex}).

The molar gaseous acid gas absorbed is calculated by:

$$H_{Acid\ Gas}^{g} = H_{Acid\ Gas,T=298.15}^{0,g} + \int_{298.15}^{T} C_{P,AcidGas}^{0} dT \quad (3\text{-}65)$$

Where $H_{Acid\ Gas,T=298.15}^{0,g}$ is the molar enthalpy of formation of gaseous acid gas at 25 °C.

3.9 Conclusion

In this chapter, thermodynamic background and structure has been addressed. The chapter starts with an overview over present thermodynamic models. Later on the acid gas thermodynamic problem and the developed density correlations followed by the basic concepts of physical and chemical equilibrium were presented. Furthermore the Extended UNIQUAC model is explained. Moreover the equations and standard states that have been used in this work for model development have been illustrated. Finally equations that relate experimental data to model parameters were presented. This section provides a better understanding of how thermodynamic concepts are related to experimentally measured quantities.

Chapter 4

Thermodynamic Modeling of CO_2-Alkanolamine (MDEA/MEA/Blend)-H_2O Systems

4 Thermodynamic Modeling of CO_2-Alkanolamine (MDEA/MEA/Blend)-H_2O Systems

4.1 Chapter Overview

The objective of this chapter is to demonstrate the developed models that can describe both thermodynamic and calorimetric properties of the mixture of CO_2-alkanolamine -H_2O systems with emphasis on MDEA, MEA and blend of both as a solvent, over whole applicable range of temperature, pressure, acid gas loading and amine concentration. Chemical absorption of CO_2 with alkanolamines as solvent has been used in a large variety of industries over years. Natural gas treating, production of hydrogen and ammonia from synthesis gas and CO_2 capture from combustion gases are among the biggest industries that are utilized chemical absorption of $CO_2$with alkanolamines (Bishnoi 2000). Removal of acid gas from process gas with alkanolamines has been developed in 1930's and since then it became a dominant technology in gas treating industry (Bishnoi 2000). Aqueous solutions of MEA and MDEA are the most commonly used solvents for acid gas removal. The use of blend amines is also increasing, this helps to reduce operating costs and improve products quality (Kim et al. 2008). Design, operation, simulation and optimization of acid gas removal from natural gas process and CO_2 capture from combustion gas plants, require accurate estimation of phase and chemical equilibrium, as well as thermal properties of the system (Zhang and Chen 2011). Hence, a thermodynamic model that can predict the behavior of the system over the applicable conditions is a vital demand in industry. The goal of this chapter is to demonstrate the developed thermodynamic models for CO_2-MDEA-H_2O, CO_2-MEA-H_2O and CO_2-Blend of MDEA/MEA-H_2O systems that can accurately describe both thermodynamic and thermal properties in the whole applicable range of temperature, pressure, acid gas loading and amine concentration.

As described earlier, Extended UNIQUAC model has been chosen for modeling the systems. This model was already applied to similar systems (Faramarzi et al. 2009), however the reported results were not satisfactory especially at high amine concentrations, and the model was not able to estimate heat of reaction which has an important contribution in calculation of heat requirements in regenerator and it also showed unrealistic freezing point. For this reason, it is attempted to improve the performance of the model. This brought about a new version of the model parameters, two main improvements is, furthermore additional type of experimental data and new experimental sources have been used to refit model parameters in order to develop an improved model.

In these chapter thermodynamic models for CO_2-MDEA-H_2O, CO_2-MEA-H_2O and CO_2-MDEA-MEA-H_2O and modeling results are presented. Firstly, modeling of CO_2-MDEA-H_2O system and its sub systems are discussed, secondly modeling of CO_2-MEA-H_2O system and subsystems are expressed and finally modeling of CO_2-MDEA-MEA-H_2O is investigated.

4.2 Literature Survey on Previous Studies for CO_2-MDEA-MEA-Blend Systems

4.3 Improvements in the New Version of Model

Improvements made in this new version of the model can be summarized as:

- **Use Vapor-Liquid Equilibria (VLE) Data as Presented in the Article**

In the literature, VLE data are reported as CO_2 partial pressures; however the measured data are total pressures. In (Faramarzi et al. 2009) model like some previous studies in the literature, partial pressure data were converted to total pressure based on the assumption that water-alkanolamine system behaves ideally, i.e. vapor phase is considered as an ideal mixture of water and CO_2, therefore total pressure was assumed to be the sum of pure water vapor and CO_2 partial pressure. Even though, low vapor pressure of amine makes this assumption not so far from reality, still it may leads to inaccurate estimation of activity coefficients. This inaccurate estimation becomes more important when an error bar around total pressure is 10 % or higher. In such cases the amine vapor pressure contribution is completely hidden. Since amine vapor pressure is much lower than water, 90% or more of the total pressure is due to water and the rest will be amine and CO_2 contribution (Bishnoi 2000). In the new version of model VLE data are exactly used as they are presented in the literature.

- **Density Correlations for Converting Volumetric Data**

Many experimental data used for parameter estimation are presented in the volumetric concentration units. In order to convert them to weight concentration unit, density of aqueous amine solution is required. For a desirable temperature density of aqueous amine solution can be found in the literature or can be obtained from correlations. In the previous model, density of aqueous amine solution was assumed to be equal to pure water, which results in inaccurate data conversion from molarity to molality scale. In the new version of model a careful conversion was performed based on density correlations found for aqueous MDEA, aqueous MEA and aqueous MDEA-MEA at 25 °C. Correlated density equations are presented in chapter 3. It is worth to mention that density equations are correlated based on density data at 25 °C, at which most probably aqueous amine solutions are prepared in the laboratories.

- **New Type of Data**

In the new version of model heat of absorption data are also used for parameter regression. Including heat of absorption improves the temperature dependency estimation of the model. It is noted that in the absence of heat of reaction, good equilibrium data set should result in good model parameters with the capability of predicting heat of absorption.

4.4 Evaluation of Parameters

This section addresses the procedure that was used for fitting the parameters, criteria for choosing the right parameters to fit and the final values of parameters.

4.4.1 Fitting Procedure

Model parameters were regressed to the large number of literature data. Different kinds of data including pure amine vapor pressure, binary and ternary VLE (total and partial pressure), freezing point (SLE), heat capacity (C_p), excess enthalpy (H^E) and heat of absorption (H_{abs}) were first evaluated and then used to fit the model parameters. Chapter 3 discussed the benefit of using each kind of data in detail. There is no regression parameter in the SRK and Debye-Huckel terms and all the regressed parameters belong to the UNIQUAC model. An advantage of local composition models such as the UNIQUAC equation is that binary parameters of a multicomponent system and of its constituent binary systems are the same and no higher-order parameters are required (Austgen 1989). Thus, best values of binary parameters for the studied systems were determined by data regression using binary and ternary system data. CO_2-alkanolamine-water mixture is the

combination of alkanolamine-water, CO_2-water and alkanolamine-water subsystems. Binary parameters of CO_2-alkanolamine-water mixture are the same as its binary constituent solutions. Therefore, binary interaction parameters were regressed to binary data and interaction parameters that are associated in the ternary system were regressed to the ternary data. Parameters of alkanolamine-water system were regressed to alkanolamine-water data and parameters of CO_2-water system were taken from (Garcia et al. 2006). Despite the two other subsystems binary parameters of CO_2-alkanolamine system has been regressed to the ternary data and not the binary data. At the time of this work, no data was found for binary CO_2-alkanolamine system. Here the procedure that was used for parameter regression will be described. For optimization to be meaningful there must be an objective function that accounts for the deviation between calculated values by the model and the experimental data. The objective function is the function that the solvers try to minimize. In this work objective function is defined as follows which is the weighted sum of square of residuals (difference between calculated values by model and experimental ones). Model parameters (volume, surface, and energy interaction), heat capacity parameters and standard state values are estimated by minimizing the following objective function named S:

$$S = \sum_{VLEdata}\left[\frac{P_{calc}- P_{exp}}{w_1\,(P_{exp}+(0.01\ bar))}\right]^2 + \sum_{P^{vap}data}\left[\frac{P_{cal}^{vap}- P_{exp}^{vap}}{w_2\,P_{exp}^{vap}}\right]^2 + \sum_{H^E data}\left[\frac{H_{calc}^{E}- H_{exp}^{E}}{w_3\,Rx}\right]^2 +$$
$$\sum_{H^{Abs}data}\left[\frac{H_{calc}^{Abs}- H_{exp}^{Abs}}{w_4\,y}\right]^2 + \sum_{C_P data}\left[\frac{C_{P,calc}- C_{P,exp}}{w_5\,J.mol^{-1}.K^{-1}}\right]^2 + \sum_{C_P^{app}data}\left[\frac{C_{P,calc}^{app}- C_{P,exp}^{app}}{w_6\,J.mol^{-1}.K^{-1}}\right]^2 +$$
$$+\sum_{SLEdata}\left[\frac{\Delta G^0 + RT\sum_i v_i ln a_i}{w_7\,RT}\right]^2 \qquad (4.1)$$

"calc" and "exp" represent values calculated with the model and experimental data, respectively. w_1 to w_7 indicate the weight number used for each kind of data. Values of weight numbers are presented in Table 4-1. P is the solution total pressure (bar) or in most cases acid gas partial pressure , P^{Vap} is the alkanolamine pure vapor pressure, H^E is the molar excess enthalpy $(J.mol^{-1})$, H^{Abs} is the heat of absorption ($J.mol^{-1}$), C_P is the molar heat capacity of ternary mixture (CO_2-H_2O-alkanolamine), C_P^{app} is the apparent [16] molar heat capacity of binary solution (H_2O-

[16] For electrolytes it is common to use apparent molar properties. Apparent molar properties are only used for binary solutions. An apparent molar property ($M_\emptyset$) of the molar property M for the salt S in an aqueous solution is defined by: $M_\emptyset = \frac{nM - n_w M_w^0}{n_S}$, where n_w is the water mole numbers, n_S is salt mole numbers, n is the total mole numbers and M_w^0 is the molar property of pure water.

alkanolamine), ΔG^0 is the change in water molar standard chemical potential between solid and liquid phase, v_i is the stochiometry coefficient of component i, a_i is the activity of i, R is the gas constant, x = 1 K and y = 1 J are included to make the equation dimensionless. 0.01 bar is added to the denominator of the VLE data in order to not to give so much weight on the low pressure data.

Table 4-1 shows weighting factors that are used in estimating process for vapor-liquid equilibrium (total pressure and partial pressure), pure alkanolamine vapor pressure, excess enthalpy, heat of absorption, ternary mixture heat capacity data, apparent heat capacity (aqueous alkanolamine mixture) and freezing point data. Weighting factors were chosen based on the quality and reliability of different kind of data and also the experience achieved in the modeling. Choosing a correct number for the weights of different kinds of data helps the model to give satisfactory results for different properties. During the optimization process, different weights for the data were tested, based on the chosen weights different parameters had been obtained, with each set of parameters results have been calculated and finally the weights that gave the best calculated results are chosen as the final weights of the data.

Table 4-1. Weights for different kinds of data in the objective function

Data Type	Weight Number
VLE* (Amine**-H_2O and CO_2-Amine**-H_2O)	0.05 (bar)
Pure amine** vapor pressure	0.0075 (bar)
Heat of absorption (CO_2-Amine**-H_2O)	0.02 (J)
Ternary heat capacity (CO_2-Amine**-H_2O)	10 (Dimensionless)
Apparent heat capacity (MDEA-H_2O and MDEA-MEA-H_2O)	25 (Dimensionless)
Apparent heat capacity (MEA-H_2O)	55 (Dimensionless)
Freezing point (MDEA-H_2O)	0.05 (Dimensionless)
Freezing point (MEA-H_2O, CO_2-MEA-H_2O, MDEA-MEA-H_2O,)	0.01 (Dimensionless)
Excess enthalpy (Amine**- H_2O)	120 (K)

** Total pressure and partial pressure.*

*** Amine indicates MDEA, MEA, blends of MDEA and MEA*

Fitting this number of parameters, in total 16 for CO_2-MDEA-H_2O, 33 for CO_2-MEA-H_2O and 1 for CO_2-MDEA-MEA-H_2O to different kinds of data is not a trivial task. Lots of try and errors is required to obtain the best fitting procedure and the best number for data weights. Optimization is a challenging work; it needs a lot of effort before obtaining satisfactory set of parameters. After lots of effort and trying different optimization methods it is realized that the best approach for fitting these systems parameters can be classified into 2 stages. The First stage is to fit r and q parameters,

as well as interaction parameters involved in the binary system of amine-water to pure alkanolamine vapor pressure, binary VLE, Excess Enthalpy, freezing point and heat capacity data, while the rest of parameters are fixed at certain values. The aim of first stage is to make a strong model for binary alkanolamine-water system. Second stage is to fit interaction parameters which are involved in ternary system to ternary VLE, H_{abs} and C_p data, while other parameters are fixed in fitted values obtained in the First stage. Regression analysis has been performed using two different routines: a modified version of the Marquardt routine (Fletcher 1971) and a modified version of Nelder-Mead routine (StatLib).

4.4.2 Determination of Effective Interaction Parameters, Selection of Interaction Parameters for Fitting

In the Alkanolamine-CO_2-water system where alkanolamine is MDEA, there are 3 molecular and 5 ionic species present in the liquid phase, primary amines like MEA form stable carbonates, thus there is one more component present in the liquid solution of CO_2-MEA-water. In each of two cases a large number of binary parameters including molecule-molecule, molecule-ion pair, and ion pair-ion pair, can be specified for the system. Nevertheless, because the concentration of many of these species present in the liquid phase is very low or negligible, parameters associated with them do not significantly affect representation of system behavior. It is important to define the effective parameters, which modeling results are sensitive to them. Knowing the chemistry of the system and concentration calculations in an ideal solution helps to determine which parameters should be included in fitting process and which ones could be neglected. Species concentration in ideal solution provides estimation about species concentrations in the real mixture and chemistry of the system provides useful information about the possibility of coexistence of different species. This kind of information clarifies which parameters have influence on representation behavior of the system. Not all the interaction parameters between all pairs are fitted in the modeling process. Primary selection of effective interaction parameters was done based on two criteria's. The First criterion is the possibility of presence of pairs together in the system. The second one is the amount if species, if both pairs have a very low concentration in the system, their interaction parameter is not important and will not be considered in the modeling. But if the amount of one pair present in the solution is low but the other pair is in high amount, then the interaction between these pairs can have influence in the system behavior. Sensitivity analysis determines which interaction parameters affect modeling results. Notice that parameters have been determined for the species that according to the chemistry of the solution may exist in the solution. R and q parameters are determined for the

species that are present at considerable amount in the solution, and binary interaction parameters are considered for the pairs that most probably are simultaneously present in the mixture. The choice of effective parameters stem from experience with the model, sensitivity studies and from requirement for fitting the experimental data appropriately. Eventually, the following set of effective parameters was chosen to adjust to the experimental data. Notice that there are more effective parameters that were not determined in this work; values of these parameters were taken from other sources. Values of effective interaction parameters for the CO_2-MDEA-H_2O system were shown in

Table 4-3 and Table 4-4. CO_2-MEA-H_2O parameters were represented in

Table 4-9 and Table 4-10. Values of ineffective interaction parameters were assigned to $u^0 = 10^{10}$ and $u^T = 0$.

- **MDEA-H_2O System**
  - ✓ MDEA-H_2O
  - ✓ $MDEAH^+$-H_2O
  - ✓ MDEA-MDEA

- **CO_2-MDEA-H_2O System**
  - ✓ $MDEAH^+$-CO_2

- **MEA-H_2O System**
  - ✓ MEA-H_2O
  - ✓ $MEAH^+$-H_2O
  - ✓ MEA-MEA
  - ✓ MEA-$MEAH^{+'}$

- **CO_2-MEA-H_2O System**
  - ✓ $MEACOO^-$-H_2O
  - ✓ CO_2-MEA
  - ✓ CO_2-$MEAH^+$
  - ✓ MEA-HCO_3^-
  - ✓ $MEAH^+$-HCO_3^-

- **CO_2-MDEA-MEA-H_2O System**
  - ✓ MDEA-MEA

The above parameters were fitted to the experimental data, by using the fitting procedure illustrated in previous, values of adjusted parameters are presented in next section.

4.4.3 Fitted Parameters

The parameters required by the UNIQUAC equation for the CO_2-alkanolamine-H_2O system include volume parameter, r, surface parameter, q, for the species and the binary interaction parameters representing energies of interaction between liquid phase species. Note that for some species heat capacity parameters and standard state properties (G_f^0, H_f^0) were also adjusted.In what follow values of the adjusted parameters for CO_2-MDEA-H_2O and CO_2-MDEA-H_2O are presented. Model parameters were adjusted to the evaluated data base (regression data base will be discussed in section 0).

4.4.3.1 CO_2-MDEA-H_2O System

This section shows equations that were used to formulateCO_2-MDEA-H_2O System. Equilibrium in the system has been represented by including both physical and chemical equilibrium.

Physical Equilibrium

As it mentioned earlier, physical equilibrium should be included in equilibrium representation of the system. CO_2 dissolves in the water, and water and MDEA present in the liquid phase have the possibility of vaporization. Note that MDEA is shown as $R_2\acute{R}N$ where $R = CH_2 - CH_2 - OH$.Vapor-liquid equilibrium condition for these molecular species can be written as follows, notice that ionic species do not vaporize and only exist in the liquid phase:

$$CO_2(aq) \leftrightarrow CO_2(g) \quad (4.2)$$

$$H_2O\ (l) \leftrightarrow H_2O\ (g) \quad (4.3)$$

$$R_2\acute{R}N\ (aq) \leftrightarrow R_2\acute{R}N\ (g) \quad (4.4)$$

Chemical Equilibrium

The chemical reactions in the CO_2-MDEA-H_2O system are as follows:

Ionization of water: $$H_2O\ (l) \leftrightarrow OH^-(aq) + H^+(aq) \quad (4.5)$$

Dissociation of carbon dioxide: $CO_2(aq) + H_2O\ (l) \leftrightarrow HCO_3^-(aq) + H^+(aq)$ (4.6)

Dissociation of bicarbonate ion: $HCO_3^-(aq) \leftrightarrow CO_3^{2-}(aq) + H^+(aq)$ (4.7)

Protonation of alkanolamine: $R_2\acute{R}N\ (aq) + H^+(aq) \leftrightarrow R_2\acute{R}NH^+(aq)$ (4.8)

Table 4-2 to Table 4-7 contain parameters that have been used in this work for modeling equilibrium thermodynamic properties of CO_2-MDEA-H_2O system. These tables show all the parameters that have been used for modeling the system, some were fitted in this work and some are from literature. Table 4-2 shows volume parameter (r) and surface area parameter (q) for the components, values in bold were regressed in this work. For CO_2, r and q values are taken form (Garcia et al. 2006) and for H_2O, OH^-, H^+, HCO_3^- and CO_3^{2-} reported values by (Thomsen et al. 1996) are used.

Table 4-2. UNIQUAC volume parameter (r) and surface area parameter (q). Bold parameters are obtained in this work.

Species	R	q
MDEA	**0.13445**	**0.54315**
$MDEAH^+$	**2.3931**	**1.0749**
H_2O	0.9200[a]	1.4000[a]
OH^-	9.3973[a]	8.8171[a]
H^+	0.13779[a]	10^{-15}[a]
HCO_3^-	8.0756[c]	8.6806[c]
CO_3^{2-}	10.828[c]	10.769[c]
CO_2	0.75[b]	2.45[b]

[a] (Thomsen et al. 1996)

[b](Garcia et al. 2006)

[c](Thomsen and Rasmussen 1999)

c(Thomsen and Rasmussen 1999)

Table 4-4 list u_{ij}^0 and u_{ij}^T parameters (u_{ij}=u_{ji}) used for calculating UNIQUAC binary interaction energy parameters for the named pairs, respectively. As it mentioned earlier, UNIQUAC binary interaction parameters are calculated in this way $u_{ij} = u_{ij}^0 + u_{ij}^T (T - 298.15)$. Parameters that are shown in bold are determined in this work and the rest of parameters are taken from the original model (Thomsen et al. 1996) and (Garcia et al. 2006). It should be mentioned that corresponds to the original model (Thomsen et al. 1996) water-water and the like cation interaction energy

parameters have been fixed at zero (Thomsen et al. 1996). Set these parameters to zero, only has an influence on numerical value of parameters, it does not affect value of binary interactions; binary interactions are calculated from differences in interaction energy parameters (Thomsen et al. 1996). As in the original model hydrogen ion is treated as a reference point for thermal properties and single ion activities (Thomsen et al. 1996). Therefore all the parameters for the hydrogen ion are fixed at chosen values (Thomsen et al. 1996). Hydrogen ion parameters are chosen on the basis of making hydrogen ion activity coefficients and other properties at all concentrations and all temperatures mostly determined by the Debye-Huckel term (Thomsen et al. 1996). For the pairs that are less probable to coexist in the mixture u_{ij}^{0} and u_{ij}^{T} values has been set to a large value and zero, respectively. These values kept these parameters away from the regression process.

Table 4-3. $u_{ij}^0 = u_{ji}^0$ Parameters for calculating UNIQUAC interaction energy parameters. Values in bold are obtained in this work.

Species	H_2O	CO_2	MDEA	OH^-	H^+	HCO_3^-	CO_3^{2-}	$MDEAH^+$
H_2O	0[a]							
CO_2	8.83825[b]	40.51756[c]						
MDEA	**-561.6682**	**10^{10}**	**-1489.795**					
OH^-	600.4952[a]	10^{10}[b]	**10^{10}**	1562.881[a]				
H^+	10^{5}[a]	10^{10}[b]	**10^{10}**	10^{10}[a]	0[a]			
HCO_3^-	577.0502[c]	651.045 [c]	**10^{10}**	10^{10}[a]	10^{10} [a]	771.0377[c]		
CO_3^{2-}	361.3877[c]	10^{10}[c]	**10^{10}**	1588.025[c]	10^{10}[a]	800.0081[c]	1458.344[c]	
$MDEAH^+$	**-294.3952**	**-727.998**	**10^{10}**	**10^{10}**	**10^{10}**	**10^{10}**	**10^{10}**	**0**

[a] *(Thomsen et al. 1996)*

[b] *(Garcia et al. 2006)*

[c] *(Thomsen and Rasmussen 1999)*

Table 4-4. $u_{ij}^T = u_{ji}^T$ Parameters for calculating UNIQUAC interaction energy parameters. Values in bold are obtained in this work.

Species	H_2O	CO_2	MDEA	OH^-	H^+	HCO_3^-	CO_3^{2-}	$MDEAH^+$
H_2O	0[a]							
CO_2	0.86293 [b]	13.629[c]						
MDEA	**0.10616**	**0**	**-2.637**					
OH^-	8.5455[a]	0[b]	**0**	5.6169[a]				
H^+	0[a]	0[b]	**0**	0[a]	0[a]			
HCO_3^-	-0.38795 [c]	2.773[c]	**0**	0[a]	0[a]	-0.019813[c]		
CO_3^{2-}	3.3516 [c]	0[b]	**0**	2.7496[a]	0[a]	1.7241 [c]	-1.3448[c]	
$MDEAH^+$	**-0.0035922**	**-2.1465**	**0**	**0**	**0**	**0**	**0**	**0**

[a] *(Thomsen et al. 1996)*

[b] *(Garcia et al. 2006)*

[c] *(Thomsen and Rasmussen 1999)*

Above tables show values that have been used for standard state heat capacity of species present in the system, aqueous and vapor (gas) phase. As in the original work (Thomsen et al. 1996) a temperature dependent correlation $\left(C^0_{P,i} = a_i + b_i\ T + \frac{c_i}{T-200}\right)$ has been used for standard state heat capacity of species present in the aqueous phase. For most of the molecular (neutral) species that exist in aqueous phase, standard state heat capacity is almost constant in the broad temperature range; thus for all molecular (neutral) species, except water, b and c parameters of equation has been assigned to zero based on the assumption that heat capacity is independent of temperature. Unlike molecular species, for ionic species standard state heat capacity cannot be assumed temperature independent, therefore it is better to consider b and c parameters for ionic species. Whenever it is possible to determine coefficients b and c, standard state heat capacity of ionic species is considered temperature dependent, which helps improving model temperature dependency. Parameters a, b and c were either fitted to the experimental heat capacity data or were taken from data compilations (Garcia et al. 2005). Data compilations could also contain standard state heat capacity at 25 °C, in such cases a coefficient is set to the value from data compilation and b and c are fixed to zero (Garcia et al. 2005). Heat capacity parameters for H_2O, OH^-, H^+, HCO_3^- and CO_3^{2-} are values reported by (Thomsen, Rasmussen et al. 1996). (Thomsen, Rasmussen et al. 1996) estimated a, b and c parameters for water from the 5 parameter (DIPPR) correlation for the heat capacity of pure water, version 1983. (Thomsen, Rasmussen et al. 1996) fitted a, b and c parameters for OH^-, HCO_3^- and CO_3^{2-} to the experimental data and set all parameters for H^+ to zero as H^+ is a reference point. Parameters for CO_2 (aq) are taken from (Garcia, Thomsen et al. 2006), these values had been taken values from (NIST) tables.

Table 4-5 represents values of heat capacity parameters (a, b and c) that has been used for calculation of standard state heat capacity of species i (C^0_{pi}) present in the aqueous phase from the mentioned correlation which yields C^0_{pi} in $J.mol^{-1}.K^{-1}$. The "a" parameter given for MDEA is the C^0_p (at T = 25 °C) presented by (Hawrylak et al. 2006). The "a" parameter for $MDEAH^+$ standard state heat capacity has been calculated from the difference between standard state heat capacity value of $MDEAH^+Cl^-$ measured by (Hawrylak et al. 2000) and Cl^- standard state heat capacity value presented by (Thomsen et al. 1996). From equation (4.11) standard state heat capacity of $MDEAH^+$ was obtained. b and c parameters for $MDEAH^+$ were assigned to zero.

$$C^0_{p,MDEAH^+\ Cl^-}(T = 25\ ^\circ C) = 194.31\ J\ mol^{-1}K^{-1} \qquad (4.9)$$

$$C^0_{p,Cl^-}(T = 25\ ℃) = -126.16\ \text{J mol}^{-1}\text{K}^{-1}(a = 400.35, b = -1.1312, c = -18574) \quad (4.10)$$

$$C^0_{p,MDEAH^+}\ (T = 25\ ℃) = C^0_{p,MDEAH^+\ Cl^-}(T = 25\ ℃) - C^0_{p,Cl^-}(T = 25\ ℃) = 321.1582 \text{J mol}^{-1}\text{K}^{-1} \quad (4.11)$$

Heat capacity parameters for H_2O, OH^-, H^+, HCO_3^- and CO_3^{2-} are values reported by (Thomsen et al. 1996). (Thomsen et al. 1996) estimated a, b and c parameters for water from the 5 parameter (DIPPR) correlation for the heat capacity of pure water, version 1983. (Thomsen et al. 1996) fitted a, b and c parameters for OH^-, HCO_3^- and CO_3^{2-} to the experimental data and set all parameters for H^+ to zero as H^+ is a reference point. Parameters for CO_2 (aq) are taken from (Garcia et al. 2006), these values had been taken values from (NIST) tables.

Table 4-5. Standard state heat capacity parameters for species in aqueous phase, C^0_{pi} (J mol^{-1}K^{-1}). Values in bold are obtained in this study.

Species	a (J mol^{-1} K^{-1})	b (J mol^{-1} K^{-2})	c (J mol^{-1})
MDEA (aq)	385[a]	0[a]	0[a]
$MDEAH^+$(aq)	**321.1582**	**0**	**0**
H_2O (l)	58.36952[b]	0.0389611[b]	523.8794[b]
OH^-(aq)	1418.157[b]	-3.445769[b]	-51473.13[b]
H^+(aq)	0[b]	0[b]	0[b]
HCO_3^-(aq)	-0.6770971[c]	0.2737451[c]	-10089.51[c]
CO_3^{2-}(aq)	894.6877[c]	-2.827237[c]	-21149.44[c]
CO_2(aq)	243[d]	0[d]	0[d]

[a] *(Hawrylak et al. 2000)*

[b] *(Thomsen et al. 1996)*

[c] *(Thomsen and Rasmussen 1999)*

[d] *(Garcia et al. 2006)*

For molecular species present in the gas (vapor) phase standard state heat capacities are taken from DIPPR data base (DIPPR). It is assumed that standard state heat capacity of molecular species in the gas phase is temperature independent and is constant over the wide range of temperature.

Table 4-6. Standard state heat capacities of species in the gas phase C_{pi}^0 (J mol^{-1}K^{-1})

Species	a (J mol^{-1} K^{-1})
MDEA (g)	100[b]
H_2O (g)	33.577[b]
CO_2 (g)	37.11[b]

[b] *(DIPPR)*

Table 4-7 includes standard state Gibbs free energy of formation (G_f^0) and standard state enthalpy of formation (H_f^0). Most of the values, were taken from NIST (NIST) tables and DIIPPR (DIPPR), standard state thermodynamic properties that could not found in NIST and DIPPR data bases, were fitted to experimental data. Notice that in NIST and DIPPR data bases, mainly standard state Gibbs free energy of formation (standard state chemical potential) are available at 25 °C. At temperatures other than 25 °C, standard state Gibbs free energy of formation has been calculated from the integration of Gibbs-Helmholtz equation using heat capacity and enthalpy data.

Table 4-7. Standard state properties G_f^0 and H_f^0 in (kJ mol^{-1}) at T = 25 °C. Values in bold are obtained in this study.

Species	G_f^0(kJ mol^{-1})	H_f^0(kJ mol^{-1})
MDEA (aq)	**-214.8709**	**-491.5275**
MDEA (g)	-169[a]	-380[a]
$MDEAH^+$ (aq)	**-264.1016**	**-528.4562**
H_2O (l)	-237.129[b]	-285.83[b]
H_2O (g)	-228.572[b]	-241.818[b]
OH^-(aq)	-157.2481[b]	-230.2433[b]
H^+(aq)	0	0
HCO_3^-(aq)	-586.77[b]	-691.99[b]
CO_3^{2-}(aq)	-527.81[b]	-677.14[b]
CO_2 (aq)	-385.98[b]	-413.8[b]
CO_2 (g)	-394.359[b]	-393.509[b]

[a] *(DIPPR)*

[b] *(NIST)*

4.4.3.2 CO_2-MEA-H_2O System

Similar to MDEA system, equilibrium in the system has been represented by including both physical and chemical equilibrium.

Physical Equilibrium

Vapor-liquid equilibrium condition for the molecular species is the same as MDEA system, equations (4.2) and (4.3) occur in the vapor phase and equation (4.4) is replaced by (4.12). Notice that MEA is shown as RNH_2 where $R = CH_2 - CH_2 - OH$

$$RNH_2(aq) \leftrightarrow RNH_2\ (g) \tag{4.12}$$

Chemical Equilibrium

The principle reactions in the MEA-CO_2-H_2O system is like the reactions for MDEA-CO_2-H_2O system, on more reaction is in addition to the reactions in the MDEA system. Because MEA is a primary amine, it reacts with bicarbonate and forms MEA carbonate:

$$HCO_3^-(aq) + RNH_2(aq) \leftrightarrow RNHCOO^-(aq) + H_2O\ (l) \tag{4.13}$$

The mentioned reactions are generally taken into account for detailed modeling of mentioned systems. Although further reactions may happen, the amounts of these further side components are very small and could be neglected. For example MEA is able to form a very small amount of a component called 2-oxazolidone, nevertheless formation reaction of oxazolidone is neglected in this study (Boettinger et al. 2008).

Table 4-8 to Table 4-13 list parameters used for modeling equilibrium thermodynamic properties of CO_2-MEA-H_2O system. Parameters that are shown in bold were determined in this work. Some parameters are obtained in this work and some are taken from literature. Table 4-8,

Table 4-9 and Table 4-10 show UNIQUAC parameters; Table 4-11, Table 4-12 and Table 4-13 present values of the standard thermodynamic properties: Heat capacity, Gibbs free energy of formation and enthalpy of formation. Table 4-8 shows volume parameter (r) and surface area parameter (q) for the present components. Parameters that are in bold were regressed in this work.

Table 4-8. UNIQUAC volume parameter (r) and surface area parameter (q). Bold parameters are determined in this work.

Species	r	q
MEA	**3.0646**	**3.5394**
$MEAH^+$	**0.70865**	**1.3546**
$MEACOO^-$	**3.0005**	**2.1871**
H_2O	Table 4.2	Table 4.2
OH^-	Table 4.2	Table 4.2
H^+	Table 4.2	Table 4.2
HCO_3^-.	Table 4.2	Table 4.2
CO_3^{2-}	Table 4.2	Table 4.2
CO_2	Table 4.2	Table 4.2

Table 4-9 and Table 4-10 present u_{ij}^0 and u_{ij}^T parameters used for calculating UNIQUAC binary interaction energy parameters ($u_{ij}=u_{ji}$). Parameters in bold were regressed in this work and the rest were taken from (Thomsen et al. 1996) and (Garcia et al. 2006). The same approach as MDEA system has been used for the pairs that are not present together in the mixture, u_{ij}^0 and u_{ij}^T values were assigned to a large value and zero, respectively. Therefore these pairs were being kept away from the regression process.

Table 4-9. $u_{ij}^0 = u_{ji}^0$ Parameters for calculating UNIQUAC interaction energy parameters. Values in bold are obtained in this work.

Species	H_2O	CO_2	MEA	OH^-	H^+	HCO_3^-	CO_3^{2-}	$MEAH^+$	$MEACOO^-$
H_2O	Table 4.3								
CO_2	Table 4.3	Table 4.3							
MEA	**188.3175**	**-3.224619**	**427.4998**						
OH^-	Table 4.3	Table 4.3	**10^{10}**	Table 4.3					
H^+	Table 4.3	Table 4.3	**10^{10}**	Table 4.3	Table 4.3				
HCO_3^-	Table 4.3	Table 4.3	**450.9179**	Table 4.3	Table 4.3	Table 4.3			
CO_3^{2-}	Table 4.3	Table 4.3	**10^{10}**	Table 4.3	Table 4.3	Table 4.3	Table 4.3		
$MEAH^+$	**159.3751**	**-199.0248**	**41.14279**	**10^{10}**	**10^{10}**	**454.2007**	**10^{10}**	**0**	
$MEACOO^-$	**114.6021**	**10^{10}**	**10^{10}**	**10^{10}**	**10^{10}**	**10^{10}**	**10^{10}**	**10^{10}**	**10^{10}**

Table 4-10. $u_{ij}^T = u_{ji}^T$ Parameters for calculating UNIQUAC interaction energy parameters. Values in bold are determined in this work.

Species	H_2O	CO_2	MEA	OH^-	H^+	HCO_3^-	CO_3^{2-}	$MEAH^+$	$MEACOO^-$
H_2O	Table 4.4								
CO_2	Table 4.4	Table 4.4							
MEA	**1.6182**	**0.024785**	**2.1171**						
OH^-	Table 4.4	Table 4.4	**0**	Table 4.4					
H^+	Table 4.4	Table 4.4	**0**	Table 4.4	Table 4.4				
HCO_3^-	Table 4.4	Table 4.4	**0**	Table 4.4	Table 4.4	Table 4.4			
CO_3^{2-}	Table 4.4	Table 4.4	**0**	Table 4.4	Table 4.4	Table 4.4	Table 4.4		
$MEAH^+$	**-2.9268**	**-2.8132**	**0.61711**	**0**	**0**	**3.9493**	**0**	**0**	
$MEACOO^-$	**12.551**	**0**	**0**	**0**	**0**	**0**	**0**	**0**	**0**

Table 4-11 and Table 4-12 present the standard state heat capacity parameters for species present in the system, aqueous and vapor (gas) phase, respectively. To avoid adding more regressed parameters for MEA, $MEAH^+$ and $MEACOO^-$ only a parameter has been regressed and b and c parameters were assigned to zero. Fitting b parameter for the mentioned ions has also been tried, but it was revealed that adding this parameter did not improve calculation results therefore it has been decided to consider the heat capacity of MEA, $MEAH^+$ and $MEACOO^-$ temperature independent.

Table 4-11. Standard state heat capacity parameters for species in aqueous phase, C_{pi}^0 ($J\ mol^{-1}K^{-1}$). Values in Bold are obtained in this work.

Species	a ($J\ mol^{-1}K^{-1}$)	b ($J\ mol^{-1}K^{-2}$)	c ($J\ mol^{-1}$)
MEA (aq)	**167.6706**	**0**	**0**
$MEAH^+$(aq)	**71.4637**	**0**	**0**
$MEACOO^-$(aq)	**-98.32253**	**0**	**0**
H_2O (l)	Table 4.5	Table 4.5	Table 4.5
OH^-(aq)	Table 4.5	Table 4.5	Table 4.5
H^+(aq)	Table 4.5	Table 4.5	Table 4.5
HCO_3^-(aq)	Table 4.5	Table 4.5	Table 4.5
CO_3^{2-}(aq)	Table 4.5[c]	Table 4.5	Table 4.5
CO_2 (aq)	Table 4.5	Table 4.5	Table 4.5

For molecular species present in the gas (vapor) phase standard state heat capacities were taken from DIPPR data base (DIPPR).

Table 4-12. Standard state heat capacities of species in the gas phase C_{pi}^0 ($J\ mol^{-1}K^{-1}$)

Species	a ($J\ mol^{-1}\ K^{-1}$)
MEA (g)	85.75[b]
H_2O (g)	Table 4.6
CO_2 (g)	Table 4.6

[b] *(DIPPR)*

Table 4-13 shows standard state Gibbs free energy of formation (G_f^0) and standard state enthalpy of formation (H_f^0).

Table 4-13. Standard state properties G_f^0 and H_f^0 in (kJ mol^{-1}) at T = 25 °C. Values in bold are obtained in this work.

Species	G_f^0(kJ.mol^{-1})	H_f^0(kJ.m, mol^{-1})
MEA (aq)	**-135.3839**	**-274.496**
MEA (g)	-103.3[a]	-206.7[a]
$MEAH^+$ (aq)	**-190.9479**	**-312.9762**
$MEACOO^-$(aq)	**-493.0246**	**-705.3813**
H_2O (l)	Table 4.7	Table 4.7
H_2O (g)	Table 4.7	Table 4.7
OH^- (aq)	Table 4.7	Table 4.7
H^+ (aq)	Table 4.7	Table 4.7
HCO_3^-(aq)	Table 4.7	Table 4.7
CO_3^{2-}(aq)	Table 4.7	Table 4.7
CO_2 (aq)	Table 4.7	Table 4.7
CO_2 (g)	Table 4.7	Table 4.7

[a] *(DIPPR)*

4.4.3.3 CO_2-MDEA-MEA-H_2O System

For modeling behavior of aqueous mixture of CO_2 and blend of MEA and MDEA, all the parameters has been kept at the values determined for the ternary systems and only the binary interaction parameter between MEA and MDEA has been fitted to the data of blend amines. Below table reports values required to calculate binary interaction parameters between MDEA and MEA.

Table 4-14. $u_{ij}^0 = u_{ij}^0$ and $u_{ij}^T = u_{ij}^T$ Parameters for calculating UNIQUAC energy interaction parameters. Values in Bold are obtained in this work.

Interaction parameter	$u_{ij}^0 = u_{ij}^0$	$u_{ij}^T = u_{ij}^T$
MDEA-MEA	**663.1154**	**2.6033**

4.5 Equilibrium Constant for MDEA

In this work the equilibrium constant for the MDEA protonation reaction is fitted to the experimental data. Recall from previous sections, in this study standard state Gibbs energy of formation and standard state enthalpy of formation for MDEA and $MDEAH^+$ are regressed to the experimental data and for other components the values are taken from NITS tables. Therefore it is of high importance to check the fitted equilibrium constant against the available experimental equilibrium constants. Notice that equilibrium constant affects the calculation results especially at law loading region, because at low concentrations, the situation is close to ideal solution and activity coefficients are close to unity, therefore the role of Extended UNIQUAC is less noticeable;

at low loading region equilibrium calculations are mainly based on equilibrium constants. The role of Extended UNIQUAC is more pronounced at higher concentration where the condition is far from reality and activities need to take into account. The equilibrium constant obtained for MDEA protonation reaction at 25 °C, standard state Gibbs energies of formation and standard state enthalpies of formation for MDEA and $MDEAH^+$ are compared with the experimental data obtained by (Kamps and Maurer 1996). Table 4-15 summarizes the regressed values in this study with the measured data from (Kamps and Maurer 1996). As it can be seen there is a good agreement with the regressed values of this study and the measured data from (Kamps and Maurer 1996).

Table 4-15. Comparison between values obtained in this study with literature data

Reference	(Kamps and Maurer 1996)	**This Study**
ΔG_f (kJ/mole)	48.81	49.2
ΔH_f (kJ/mole)	34	36.9
K (equilibrium Constant)	2.81E-9	2.37E-9

4.6 Regression Data Base and Results

In this work pure, binary and ternary VLE, SLE, heat capacity, excess enthalpy and heat of absorption data were used for regression model parameters. In order to create a data base which covers extensive pressure, temperature, amine concentration and acid gas loading range, it is attempted to collect almost all the available data in the open literature. Although there are a high number of data, especially VLE, available in the open literature, only some of them are qualified and consistent, many show discrepancies. Therefore in order to obtain a good fit, it is crucial to create a reliable and consistent data base for parameter regression. There are many ways to distinguish between consistent and inconsistent data. In this work three different ways were tried to analyze consistency of data:

- *Literature study*: a literature survey on the data source citations often provide good information about reliability of the data source.
- *Comparing different data sources*: Comparing data from different publications at the same conditions is a way to test quality of the data. In case of disagreement with other sources or a difference in trend line, the data were discarded from regression data base.
- *Analyze the data by itself:* Details of experimental procedure, uncertainty value reported for the data can be used for determining the quality of data.

Not all the data were used for parameter estimation. Consistent and accurate data were chosen to for parameter regression. Data that are either inconsistent with other sources or including them in the parameter regression affect other sources results, were discarded from regression data base. Data sources used for parameter regression with model deviations are tabulated in tables. Average absolute relative deviation (AARD) is calculated from the following formula:

$$AARD = 100\left(\frac{\sum_{i=1}^{N}\frac{\left(\left|Z_{i,exp}-Z_{i,calc}\right|\right)}{Z_{i,exp}}}{N}\right) \quad (4.14)$$

N is the total number of data, $Z_{i,exp}$ is the experimental value and $Z_{i,calc}$ is the calculated value with the model.

As mentioned by (Thomsen and Rasmussen 1999) typical accuracy for vapor pressure measurements using modern equipment is up to $\pm 5\%$ (RUMPF et al. 1994). The usual accuracy of partial pressure measurements is about 5-10 % (Goppert and Maurer 1988) and can increase to 15 % in some conditions. According to Rochellle (Rochelle 1991)acid gas solubility in MDEA data have an average error of around 10 % (Chang et al. 1993). Hence it is expected that the model calculates vapor pressure and partial pressure data within acceptable accuracy (less than 10%). In the following sections the data used for the parameter estimation are discussed and compared with the modeling results.

4.7 MDEA System

The parameters required for CO_2-MDEA-H_2O system were fitted based on totally 1408 data points. Different kinds of data of pure, binary mixture of water and amine and CO_2 loaded mixture have been used for regression model parameters. In what follows, different types of data that have been used for regression model parameters and the regression results are given.

4.7.1 Pure MDEA Vapor Pressure Data and Regression Results

Pure MDEA vapor pressure has been used for model parameters regression. An overview over the experimental pure MDEA vapor pressure used for parameter estimation and the modeling results is given in Table 4-16. Totally 13 pure vapor pressure data points were used for model parameters estimation. Vapor pressure of pure components is very important for calculation of activity coefficients (Kim et al. 2008). As mentioned in chapter 3, this kind of data helps to get better estimation for infinite dilution activity coefficient. Pure MDEA vapor pressure data could improve

estimation of MDEA r and q parameters, and MDEA-MDEA and MDEA-water interaction parameters.

Table 4-16. Regression results for MDEA vapor pressure

Temperature , °C	Reference Number	Number of Data Points	AARD %
147.3-194.7	(VonNiederhausern et al. 2006b)	7	3.53
136.54-157.33	(Kim et al. 2008)	6	8.89

Figure 4-1 shows model regression results for vapor pressure of pure MDEA. The model represents vapor pressure of pure MDEA with an average absolute relative devaiaton of 8.89 %.

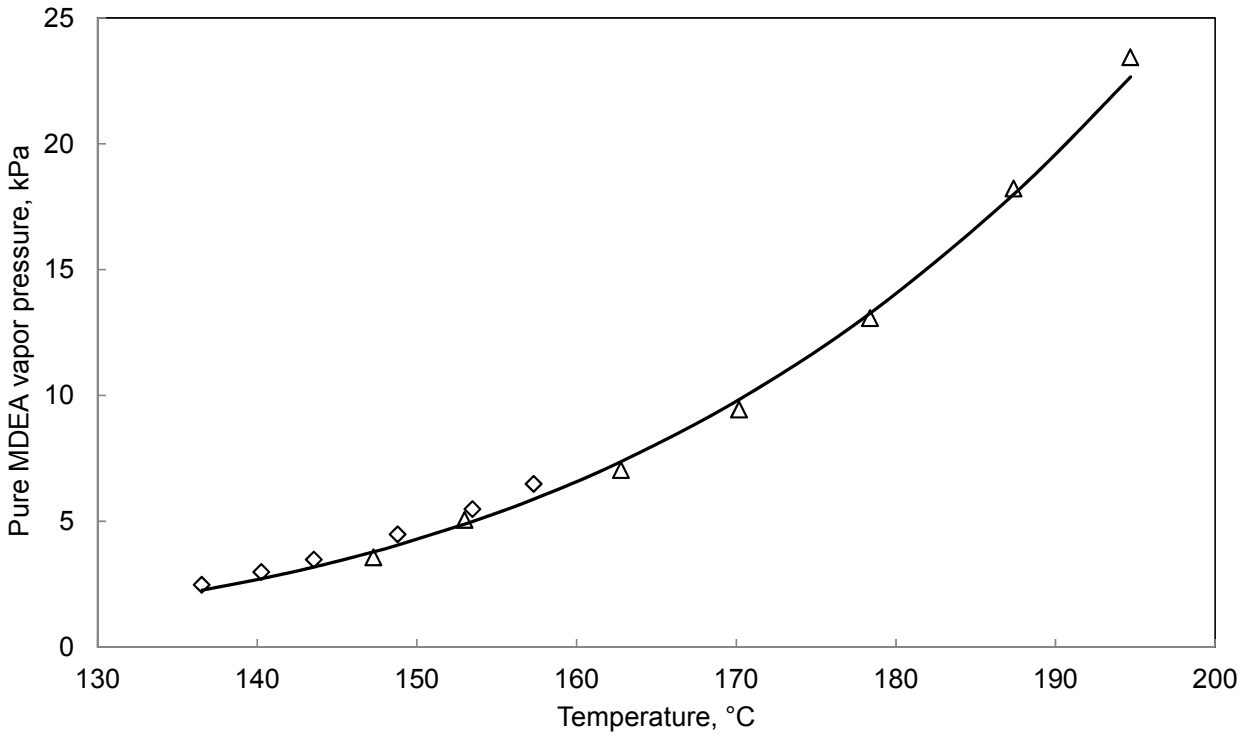

Figure 4-1. Vapor pressure of pure MDEA. Symbols stand for the experimental data and curve (line) refer to the calculated values using the developed thermodynamic model. □**,** (Kim et al. 2008)**;** Δ**,** (VonNiederhausern et al. 2006a)

Data from (VonNiederhausern et al. 2006a) at temperatures higher than 200 °C were discarded from regression data base, because data for CO_2-MDEA-H_2O systems were only available up to 140°C

and it was therefore not relevant to model the pure component vapor pressure to higher temperatures.

4.7.2 Binary MDEA-H_2O Data and Regression Results

As the loading in CO_2-MDEA-H_2O system approaches zero, a binary mixture of amine and water forms. Binary MDEA-H_2O data are good to determine the MDEA activity coefficient which helps to calculate MDEA lost in absorber column (Posey 1997) and it also helps to have better estimation of MDEA infinite dilution activity coefficient (Kim et al. 2008; Posey 1997). As mentioned in section 4.4.1, interaction parameters of MDEA-water system were established prior to treat the loaded solution. This section will discuss the modeling results of the created model for binary MDEA-Water system.551 binary MDEA-H_2O data points including total pressure, freezing point (SLE), H^E and heat capacity have been used to determine model parameters. (Posey 1997) showed that including total pressure, freezing point, Enthalpy of mixing (H^E) and VLE (partial pressure) data result in best set of parameters for NRTL model and best results consequently. Since UNIQUAC and NRTL are both G^E models, it is concluded that including different kind of data will improve modeling results.

Table 4-17 lists the data sets upon which the parameters were regressed. In what follows modeling results for different kind of data are given.

Table 4-17. Review over binary MDEA-H_2O data used for model parameter regression and modeling results

	T ,°C	P, kPa	Data Type	Reference	Number of Data Points	AARD %
17.5 to 98.92	25, 40	Na*	H^E	(Maham et al. 1997)	26	16
16.25 to 65.94	65	Na*	H^E	(Maham et al. 2000)	9	41
9.58 to 94.91	25, 69.3	Na*	H^E	(Posey 1997)	19	14
25.68 to 46.85	25,40,75	2.7 to 5.47 (P_{Total})	VLE	(Sidi-Boumedine et al. 2004)	5	5.22
77.05 to 185.55	3.66 to 98.92	40,53.3,66.7(P_{Total})	VLE	(Voutsas et al. 2004)	27	10
3 to 78.61	40 to 100	7.27 to 100 (P_{Total})	VLE	(Kim et al. 2008)	57	0.76
9.98, 19.99, 29.98, 49.92, 70.02	53.1 to 108.05	13.08 to 101.67 (P_{Total})	VLE	(Xu et al. 1991)	34	2.69
18.84, 32.11	120,140	186.2 to 346.4 (P_{Total})	VLE	(Kuranov et al. 1996)	4	0.72
23 , 50	25, 50, 75	Na*	C_P	(Hayden et al. 1983)	6	3.58
62.3, 81.51,90.84,96.35	30 to 80	Na*	C_P	(Chen et al. 2001)	44	4.78
16.82 to 99.01	5 to 95	Na*	C_P	(Zhang et al. 2002)	228	2.38
23 to 50	30 to 80	Na*	C_P	(Chiu and Li 1999)	22	1.43
1.41 to 20.47	10 to 55	100 (P_{Total})	Apparent C_P	(Hawrylak et al. 2006)	37	3.65
29.99, 40, 49.99, 59.99	25	Na*	C_P	(Weiland et al. 1997)	4	1.86
18.18 to 35.26	-4 to -12	101.3 (P_{Total})	Freezing point	(Song et al. 2006)	13	11
5.17 to 39.65	-1 to -15	101.3 (P_{Total})	Freezing point	(Fosbol et al. 2011)	6	5.89
17.40 to 39.15	-4 to -14	101.3 (P_{Total})	Freezing point	(Chang et al. 1993)	10	10

**Not available*

4.7.2.1 Total pressure data

Recall from chapter 3, total pressure vapor data do not allow for the direct calculation of individual activity coefficients. However the accuracy of activity coefficients derived from total pressure measurements are comparable with the ones determined from partial pressure data (BARKER 1953). For low volatile species like MDEA, partial pressure measurements are difficult to handle and usually uncertain; however total pressure measurement are easier to do and more accurate than partial pressure measurements for mixture of MDEA and water. Therefore, like (Hessen et al. 2010), for binary mixture of water and MDEA, model parameters have been regressed to total pressure data and not partial pressure (Barker method (BARKER 1953)). Total pressure data of (Sidi-Boumedine et al. 2004), (Voutsas et al. 2004), (Kim et al. 2008) and (Xu et al. 1991) have been used for parameter regression. Figure 4-2 shows that total pressure data for binary system fit quiet well.

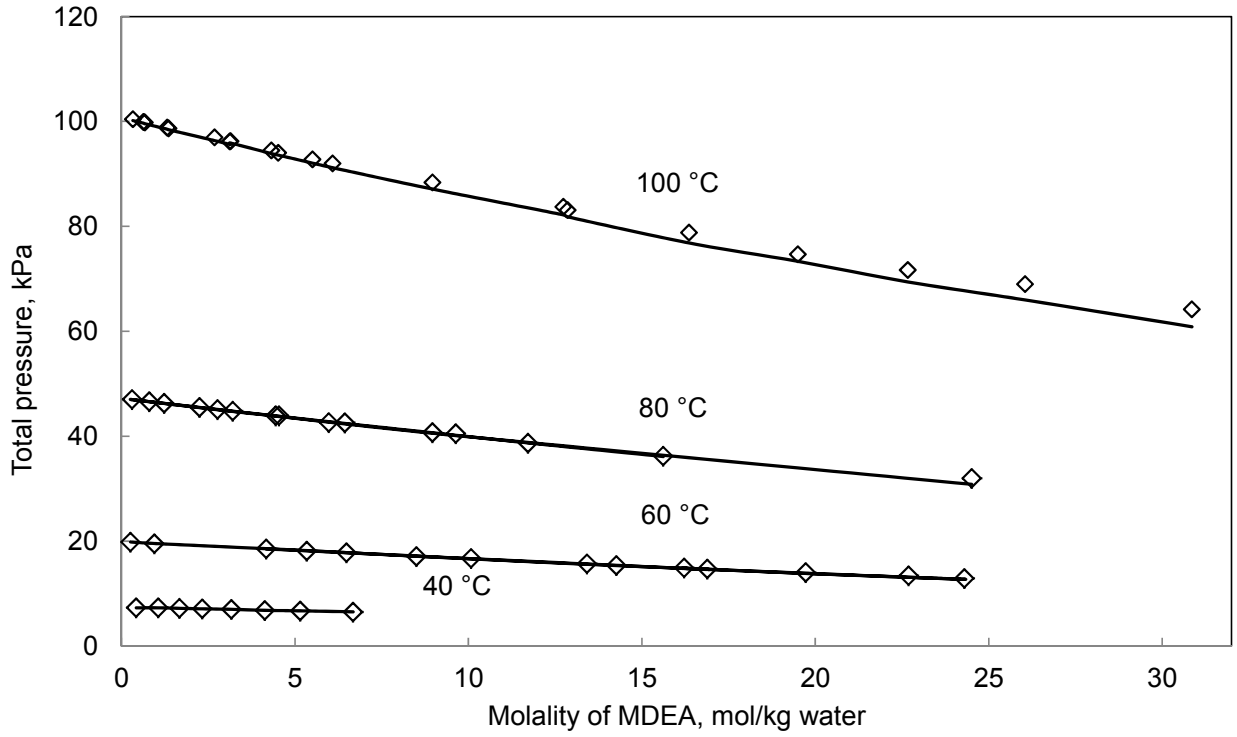

Figure 4-2. Total vapor pressure of MDEA-H_2O solutions. Symbols stand for the experimental data and curves (lines) refer to the calculated values using the developed thermodynamic model. □, (Kim et al. 2008)

Figure 4-3 is a parity plot which represents model calculated results against experimental data at various conditions; the curve has the slope of 0.98 which confirms model capability for well

representing total pressure of MDEA-water subsystem. Overall, model reproduce total pressure of MDEA-water mixture within 3.87 AARD %.

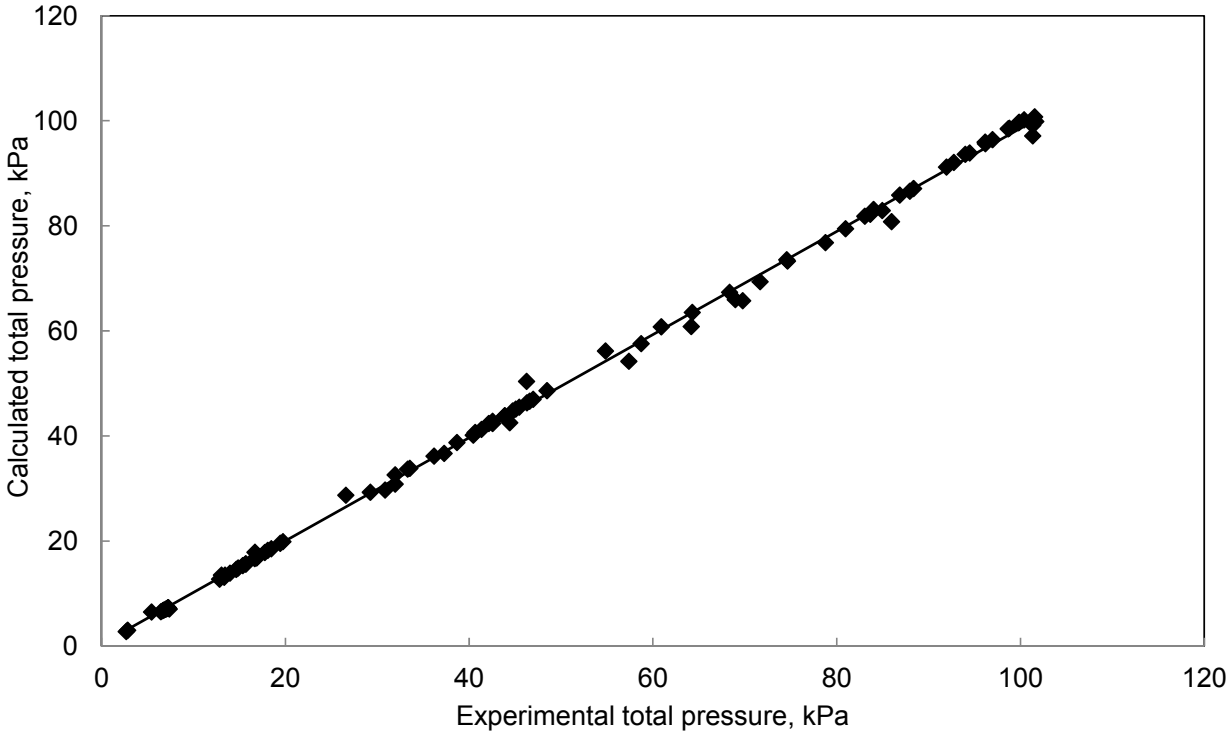

Figure 4-3. Parity plot for binary MDEA-H_2O system.■, Experimental data points

4.7.2.2 Excess Enthalpy Data

Excess enthalpy data is directly related to temperature dependence of excess Gibbs energy. Thus using excess enthalpy data for regressing parameters of a G^E model will provide a more accurate temperature dependence of excess Gibbs energy. Data of (Maham et al. 1997), (Maham et al. 2000) and (Posey 1997) have been used for adjusting model parameters. Figure 4-4 displays the excess enthalpy data for mixtures of MDEA and water at 25 °C. As it can be seen excess enthalpy data are not fit well due to the influence of other data types used in the regression. Altogether, model fit excess enthalpy data within 23 AARD %.

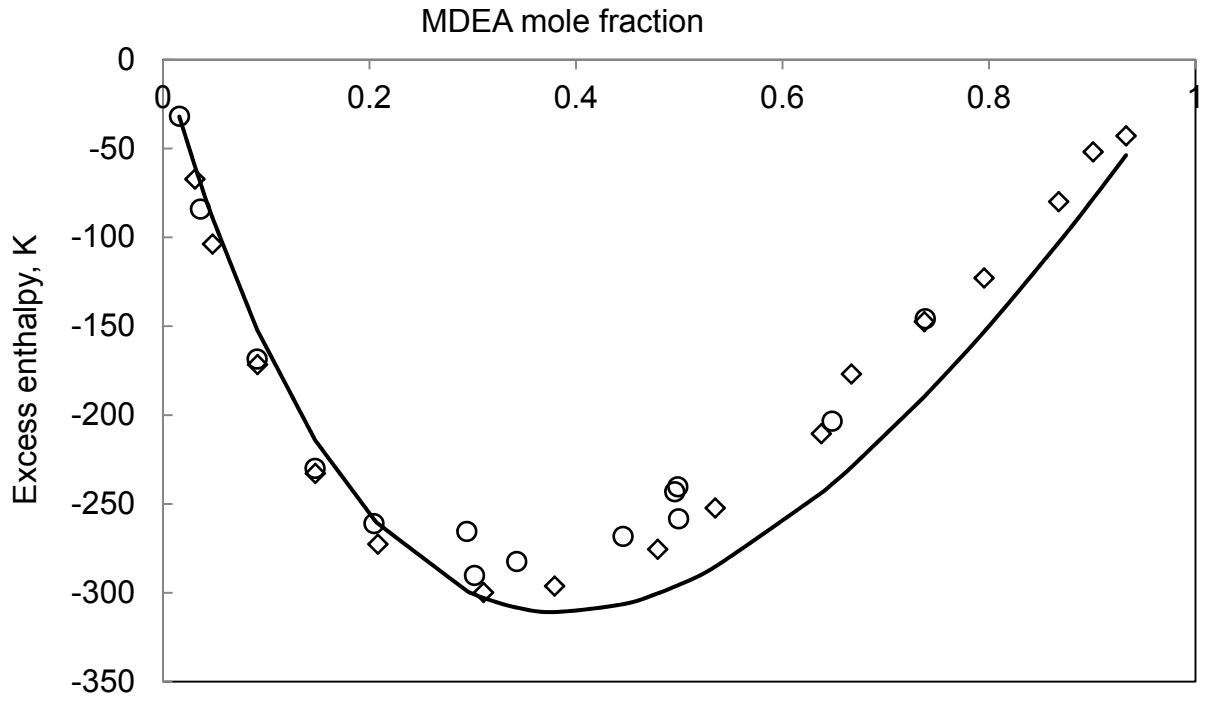

Figure 4-4. Excess enthalpy of MDEA-H_2O solutions. Symbols stand for the experimental data and curves (lines) refers to the calculated values using the developed thermodynamic model.◊, (Maham et al. 1997)**;** ○**,** (Posey 1997)

4.7.2.3 Heat Capacity Data

The liquid phase heat capacity of a mixture is obtained by taking the derivative of the liquid enthalpy at constant pressure. Mixture heat capacity data as a function of temperature and concentration has been used to adjust water and MDEA activity coefficients through the simultaneous regression of the binary interaction parameters. Data of (Hayden et al. 1983), (Chen et al. 2001), (Zhang et al. 2002), (Chiu and Li 1999), (Weiland et al. 1997) and (Hawrylak et al. 2006) have been used for adjusting model parameters. Figure 4-5 plots heat capacity of binary MDEA-water mixture calculated by the model together with the experimental data from (Zhang et al. 2002), results at selected temperatures; 5, 50 and 95 °C, are shown in the Figure 4-5.

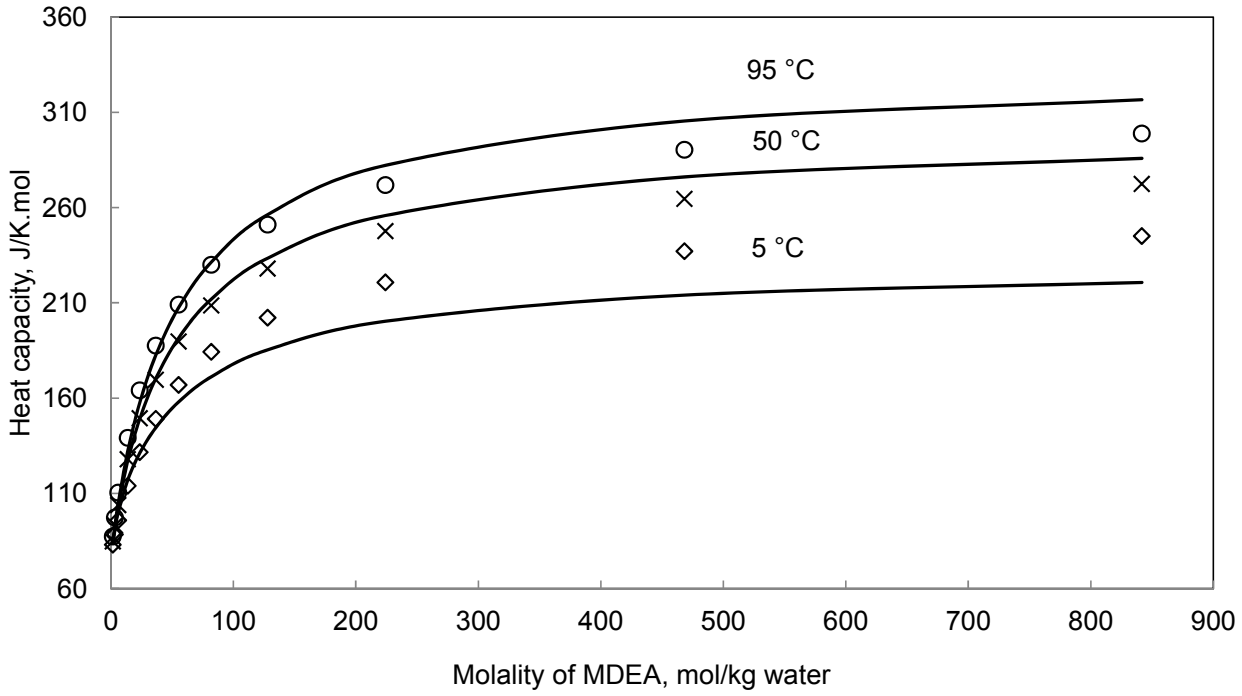

Figure 4-5. Heat capacity of MDEA-H_2O solutions at 5 °C, 50 °C and 95 °C. Symbols stand for the experimental data and curves (lines) refer to the calculated values using the developed thermodynamic model.◊, 5 °C (Zhang et al. 2002)**; ×, 50 °C** (Zhang et al. 2002)**; ○, 95 °C** (Zhang et al. 2002)

Heat capacity data available in literature for MDEA-water mixture often show some discrepancies s. Figure 4-6 compares data from (Chiu and Li 1999) and (Hayden et al. 1983) for 22.99 and 49.99 wt % MDEA, as it can be seen from the figure data from (Chiu and Li 1999) are between 2 to 3.5 % higher than data from (Hayden et al. 1983).

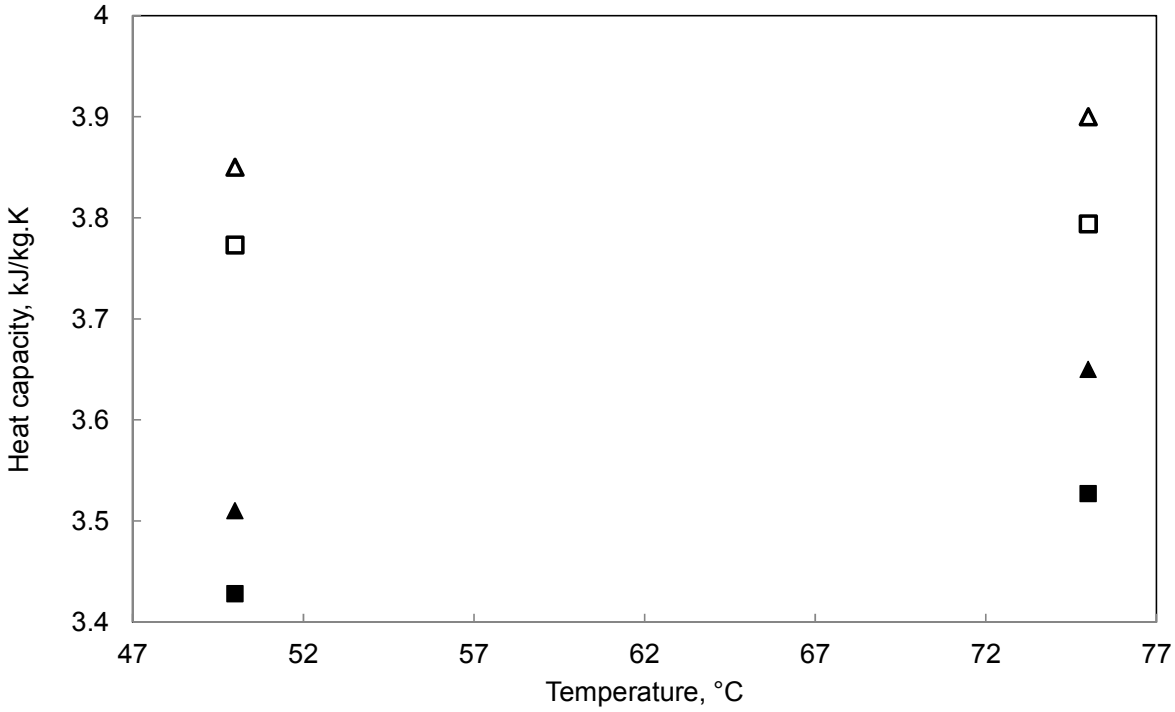

Figure 4-6. Comparison between experimental heat capacity data for MDEA-H_2O solutions. Δ, 22.95 wt % MDEA (Chiu and Li 1999)**; □, 22.95 wt % MDEA** (Hayden et al. 1983)**; ▲, 49.99 wt % MDEA** (Chiu and Li 1999)**; ■, 49.99 wt % MDEA**(Chiu and Li 1999)

All in all, model fit heat capacity data with average absolute relative deviation of 2.94 %.

4.7.2.4 Freezing Point Depression Data

This kind of data is useful to get a better estimation for water activity. Activity of water is directly related to the freezing point depression of water. Three different freezing point data sources have been used for regression model parameters. Figure 4-7 represents freezing point of aqueous MDEA mixture calculated by the model against different experimental sources. Calculated results are in good agreement with the experimental data. Overall, model represent freezing point of aqueous MDEA solution within 8.96 AARD %.

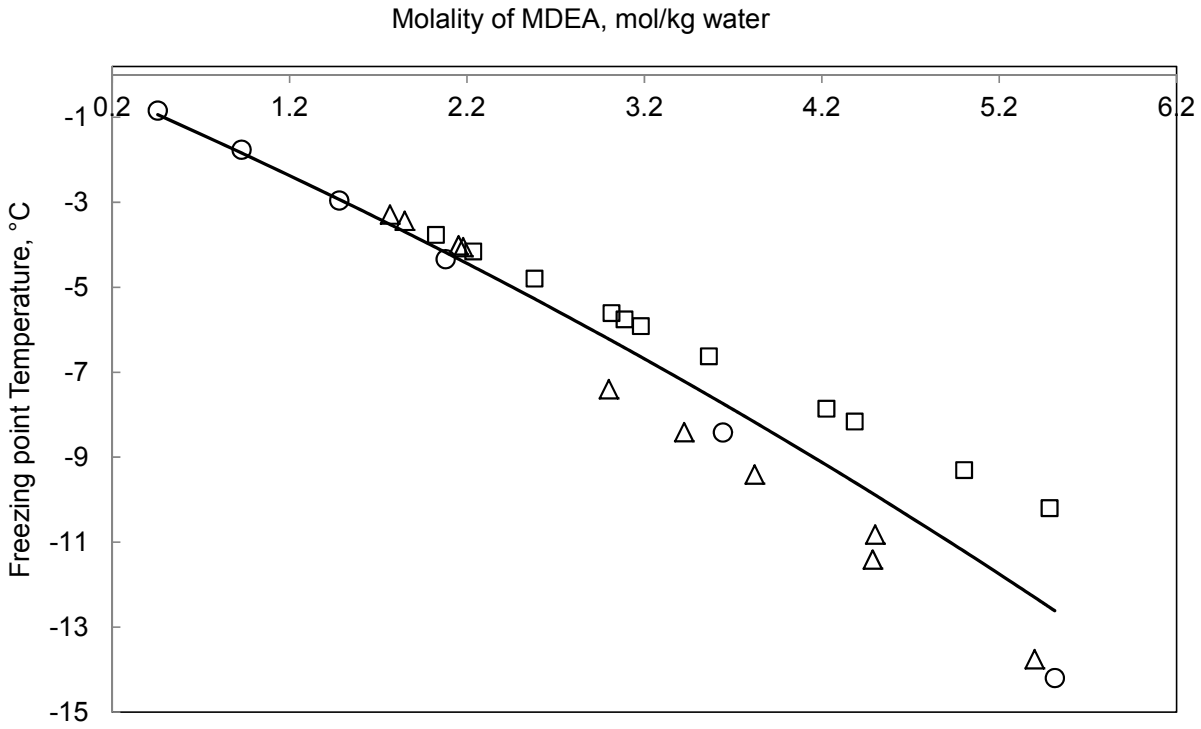

Figure 4-7. Comparison between experimental and regressed values of MDEA-H_2O freezing point. Symbols stand for the experimental data and curve (line) refers to the calculated values using the developed thermodynamic model. Δ, (Chang et al. 1993); ○, (Fosbol et al. 2011), □, (Song et al. 2006)

Overall, the results presented above indicate that the Extended UNIQUAC model, through simultaneous regression gave a set of optimum binary interaction parameters for the binary mixture of MDEA-water. The developed model adequately represents the literature data for MDEA-water mixtures, the average absolute relative deviation for all kinds of MDEA-water data is 7.93%.

4.7.2.5 MDEA Vapor Pressure, Model Predictions

It is of high importance that the model can well describe amine losses from absorber and stripper columns. Figure 4-8 and Figure 4-9 show model predictions for MDEA volatility at 9.98, 19.99, 29.98, 49.92 and 70.02 wt % MDEA versus temperature. The temperature range shown in the figure covers absorber and stripper operational conditions.

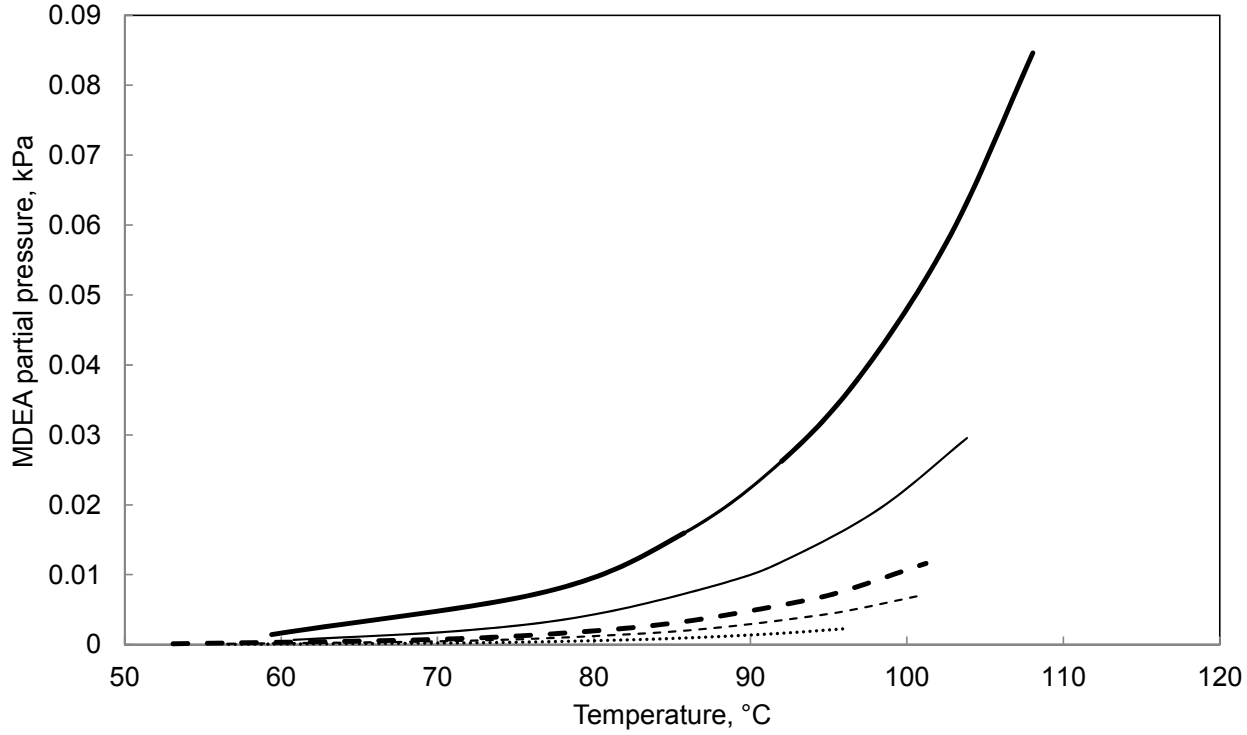

Figure 4-8. Predicted MDEA volatility in 9.98, 19.99, 29.98, 49.92 and 70.02 wt % aqueous MDEA solution. Curves (lines) refer to the calculated values using the developed thermodynamic model. Dot Line, 9.98 wt % MDEA; Dash Line, 19.99 wt % MDEA; Bold Dash Line, 29.98 wt % MDEA; Solid Line, 49.92 wt % MDEA; Bold Solid Line, 70.02 wt % MDEA

To have better illustration of the predicted MDEA volatility, results were shown also in a semi-log plot (logarithmic y axis).

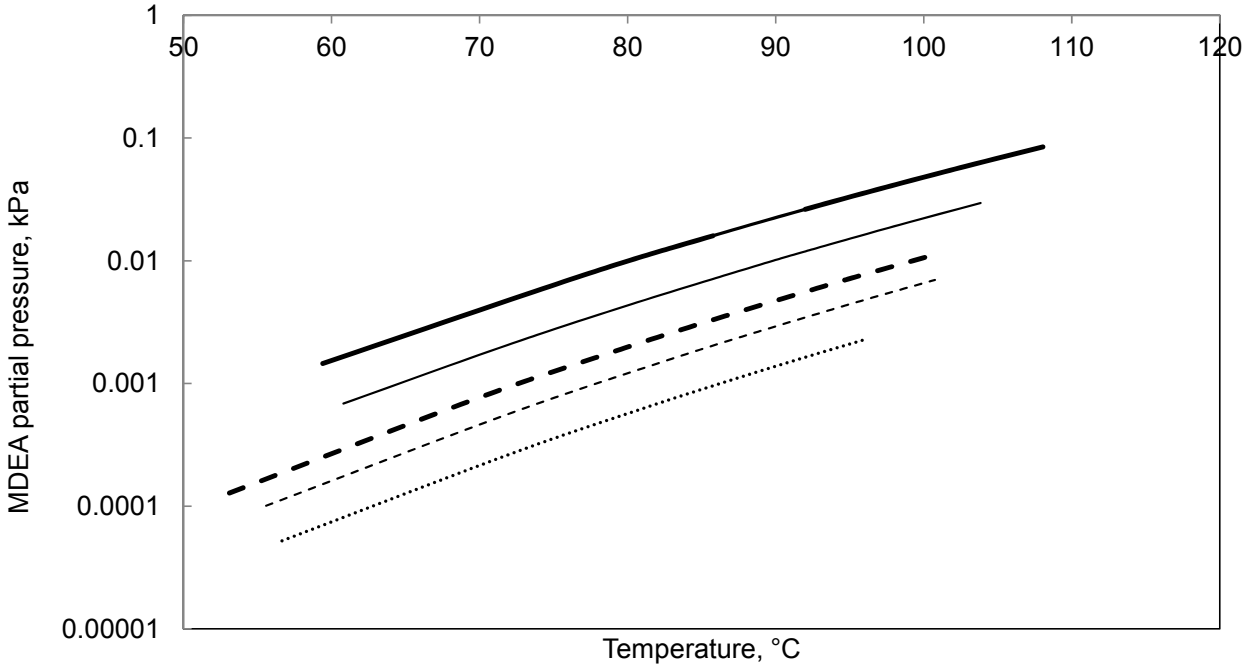

Figure 4-9. Semi-log plot-predicted MDEA volatility in 9.98, 19.99, 29.98, 49.92 and 70.02 wt % MDEA aqueous solution. Curves (lines) refer to the calculated values using the developed thermodynamic model. Dot Line, 9.98 wt % MDEA; Dash Line, 19.99 wt % MDEA; Bold Dash Line, 29.98 wt % MDEA; Solid Line, 49.92 wt % MDEA; Bold Solid Line, 70.02 wt % MDEA

4.7.3 Ternary CO_2-MDEA-H_2O Data and Regression Results

To this point modeling results has only been presented for MDEA-water subsystem. Adding CO_2 to the system causes lots of reactions happen in the system, many ions will be formed, therefore modeling of the CO_2 loaded system requires accounting for interactions between molecules-ions and ions-ions. Model parameters for CO_2-MDEA-H_2O system have been determined through simultaneous regression of total pressure, CO_2 solubility (CO_2 partial pressure), heat capacity and heat of absorption data with the Extended UNIQUAC model. Speciation data from NMR analysis have not been used for regression model parameters, since the availability of this kind of data are low and the uncertainty associated with these measurements is significant; whereas these data have been used to compare with model predictions. pH data were also excluded from the data base used for regression parameters, since these data are rarely available in open literature and uncertainty connected to them is usually high. As stated by (Hessen et al. 2010), it should be discussed whether or not pH is a good measure of the proton activity since single ions activity cannot be measured

directly (Hessen et al. 2010). 895 number of data composed of total pressure and CO_2 partial pressure, heat capacity and heat of absorption over vast range of temperature, pressure and composition were used to fit model parameters.

Table 4-18 represents a summary of the data that were used for parameter estimation. The remainder of this section will discuss different kinds of data that have been used for regression parameters and regression results.

Table 4-18. Overview on ternary data used for parameter estimation and regression results

MDEA Concentration, wt %	T (°C)	P (kPa)	Data Type	Reference	Number of Data Points	AARD %
19, 32.11	40 to 140	139 to 5037 (P_{Total})	VLE	(Kuranov et al. 1996)	77	6.62
26, 47	25, 40, 75	3 to 4559 (P_{Total})	VLE	(Sidi-Boumedine et al. 2004)	80	8.16
19	40	791 to 4739 (P_{Total})	VLE	(Kamps et al. 2002)	5	3.38
32, 49	40, 80, 120	176.5 to 7565 (P_{Total})	VLE	(Kamps et al. 2001)	27	11
24	40	1155 to 3029 (P_{Total})	VLE	(Addicks et al. 2002)	3	9.87
24	40	12 to 3029 (P_{Total})	VLE	(Silkenbaumer et al. 1998)	10	17
19, 32, 48	40, 80, 120	0.12 to 69.3 (P_{CO_2})	VLE	(Ermatchkov et al. 2006a)	101	8.26
5, 20, 50, 75	50, 75, 100	0.775 to 268.3 (P_{CO_2})	VLE	(Rho et al. 1997)	99	18
23, 47	40	0 to 93.6 (P_{CO_2})	VLE	(Austgen et al. 1991)	13	14
35	40, 100	0 to 262 (P_{CO_2})	VLE	(Jou et al. 1993)	37	27
50	25, 50, 75, 100	8.27 to 95.83 (P_{CO_2})	VLE	(Park and Sandall 2001)	29	19
23, 50	40	0 to 0.55 (P_{CO_2})	VLE	(Rogers et al. 1998)	27	18
23, 50	40, 70, 100, 120	0.002 to 5188 (P_{CO_2})	VLE	(Huang and Ng 1998)	66	22
11.8, 20, 23	25,38,50,65.5,115.5	11.1 to 6161.5(P_{CO_2})	VLE	(Maddox et al. 1987)	99	19
50	55, 70, 85	65.75 to 813.4 (P_{CO_2})	VLE	(Ma'mun et al. 2005)	31	8.94
30, 40, 50, 60	25	Na*	C_P	(Weiland et al. 1997)	39	1.25
15, 30	49.3	Na*	H_{abs}	(Arcis et al. 2008)	101	3.19

Not available

4.7.3.1 Total Pressure Data

Equations that relate total pressure data to model parameters have already been illustrated. Total pressure data that have been used for regression have been listed in

Table 4-18. (Mathonat et al. 1997) data and data of (Baek and Yoon 1998) have been excluded from regression data base since these data affect other sources results. Figure 4-10 shows the results of fit for experimental total pressure at 40 °C and 19.9 wt % MDEA versus loading (mole CO_2/mole MDEA), experimental data are from (Kuranov et al. 1996) and (Kamps et al. 2002).

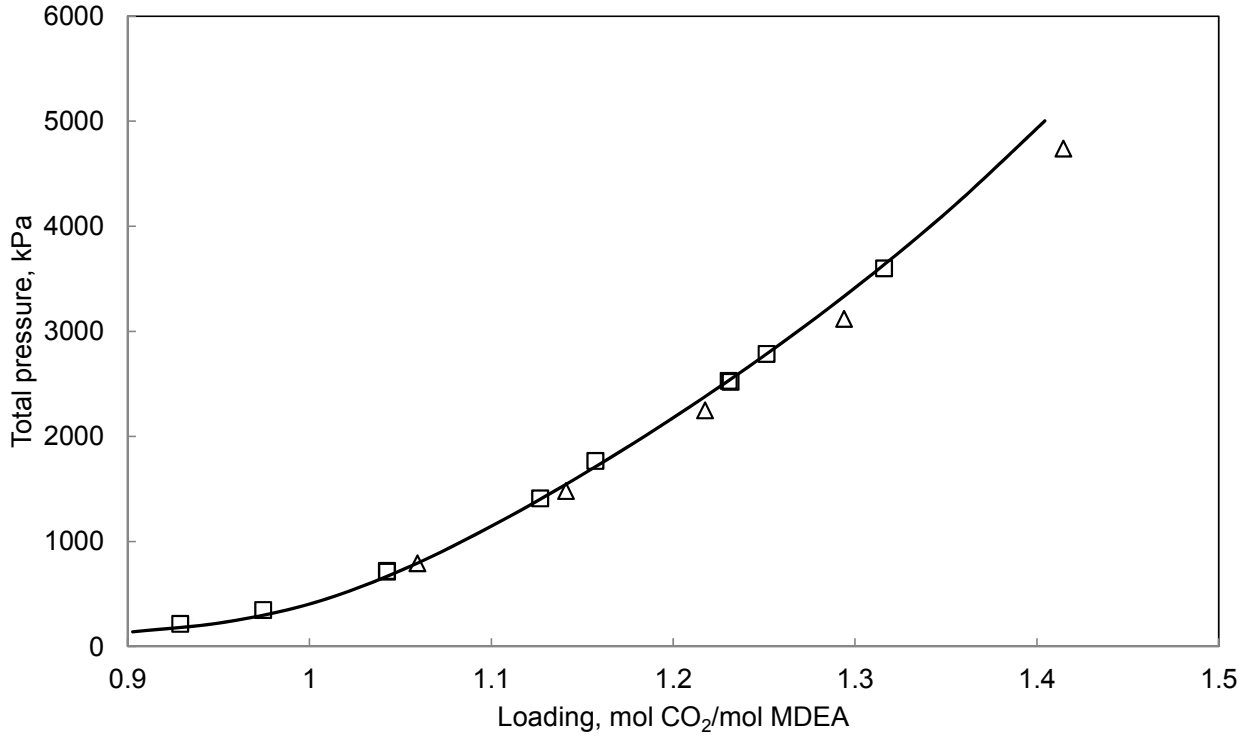

Figure 4-10. Comparison between experimental and regressed total pressure for CO_2-MDEA-H_2O solutions in 19.19 wt % MDEA and at 40 °C. Symbols stand for the experimental data and curve (line) refers to the represented values using the developed thermodynamic model. Δ, (Kamps et al. 2002), □, (Kuranov et al. 1996)

Figure 4-14 plot experimental measurements of total pressure of CO_2-MDEA-H_2O solution at 50 wt % MDEA and from 40 to 120 °C, over the whole loading range, against calculated results of the developed model. Amine concentration, temperature and pressure range of these data points corresponds to industrial acid gas removal plants. Data points also cover the whole loading range.

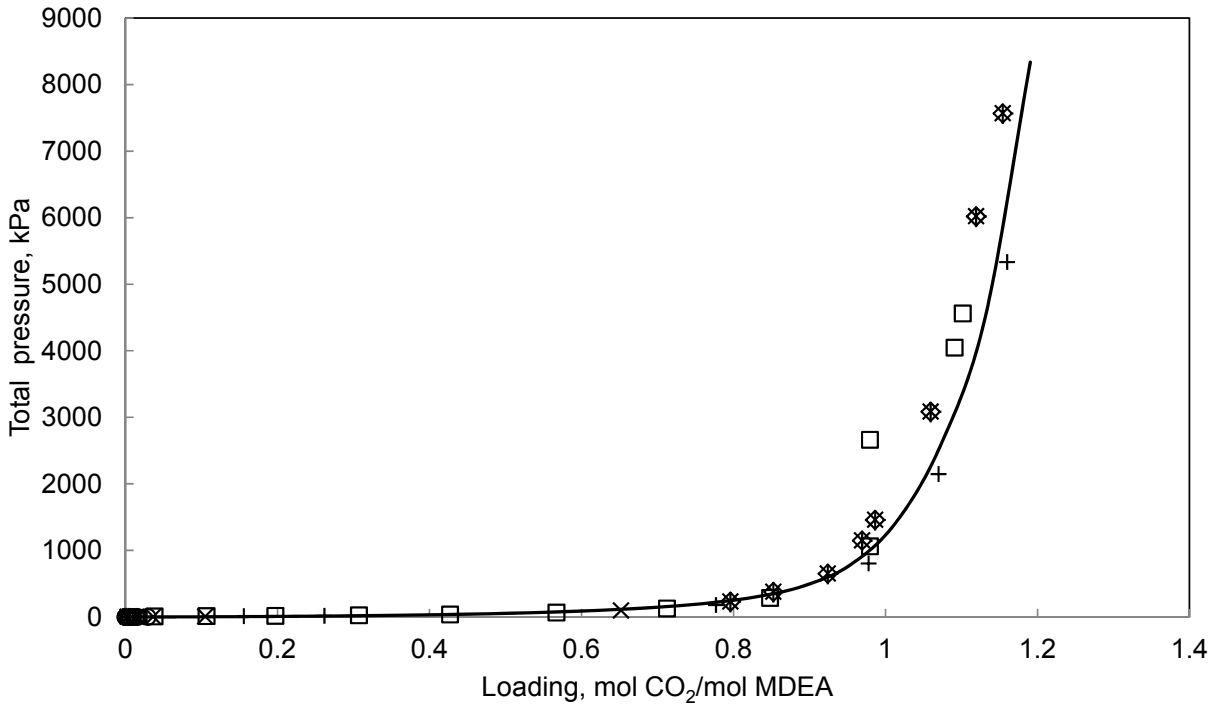

Figure 4-11. Comparison between experimental and regressed total pressure for CO_2-MDEA-H_2O solutions in 50 wt % MDEA and at 40 °C. Symbols stand for the experimental data and curve (line) refers to the represented values using the developed thermodynamic model. ◊**,** (Ermatchkov et al. 2006a)**;** □**,** (Sidi-Boumedine et al. 2004)**;** ×**,** (Austgen et al. 1991)**,** *****, (Kamps et al. 2001)**;** ○**,** (Rogers et al. 1998)**;** +**,** (Huang and Ng 1998)

In Figure 4-12 low loading region of Figure 4-11 is magnified, in order to be able to compare modeling results with experimental values, easier.

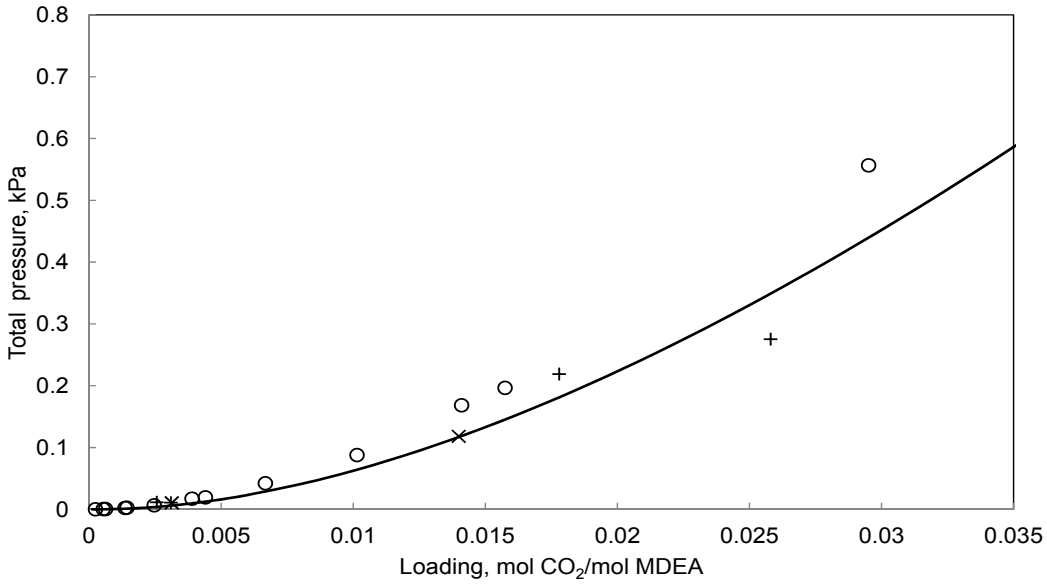

Figure 4-12. Magnified of Figure 4-11 in low loading region. Comparison between experimental and regressed total pressure for CO_2-MDEA-H_2O solutions in 50 wt % MDEA and at 40 °C. ◊**,** (Ermatchkov et al. 2006a)**;** □**,** (Sidi-Boumedine et al. 2004)**;** ×**,** (Austgen et al. 1991)**,** *****, (Kamps et al. 2001)**;** ○**,** (Rogers et al. 1998)**;** +**,** (Huang and Ng 1998)

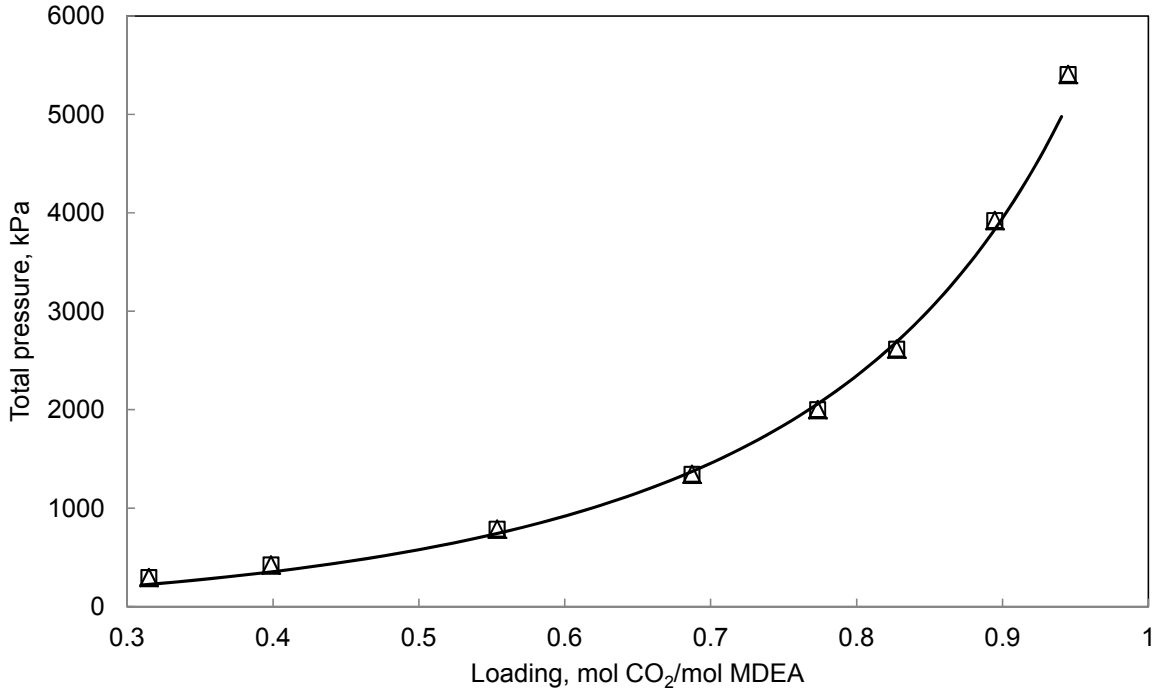

Figure 4-13. Comparison between experimental and regressed total pressure for CO_2-MDEA-H_2O solutions in 50 wt % MDEA and at 80 °C. Symbols stand for the experimental data and curve (line) refers to the represented values using the developed thermodynamic model. □**,** (Ermatchkov et al. 2006a)**;** Δ**,** (Kamps et al. 2001)

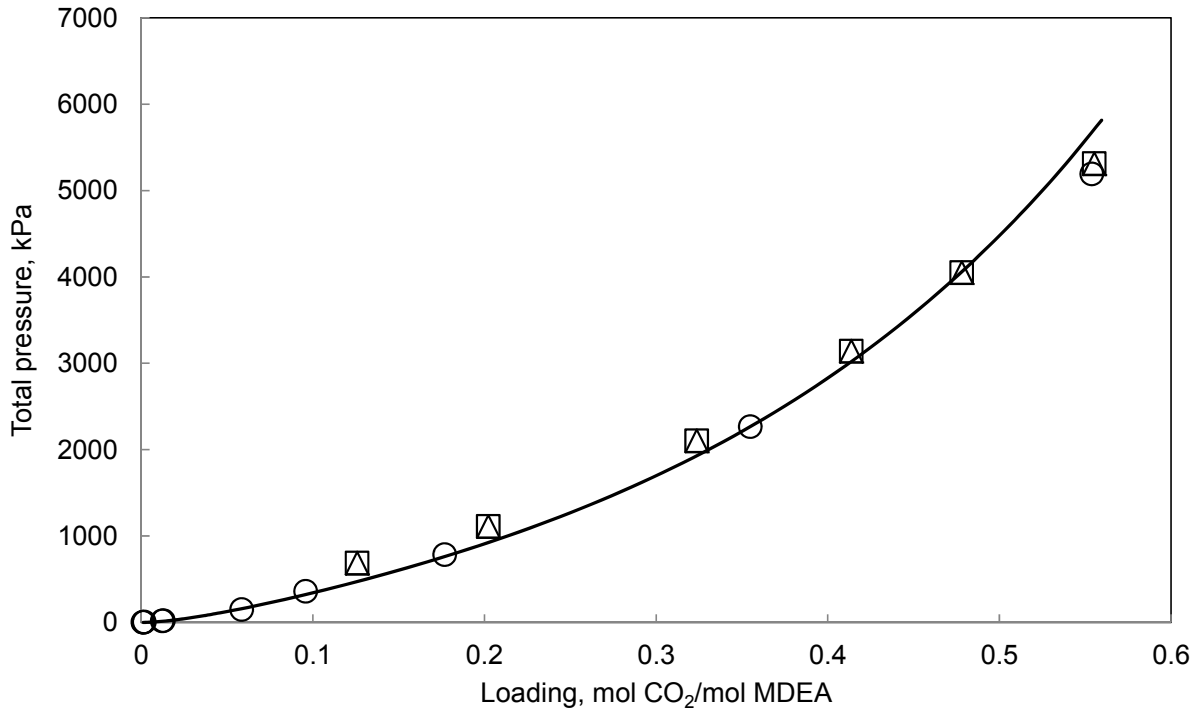

Figure 4-14. Comparison between experimental and regressed total pressure for CO_2-MDEA-H_2O solutions in 50 wt % MDEA and at 120 °C. Symbols stand for the experimental data and curve (line) refers to the represented values using the developed thermodynamic model. □,(Ermatchkov et al. 2006a); Δ, (Kamps et al. 2001); ○, (Huang and Ng 1998)

As it can be seen from Figure 4-11 to Figure 4-14, in terms of industrial applications the developed model can adequately represent total pressure of CO_2-MDEA-H_2O solutions. Overall the model can adequately describe total pressure of CO_2-MDEA-water mixtures with an average absolute deviation of 9.33 %.

4.7.3.2 CO_2 Solubility Data

CO_2 solubility data refers to measurements of CO_2 partial pressure over aqueous mixture of MDEA (P_{CO2}). Many experimental data on the solubility of CO_2 in MDEA solutions could be found in the literature, after the evaluation, data sets which are listed in

Table 4-18 have been chosen for regression parameters. As stated by (Hessen et al. 2010) and (Posey 1997) trend of data by (Li and Shen 1992) significantly deviate from the majority of other sources therefore were discarded from regression data base, they are lower than other data sets by factor of two (Posey 1997). (Chakma and Meisen 1987) data was excluded from regression data

base due to the high uncertainty associated with this data set. According to (Huttenhuis et al. 2007) experiments of (Chakma and Meisen 1987) were performed at high temperatures (373-473 K) without considering any correction for water evaporation and change in liquid density, possibility of MDEA degradation at high temperatures was also neglected in these experiments (Huttenhuis et al. 2007). Data of (JOU et al. 1982) were discarded from regression data base since these data systemically under predict acid gas partial pressure, the same observation was made by (Huttenhuis et al. 2007). Data of (Xu et al. 1998a), (Jenab et al. 2005), (Kicrzkowska-Pawlak 2007), (Ali and Aroua 2004), (Mathonat et al. 1997), (Kundu and Bandyopadhyay 2005), (Macgregor and Mather 1991) and (Lemoine et al. 2000b) data were also discarded from regression data base as these data affect modeling results for other sources (Ermatchkov and Maurer 2011) mentioned that their model show larger deviations for (Jenab et al. 2005) and (Ali and Aroua 2004) data sets. (Hessen et al. 2010) observed that data of (Macgregor and Mather 1991) largely deviate from their model predictions.

In what follows the results of fit for experimental CO_2 solubility at different conditions are presented. Regarding the modeling of the absorber column, it is of high importance that the model describes CO_2 partial pressure accurately at absorber temperature in order to assess the efficiency of the absorber column. To have better design of desorber column, it is very important to have precise prediction of CO_2 partial pressures at elevated temperatures (desorber operational temperatures). Figure 4-15 and Figure 4-16 show calculated results against experimental data for 50 wt % MDEA and at 40 °C (typical absorber temperature) and 100 °C (desorber condition), respectively. Figure 4-17 is the magnified images of Figure 4-16**,** in low loading range region.

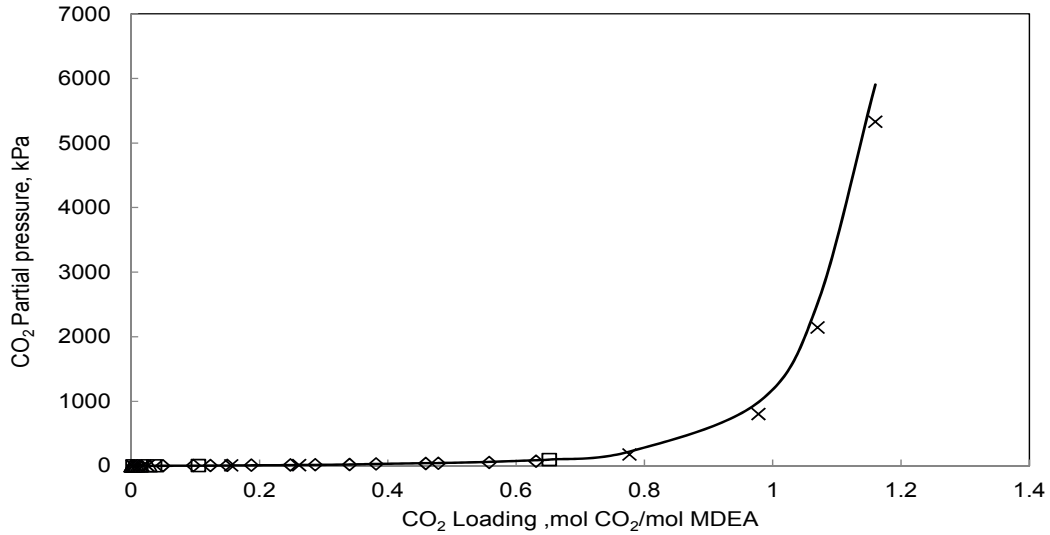

Figure 4-15. Comparison between experimental and regressed CO_2 solubility in aqueous MDEA solutions in 50 wt % MDEA and at 40°C. Symbols stand for the experimental data and curve (line) refers to the represented values using the developed thermodynamic model. ◊**,** (Ermatchkov et al. 2006a)**;** □**,** (Austgen et al. 1991)**;** Δ**,** (Rogers et al. 1998)**;** ×**,** (Huang and Ng 1998)

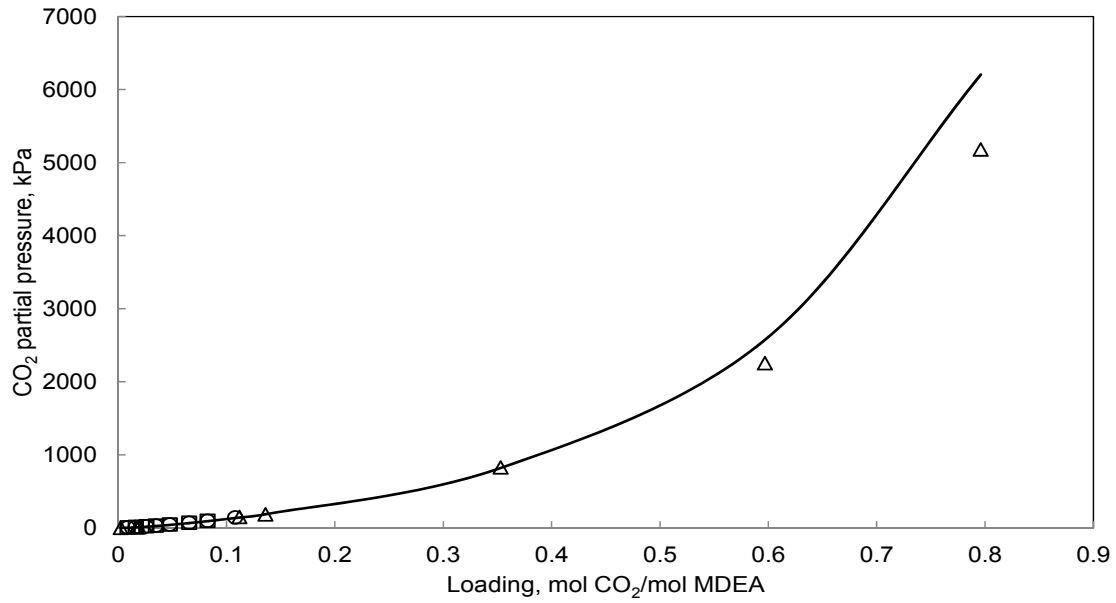

Figure 4-16. Comparison between experimental and regressed CO_2 solubility in aqueous MDEA solutions in 50 wt % MDEA and at 100°C. Symbols stand for the experimental data and curve (line) refers to the represented values using the developed thermodynamic model. ○**,** (Ermatchkov et al. 2006b)**;** □**,** (Park and Sandall 2001)**,** Δ**,** (Huang and Ng 1998)

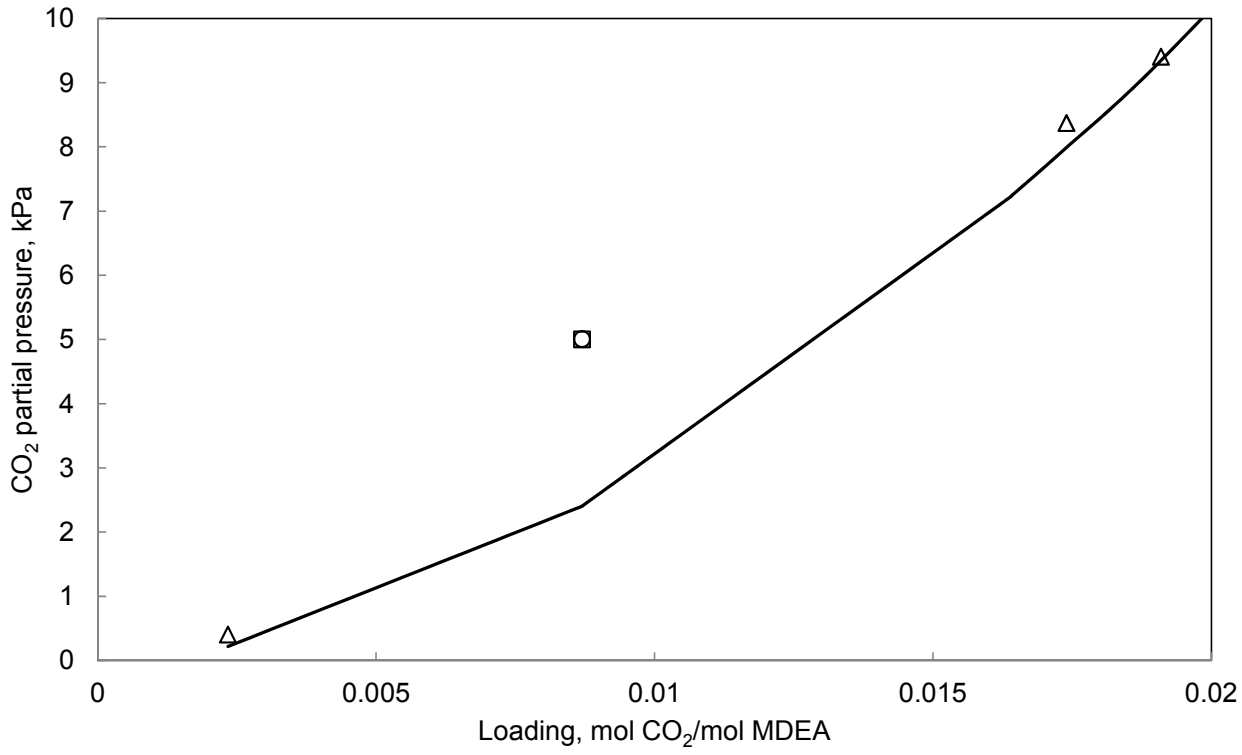

Figure 4-17. Magnified of Figure 4-16 in low loading range. Comparison between experimental and regressed CO_2 solubility in aqueous MDEA solutions in 50 wt % MDEA and at 100°C. Symbols stand for the experimental data and curve (line) refers to the represented values using the developed thermodynamic model. ○**,** (Ermatchkov et al. 2006b)**;** □**,** (Park and Sandall 2001)**,** Δ**,** (Huang and Ng 1998)

Figure 4-18 and Figure 4-19 give results of fit for the experimental CO_2 partial pressure as a function of loading at 5 and 75 wt % MDEA and from 50 °C to 100 °C. To the best of our knowledge, at the time of this work, measurements of (Rho et al. 1997) for CO_2 solubility in aqueous MDEA solutions cover the lowest and highest values available in open literature for MDEA concentration, 5 to 75 wt %. Hence, it is worthwhile to present the results of fit for this source to evaluate model performance in a wide span of amine concentration.

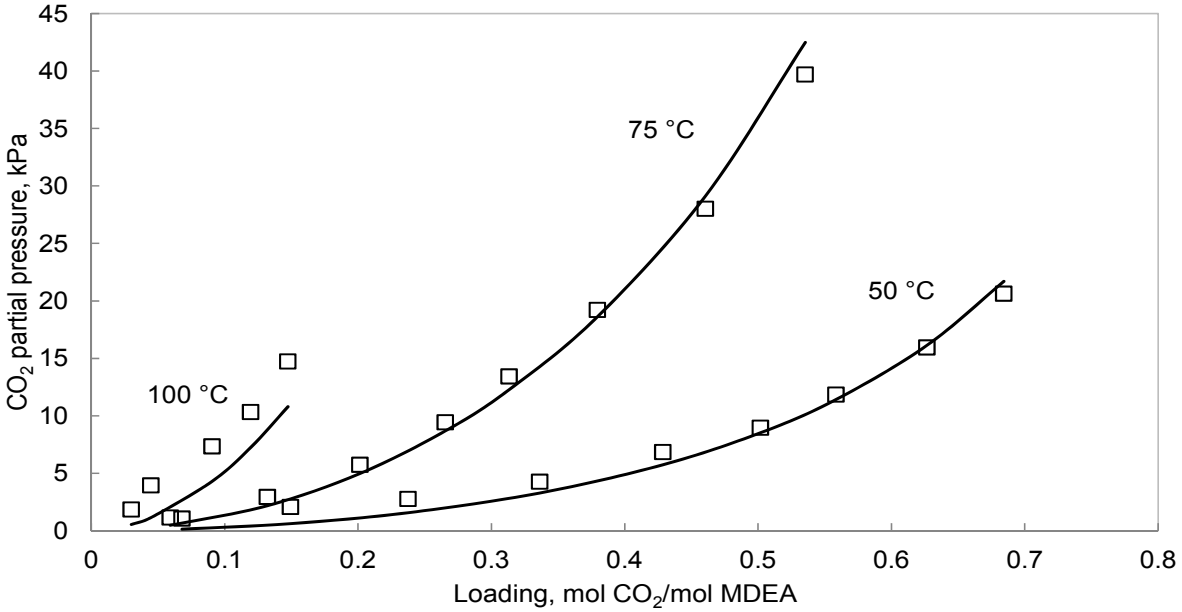

Figure 4-18. Comparison between experimental and regressed CO_2 solubility in in 5 wt % MDEA aqueous solutions and at 50 °C, 75 °C and 100°C. Symbols stand for the experimental data and curve (line) refers to the represented values using the developed thermodynamic model. □, (Rho et al. 1997)

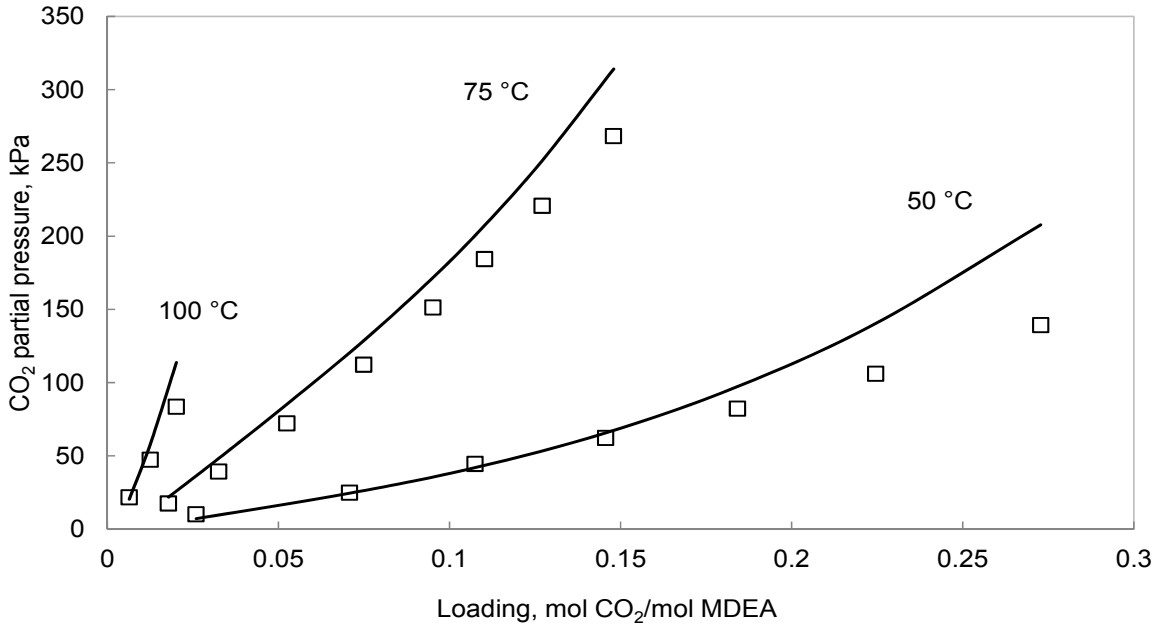

Figure 4-19. Comparison between experimental and regressed CO_2 solubility in in 75 wt % MDEA aqueous solutions and at 50 °C, 75 °C and 100°C. Symbols stand for the experimental data and curve (line) refers to the represented values using the developed thermodynamic model. □, (Rho et al. 1997)

As it can be seen from Figure 4-18 and Figure 4-19, the model is capable of representing CO_2 solubility in very low and very high concentrations of aqueous MDEA solutions. All in all, the model adequately represents CO_2 solubility in aqueous MDEA solutions. The average absolute relative deviation for estimated CO_2 solubility in aqueous MDEA is 17 %.

4.7.3.3 Heat Capacity Data and Regression Results

Using Heat capacity data for parameter regression improve model temperature dependency. Figure 4-20 compares experimental data from (Weiland et al. 1997) to the regressed results at 25 °C and 29.99 wt % MDEA, 40 wt % MDEA, 49.99 wt % MDEA and 59.99 wt % MDEA. To best of our knowledge, this data set is the only measurements available for heat capacity of CO_2 loaded solutions of aqueous MDEA. As it can been from the figure there is a good agreement between calculated and experimental results.

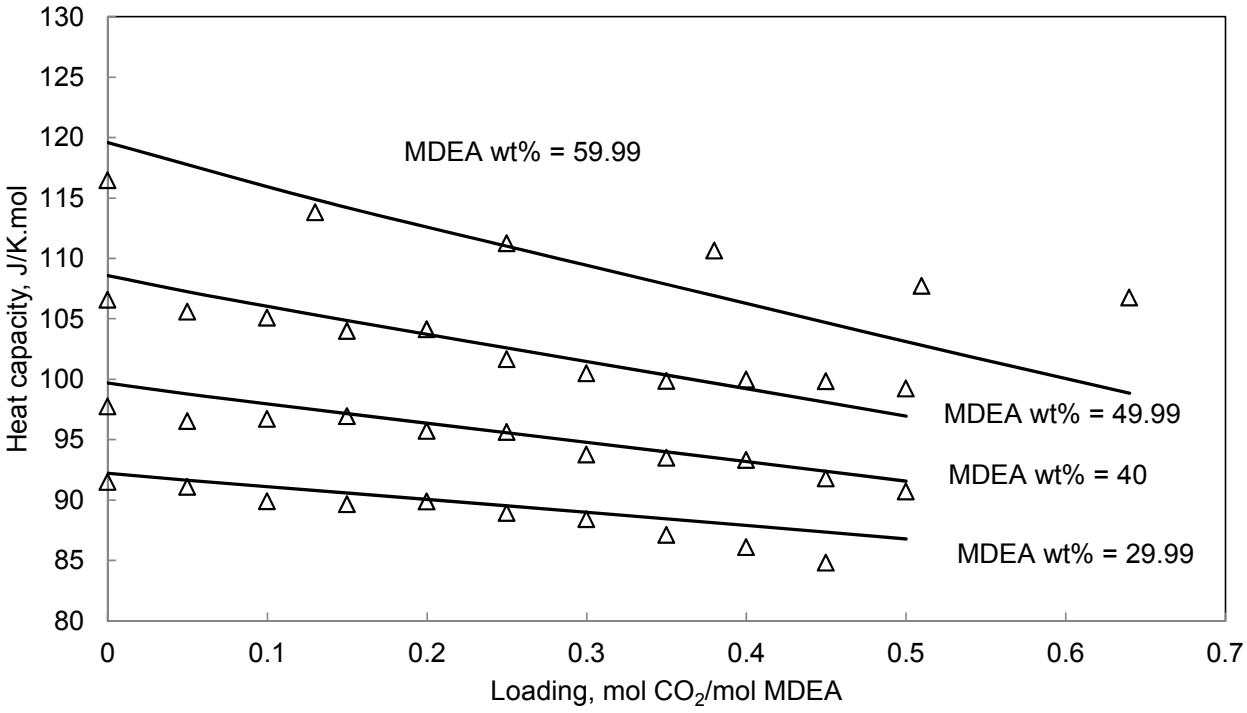

Figure 4-20. Comparison between experimental and regressed heat capacity at 25 °C and for ternary mixtures of CO_2-MDEA-H_2O at different wt % MDEA. Symbols stand for the experimental data and curves (lines) refer to the represented values using the developed thermodynamic model. Δ, (Weiland et al. 1997)

4.7.3.4 Heat of Absorption Data, Regression and Prediction Results

Regression model parameters to heat of absorption data helps to improve temperature dependency of the model. Notice that model parameters have been regressed to the integral heat of absorption

data. Hence, differential heat of absorption data is transformed to integral type of data before using for regression parameters. Heat of CO_2 absorption data from (Arcis et al. 2008) has been used simultaneously with other kinds of data to regress model parameters. Figure 4-21 shows the result of fit for the experimental data at 49.35 °C, in 15 wt % MDEA and at different total pressures, 520 kPa, 980 kPa and 5170 kPa.

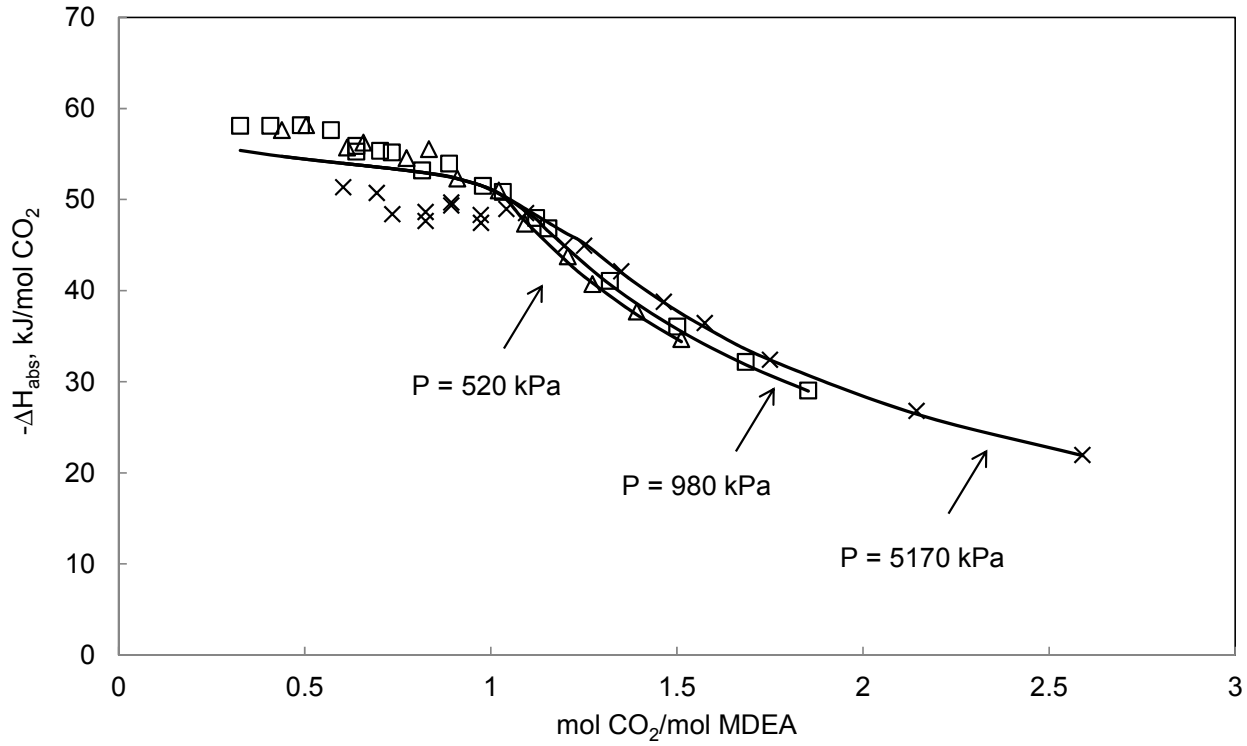

Figure 4-21. Comparison between estimated and measured heat of CO_2 absorption into 15wt % MDEA aqueous solutions at temperature of 49.35 °C and total pressure of 520, 980 and 5170 kPa. Symbols stand for the experimental data and curve (line) refers to the represented values using the developed thermodynamic model. Δ (P = 520 kPa), □ (P = 980 kPa), × (p = 5170 kPa), (Arcis et al. 2008)

Heat of CO_2 absorption data from (Carson et al. 2000), (Oscarson et al. August, 1995) and (Arcis et al. 2009) have been used to verify the model; these data have been used to examine ability of the model as a predictive tool. Model predictions against the experimental values for data of (Oscarson et al. August, 1995) and (Arcis et al. 2009) are shown in Figure 4-22 and Figure 4-23, respectively. Figure 4-22 shows the effect of temperature on heat of CO_2 absorption into aqueous MDEA solution and Figure 4-23 demonstrates the effect of pressure on enthalpy of CO_2 absorption.

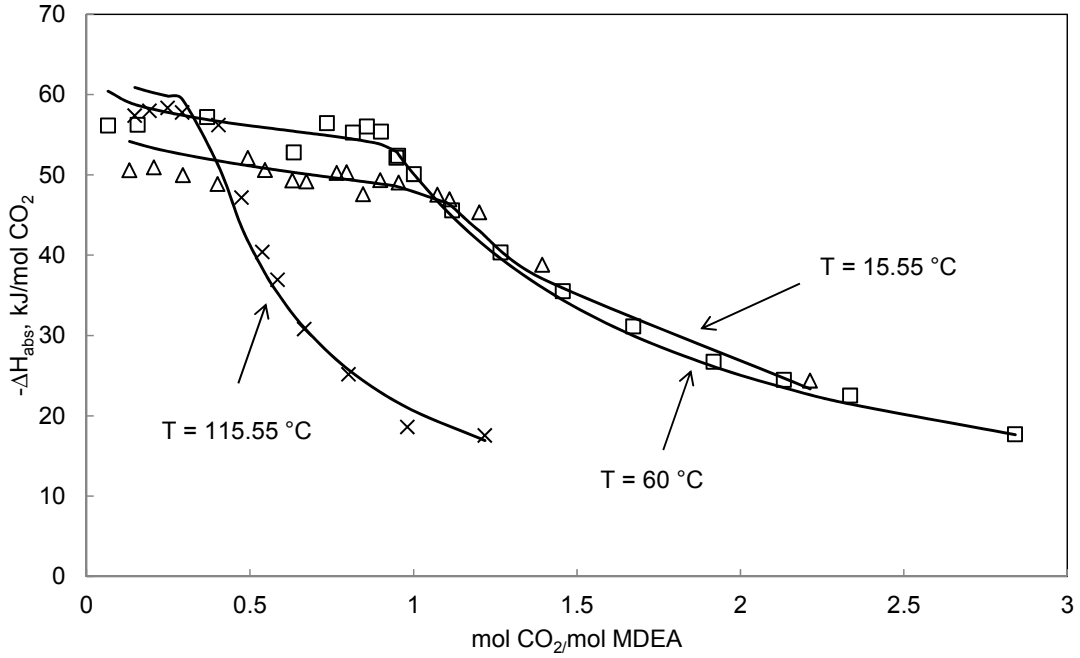

Figure 4-22. Comparison between estimated and measured heat of CO_2 absorption into 40 wt % MDEA aqueous solution at 1120.96 kPa and at 15.55, 60 and 115.55 °C. Symbols stand for the experimental data and curves (lines) refer to the represented values using the developed thermodynamic model. Δ (T = 15.55 °C), □ (T = 60°C), × (T = 115.55 °C), (Oscarson et al. August, 1995)

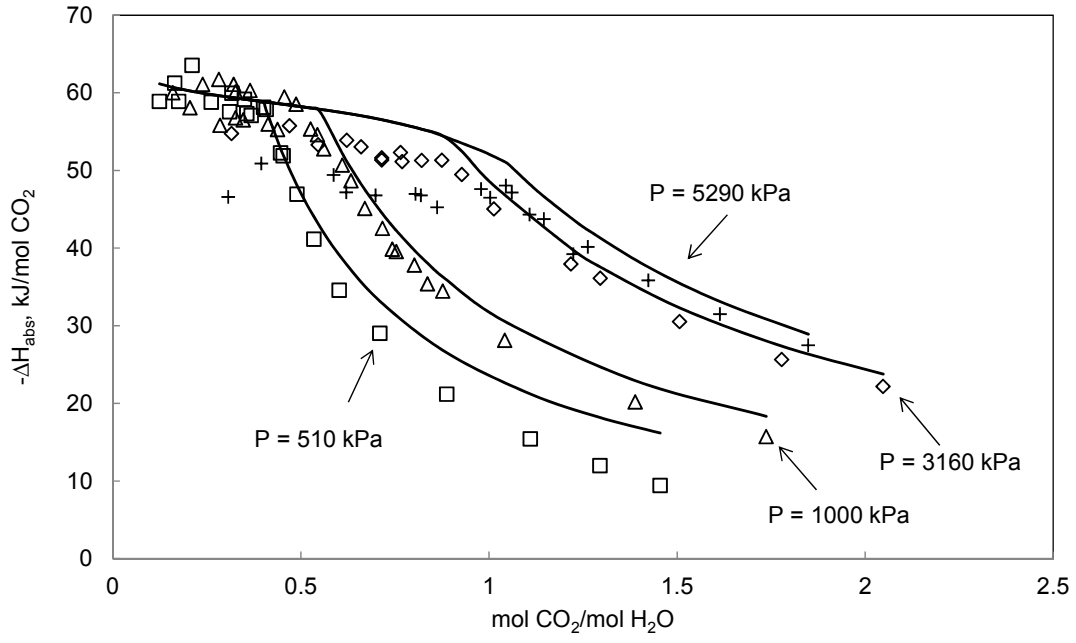

Figure 4-23. Comparison between estimated and measured heat of CO_2 absorption into 30 wt % MDEA aqueous solution at 99.75 °C and at 510, 1000, 3160 and 5290 kPa. Symbols stand for the experimental data and curve (line) refers to the represented values using the developed thermodynamic model. □ (P = 510 kPa), Δ (P = 1000 kPa), ◊ (P = 3160 kPa), + (P= 5290 kPa), (Arcis et al. 2009)

As stated by (Arcis et al. 2008), for all MDEA concentrations, pressure rise leads to decreased heat of CO_2 absorption into aqueous MDEA solutions (decrease in exothermic effect). Generally, for all MDEA concentration, temperature increase causing increased heat of CO_2 absorption in aqueous MDEA solutions (increase in exothermic effect). Table 4-19 shows experimental heat of CO_2 absorption data that have been used for model verification.

Table 4-19. Heat of CO_2 absorption data used for model verification

MDEA Concentration, wt %	T ,°C	Total Pressure, kPa	Reference	Number of Data Points	AARD %
10, 20, 30	25	Na*	(Carson et al. 2000)	40	41
20, 40, 60	15.5, 60, 115.5, 148.8	155.8, 1120.9, 1465.6	(Oscarson et al. August, 1995)	296	11
15, 30	99.7	510, 1000, 3160, 5290	(Arcis et al. 2009)	170	11

**Not available*

Altogether, the model predicts heat of CO_2 absorption in aqueous MDEA solutions within 21 % average absolute relative deviation. Overall results show that the model could be used confidently for calculation enthalpy of solution over the range of temperature, pressure and MDEA concentration.

4.7.3.5 NMR Speciation Data and Prediction Results

As it mentioned in section earlier, speciation data have not used in regression process, however model predictions were checked against available experimental NMR data. The below figure demonstrates prediction results for NMR speciation data.

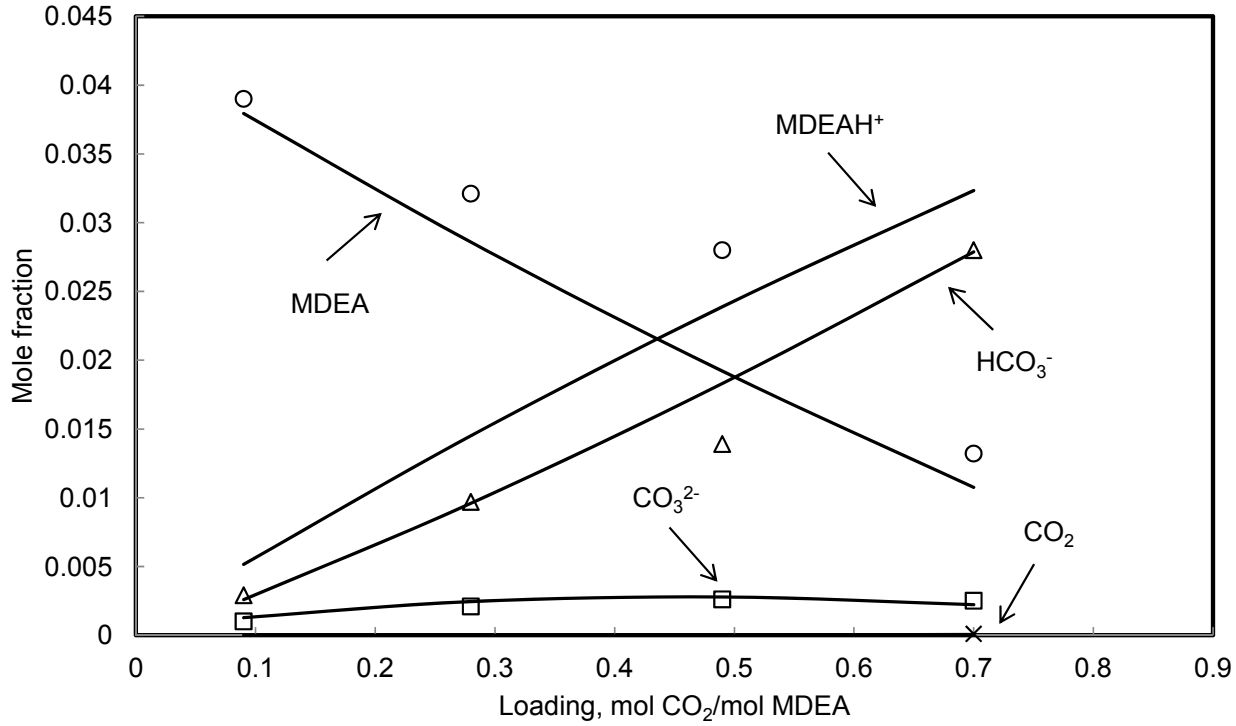

Figure 4-24 .Comparison between model predictions and NMR speciation data. Symbols stand for the experimental data and curve (line) refers to the represented values using the developed thermodynamic model. ○ (MDEA), Δ (HCO_3^-), □ (CO_3^{2-}), × (CO_2), (Jakobsen et al. 2005)

Table 4-20 shows deviations between predicted and NMR data for each species.

Table 4-20. AARD % for the predicted NMR speciation data

Species	AARD %
MDEA	14
CO_2	39
HCO_3^-	12
CO_3^{2-}	40

4.7.4 Comparison between Different Models

This section compare the results of the developed Extended UNIQUAC model in this study with the Extended UNIQUAC model with parameters from (Faramarzi et al. 2009) and e-NRTL model with parameters from (Hessen et al. 2010). Table 4-21 shows comparison between different models results for some selected sources for CO_2solubility in aqueous solutions of MDEA

Table 4-21. Comparison between different models results for CO_2solubility in aqueous solutions of MDEA

Reference	MDEA Concentration, wt %	Temperature, °C	Pressure, kPa	AARD%		
				This Study	(Faramarzi et al. 2009)	(Hessen et al. 2010)
(Austgen et al. 1991)	23, 47	40	0.005 to 100 (P_{CO_2})	14	51	21
(Rho et al. 1997)	5, 19, 49, 75	50, 75,100	0.77 to 264 (P_{Total})	18	42	25
(Kamps et al. 2001)	32, 48	40, 80, 120	176.5 to 7565 (P_{Total})	11	16	Na*
(Ermatchkov et al. 2006a)	19, 32, 48	40, 80, 120	0.12 to 69.3 (P_{CO_2})	8	24	18

Na: Not available

4.8 MEA System

Model parameters for CO_2-MEA-H_2O system were fitted to various types of data. Model parameters were regressed to 716 data points of pure, binary (MEA-H_2O) and CO_2 loaded mixtures. In what follows only modeling results for each data type will be discussed.

4.8.1 Pure MEA Vapor Pressure Data and Regression Results

Table 4-22 provides a summary of the experimental pure MEA vapor pressure data used for parameter estimation and modeling results. Totally 45 pure vapor pressure data points were used for model parameters estimation.

Table 4-22. Regression results for MEA pure vapor pressure

Temperature , °C	Reference Number	Number of Data Points	AARD %
89.85 to 166.85	(Tochigi et al. 1999)	26	0.89
78 and 91.7	(Nath and Bender 1983)	2	6.11
158.24 and 170.23	(Cai et al. 1996)	2	1.66
84.31 to 158.46	(Kim et al. 2008)	15	0.70

Table 4-22 shows model regression results for vapor pressure of pure MEA. All in all the model represent pure MEA vapor pressure with average 2.34 AARD %.

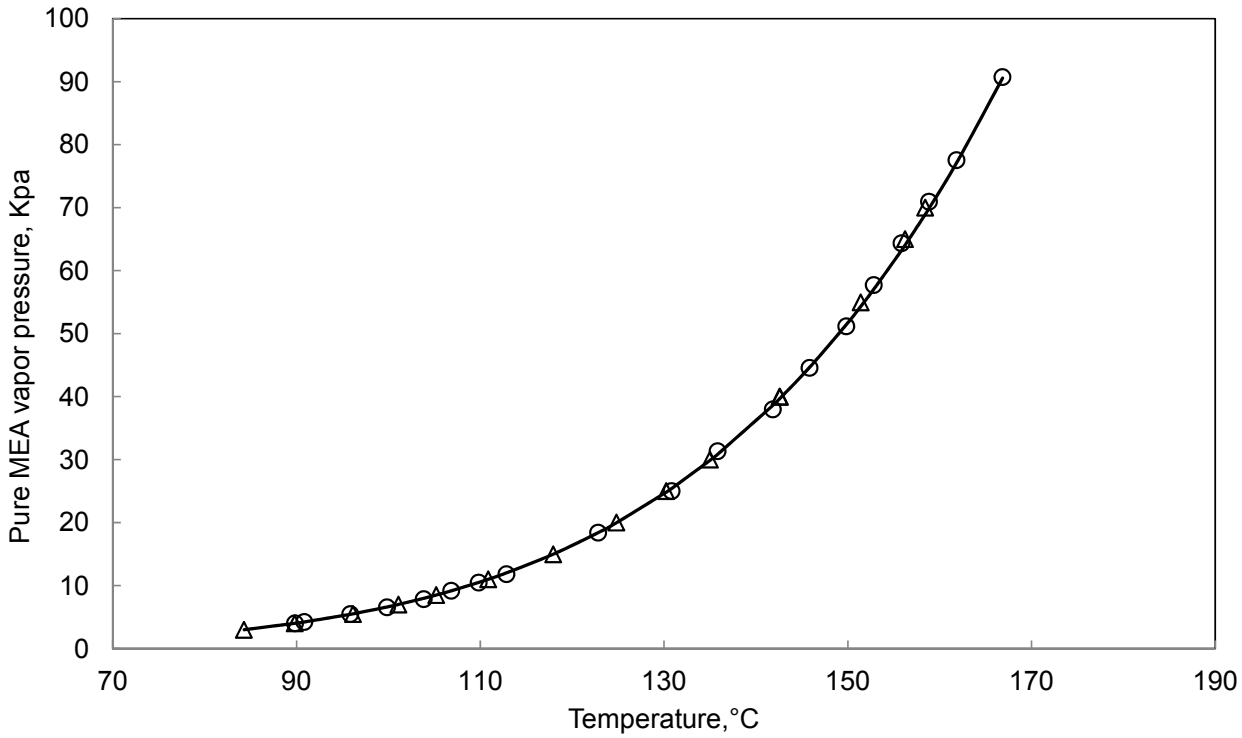

Figure 4-25. Vapor pressure of pure MEA. Symbols stand for the experimental data and curve (line) refers to the calculated values using the developed thermodynamic model.○**,**(Tochigi et al. 1999)**;** Δ**,** (Kim et al. 2008)

4.8.2 Binary MEA-H_2O Data and Regression Results

266 binary MEA-H_2O data points has been used for model parameter determination. Different types of binary data including total pressure, freezing point (SLE) and heat capacity were used for determining model parameters. Table 4-23 lists the data sets upon which the parameters are regressed. In what follows modeling results for different kind of data are given.

Table 4-23. Review over binary MEA-H_2O data used for model parameter regression and modeling results for binary mixture

MEA Concentration, wt %	T ,°C	P, kPa	Data Type	Reference	Number of Data Points	AARD %
42.5 to 97.86	89.85	4.02 to 68.15 (P_{Total})	VLE	(Tochigi et al. 1999)	10	22
16.74 to 97.86	60, 78, 90.7	1.31 to 69.1 (P_{Total})	VLE	(Nath and Bender 1983)	36	3.09
53.05, 77.24, 91.04	37.51 to 137.49	4.32 to 92.2 (P_{Total})	VLE	(Kling and Maurer 1991)	20	4.22
14.68 to 97.69	89.66 to 158.7	66.66, 101.33 (P_{Total})	VLE	(Cai et al. 1996)	25	7.02
3.98 to 75.58	40, 60, 80, 100	7.28 to 46 (P_{Total})	VLE	(Kim et al. 2008)	85	1.51
10, 20, 30, 40	25	Na*	C_p	(Weiland et al. 1997)	4	1.10
45.87, 69.32, 83.56, 93.13	30 to 80	Na*	C_p	(Chiu and Li 1999)	44	1.91
5.03 to 30.64	-1.6 to -16.27	Na*	Freezing point	(Fosbol et al. 2011)	6	1.80
9.01 to 35.87	-3.11 to -20.48	Na*	Freezing point	(Chang et al. 1993)	30	3.57
2.48 to 32	-0.70 to -16.93	Na*	Freezing point	(Song et al. 2006)	6	6.66

**Not available*

4.8.2.1 Total pressure data and Regression Results

Figure 4-26 shows the results of fit for total pressure of binary mixture of MEA and water.

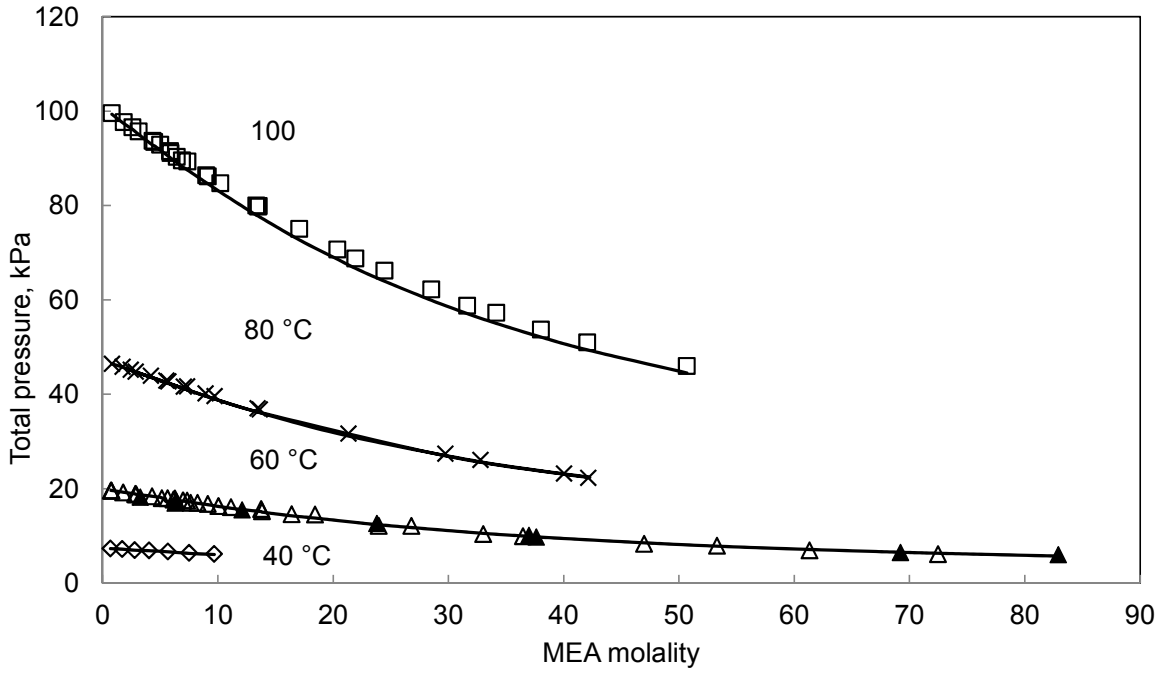

Figure 4-26. Comparison between experimental and fitted results for total pressure of MEA-H_2O solutions. **Symbols stand for the experimental data and curves (lines) refer to the calculated values using the developed thermodynamic model. ◊ (T = 40 °C), Δ (T = 60 °C), × (T = 80 °C), □ (T = 100 °C),** (Kim et al. 2008)**; ▲(T = 40 °C),** (Nath and Bender 1983)

Figure 4-27 is a parity plot shows model calculated results versus all regressed experimental data; the curve has the slope of 0.96 which confirms model capability for representing total pressure of MEA-water subsystem. Overall the model represents total pressure of MEA-H_2O sub molecular system with an average absolute relative deviation of 7.56 %.

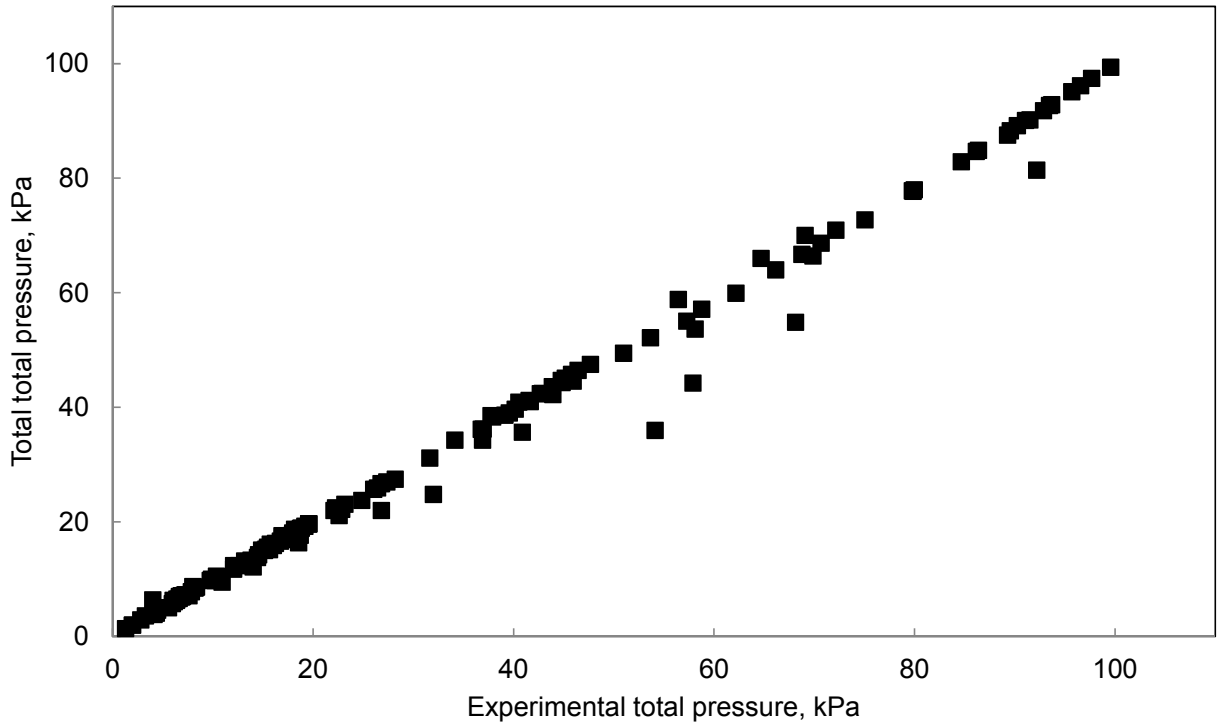

Figure 4-27. Parity plot for binary MEA-H_2O system.■, Experimental data points at various conditions

4.8.2.2 Heat Capacity Data and Regression Results

(Weiland et al. 1997) and (Chiu and Li 1999) heat capacity data for binary mixture of MEA-H_2O have been used simultaneously with other data types to regress model parameters. Figure 4-28 compares results of fit for heat capacity of MEA-water mixture with the experimental data from (Chiu and Li 1999). All in all, average AARD % for results of fit of heat capacity of binary MEA-H_2O system is 1.50 %.

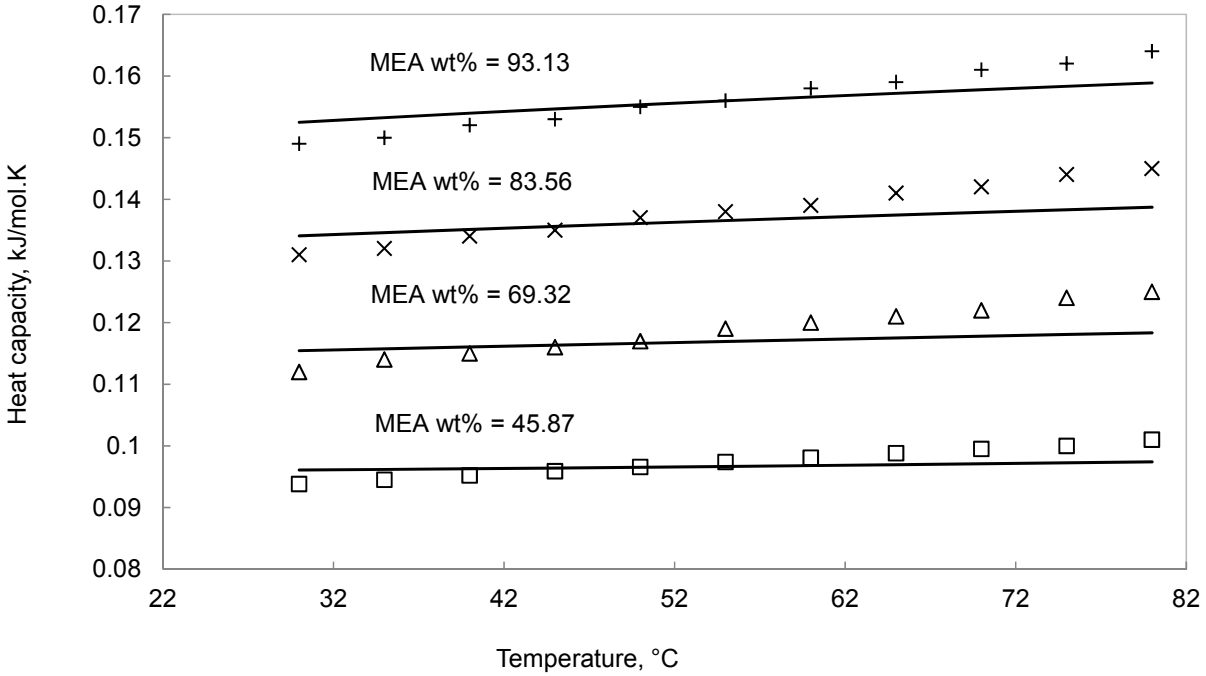

Figure 4-28. Comparison between experimental and calculated values of heat capacity of MEA-H_2O solutions at 45.87, 69.32, 83.56 and 93.13 wt % MEA. Symbols stand for the experimental data and curves (lines) refer to the calculated values using the developed thermodynamic model. □ (45.87 wt % MEA), Δ (69.32 wt % MEA),× (83.56 wt % MEA), + (93.13 wt % MEA), (Chiu and Li 1999)

4.8.2.3 Freezing Point Depression Data and Regression Results

MEA-H_2O freezing point data of (Fosbol et al. 2011), (Chang et al. 1993) and (Song et al. 2006) have been used to regress model parameters. Figure 4-29 shows freezing point of aqueous MEA mixture calculated by the model against different experimental sources. As it can be seen from the Figure 4-29, calculated results are in good agreement with the experimental data. All in all, the developed model calculates freezing point of MEA-H_2O solution within 4.01 AARD %.

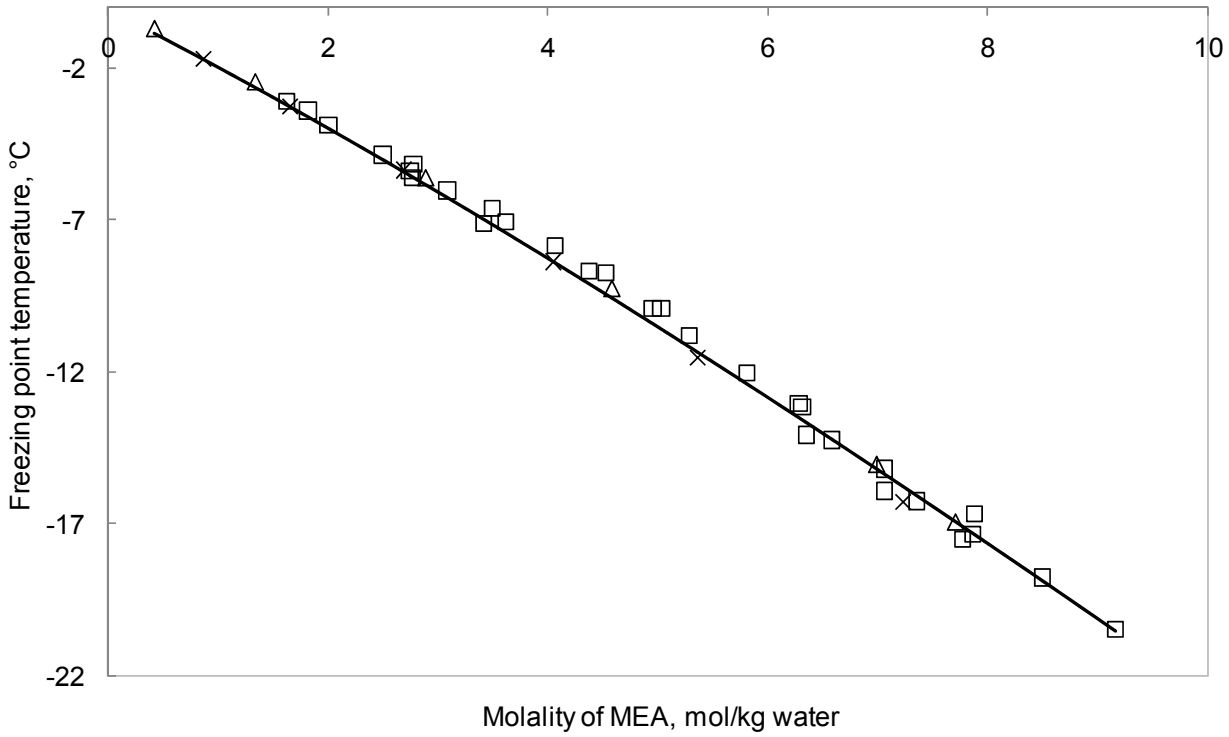

Figure 4-29. Freezing point of MEA-H_2O solutions. Symbols stand for the experimental data and curve (line) refers to the calculated values using the developed thermodynamic model. Δ, (Song et al. 2006); ×, (Mason and Dodge 1936); □, (Song et al. 2006)

Overall, the results presented above indicate that the Extended UNIQUAC model, through simultaneous regression gave a set of optimum binary interaction parameters for the binary mixture of MEA-water. The developed model adequately represents the literature data for MEA-water mixtures.

4.8.2.4 MEA Vapor Pressure, Model Predictions

MEA is more volatile than MDEA and the amount of MEA losses from absorber and stripper columns are greater than MDEA. Accurate estimation of MEA volatility at absorber and stripper conditions leads to better design of columns. Thus it is of great need that thermodynamic model could represent MEA vapor pressure over operational conditions accurately. Figure 4-30 plots model predictions for MEA vapor pressure over aqueous mixtures of MEA at 53.05, 77.22 and 91.04 wt % MEA. The temperature range shown in the figure covers absorber and stripper operational conditions.

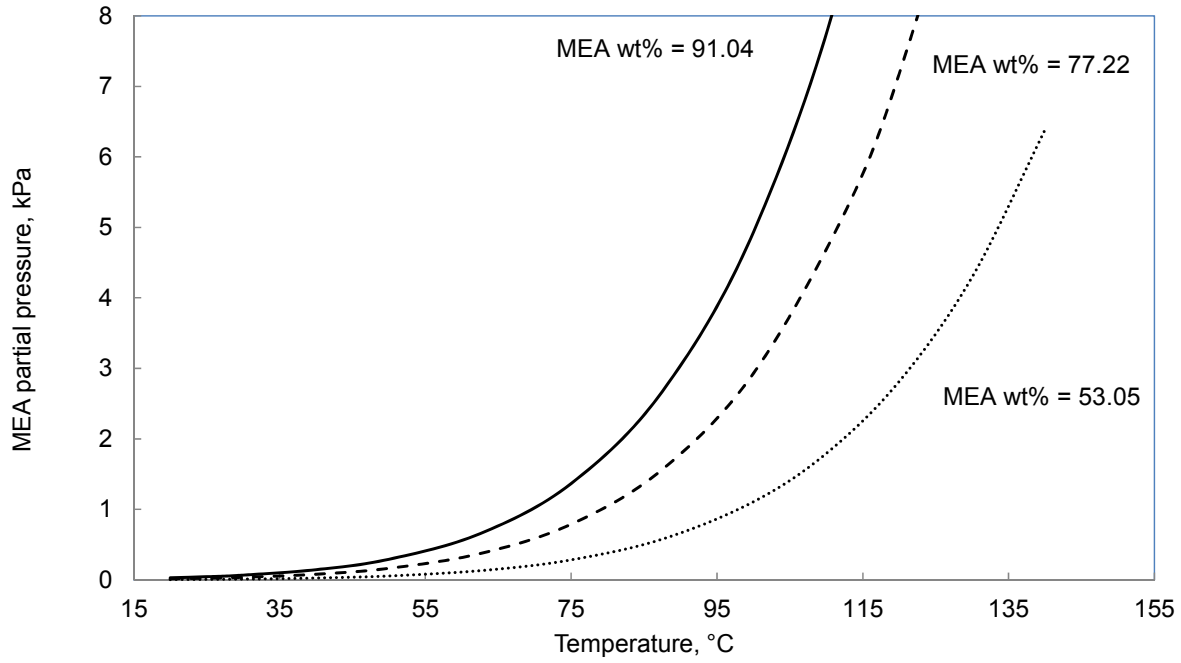

Figure 4-30. Predicted MEA volatility for MEA-H_2O solutions in 53.05, 77.22 and 91.04 wt % MEA. Curves (lines) refer to the predicted values using the developed thermodynamic model. Dot Line, 53.05 wt % MEA; Dash Line, 77.22 wt % MEA; Solid Line, 91.04 wt % MEA

4.8.3 Ternary CO_2-MEA-H_2O Data and Regression Results

Modeling results for MEA-water molecular subsystem were presented in previous section. This section will go through CO_2 loaded system results. Data that have been used to regress model parameters and modeling results will be described in what follows. Interaction parameters involved in CO_2-MEA-H_2O system have been determined through simultaneous regression of total pressure, CO_2 solubility (CO_2 partial pressure), heat capacity, heat of absorption and freezing point depression data with the Extended UNIQUAC model. 405 numbers of data over vast range of temperature, pressure and composition were used to fit model parameters. Table 4-24 presents a summary of the data that were used for parameter estimation.

Table 4-24. Overview on ternary (CO_2-MEA-H_2O) data used for parameter estimation and regression results

MEA Concentration, wt %	T (°C)	P (kPa)	Data Type	Reference	Number of Data Points	AARD %
15.17	25, 60, 80	6.84 to 6085.46 (P_{CO_2})	VLE	(Maddox et al. 1987)	60	13
15.17	80, 100	0.00896 to 1.64 (P_{CO_2})	VLE	(ISAACS et al. 1980)	19	74
15.29, 30	40, 60, 80, 100	1.1 to 2550 (P_{CO_2})	VLE	(Shen and Li 1992)	61	19
15.17	40, 80	0.09 to 228.7 (P_{CO_2})	VLE	(Austgen et al. 1991)	8	13
15.20	40, 60, 80, 100, 120, 140	1.33 to 2786.44 (P_{CO_2})	VLE	(Lawson and Garst 1976)	20	13
30	120	7.3 to 191.9 (P_{CO_2})	VLE	(Ma'mun et al. 2005)	19	16
15.29	0.43, 40, 80, 100, 120, 140	0.002 to 930.99 (P_{CO_2})	VLE	(Jones et al. 1959)	54	30
10, 20, 30, 40	25	Na*	C_p	(Weiland et al. 1997)	24	13
9.99, 20, 29.99	25	Na*	H_{abs}	(Carson et al. 2000)	40	1.55
29.99	40, 80, 120	Na*	H_{abs}	(Kim and Svendsen 2007)	85	13
29.99	-15.55 to -15.09	Na*	Freezing Point	(Source1)(Iliuta and Larachi 2007)	4	2.78
29.99	-16.42 to -14.88	Na*	Freezing Point	(Source2)	11	3.86

Not available

The remainder of this section will present different kinds of data that have been used for regression parameters of CO_2-MEA-H_2O system and regression results.

4.8.3.1 CO_2 Solubility Data

CO_2 partial pressure data over aqueous mixture of MEA have been used to regress model parameters. A large number of experimental data on solubility of CO_2 in aqueous MEA solutions are available in the literature, however many of them are dispersed and scattered. Lots of the

available data show discrepancies at the same conditions. Thus it is necessary to evaluate the data before including them in regression data base. According to (JOU et al. 1995), because of inaccurate experimental procedure, data of (Lee et al. 1974) and (LEE et al. 1976) are about 0.04 mole of CO_2/mole of MEA less than real values, therefore data of (Lee et al. 1974) and (LEE et al. 1976) should be biased with the factor of 0.04. Nevertheless, data of (Lee et al. 1974) and (LEE et al. 1976) were discarded from the regression data base in this work, since it seems unreasonable to bias all the data with the same factor of 0.04. As stated by Hessen (Hessen et al. 2010) low pressures data of (JOU et al. 1995) deviate from the biased data of (LEE et al. 1976). Similar to (Faramarzi et al. 2009), data of (JOU et al. 1995)were excluded from regression data base in this study. As stated by (Hessen et al. 2010) and (JOU et al. 1995), data of (Shen and Li 1992) deviate from other sources, thus these data were discarded in this work. Data of (ISAACS et al. 1980) were discarded by (Hessen et al. 2010), however (Weiland et al. 1993) believe that 30 % of these data are inaccurate. In this work 50 % of (ISAACS et al. 1980) were excluded from regression data base as they are inconsistent with other data. (Ma'mun et al. 2005)data were not included by Hessen for regressing parameters, 48% of (Ma'mun et al. 2005) data were also discarded from regression data base in this work. (LEE et al. 1975) data is referred as inaccurate data by (Lemoine et al. 2000a) and (Weiland et al. 1993), (LEE et al. 1975) data were also evaluated as inconsistent data in this work and therefore excluded from regression data base. As stated by (JOU et al. 1995), (Mason and Dodge 1936) data deviate from other measurements, thus have been taken out from regression data base. The same as (Faramarzi et al. 2009), (Daneshvar et al. 2004) data were excluded from regression data base. According to (JOU et al. 1995), data of (Murrietaguevara et al. 1993) seems to deviate from other measurements and were discarded from regression data base in this study.

After evaluation, sources that are listed in Table 4-24 were chosen for parameter regression. It was found out that a few measurements in some of the listed data sets deviate greatly from the majority. A direct comparison between measurements from different sources at the same conditions, make it possible to determine which measurements within a given data set are errant. However, a large number of parameters varying from measurement to measurement make this comparison risky, but this is one of the few available methods to determine beforehand the reliability of data points. Following figures show comparison between different measurements that leads to eliminate of bad data from listed data sets in Table 4-24. Figure 4-31 and Figure 4-32 show the comparison between different data sets at 40 °C and 15 wt % MEA. As it can be seen from the figures, at 0.68 loading CO_2 partial pressure reported by (Jones et al. 1959) and (Lawson and Garst 1976) is lower than the values from (Shen and Li 1992) and (Austgen et al. 1991). Therefore (Jones et al. 1959) data point

at loading = 0.68 and (Lawson and Garst 1976) data points at loading = 0.673 and 0.678 were withdrawn from data set.

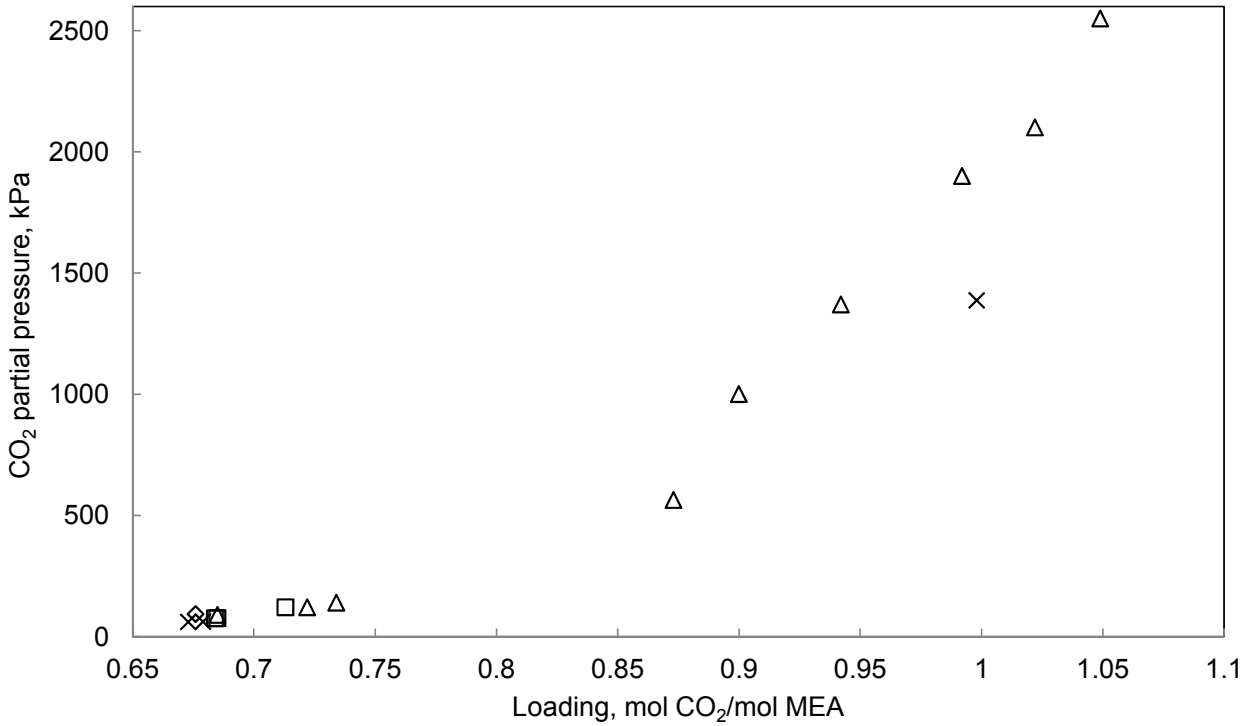

Figure 4-31. Comparison between experimental CO_2 partial pressure from different data sources at 40 °C and 15 wt % MEA. ◊; (Austgen et al. 1991), □; (Jones et al. 1959); Δ, (Shen and Li 1992); ×, (Lawson and Garst 1976)

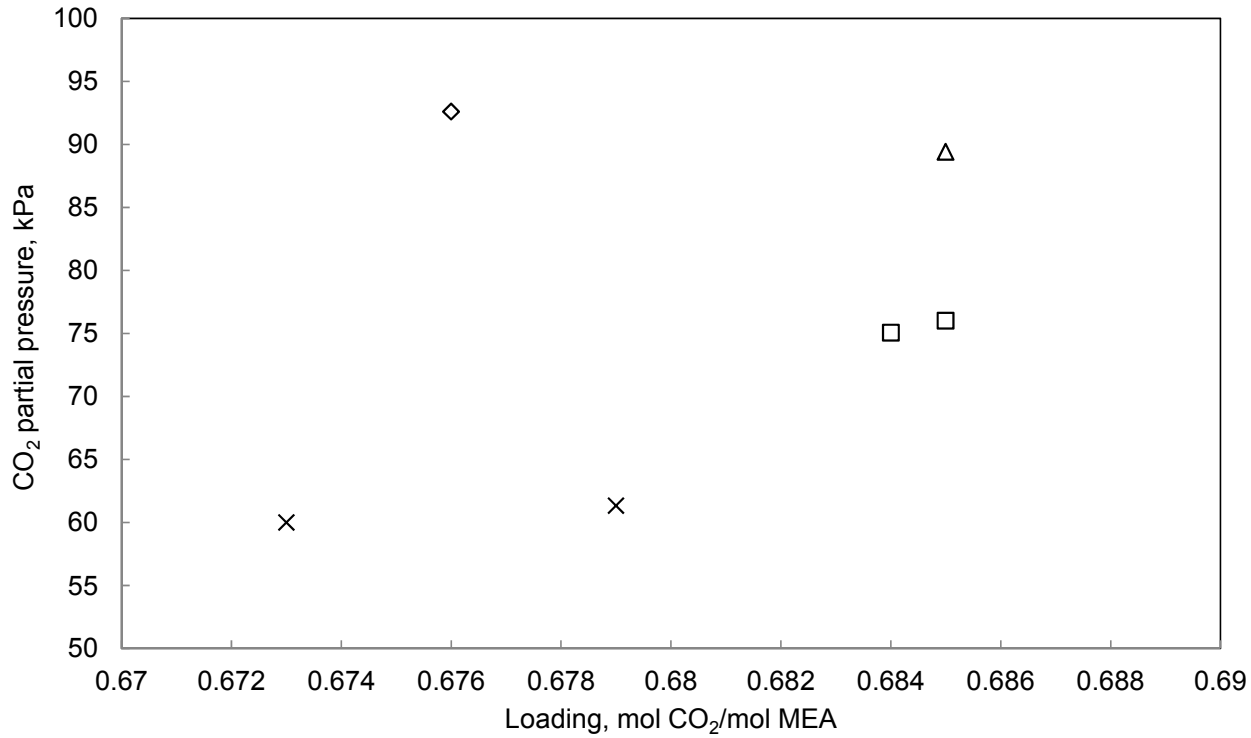

Figure 4-32. A magnified portion of Figure 4-31 in limited loading range.Comparison between experimental CO_2 partial pressure from different data sources at 40 °C and in 15 wt % MEA solutions. ◊**,** (Austgen et al. 1991)**;** □**,** (Jones et al. 1959)**;** Δ**,** (Shen and Li 1992)**;** ×**,** (Lawson and Garst 1976)

Figure 4-33 and Figure 4-34 compare different data sets at 80 °C and 15 wt %. Results reveal that (Maddox et al. 1987) generally show higher measured values than other data sets. (ISAACS et al. 1980) data point at loading of 0.26 is lower than the value reported by (Austgen et al. 1991), thus data point of (ISAACS et al. 1980) at loading = 0.26 is discarded from regression data base. At loading =0.483 and 0.489, CO_2 partial pressure values from (Maddox et al. 1987) are higher than (Jones et al. 1959) values, points from (Maddox et al. 1987) were discarded from regression data base. At loading of 0.88, the reported value by (Maddox et al. 1987) is above the value from (Lawson and Garst 1976), data point from (Maddox et al. 1987) is dropped from regression data base.

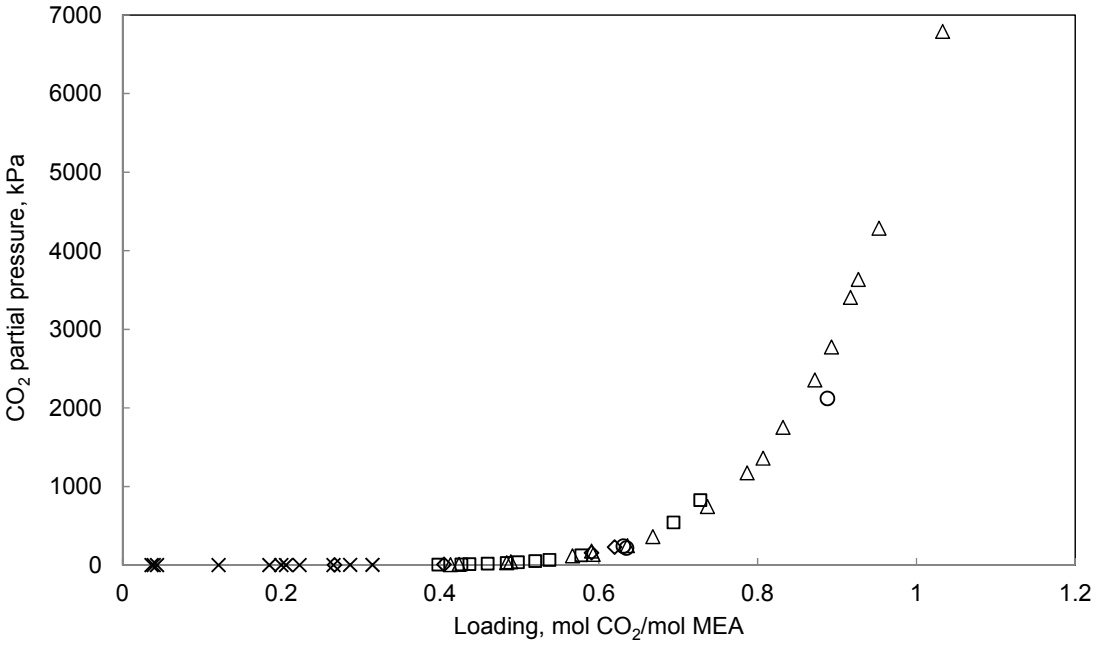

Figure 4-33. Comparison between experimental CO_2 partial pressure from different data sources at 80 °C and in 15 wt % MEA solutions. ◊**,** (Austgen et al. 1991)**;** □**,** (Jones et al. 1959)**(Jones et al. 1959)(Jones et al. 1959);** Δ**,** (Maddox et al. 1987)**;**○(Lawson and Garst 1976)**;** ×**,** (ISAACS et al. 1980)

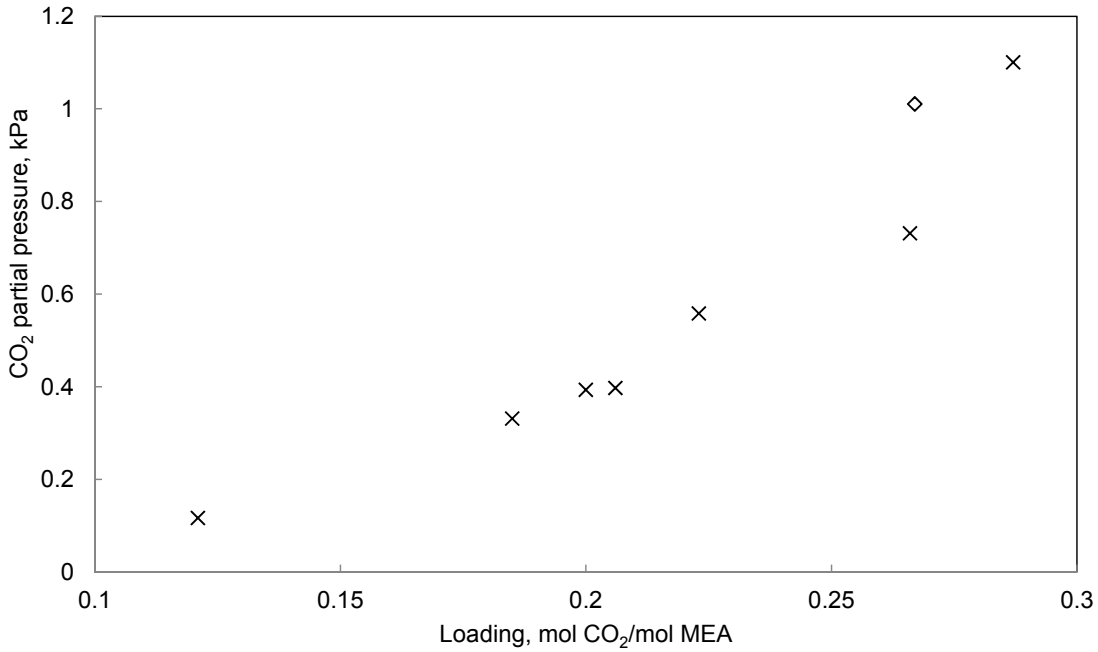

Figure 4-34.Magnified portion of Figure 4-33.Comparison between experimental CO_2 partial pressure from different data sources at 80 °C and in 15 wt % MEA solutions.◊**,** (Austgen et al. 1991)**;** □**,** (Jones et al. 1959)**(Jones et al. 1959)(Jones et al. 1959);** Δ**,** (Maddox et al. 1987)**;**○(Lawson and Garst 1976)**;** ×**,** (ISAACS et al. 1980)

Comparing different data sets at 100 °C and 15 wt % MEA indicates that at loading = 0.59 and 0.60 values from (Lawson and Garst 1976) are below the ones from (Jones et al. 1959), values from (Lawson and Garst 1976) are withdrawn from regression data base. CO_2 partial pressures reported by (ISAACS et al. 1980) at 100 °C are not in agreement with other sources, these values were also discarded from regression data base. The remainder of this section discusses modeling results for CO_2 solubility in aqueous MEA solutionsin15 wt % at 40 and 80 °C and in 30 wt % MEA at 120 °C.

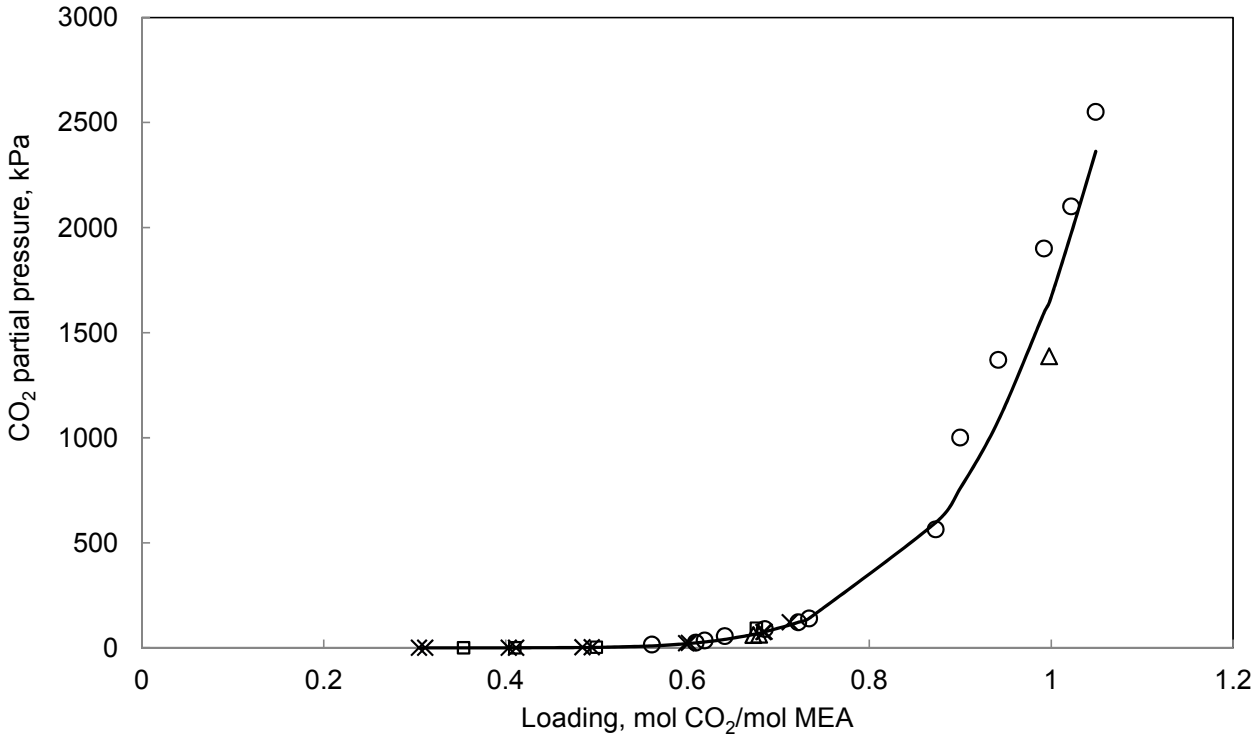

Figure 4-35. Comparison between experimental and regressed CO_2solubility in 15 wt % aqueous MEA solutions at 40 °C. Symbols stand for the experimental data and curve (line) refers to the represented values using the developed thermodynamic model. ○**,** (Shen and Li 1992)**;** □**,** (Austgen et al. 1991)**;** Δ**,** (Lawson and Garst 1976)**;** ×**,** (Jones et al. 1959)

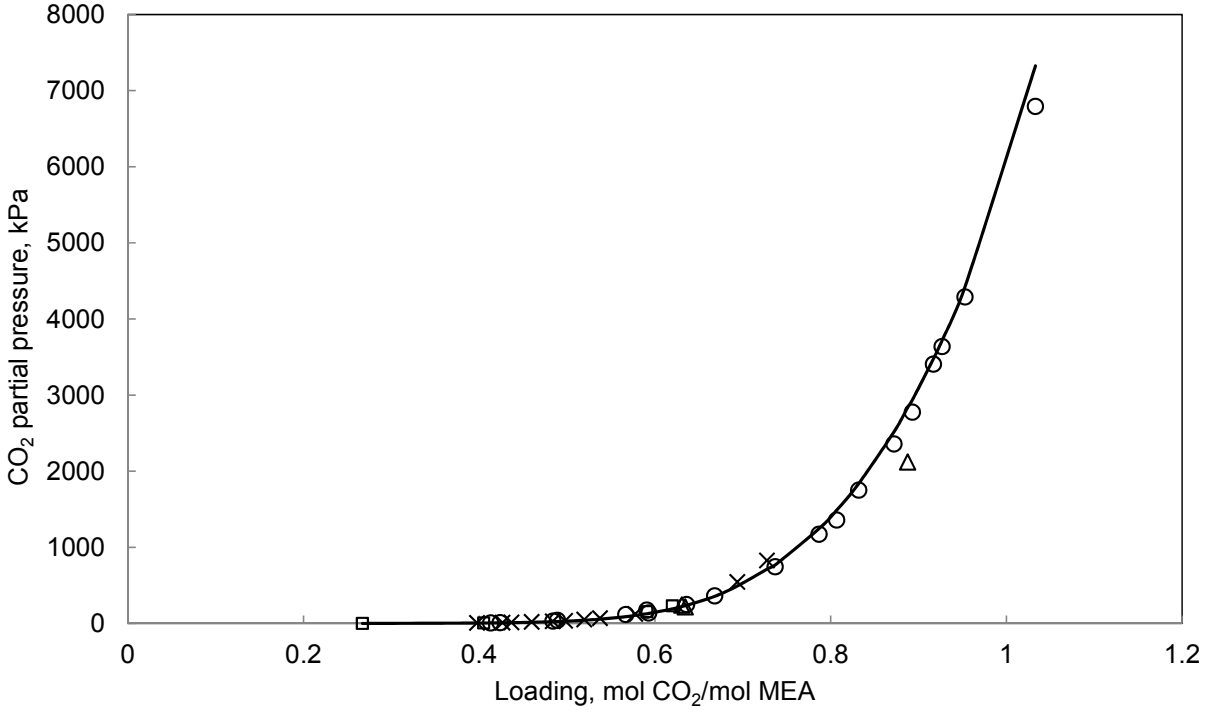

Figure 4-36. Comparison between experimental and regressed CO_2 solubility in 15 wt % aqueous MEA solutions at 80 °C. Symbols stand for the experimental data and curve (line) refers to the represented values using the developed thermodynamic model. ○**,** (Shen and Li 1992)**;** □**,** (Austgen et al. 1991)**;** Δ**,** (Lawson and Garst 1976)**;** ×**,** (Jones et al. 1959)

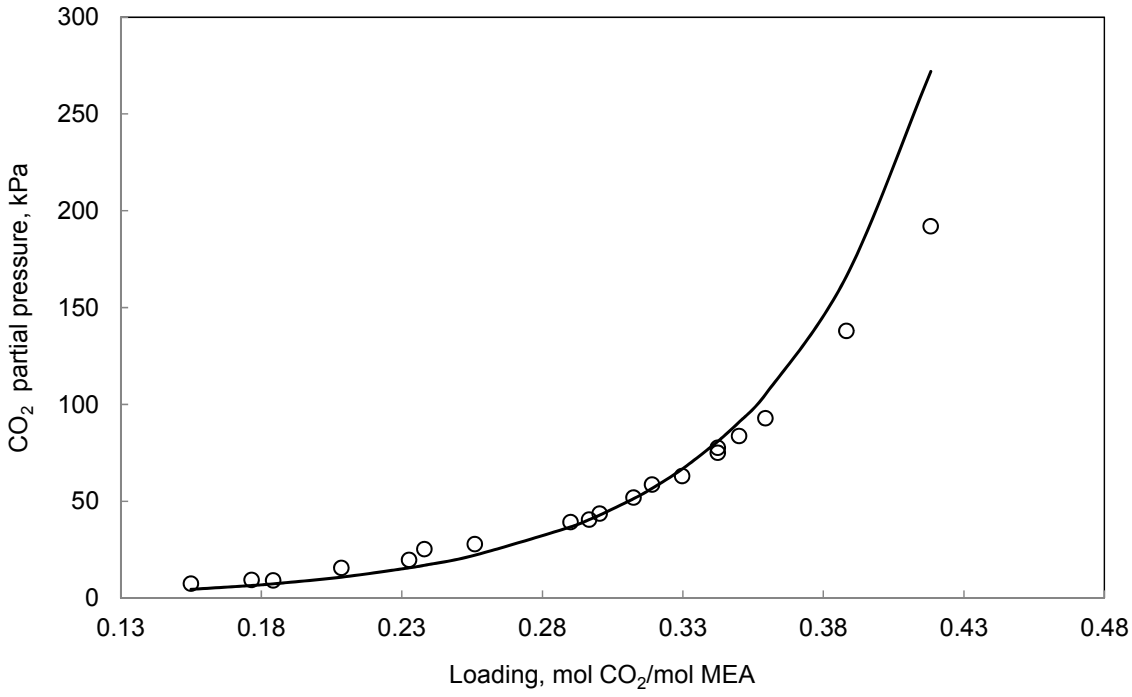

Figure 4-37. Comparison between experimental and regressed CO_2 solubility in 30 wt % aqueous MEA solutions at 120 °C. Symbols stand for the experimental data and curve (line) refers to the represented values using the developed thermodynamic model.○**,** (Ma'mun et al. 2005)

All in all model represent CO_2 solubility in aqueous MEA solution within 25% AARD.

4.8.3.2 Heat of Absorption Data, Regression and Prediction Results

Figure 4-38 presents the result of fit for heat of CO_2 absorption data at 40, 80 and 120 °C, in 30wt % aqueous MEA solutions.

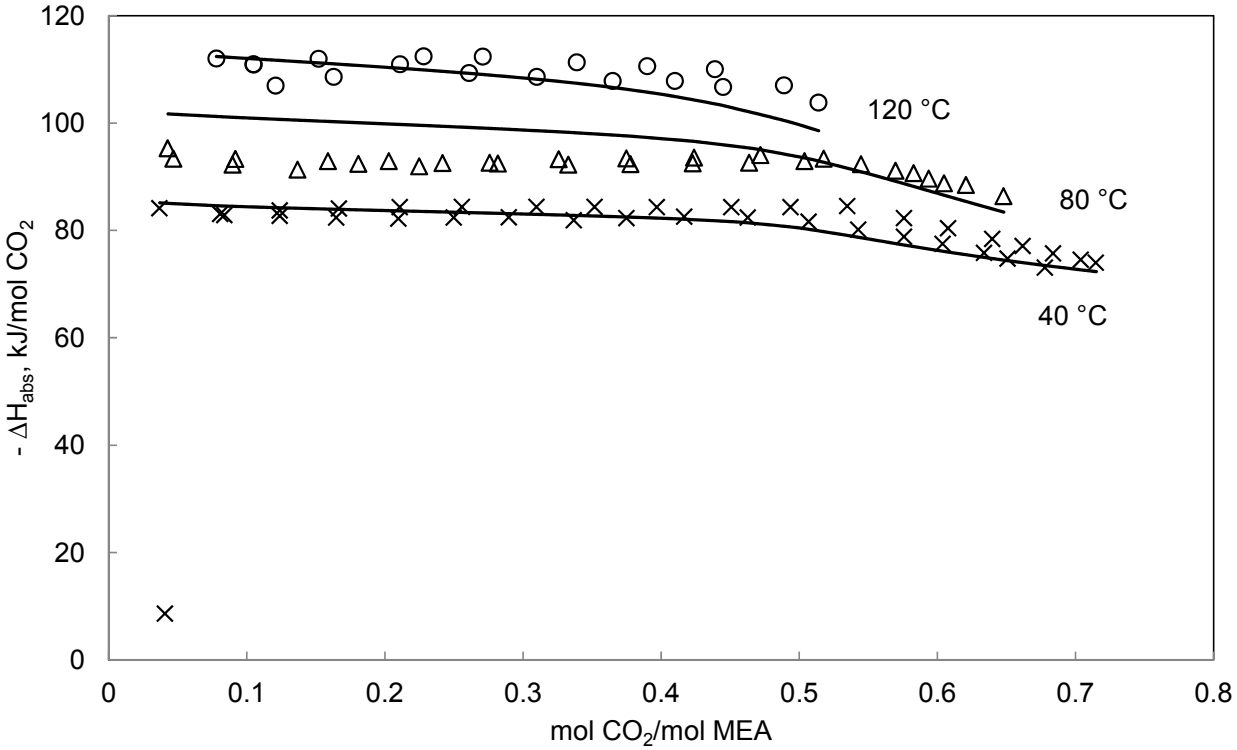

Figure 4-38. Comparison of the enthalpy of CO_2 absorption at 40, 80 and 120 °C and in 30 wt % aqueous MEA solutions. Symbols stand for the experimental data and curves (lines) refer to the represented values using the developed thermodynamic model. × (T = 40 °C), Δ (T = 80 °C), ○ (T = 120 °C), (Kim and Svendsen 2007)

As it is shown in Figure 4-38 the agreement between model and experiments are satisfactory. All in all model represents CO_2 heat of absorption in aqueous MEA solutions within 7.63 AARD %.

4.8.3.3 Freezing Point Depression Data and Regression Results

Figure 4-39 shows results of fit for freezing point of CO_2 loaded aqueous MEA solution for MEA concentration of 30 wt %. Experiments were performed at CERE laboratories. These measurements have been used simultaneously to regress model parameters. Including these data in the regression data base improve model capability to represent freezing point of the loaded solution.

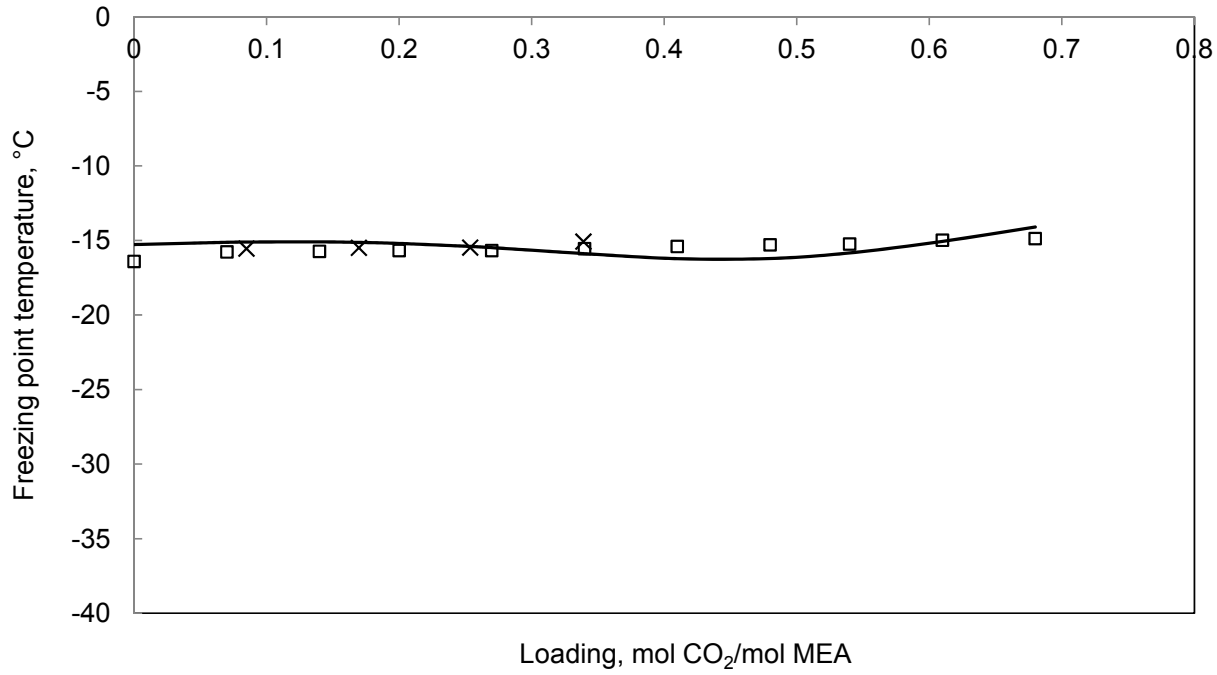

Figure 4-39. Comparison between estimated and experimental freezing point in 30 wt % aqueous MEA solutions. Symbols stand for the experimental data and curve (line) refers to the represented values using the developed thermodynamic model. ×,(Source1)**;** □**,** (Source2)

4.8.3.4 NMR Speciation Data and Prediction Results

This section show model predictions for NMR speciation data, like MDEA system these data have not been used for regression model parameters. Figure 4-40 plots model predictions against NMR speciation datain30 wt % MEA and at 40 °C. Due to fast proton transfer between MEA and MEA protonated, it was not possible to experimentally determine MEA and $MEAH^+$ concentrations, therefore only sum of MEA and $MEAH^+$ concentrations were presented by (Boettinger et al. 2008). Despite this, the model can calculate concentration of all constituents of liquid phase. Figure 4-41 shows model predictions for liquid phase distribution in solution of CO_2-MEA-H_2O for 30 wt % MEA and at 40 °C.

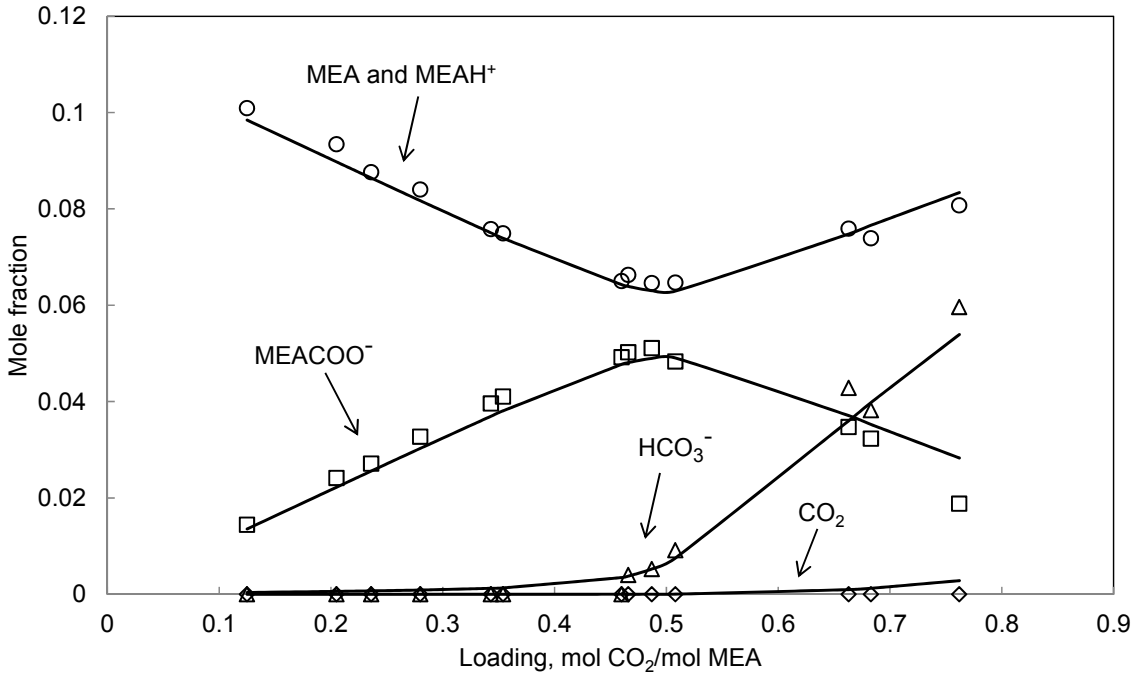

Figure 4-40. Comparison between model predictions and speciation NMR data at 40 °C and in 30 wt % MEA. Symbols stand for the experimental data and curves (lines) refer to the calculated values using the developed thermodynamic model.○ (MEA and $MEAH^+$), Δ (HCO_3^-), □ ($MEACOO^-$), ◊(CO_2) ,(Boettinger et al. 2008)

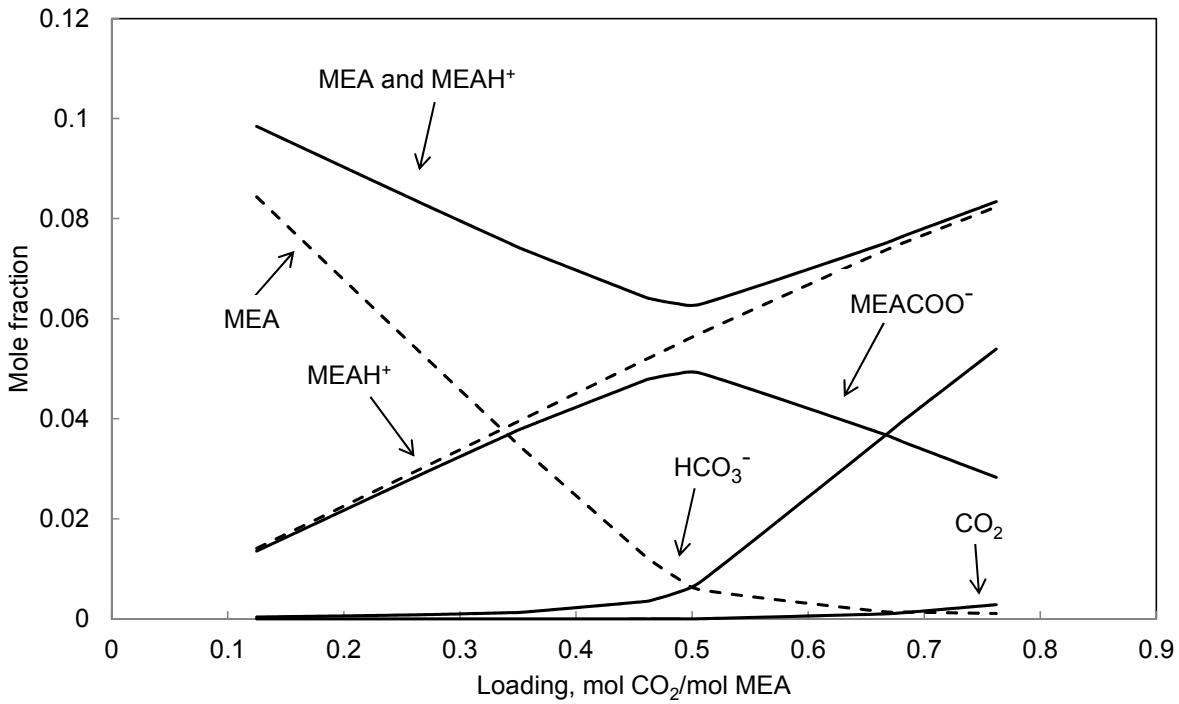

Figure 4-41. Model predictions for liquid phase distribution in CO_2-MEA-H_2O solution at 40 °C and in 30 wt % MEA.

When CO_2 is added to the system, many reactions will occur in the system. Reactions between CO_2 and aqueous MEA form $MEACOO^-$ and $MEAH^+$ as primary products. The concentration of MEA drops while the MEA carbonate and MEA protonated concentrations rise. At loading around 0.5 MEA concentration almost becomes zero since MEA totally consumed by the reactions. However $MEAH^+$ concentration continues to increase with the loading. Thus $MEACOO^-$ starts to decline after loading 0.5. This makes more MEA available for the formation of $MEAH^+$. It also creates more HCO_3^- and consequently more CO_2. Table 4-25 shows deviations between model predictions and NMR speciation data from (Boettinger et al. 2008) for the concentration of the species present in the liquid phase.

Table 4-25. AARD % for the NMR speciation data

Species	AARD%
MEA and $MEAH^+$	2.40
$MEACOO^-$	9.21
HCO_3^-	4.12

Figure 4-41 illustrates that the model has done a good job fitting NMR data considering no parameters were regressed upon these data. Modeling results reveal that the model can accurately predict distribution of the liquid phase.

4.8.4 Comparison between Different Models

This section compare the results of the developed Extended UNIQUAC model in this study with the Extended UNIQUAC model with parameters from (Faramarzi et al. 2009) and e-NRTL model with parameters from (Hessen et al. 2010). Table 4-26 shows comparison between different models results for some selected sources for CO_2 solubility in aqueous MEA solutions.

Table 4-26. Comparison between different models results for CO_2 solubility in aqueous MEA solutions

Reference	MDEA Concentration, wt %	Temperature, °C	Pressure, kPa	AARD%		
				This Study	(Faramarzi et al. 2009)	(Hessen et al. 2010)
(Austgen et al. 1991)	15.17	40, 80	0.09 to 228.7 (P_{CO_2})	13	36	28
(Shen and Li 1992)	15.29, 30	40, 60, 80, 100	1.1 to 2550 (P_{CO_2})	19	29	53
(Maddox et al. 1987)	15.17	25, 60, 80	6.48 to 6085.46 (P_{CO_2})	13	15	Na*
(Ma'mun et al. 2005)	30	120	7.3 to 191.9 (P_{CO_2})	16	64	31

Na : Not available

4.9 Blend of MDEA and MEA System

As it mentioned earlier, only binary interaction parameter between MDEA and MEA has been regressed to the experimental data for the blend systems and the rest of the parameters remained fixed at the determined values for subsystems. 397 data points including different kinds of data that have been used for regression MDEA-MEA interaction parameter. Next sections show data that used for regression model parameters and regression results.

4.9.1 Ternary MDEA-MEA-H_2O Data and Regression Results

Ternary MDEA-MEA-H_2O data including total pressure, freezing point and heat capacity have been used for model parameter determination. Table 4-27 lists the data sets upon which the parameters are regressed. In what follows modeling results for different kind of data have been shown.

Table 4-27. Review over ternary MDEA-MEA-H_2O data used for model parameter regression

MDEA /MEA Concentration, mole fraction/mole fraction	T ,°C	P, kPa	Data Type	Reference	Number of Data Points	AARD %
3, 1, 0.33	40 to 100	5.98 to 90.3 (P_{Total})	VLE	(Kim et al. 2008)	12	0.50
0.25 to 4	30 to 80	Na*	C_p	(Chen et al. 2001)	176	3.76
0.25 to 4	-0.96 to -20.15	Na*	Freezing Point	(Fosbol et al. 2011)	32	3.58

Na: Not Available

4.9.1.1 Total Pressure Data and Regression Results

Total pressure data of (Kim et al. 2008) have been used to regress binary interaction parameter between MEA and MDEA. Results of the fit are shown in Figure 4-42.

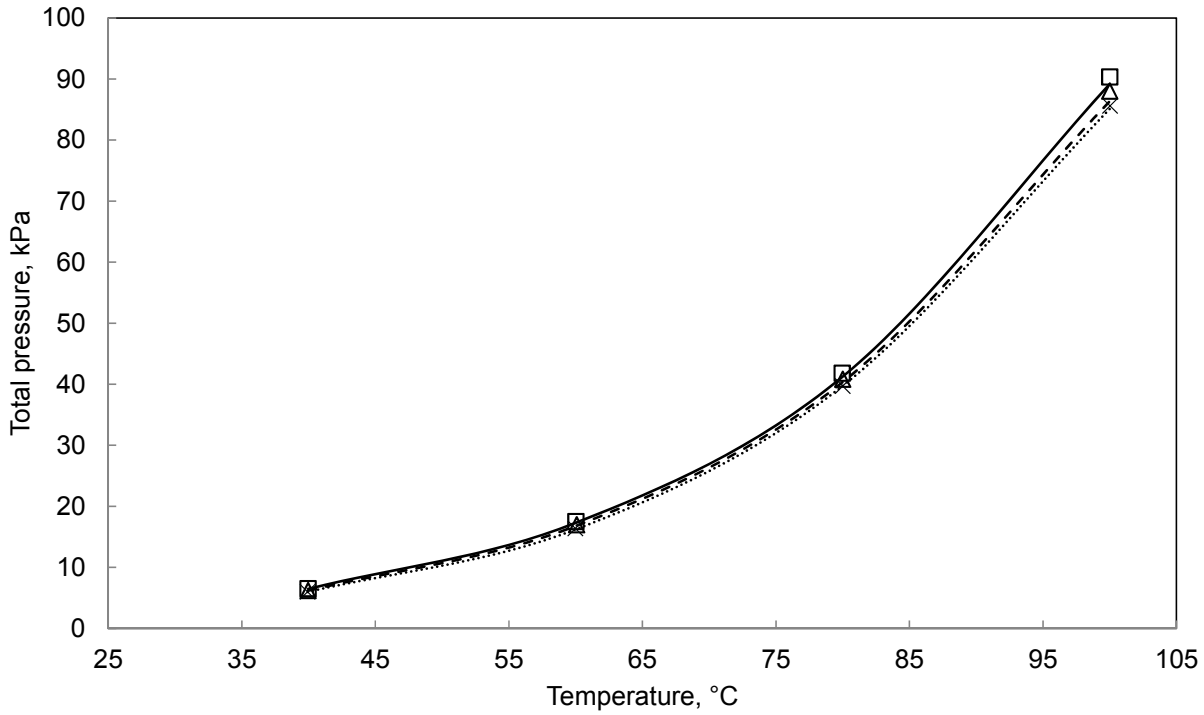

Figure 4-42. Comparison between estimated and experimental total pressure of MDEA-MEA-H_2O solutions. Symbols stand for the experimental data and curves (lines) refer to the calculated values using the developed thermodynamic model. □ (MDEA mole fraction/ MEA mole fraction = 3), Δ(MDEA / MEA mole fraction = 1), × (MDEA mole fraction / MEA mole fraction = 0.33), (Kim et al. 2008)**; Solid line (MDEA mole fraction / MEA mole fraction = 3), Dash line (MDEA mole fraction / MEA mole fraction = 1), Dot line (MDEA mole fraction / MEA mole fraction = 0.33)**

As it can be seen from the above figure agreement between experimental and estimated values by are very satisfactory.

4.9.1.2 Heat Capacity Data and Regression Results

Heat capacity data from (Chen et al. 2001) for mixtures of MDEA-MEA-H_2O have been used to tune MDEA-MEA binary interaction parameters. Figure 4-43 plots estimated values against the experimental data at water mole fraction of 0.4.

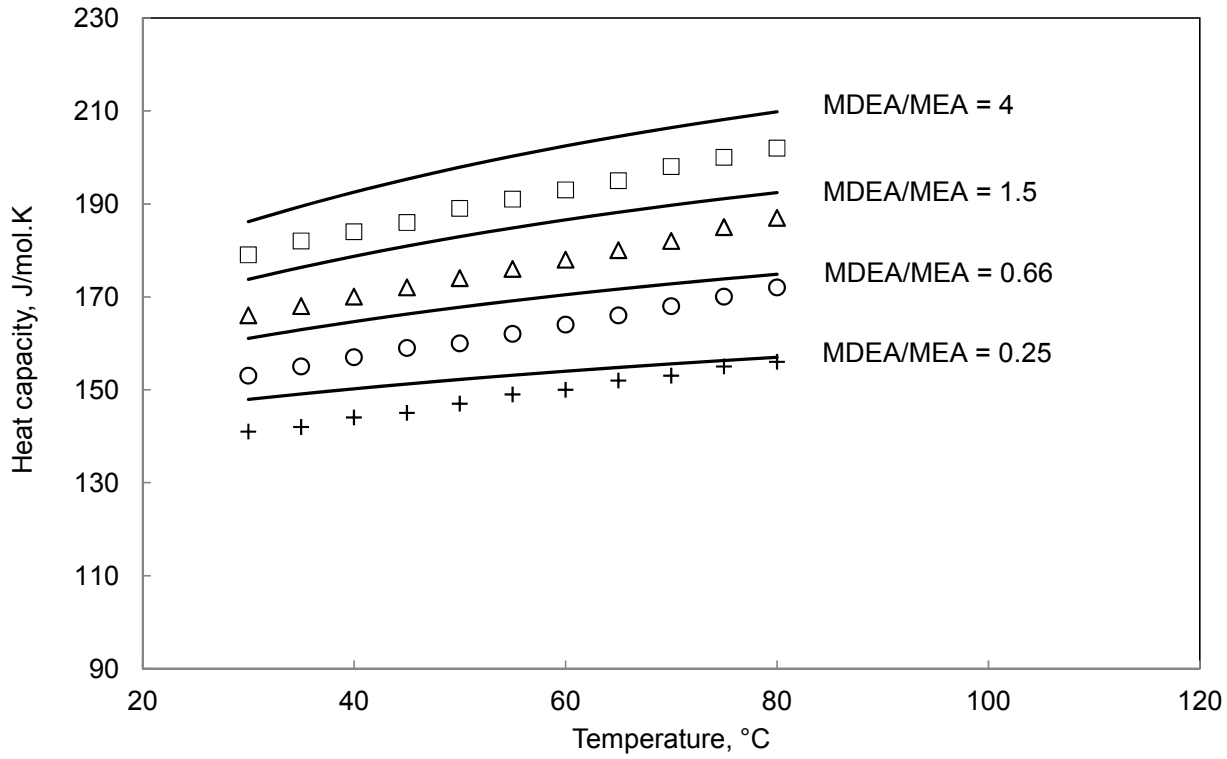

Figure 4-43. Heat capacity of MDEA-MEA-H_2O solutions for water mole fraction = 0.4. Symbols stand for the experimental data and curves (lines) refer to the calculated values using the developed thermodynamic model. □ (MDEA molality / MEA molality = 4), Δ (MDEA molality / MEA molality = 1.5), ○ (MDEA molality / MEA molality = 0.66), + (MDEA molality / MEA molality = 0.25),(Chen et al. 2001)

Results of fit show that heat capacity of aqueous mixture of MDEA and MEA are well described by the developed model.

4.9.1.3 Freezing Point Data and Regression Results

Freezing point depression data of (Fosbol et al. 2011) have been simultaneously used to regress binary interaction parameter between MDEA and MEA. Regression results are plotted in Figure 4-44.

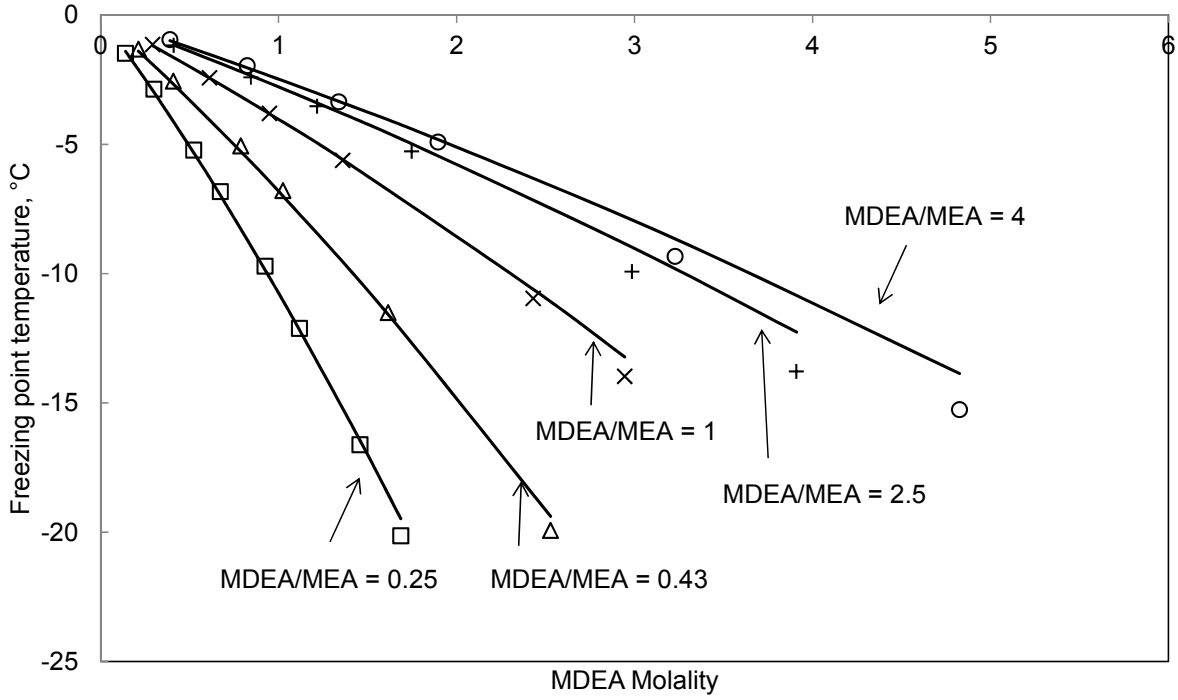

Figure 4-44.Freezing point of MDEA-MEA-H_2O solutions. **Symbols stand for the experimental data and curves (lines) refer to the calculated values using the developed thermodynamic model. □ (MDEA molality / MEA molality = 0.25), Δ (MDEA molality / MEA molality = 0.43), × (MDEA molality / MEA molality =1), + (MDEA molality / MEA molality = 2.5), ○ (MDEA molality / MEA molality = 4),** (Fosbol et al. 2011)

4.9.2 Quaternary CO_2-MDEA-MEA-H_2O Data and Regression Results

CO_2 solubility data in aqueous mixture of MDEA and MEA have been used to regress binary interaction parameter between MDEA and MEA. Table 4-28 shows quaternary data that have been used for regressing model parameters. Next section will present modeling results.

Table 4-28. Review over quaternary CO_2-MDEA-MEA-H_2O regressed data

MDEA /MEA Concentration, mole fraction/mole fraction	T ,°C	P, kPa	Data Type	Reference	Number of Data Points	AARD %
0.76, 0.12	40, 60, 80, 100	0.9 to 2016(P_{CO_2})	VLE	(Shen and Li 1992)	94	54
4.25, 1	70, 100, 120, 140, 160, 180	137 to 3876 (P_{CO_2})	VLE	(DAWODU and MEISEN 1994)	68	52
1	40,80	0.05 to 258.2 (P_{CO_2})	VLE	(Austgen et al. 1991)	15	42

4.9.2.1 CO_2 Solubility Data and Regression Results

This section shows result of fit for CO_2 solubility in aqueous mixture of MDEA and MEA. Figure 4-45 compares results of fit with experimental data from (Austgen et al. 1991).

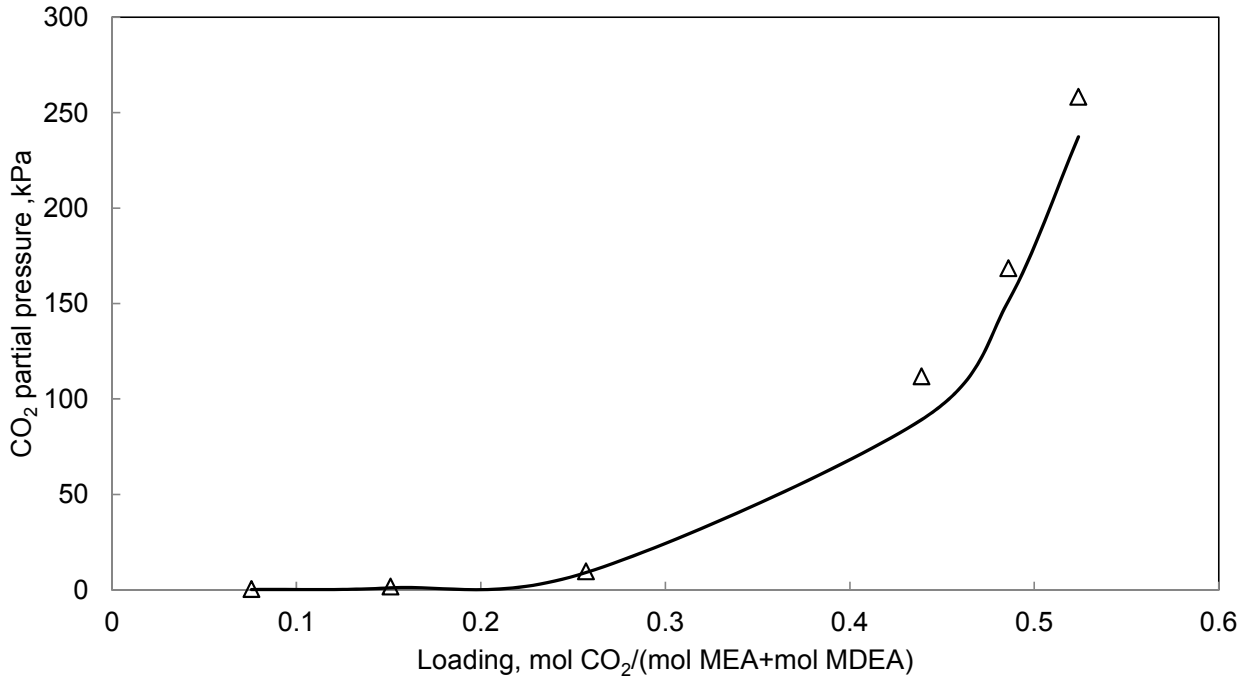

Figure 4-45. Comparison between estimated and experimental values of CO_2 solubility in aqueous mixture of MDEA-MEA at 80 °C and with molar ratio of 1. Symbols stand for the experimental data and curve (line) refers to the calculated values using the developed thermodynamic model. Δ (MDEA molality /MEA molality = 1), (Austgen et al. 1991)

All in all, model describes CO_2 partial pressure in aqueous MDEA-MEA solution within 49 % average absolute relative deviation.

4.10 Conclusion

In this chapter developed thermodynamic models for MDEA-H_2O, MEA-H_2O, MDEA-MEA-H_2O, CO_2-MDEA-H_2O, CO_2-MEA-H_2O and CO_2-Blend of MDEA and MEA-H_2O systems and modeling results has been discussed. Three improvements were utilized in this model and parameters were fitted to a more various and extensive data base than the previous model. The experimental data available in the open literature were found to be discrepant and scattered, the regression data base was selected after evaluation of the available data. The model for the CO_2-amine-H_2O system begins with a strong model for the amine-water system. Binary interaction parameters for the MDEA-H_2O and MEA-H_2O subsystems have been regressed to experimental data on total pressure,

excess enthalpy, heat capacity and freezing point. Including different kinds of data for regression process, improve model predictions of amine activity coefficient in aqueous amine solutions. Amine activity coefficients are required to calculate amine concentration in the vapor phase, also are important in the acid gas VLE calculations (Posey 1997). Good values for amine activity coefficients lead to accurate estimation of amine losses from the top of the absorber which is one of important operational considerations. The overall fit of the two subsystems were quiet good and the developed models adequately represent thermodynamic and thermal properties of the subsystems. The models also properly predict amine volatility. After modeling amine-water subsystems, interaction parameters for the CO_2-amine-water systems were regressed to experimental total pressure, CO_2 partial pressure, heat capacity, heat of absorption and in case of MEA system, freezing point data. The models were confirmed to be able to represent thermodynamic and thermal properties over a broad range of conditions. After developing a rigorous model for CO_2-MDEA-H_2O and CO_2-MEA-H_2O systems, binary interaction parameter between MDEA and MEA was adjusted to experimental total pressure, freezing point and heat capacity of MDEA-MEA-H_2O systems, CO_2 solubility data in aqueous MDEA-MEA mixture were also used to tune MDEA-MEA interaction parameter. All in all results of fit for CO_2-blend of MDEA and MEA-water system were found to be satisfactory, although the deviations are larger than binary and ternary systems.

Overall the results presented above indicate that the developed model, through simultaneous regression to different kind of data, gave a set of optimum parameters for MDEA-H_2O, MEA-H_2O, MDEA-MEA-H_2O, CO_2-MDEA-H_2O, CO_2-MEA-H_2O and CO_2-MDEA-MEA-H_2Osystems. The developed models adequately represent thermodynamic and thermal properties of the systems. Modeling results show that the developed models improved significantly over previously existing models.

Chapter 5

Thermodynamic Modeling of H_2S-MDEA-H_2O and H_2S-MDEA-CH_4-H_2O Systems

5 Thermodynamic Modeling of H_2S-MDEA-H_2O and H_2S-MDEA-CH_4-H_2O Systems

5.1 Chapter Overview

The goal of this chapter is to develop a thermodynamic model that can represent thermodynamic and calorimetric properties of H_2S-MDEA-H_2O and H_2S-CH_4-MDEA-H_2O systems over a wide range of temperature, pressure, acid gas loading and amine concentration. The modeling of H_2S system is more difficult and complicated than CO_2 system due to the fact that much less data is available for H_2S systems and also because the concentration of some of the present ions in the system is very small. In the petroleum industry, aqueous solutions of alkanolamines are generally used to remove acid gases (H_2S and CO_2) from gas streams. Among alkanolamines, MDEA is the most preferable amine in acid gas treating process. The main advantage of MDEA over other amines is its capability for selective removal of H_2S from its mixture with CO_2. The selectivity of absorption is due to the higher rate of the reaction of MDEA with H_2S than the reaction of MDEA with CO_2 (Anufrikov et al. 2007). H_2S has H^+ that can give directly to MDEA; the proton transfer reaction is always fast and spontaneous. Moreover, comparing to other amines, MDEA is more stable, less volatile and less corrosive, it has lower heat of reaction and higher absorption capacity (Anufrikov et al. 2007). Precise representation of the thermodynamic data for the acid gas-MDEA-water system is required for a better design and operation of acid gas treating process. Because of MDEA wide application in acid gas treating industry, it was determined that this chapter would emphasis modeling MDEA. In natural gas cleaning industry, generally in the absorber column the pressure is high and generally hydrocarbons, mainly methane, are encountered, therefore it is important to model methane effect on the solubility of acid gas in aqueous MDEA solutions. This chapter describes modeling methodology, data regression and model predictions for H_2S-H_2O, CH_4-H_2O, H_2S-MDEA-H_2O and H_2S-CH_4-MDEA-H_2O systems.

The regression of data to pure H_2S and H_2S-H_2O binary subsystem are discussed first. Based on the proposed model for H_2S-H_2O and MDEA-H_2O subsystems (MDEA-H_2O model was already discussed in chapter 4) the model is further developed for H_2S-MDEA-H_2O systems. Afterwards, modeling of CH_4-H_2O system is presented. The last section describes model predictions for H_2S-CH_4-MDEA-H_2O and CO_2-CH_4-MDEA-H_2O systems. Finally the methane effect on acid gas equilibrium is investigated.

5.2 Evaluation of Parameters

This section represents the fitting procedure, selection of interaction parameters for fitting and the regressed value of parameters.

5.2.1 Fitting Procedure

Available data in the open literature were first evaluated and then used to regress model parameters. Regressed data include pure H_2S vapor pressure, VLE (total and partial pressure) and heat of absorption (H_{abs}). As previously explained, all the regressed parameters belong to UNIQUAC model and no adjustable parameter is considered for Debye-Huckel and SRK terms. Table 5-1 shows weighting factors that have been used for VLE, pure H_2S vapor pressure and heat of absorption data in the objective function (objective function is already illustrated in chapter 4). The choice of values for weighting factors stems from the experience with the model and also depends on the quality and reliability of different kinds of data.

Table 5-1. Weights for different kinds of data in the objective function used for estimation model parameters

Data Type	Weight Number
VLE*	0.05 (bar)
Pure H_2S vapor pressure	0.0075 (bar)
Heat of H_2S absorption	0.02 (J)

**Total and partial pressure data used for regression parameters of H_2S-H_2O, CH_4-H_2O, H_2S-MDEA-H_2O systems.*

Optimization model parameter for H_2S-MDEA-H_2O system is not a trivial task. After trying different optimization methods it was found out that the best approach for optimizing parameters of H_2S-MDEA-H_2O system comprise of two steps. In the first step, r and q parameters and effective interaction parameters in the binary system were being fitted to the pure H_2S vapor pressure and binary H_2S-H_2O data, eventually the effective interaction parameters in the ternary system are tuned to the ternary data while the rest of the parameters were retained at the best adjustable values obtained in previous step. In the other words, first a strong model for H_2S-H_2O binary system is

proposed, and based on the H_2S-H_2O binary model, a model for H_2S-MDEA-H_2O is developed. All in all, 8 parameters (including 4 pure component (r and q) and 4 interaction parameters) for H_2S-H_2O binary subsystem were adjusted to the experimental data. H_2S-H_2O model parameters were fitted to pure H_2S vapor pressure data, total pressure data of H_2S-H_2O system and H_2S solubility in water data (H_2S partial pressure). H_2S solubility and heat of H_2S absorption data in aqueous MDEA have been used to regress10 interaction parameters involved in ternary H_2S-MDEA-H_2O system. Altogether, 18 parameters were adjusted to model the behavior of H_2S-MDEA-H_2O system (8+10=18). For the CH_4-H_2O system, totally 4 parameters including r and q parameters for methane and CH_4-H_2O binary interaction parameters (u^0 and u^T) were fitted to binary total pressure data of CH_4-H_2O system. Regressed parameters for H_2S-MDEA-H_2O and CH_4-H_2O systems have been used to model (predict) the behavior of H_2S-CH_4-MDEA-H_2O system, no additional parameters is going to be adjusted on quaternary H_2S-CH_4-MDEA-H_2O data.

5.2.2 Determination of Effective Interaction Parameters, Selection of Interaction Parameters for Fitting

In the H_2S-MDEA-H_2O system, there are 3 molecular and 5 ionic species present in the liquid phase, for H_2S-CH_4-MDEA-H_2O system, one more component (CH_4) is added to the number of molecular species present in the liquid solution. Hence an achingly large number of possible interactions could be formulated in the system. For example in the system of CO_2-H_2S-primary or secondary amine-H_2O, 78 possible interactions (by considering for symmetry) could be specified (Weiland et al. 1993). Fitting this large number of parameters is not a realistic goal. Therefore, it is necessary to disregard ineffective interaction parameters in order to reduce the number of fitting parameters to a manageable set. Knowing the chemistry of solution and calculating concentration of species in ideal solution helps to discard ineffective parameters. Concentration of some of the species is quiet small, thus, parameters associated with them have negligible effect on representation the behavior of system (when the concentration is low, even if the interactions were strong, they make negligible contribution to the total interaction term). The choice of important parameters of the system, those that affected representation of system behavior, arises from experience with the model, sensitivity studies of parameters and necessity to adequately fit the experimental data. Finally, the following set of effective parameters was chosen to tune to experimental data. Values of effective interaction parameters were shown in

Table 5-3 and Table 5-4, for ineffective interaction parameters u^0 is fixed at 0 and u^T is assigned at 10^{10}.

- **H_2S- H_2O System**
  - ✓ H_2S-H_2S
  - ✓ H_2S-H_2O
- **H_2S-MDEA-H_2O System**
  - ✓ MDEA-HS^-
  - ✓ $MDEAH^+$-HS^-
  - ✓ HS^--HS^-
  - ✓ MDEA-H_2O (Determined in previous chapter)
  - ✓ MDEA-MDEA (Determined in previous chapter)
  - ✓ $MDEAH^+$-H_2O (Determined in previous chapter)
- **CH_4- H_2O System**
  - ✓ CH_4-H_2O

The mentioned interaction parameters were fitted to the experimental data, by using the fitting procedure illustrated in section 5.2.1, values of adjusted parameters are presented in section 5.2.3.

5.2.3 Fitted Parameters

The parameters required by the UNIQUAC equation for modeling the H_2S-MDEA-H_2O and H_2S-CH_4-MDEA-H_2O system include volume parameter, r, surface parameter, q, for the components present in the liquid phase and the binary interaction parameters representing energies of interaction between liquid phase species. Model parameters were adjusted to the evaluated data base (regression data base will be discussed in section 5.3). In following section the best adjusted values for the parameters involved in H_2S-MDEA-H_2O and CH_4-H_2O system (required for predicting the behavior ofH_2S-CH_4-MDEA-H_2O system) will be presented.

5.2.3.1 H_2S-MDEA-H_2O System

This section illustrates the proposed equations to correlate H_2S solubility in aqueous MDEA solution. Modeling the behavior of such a system is rather complex as chemical and physical equilibria are coupled. To do the thermodynamic modeling of this system rigorously, both physical and chemical equilibrium should be taken into account.

Physical Equilibrium

As it mentioned, physical equilibrium should be included in equilibrium representation of the system. Dissolution of gaseous H_2S into the solution and vaporization of liquid MDEA and water creates the following vapor-liquid equilibria equations:

$$H_2S(aq) \leftrightarrow H_2S\,(g) \tag{5.1}$$

$$H_2O(l) \leftrightarrow H_2O(g) \tag{5.2}$$

$$MDEA(aq) \leftrightarrow MDEA\,(g) \tag{5.3}$$

Chemical Equilibrium

Dissolution of H_2S in the aqueous MDEA solution is accompanied with different acidic and basic reactions which are listed below. "Due to chemical reactions in the solution hydrogen sulfide is dissolved in the liquid phase not only in neutral, but also in nonvolatile, ionic form (Kuranov et al. 1996)."

Water dissociation: $H_2O\,(l) \leftrightarrow OH^-(aq) + H^+(aq)$ (5.4)

Hydrogen sulfide dissociation: $H_2S(aq) \leftrightarrow H^+(aq) + HS^-(aq)$ (5.5)

Bisulfide ion dissociation: $HS^-(aq) \leftrightarrow H^+(aq) + S^{2-}(aq)$ (5.6)

S^{2-} concentration is very small in the solution since dissociation constant for equation (5.6) is three to four orders of magnitude smaller than the dissociation constant for equation (5.5). Ideal solution calculations also show the concentration of sulfide ion is extremely low. Owing to the extremely low concentration of S^{2-} in the aqueous phase, its presence in the aqueous phase is neglected; hence reaction (5.6) is disregarded. This realistic assumption yields to reduce the number of adjustable interaction parameters. Table 5-2 and Table 5-4 represent parameters that have been determined in this work for modeling behavior of H_2S-MDEA-H_2O system. Table 5-2 shows determined UNIQUAC r and q parameters for the components present in the liquid phase.

Table 5-2. UNIQUAC volume parameter (r) and surface area parameter (q). Bold parameters are obtained in this work.

Species	r	q
MDEA	Table 4.2	Table 4.2
$MDEAH^+$	Table 4.2	Table 4.2
H_2O	Table 4.2	Table 4.2
OH^-	Table 4.2	Table 4.2
H^+	Table 4.2	Table 4.2
H_2S	**0.64453**	**0.11014**
HS^-	**9.9317**	**15.031**

Table 5-3 and Table 5-4 list u_{ij}^0 and u_{ij}^T parameters determined for calculating UNIQUAC binary interaction energy parameters $(u_{ij} = u_{ji} = u_{ij}^0 + u_{ij}^T (T - 298.15))$ for the named pairs, respectively. For the pairs that are less probable to coexist in the mixture u_{ij}^0 and u_{ij}^T values has been set to a large value and zero, respectively. These assigned values eliminate the effect of these parameters over other parameters.

Table 5-3. $u_{ij}^0 = u_{ji}^0$ Parameters for calculating UNIQUAC interaction energy parameters. Values in bold are obtained in this work.

Species	H_2O	H_2S	MDEA	OH^-	H^+	HS^-	$MDEAH^+$
H_2O	Table 4.3						
H_2S	**-183.341**	**-1499.484**					
MDEA	Table 4.3	**10^{10}**	Table 4.3				
OH^-	Table 4.3	**10^{10}**	Table 4.3	Table 4.3			
H^+	Table 4.3	**10^{10}**	Table 4.3	Table 4.3	Table 4.3		
HS^-	**113.5498**	**10^{10}**	**-216.2905**	**10^{10}**	**10^{10}**	**58.7296**	
$MDEAH^+$	Table 4.3	**10^{10}**	Table 4.3	Table 4.3	Table 4.3	**-51.41282**	Table 4.3

Table 5-4. $u_{ij}^T = u_{ji}^T$ Parameters for calculating UNIQUAC interaction energy parameters. Values in bold are obtained in this work.

Species	H_2O	H_2S	MDEA	OH^-	H^+	HS^-	$MDEAH^+$
H_2O	Table 4.4						
H_2S	**-5.8785**	**-31.563**					
MDEA	Table 4.4	**0**	Table 4.4				
OH^-	Table 4.4	**0**	Table 4.4	Table 4.4			
H^+	Table 4.4	**0**	Table 4.4	Table 4.4	Table 4.4		
HS^-	**-0.76892**	**0**	**-0.1475**	**0**	**0**	**-0.93466**	
$MDEAH^+$	Table 4.4	**0**	Table 4.4	Table 4.4	Table 4.4	**-4.993**	Table 4.4

Values of standard state heat capacity of species present in the aqueous phase and gas phase are presented in Table 5-5 and Table 5-6, respectively.

Table 5-5. Standard state heat capacity parameters for species in aqueous phase, C_{pi}^0 (J mol^{-1}K^{-1}).

Species	a (J mol^{-1} K^{-1})	b (J mol^{-1} K^{-2})	c (J mol^{-1})
H_2S (aq)	110	0	0
HS^- (aq)	-94[a]	0[a]	0[a]
MDEA (aq)	Table 4-5	Table 4-5	Table 4-5
$MDEAH^+$(aq)	Table 4-5	Table 4-5	Table 4-5
H_2O (l)	Table 4-5	Table 4-5	Table 4-5
OH^-(aq)	Table 4-5	Table 4-5	Table 4-5
H^+(aq)	Table 4-5	Table 4-5	Table 4-5

[a] (Marcus 1997)

Table 5-6. Standard state heat capacities of species in the gas phase C_{pi}^0 (J mol^{-1}K^{-1})

Species	a (J mol^{-1} K^{-1})
H_2S(g)	34.23[a]
MDEA (g)	Table 4-6.
H_2O (g)	Table 4-6.

[a] (NIST)

Values of standard state Gibbs free energy of formation (G_f^0) and standard state Enthalpy of formation (H_f^0) are presented in Table 5-7.

Table 5-7. Standard state properties G_f^0 and H_f^0 in (kJ mol^{-1}) at T = 25 °C

Species	G_f^0(kJ mol^{-1})	H_f^0(kJ mol^{-1})
H_2S(aq)	-27.83[a]	-39.7[a]
HS^- (aq)	12.08[a]	-17.6[a]
H_2S(g)	-33.56[a]	-20.63[a]
MDEA (aq)	Table 4-7	Table 4-7
MDEA (g)	Table 4-7	Table 4-7
$MDEAH^+$ (aq)	Table 4-7	Table 4-7
H_2O (l)	Table 4-7	Table 4-7
H_2O (g)	Table 4-7	Table 4-7
OH^-(aq)	Table 4-7	Table 4-7
H^+(aq)	Table 4-7	Table 4-7

[a] *(NIST)*

5.2.3.2 CH_4-H_2O System (Required for predictions of H_2S-CH_4-MDEA-H_2OSystem)

Methane dissolved only physically in the water. Therefore it is important to take the vapor-liquid equilibrium for the dissolved methane into account:

$$CH_4(g) \leftrightarrow CH_4(aq) \tag{5-7}$$

For modeling behavior of quaternary mixture of H_2S-CH_4-MDEA-H_2O, all the parameters were retained at the values determined for the ternary system and only the binary interaction parameter between CH_4 and H_2O has been fitted to the binary VLE data of CH_4-H_2O, r and q parameters for methane are taken from (Addicks 2002). Table 5-8 shows regressed parameters required for calculation of binary interaction parameter between CH_4 and H_2O.

Table 5-8 . $u_{ij}^0 = u_{ij}^0$ and $u_{ij}^T = u_{ij}^T$ parameters for calculating UNIQUAC energy interaction parameters. Values in bold are determined in this work.

Interaction parameter	u_{ij}^0	u_{ij}^T
CH_4-H_2O	**44.16483**	**1.4836**

Table 5-9 reports r and q parameters for CH_4which are taken from (Addicks 2002).

Table 5-9. UNIQUAC volume parameter (r) and surface area parameter (q)

Species	r	q
CH_4	5*	5*

* *(Addicks 2002)*

Values of standard state heat capacity of methane in the aqueous phase and gas phase are reported in Table 5-10.

Table 5-10. Standard state heat capacity parameters for species in aqueous phase, C_{pi}^0 (J $mol^{-1}K^{-1}$).

Species	a (J mol^{-1} K^{-1})	b (J mol^{-1} K^{-2})	c (J mol^{-1})
$CH_4(aq)$	0	0	0
$CH_4(g)$	35.309[a]	0	0

[a] *(NIST)*

Values of standard state Gibbs free energy of formation (G_f^0) and standard state Enthalpy of formation (H_f^0) for methane are presented in Table 5-11.

Table 5-11. Standard state properties G_f^0 and H_f^0 in (kJ mol^{-1}) at T = 25 °C

Species	G_f^0(kJ mol^{-1})	H_f^0(kJ mol^{-1})
$CH_4(aq)$	-34.33[a]	-89.04[a]
$CH_4(g)$	-50.72[a]	-74.81[a]

[a] (NIST)

5.3 Regression Data Base and Results

Comparing to the CO_2-H_2O and CO_2-MDEA-H_2O systems, the number of data available for H_2S-H_2O and H_2S-MDEA-H_2O are limited. Some of these available data show discrepancies. Therefore, before determining the model parameters values, it is crucial to create a reliable and consistent regression data base. It is necessary to omit the discrepant data as they would cause the fitting procedure to fail. In what follows the data that have been used for parameter estimation are discussed and compared with the modeling results. The parameters required for H_2S-MDEA-H_2O system were fitted based on totally 1353 data points. Pure H_2S vapor pressure data, VLE data of binary mixture of water and H_2S and ternary VLE and heat of absorption data have been used for regression model parameters. Binary VLE data of CH_4-H_2O system were used to regress binary interaction parameter between CH_4-H_2O. Finally the determined set of parameters has been used to predict the behavior of H_2S-CH_4-MDEA-H_2O system. Following sections will present different types of data and the regression results for pure H_2S vapor pressure, H_2S-H_2O molecular subsystem, H_2S-MDEA-H_2O ternary system, and CH_4-H_2O molecular subsystem. Results of model predictions for H_2S-CH_4-MDEA-H_2O quaternary system will be shown in last section.

5.4 H_2S-MDEA-H_2O ternary system

This section addresses regression data base and modeling results for H_2S-MDEA-H_2O ternary system. It includes regression results for developed H_2S-H_2O binary model and results of created model for H_2S-MDEA-H_2O ternary.

5.4.1 Pure H_2S Vapor Pressure Data and Regression Results

Table 5-12 provides an overview over experimental pure H_2S vapor pressure data used for parameter estimation, modeling results are also shown in this table. H_2S-H_2O model parameters have been regressed to totally 64 pure H_2Svapor pressure data points. As previously explained,

modeling H_2S-MDEA-H_2O ternary system starts with creating a model for H_2S-H_2O binary molecular subsystem. Pure H_2Svapor pressure data and binary H_2S-H_2O, VLE data were utilized to regress H_2S-H_2O model parameters.

Table 5-12. Regression results for H_2S pure vapor pressure

Temperature , °C	Reference Number	Number of Data Points	AARD %
4.44 to 100.39	(Reamer et al. 1950)	9	0.98
0 to 96.85	(West 1948)	19	1.04
0 to 100.4	(Cardoso 1921)	16	0.72
-28.51 to 29.98	(Clarke and Glew 1970)	20	0.39

Figure 5-1 compares the experimental and calculated H_2S pure vapor pressure.Overall, all the calculation results of the model for pure H_2S vapor pressure are within an AARD of 0.78 %

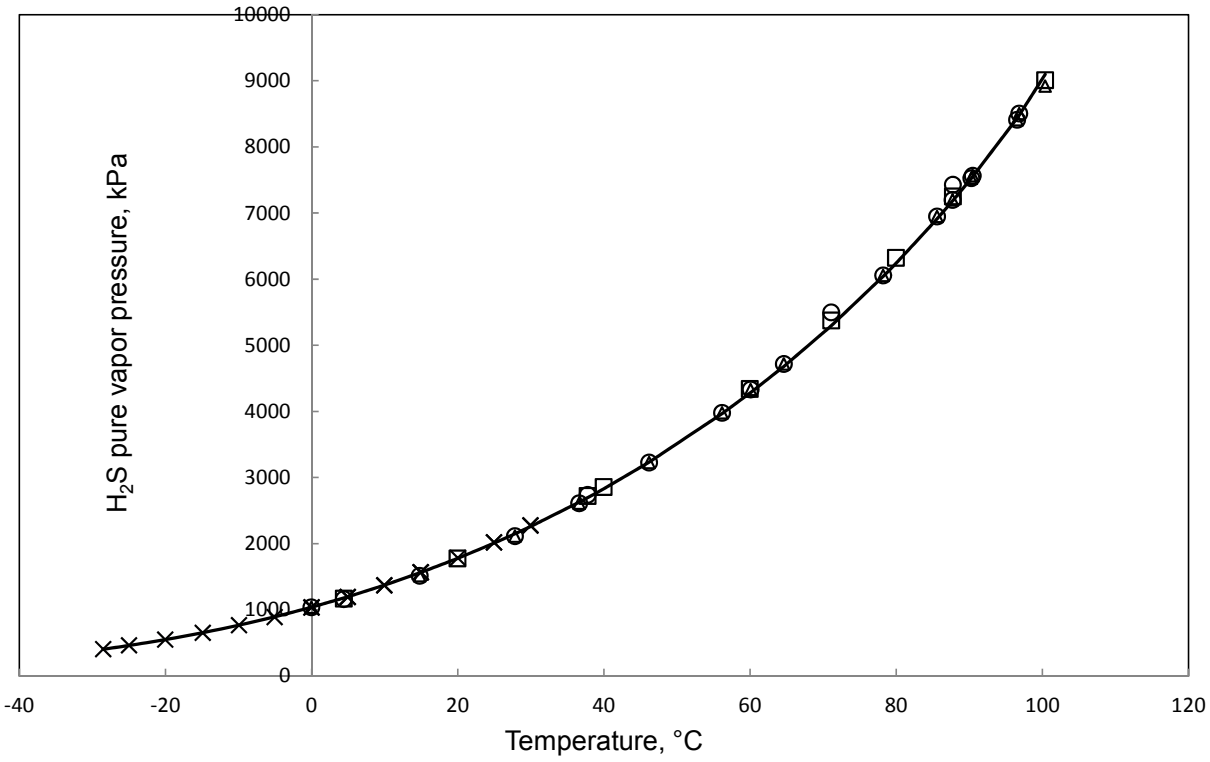

Figure 5-1. Comparison of model predictions with experimental pure H_2S vapor pressure data. Symbols stand for the experimental data and curve (line) refers to the calculated values using the developed thermodynamic model.○,(West 1948); Δ, (Cardoso 1921); □, (Reamer et al. 1950); ×, (Clarke and Glew 1970)

5.4.2 Binary H_2S-H_2O Data and Regression Results

499 binary H_2S-H_2O data points have been regressed to obtain the UNIQUAC parameters required to model H_2S-H_2O binary system. Total pressure and H_2S partial pressure data were used to determine model parameters. Table 5-13 shows H_2S-H_2O binary data upon which model parameters were regressed. Modeling results for different kind of data are given in following sections. Binary H_2S-H_2O data that have been used for adjusting model parameters are in agreement with each other and no point is eliminated from them. (Kuranov et al. 1996) compares their data with (Lee and Mather 1977) data; their comparison showed that relative deviation in total pressure is below 3 %. Evaluation analysis over these data and other data sources listed in Table 5-13 shows that regressed binary data are fairly accurate and in agreement with each other.

Table 5-13. Overview over binary H_2S-H_2O data

H_2SConcentration, wt %	T ,°C	P, kPa	Data Type	Reference	Number of Data Points	AARD %
0.81 to 6.43	25.01 to 65.19	483 to 3475 (P_{Total})	VLE	(Chapoy et al. 2005)	30	3.74
0.06 to 7.20	10 to 180	154.8 to 6670.4 (P_{Total})	VLE	(Lee and Mather 1977)	325	4.50
0.82 to 7.51	37.77 to 148.88	344.73 to 3102.64 (P_{Total})	VLE	(Gillespie and Wilson 1982)	11	5.18
1.12 to 5.53	40	470.4 to 2489.5 (P_{Total})	VLE	(Kuranov et al. 1996)	9	1.89
0.09 to 0.57	0 to 50	46.76 to 96.29 (P_{Total})	VLE	(Clarke and Glew 1971)	36	2.02
0.12 to 1.40	5 to 60	35.73 to 474.36 (P_{H_2S})	VLE	(Wright. and Maass 1932)	52	3.56
0.54 to 8.41	37.77 to 171.11	548.96 to 8329.71 (P_{H_2S})	VLE	(Selleck et al. 1952)	33	5.18

5.4.2.1 Total pressure data and Regression Results

Model parameters have been regressed to 411 total pressure data of binary mixture of H_2S-H_2O. From the total pressure data listed in Table 5-14 no data points were omitted, however binary total pressure data from (Koschel et al. 2007) and (von Kiss et al. 1937) were excluded from the regression since 3 data points from (von Kiss et al. 1937) are isobaric and the accuracy related to the 3 data points from (Koschel et al. 2007) is questionable. Figure 5-2 compares the results of fit for total pressure of binary mixture of hydrogen sulfide and water. Figure 5-3 shows the magnified portion of Figure 5-2 in the low loading range.

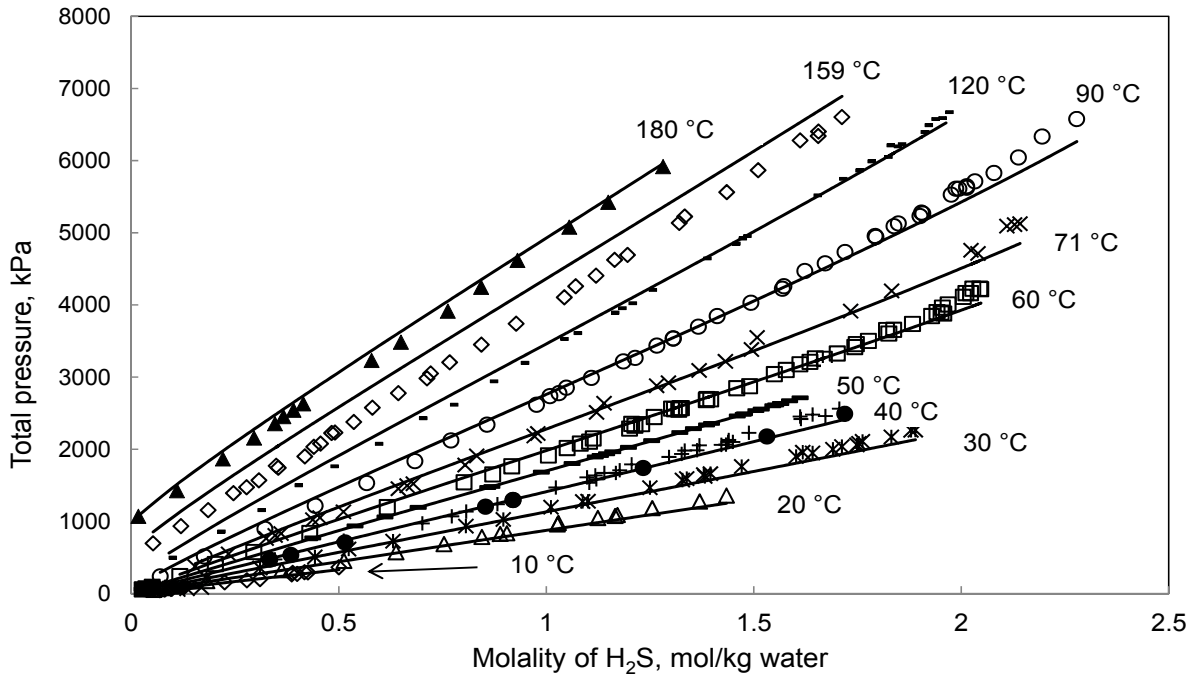

Figure 5-2. Comparison between experimental and fitted results for total pressure of H_2S-H_2O solutions. **Symbols stand for the experimental data and curves (lines) refer to the calculated values using the developed thermodynamic model.** ○ **(T = 0 °C),** ♦ **(T = 10 °C),** ▲ **(T = 20 °C),** * **(T = 30 °C),** + **(T = 40 °C),** - **(T = 50 °C),** (Clarke and Glew 1971)**;** ● **(T = 40 °C),** (Kuranov et al. 1996)**;** ◊ **(T = 10 °C),** Δ **(T = 20 °C),** * **(T = 30 °C),** + **(T = 40 °C),** ■ **(T = 50 °C),** □ **(T = 60 °C),** × **(T = 71 °C),** ○ **(T = 90 °C),** - **(T = 120 °C),** ◊ **(T = 159 °C),** ▲ **(T = 180 °C),** (Lee and Mather 1977)

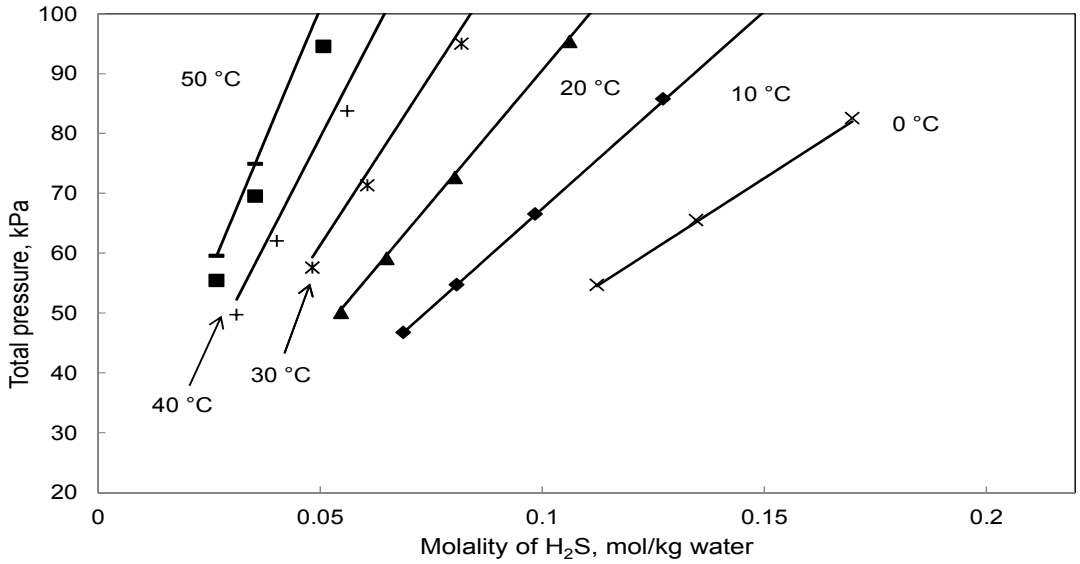

Figure 5-3. Magnified portion of Figure 5-2 in low loading region. Symbols stand for the experimental data and curves (lines) refer to the calculated values using the developed thermodynamic model. ○ (T = 0 °C), ♦ (T = 10 °C), ▲ (T = 20 °C), * (T = 30 °C), + (T = 40 °C), ■ (T = 50 °C), (Clarke and Glew 1971)**; - (T = 50 °C),**(Lee and Mather 1977)

Eventually, the model represents total pressure of H_2S-H_2O sub molecular system with an average absolute relative deviation of 3.46 %.

5.4.2.2 H_2S Solubility Data and Regression Results

Model parameters have been regressed to H_2S solubility in water data (H_2S partial pressure data of (Wright. and Maass 1932) and (Selleck et al. 1952). Figure 5-4 compares model results to regressed data set of (Wright. and Maass 1932).

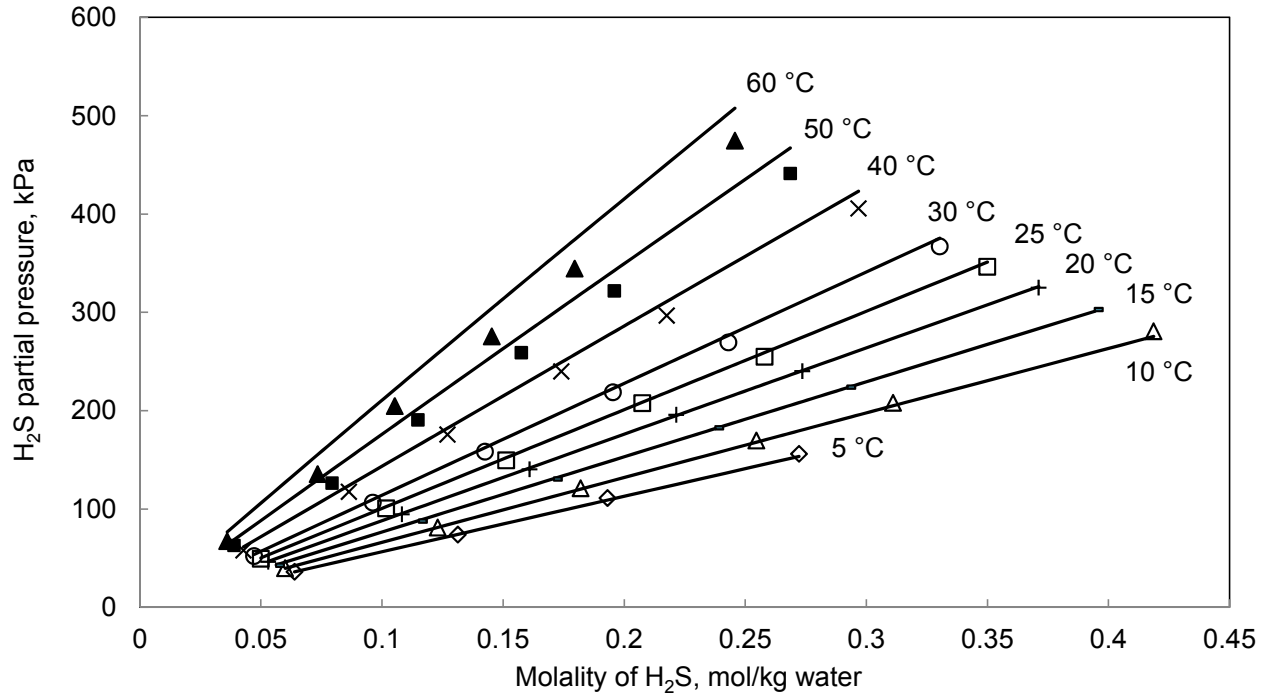

Figure 5-4. Comparison between experimental and fitted results for H_2Ssolubility in water. Symbols stand for the experimental data and curves (lines) refer to the calculated values using the developed thermodynamic model. ◊ (T = 5 °C), Δ (T = 10 °C), - (T = 15 °C), + (T = 20 °C), □ (T = 25 °C), ○(T = 30 °C),×(T = 40 °C), ■(T = 50 °C),▲(T = 60 °C),(Wright. and Maass 1932)

Figure 5-5 is a parity plot for H_2S partial pressure in binary mixture of hydrogen sulfide and water. The figure plots model calculated results against regressed experimental data points; the trend line curve has the slope of 0.96 which shows how well the model can represent H_2S solubility in water.

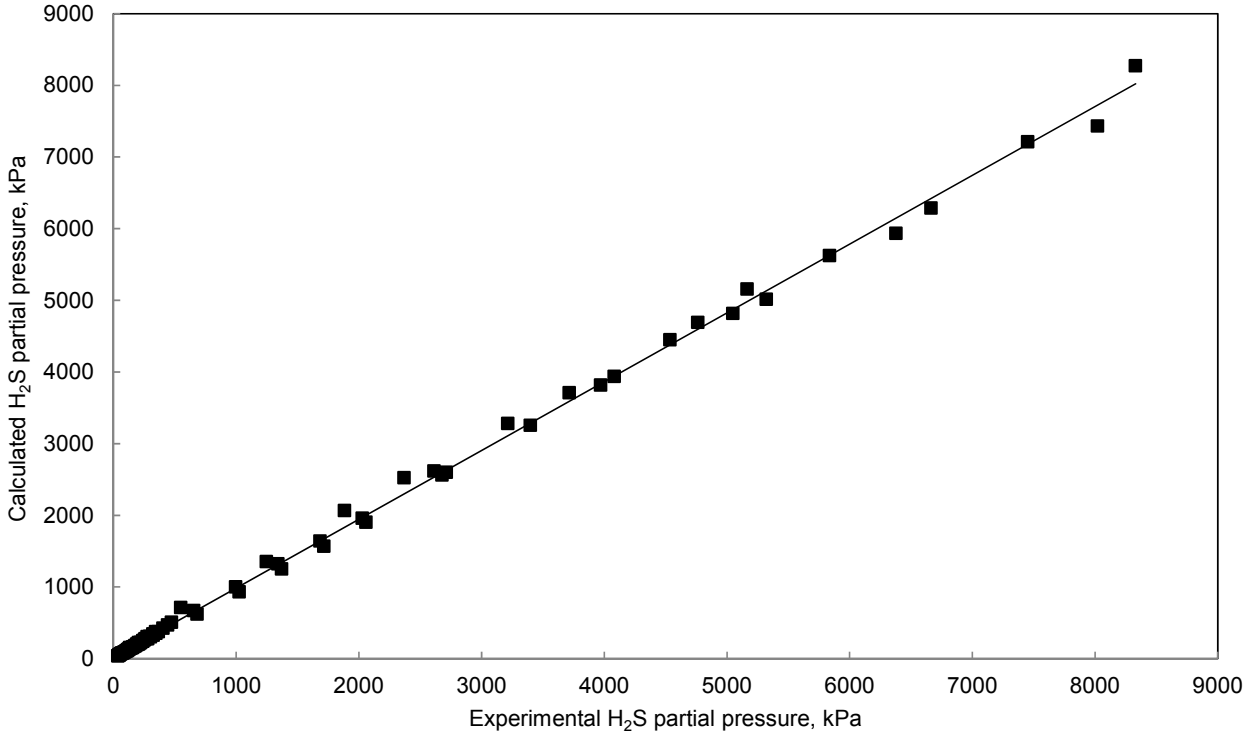

Figure 5-5. Parity plot for H_2S solubility in water

Overall the model represents H_2S partial pressure over binary mixture of H_2S and H_2O within 8.74 AARD %.

5.4.3 Ternary H_2S-MDEA-H_2O Data and Regression Results

Modeling results for hydrogen sulfide-water molecular subsystem were described in previous section. This section will go through regressed data and modeling results for H_2S loaded systems. Interaction parameters required for describing the H_2S-MDEA-H_2O system have been determined by regression to total pressure, H_2S solubility (H_2Spartial pressure) and H_2S heat of absorption data. Table 5-14 presents a summary of the data upon which model parameters were regressed.

Table 5-14. Overview on ternary, H_2S-MDEA-H_2O,data used for parameter estimation and regression results

MDEA Concentration, wt %	T (°C)	P (kPa)	Data Type	Reference	Number of Data Points	AARD %
18.68, 32.20	40 to 140	165.2 to 4895.9 (P_{Total})	VLE	(Kuranov et al. 1996)	71	3.83
48.80	40, 80, 120	147.9 to 2783 (P_{Total})	VLE	(Kamps et al. 2001)	26	7.23
11.82, 19.99	25 to 115.5	13.23 to 1536.6(P_{H_2S})	VLE	(Maddox et al. 1987)	47	10
23.10, 49.99	40 to 120	0.0033 to 3673(P_{H_2S})	VLE	(Huang and Ng 1998)	42	20
49.99	40	0.25 to 4.94(P_{H_2S})	VLE	(Ter Maat et al. 2004)*	7	6.75
34.99, 49.99	9.85, 24.85	0.14 to 1.49(P_{H_2S})	VLE	(Huttenhuis et al. 2007)*	10	16
11.35, 21.63, 33.88	26.65 to 126.65	87 to 1121(P_{Total})	H_{abs}	(Oscarson and lzatt 1990)	368	12

** Includes Methane as a makeup gas.*

Interaction parameters involved in the ternary system were determined by regression to the data listed in Table 5-14. Notice that data of (Ter Maat et al. 2004)and (Huttenhuis et al. 2007) are measured in presence of methane. 7 Data points from (Ter Maat et al. 2004) at total pressure of 350 kPa and 10 data points of (Huttenhuis et al. 2007) at total pressure of 690 kPa were included in regression parameters of the ternary system. It was noticed that including these low pressure data points which has methane as make up gas improves modeling results both for ternary and quaternary systems (with methane). Keep in mind that only data at low total pressure from quaternary system were used to regress model parameters. The remainders of this section will describe different kinds of data that have been used for regression parameters of H_2S-MDEA-H_2O system and regression results, furthermore model predictions will be presented.

5.4.3.1 Total Pressure Data and Regression Results

Total pressure data of two sources, (Kuranov et al. 1996) and (Kamps et al. 2001) have been used for adjusting effective interaction parameters in the ternary system. No data points were omitted from data sets. Results of fit for total pressure over the ternary mixture have been shown in Figure 5-6 and Figure 5-7. Figure 5-6 compares total pressure of H_2S-MDEA-H_2O mixtures for two different MDEA concentration, 32.20 and 48.80 wt % MDEA at 40 and 120 °C.

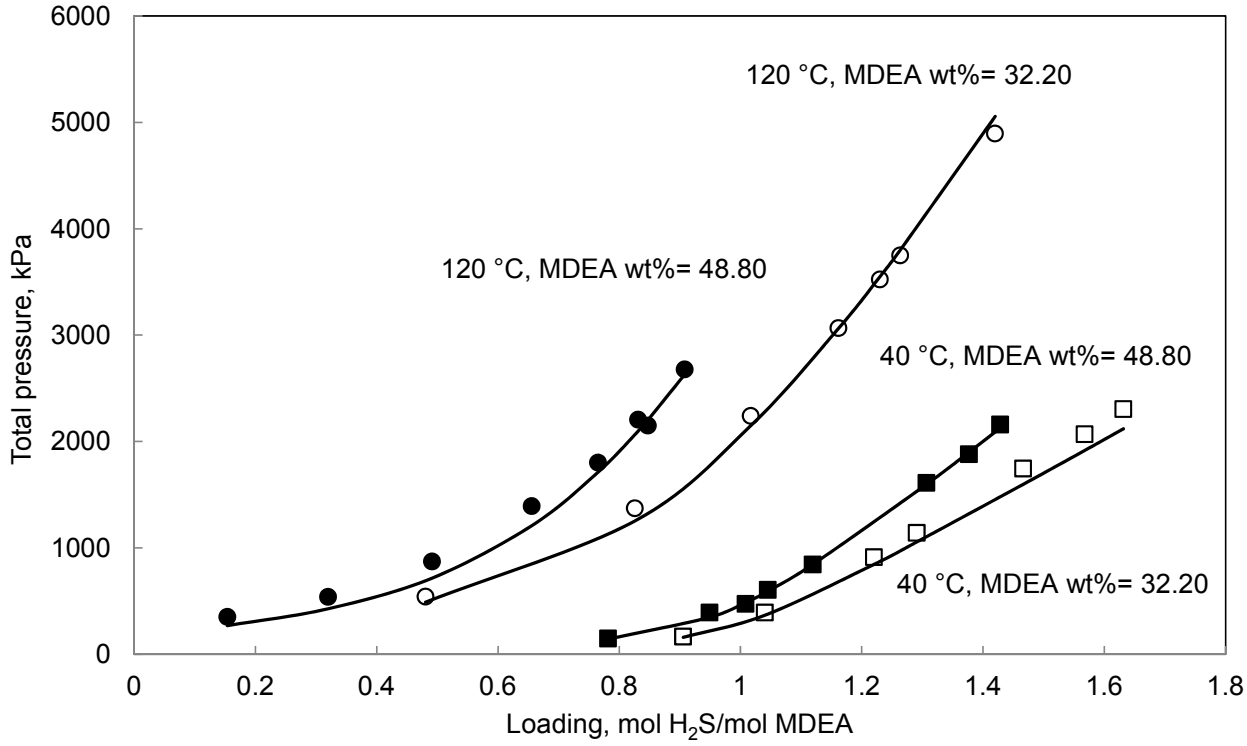

Figure 5-6. Comparison between experimental and fitted results for total pressure of H_2S-MDEA-H_2Osolutions for32.20 and 48.80 wt % MDEA and at 40 and 120 °C. Symbols stand for the experimental data and curves (lines) refer to the calculated values using the developed thermodynamic model. □ (T = 40 °C, MDEA wt % = 32.20), ○ **(T = 120 °C MDEA, wt % = 32.20),** (Kuranov et al. 1996)**;** ■ **(T = 40 °C, MDEA wt % = 48.80),** ● **(T = 120 °C, MDEA wt % = 48.80),** (Kamps et al. 2001)

Figure 5-7 shows effect of temperature on the absorption capacity for 18.68 wt % MDEA, as it is shown in Figure 5-7 at the same pressure and amine concentration decreasing temperature leads to increase in absorption capacity. This is an expected behavior since the reaction of H_2S with aqueous MDEA is exothermic. It is known from basic thermodynamics if a chemical system at equilibrium experience a change in temperature, then equilibrium shift to counteract the imposed change and a new equilibrium is formed. For exothermic reactions lowering the temperature would cause the reaction to produce more heat, since the reaction between acid gas and aqueous alkanolamine is exothermic, this would be in favor of absorbing more acid gas in the aqueous phase in forms of ionic nonvolatile species.

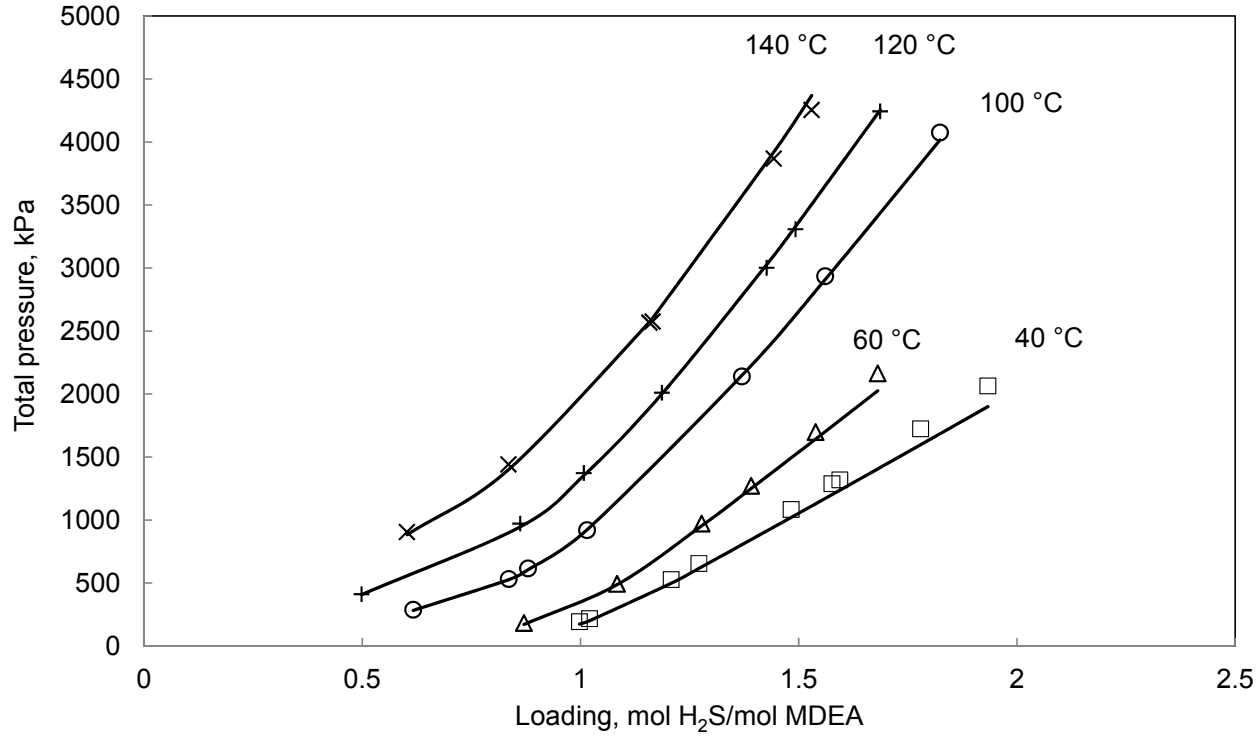

Figure 5-7. Results of fit for total pressure of H_2S-MDEA-H_2O solutions for 18.68 wt % MDEA solvent. Symbols stand for the experimental data and curves (lines) refer to the calculated values using the developed thermodynamic model. □ (T = 40 °C), Δ (T = 60 °C),),○ (T = 100 °C), + (T = 120 °C),× (T = 140 °C), (Kuranov et al. 1996)

Altogether, the model fit the total pressure data of H_2S-MDEA-H_2O solutions within 5.53 AARD%.

5.4.3.2 H_2S Solubility Data and Regression Results

H_2S solubility data in aqueous MDEA solutions were utilized to adjust model parameters. As it was mentioned previously, much less data exists for H_2S solubility in aqueous MDEA solutions compare to CO_2 solubility. Available data show some discrepancies at the same conditions. Hence it is important to evaluate the data before choosing them for regression. For the H_2S partial pressure, four data sets (two data sets have methane as make up gas) were regressed to obtain UNIQUAC parameters. From (Maddox et al. 1987) and (Huang and Ng 1998) no data points were omitted. As it has already explained, (Ter Maat et al. 2004) and (Huttenhuis et al. 2007) have used methane as a makeup gas, from these two sources only data at low total pressure, 7 data points from (Ter Maat et al. 2004) at total pressure of 350 kPa and 10 data points from (Huttenhuis et al. 2007) at total pressure of 690 kPa were used for parameters regression. Note that including data of (Lemoine et al. 2000b) in regression data base does not improve modeling results, therefore to avoid regressing model parameters to more data sets, these data were excluded from data base. Model properly

predicts data of (Lemoine et al. 2000b), prediction results are shown in Figure 5-11. Four data sets for H_2S-MDEA-H_2O mixtures were excluded from regression data base including data of (Macgregor and Mather 1991) , (LI and SHEN 1993), (Jou et al. 1993) and (JOU et al. 1982). Data of (Macgregor and Mather 1991) and (LI and SHEN 1993) were eliminated from regressed data sets as they show a downward trend which is away from other sources (Posey 1997). (Posey 1997) claimed that the error in the reported H_2S partial pressure may be happened because of H_2S adsorption onto the walls of equilibrium cell or analytical devices (Posey 1997). (Posey 1997) also did not use (Macgregor and Mather 1991) and (LI and SHEN 1993) data for regressing e-NRTL parameters. Data of (Jou et al. 1993) were omitted from regression data base in this work, as these data set deviate downward from other sources. This conclusion is in accordance with others investigations. Investigations over (Jou et al. 1993) data available in literature can be summarized as follows:

Comparison between experimental data from (Jou et al. 1993) and results from the correlation of (Kamps et al. 2001) shows that for 34.90 wt % MDEA and at 313 K, (Jou et al. 1993) data are lower than correlated partial pressures. Relative deviation between (Jou et al. 1993) data and correlated results by (Kamps et al. 2001) at temperature of 313K and 34.90 MDEA wt %, up to H_2S molality of 3, ranges from 165 % (at the lowest loading point) to 4.4 %, for H_2S modalities above 3, deviation is even higher. At 34.90 MDEA wt % and 373K, average relative deviation between (Jou et al. 1993) data and correlated results by (Kamps et al. 2001) is 18%, however deviation is not systematic. For 50 wt % MDEA, excluding the two data points with experimental H_2S partial pressure lower than 110 Pa, hydrogen sulfide partial pressures predicted with the (Kamps et al. 2001) correlation are systematically 45 % larger than experimental points from Jou et al. data (1993)(Kamps et al. 2001). According to (Ter Maat et al. 2004), for loadings up to 0.3 or 0.4 a log-log plot of acid gas partial pressure versus loading should be a straight line, however data of (Jou et al. 1993) shows a different behavior for loading range of 0.01 to 0.04 mole/mole, hence they considered as inaccurate data by (Ter Maat et al. 2004). At H_2S molalities higher than 3, (Kuranov et al. 1996) H_2S partial pressure data are larger than (Jou et al. 1993) measured values. Literature survey over (Jou et al. 1993) confirmed their downward deviation, therefore it was concluded that (Jou et al. 1993) should be discarded from this work regression data base.

Data of (JOU et al. 1982) were not used in this work for fitting parameters since these data deviate largely from other sources. Relative deviation between measured H_2S partial pressure data by (JOU

et al. 1982) and correlated values from (Kamps et al. 2001) at 50 wt % MDEA and at 298, 313, 343, 373 and 393 K are 307,409,369,227 and 218 % at lowest loadings and are 9, 4, -16, -18 and -20 % at the highest loadings , respectively. These large deviations show that these data are suspect.

Despite of (Posey 1997), data of (Huang and Ng 1998) have been used to regress model parameters in this work.(Posey 1997) claimed that measured H_2S partial pressures by (Huang and Ng 1998)at H_2S loadings lower than 0.1 are slightly high, however as stated by (Ter Maat et al. 2004) comparison with other sources shows that this data are in agreement with other data sets. Figure 5-8 show the comparison between data of (Huang and Ng 1998), (Rogers et al. 1998), (Ter Maat et al. 2004) and (JOU et al. 1982). As it can be seen from the figure, data of (Huang and Ng 1998), (Rogers et al. 1998) and (Ter Maat et al. 2004) are in agreement with each other but (JOU et al. 1982) data deviates from the rest.

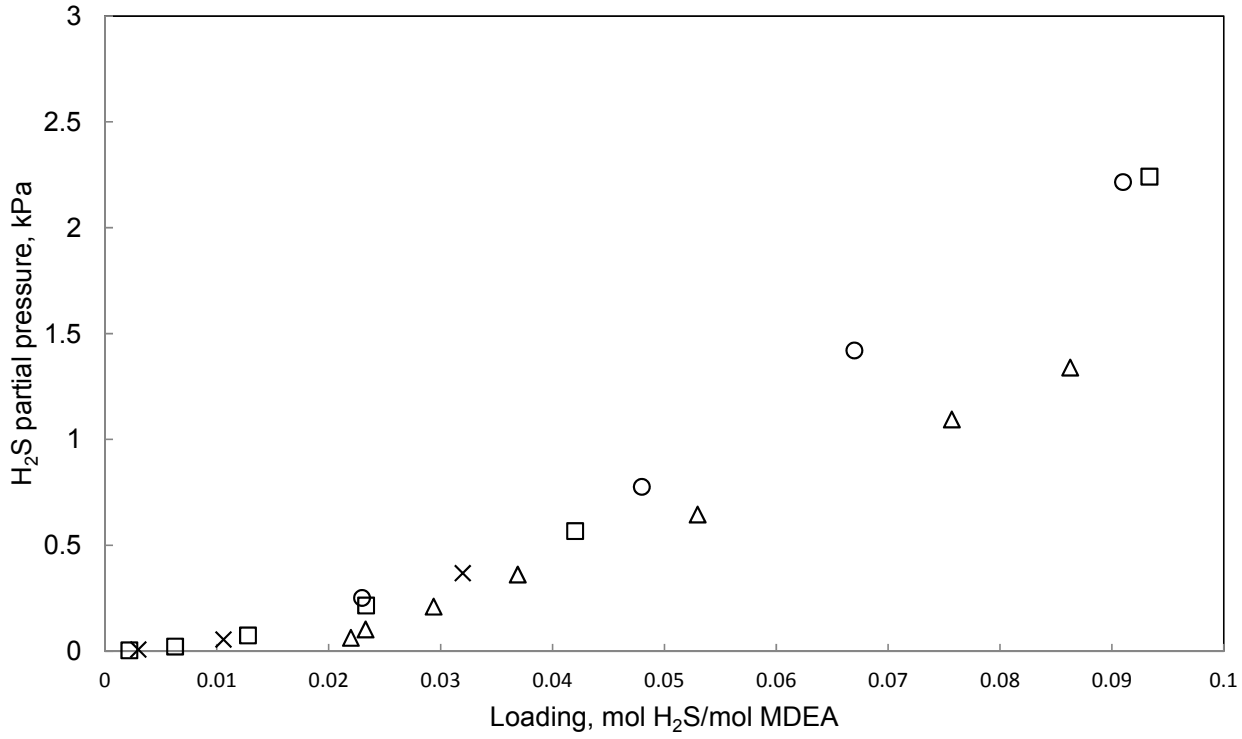

Figure 5-8. Comparison between H_2S partial pressure from different data sets at 40 °C and 50.02 wt % MDEA. □, (Rogers et al. 1998); Δ ,(JOU et al. 1982);○,(Ter Maat et al. 2004); ×, (Huang and Ng 1998)

As it explained in Table 5-14, 106 H_2S partial pressure data were regressed, they were fit with an average absolute relative deviation of 13%. Results of fit for 19.99 and 49.99 wt % MDEA at

different temperatures span from 37.8 to 120 °C are shown in Figure 5-9 and Figure 5-10, respectively.

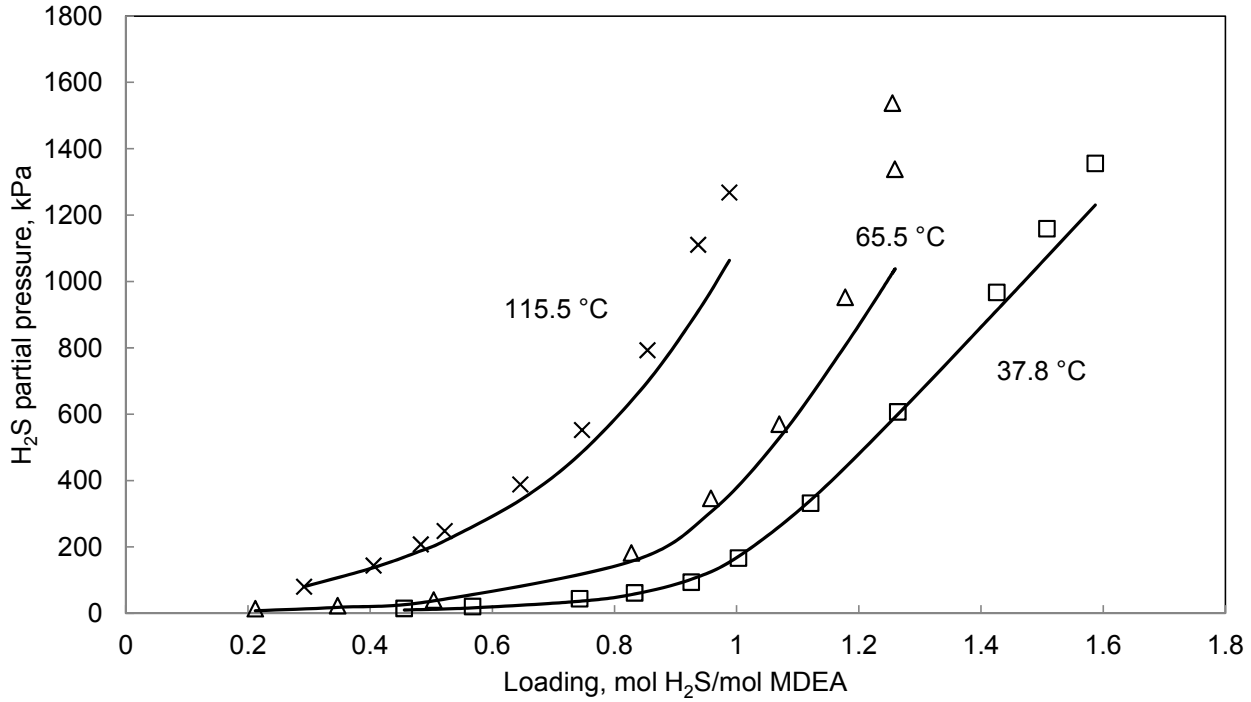

Figure 5-9. Comparison between experimental and regressed H_2Ssolubility in 19.99 wt % aqueous MDEA solutions and at different temperatures. Symbols stand for the experimental data and curves (lines) refers to the represented values using the developed thermodynamic model. □, (T=37.8 °C), Δ, (T=65.5 °C),×, (T=115.5 °C), (Maddox et al. 1987)

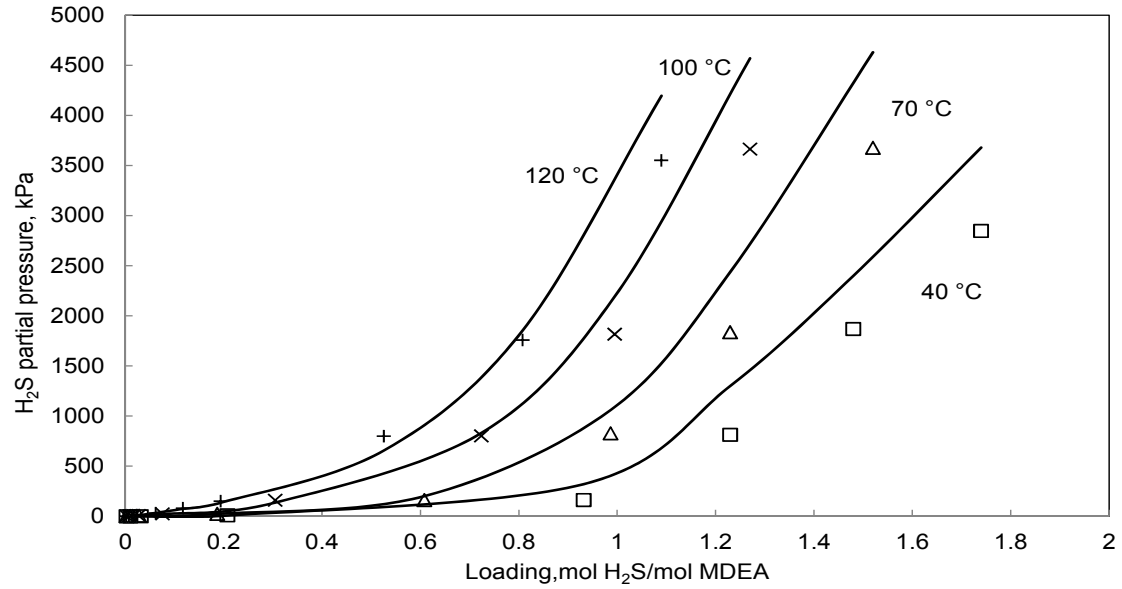

Figure 5-10. Comparison between experimental and regressed H_2S solubility in 49.99 wt % aqueous MDEA solutions and at different temperatures. Symbols stand for the experimental data and curves (lines) refers to the represented values using the developed thermodynamic model. □, (T=40°C), Δ, (T=70°C), ×, (T=100 °C), + (T=120 °C), (Huang and Ng 1998)

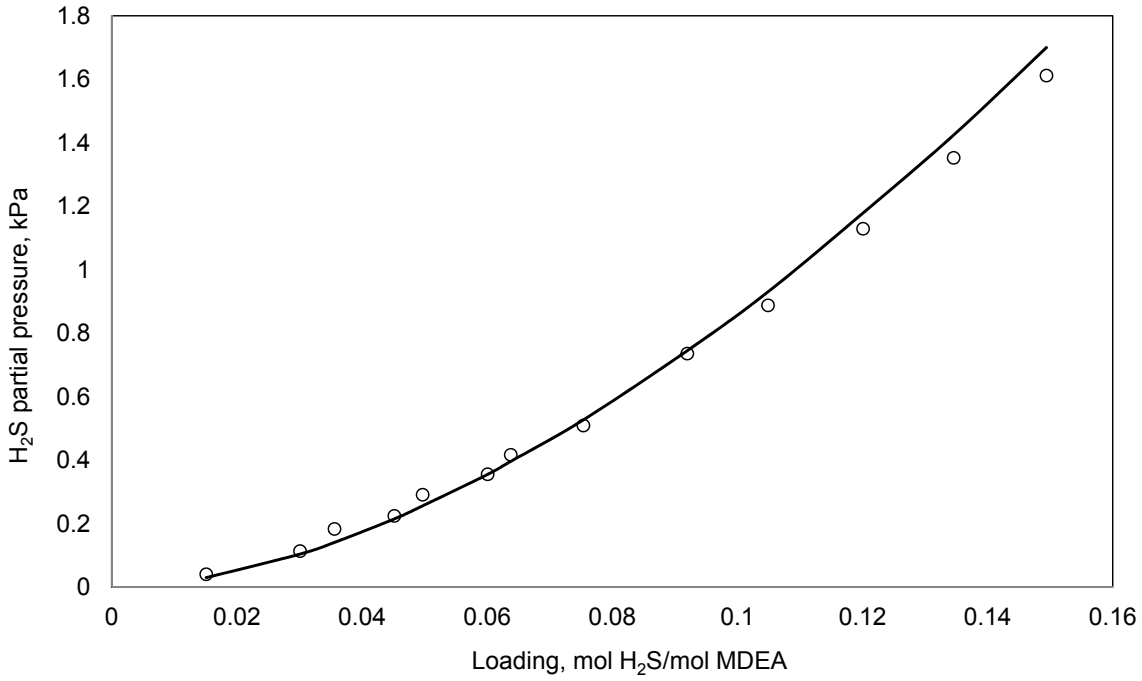

Figure 5-11. Comparison between experimental and predicted H_2S solubility in 23.6 wt % aqueous MDEA solutions and at 40 °C. Symbols stand for the experimental data and curves (lines) refers to the represented values using the developed thermodynamic model. ○, (Lemoine et al. 2000b)

Figure 5-11, shows that model adequately predicts H_2S solubility in low loading region. As it can be seen from the above figures, results of fit well agree with the expermental data points. In addition developed model appropiately predicts H_2S soubility in aqueous MDEA solutions.

5.4.4 Heat of Absorption Data and Regression Results

368 data of heat of H_2S absorption into aqueous MDEA solution were fit within an average absolute relative deviation of 12 %. Regression results at 126.65 °C and 1121 kPa at 20, 35 and 50 wt % MDEA are demonstrated in Figure 5-12.

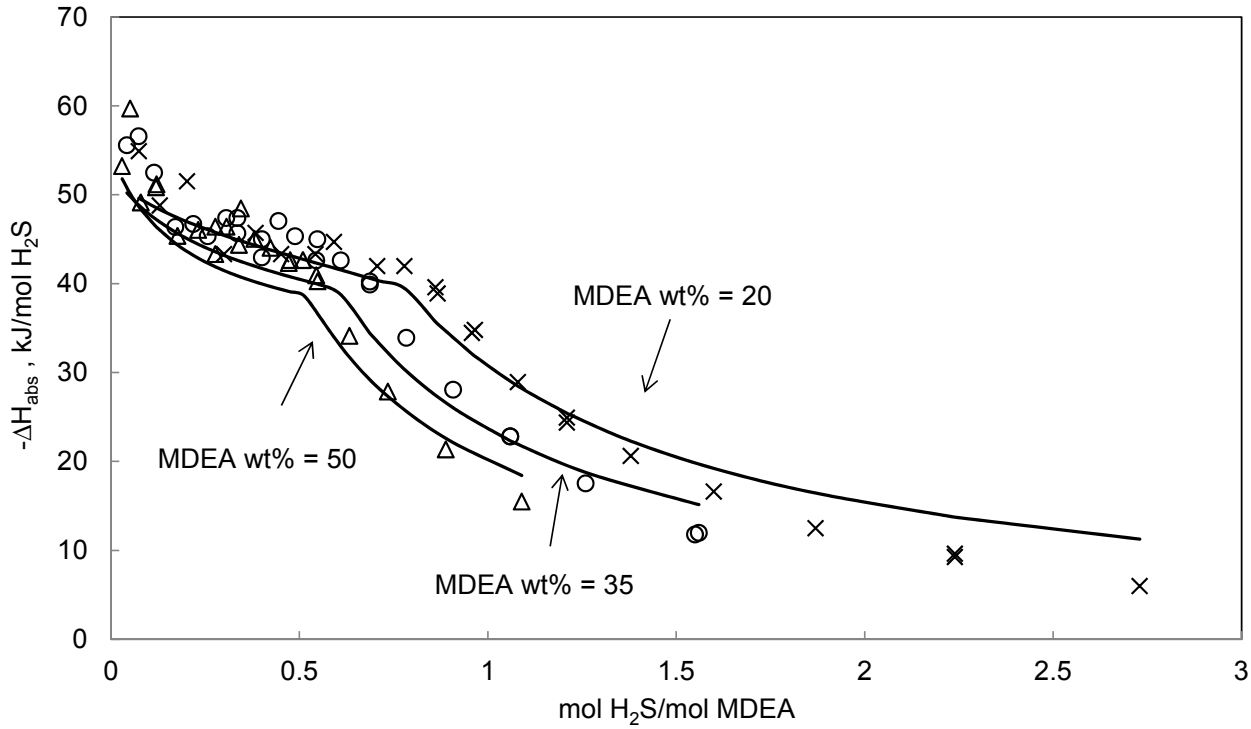

Figure 5-12. Comparison of the enthalpy of H_2S absorption at 126.65 °C and 1121 kPa and in 20, 35 and 50 wt % aqueous MDEA solutions. Symbols stand for the experimental data and curves (lines) refer to the represented values using the developed thermodynamic model. × (MDEA wt % = 20), ○ (MDEA wt % = 35), Δ (MDEA wt % = 50), (Oscarson and lzatt 1990)

As it is shown in Figure 5-12**,** the agreement between model and experiments are satisfactory. The developed model can describe the heat of H_2S absorption into aqueous MDEA solution quiet well. Altogether, results of fit show that developed models for H_2S-H_2O and H_2S-MDEA-H_2O systems consistently represent thermodynamic and thermal properties of the binary and ternary systems.

5.5 CH_4 System

This section will describe modeling results for absorption of H_2S into aqueous MDEA solutions for systems that have methane as a makeup gas. Before quaternary system of H_2S-CH_4-MDEA-H_2O could be simulated, first CH_4-H_2O binary system has to be studied. The CH_4-H_2O interaction parameters and r and q values for CH_4 are the only additional parameters that are required when methane is added to H_2S-MDEA-H_2O system. In what follows regression results for binary CH_4-H_2O system and prediction results for H_2S-CH_4-MDEA-H_2O quaternary system will be presented. Finally the effect of methane on H_2S solubility will be discussed.

5.5.1 CH_4-H_2O System, Regression Results

Methane is physically dissolved in water. The hydrocarbon solubility, i.e. methane, is an important parameter for the correct design of high pressure gas treating equipment. As explained in section 5.2.1, CH_4-H_2O binary interaction parameter is required to model CH_4-H_2O system. In addition to CH_4-H_2O interaction parameter, r and q parameter for CH_4should be determined in order to model the CH_4-H_2O binary system. It was important to determine whether or not CH_4-MDEA and CH_4-$MDEA^+$ interaction parameters are effective in modeling the behavior of CH_4-H_2O system. Therefore four regression cases were performed for modeling CH_4-H_2O system. In case (I) only CH_4-H_2O interaction parameter was regressed, in case (II) CH_4-H_2O and CH_4-MDEA interaction parameters were fitted, in case (III) CH_4-H_2O and CH_4-$MDEA^+$ interaction parameters were adjusted and in case (IV) all three CH_4-H_2O, CH_4-MDEA and CH_4-$MDEA^+$ interaction parameters were regressed. Notice that CH_4-MDEA and CH_4-$MDEA^+$ parameters were regressed to CH_4-MDEA-H_2O ternary data of (Jou et al. 1998). Comparing results of four regression cases demonstrates that by adjusting only CH_4-H_2O interaction parameter, the model could fairly describe the behavior of the binary system and there is no need to consider more adjustable parameters. The value of the interaction parameter is determined by regressing this interaction parameter with total pressure data of CH_4-H_2O system, r and q values are taken from (Addicks 2002). Table 5-15 lists data sets upon which the CH_4-H_2O interaction parameter was regressed. In what follows modeling results for total pressure data of CH_4-H_2O system have been shown.

Table 5-15. Review over binary CH_4-H_2O data used for regression

CH_4 Concentration	T ,°C	P, kPa	Data Type	Reference	Number of Data Points	AARD %
0.04 to 14	25, 50	3000 to 8000 (P_{Total})	VLE	(Yokoyama et al. 1988)	6	1.86
0.05 to 0.36	10.05, 20.05, 30.05	2000 to 40030 (P_{Total})	VLE	(Wang et al. 2003)	17	7.61
0.02 to 0.14	25, 41	993 to 9981(P_{Total})	VLE	(Awan et al. 2010)	8	5.06

Results of fit for total pressure of CH_4-H_2O binary system at 25, 40 and 50 °C plotted in Figure 5-13.

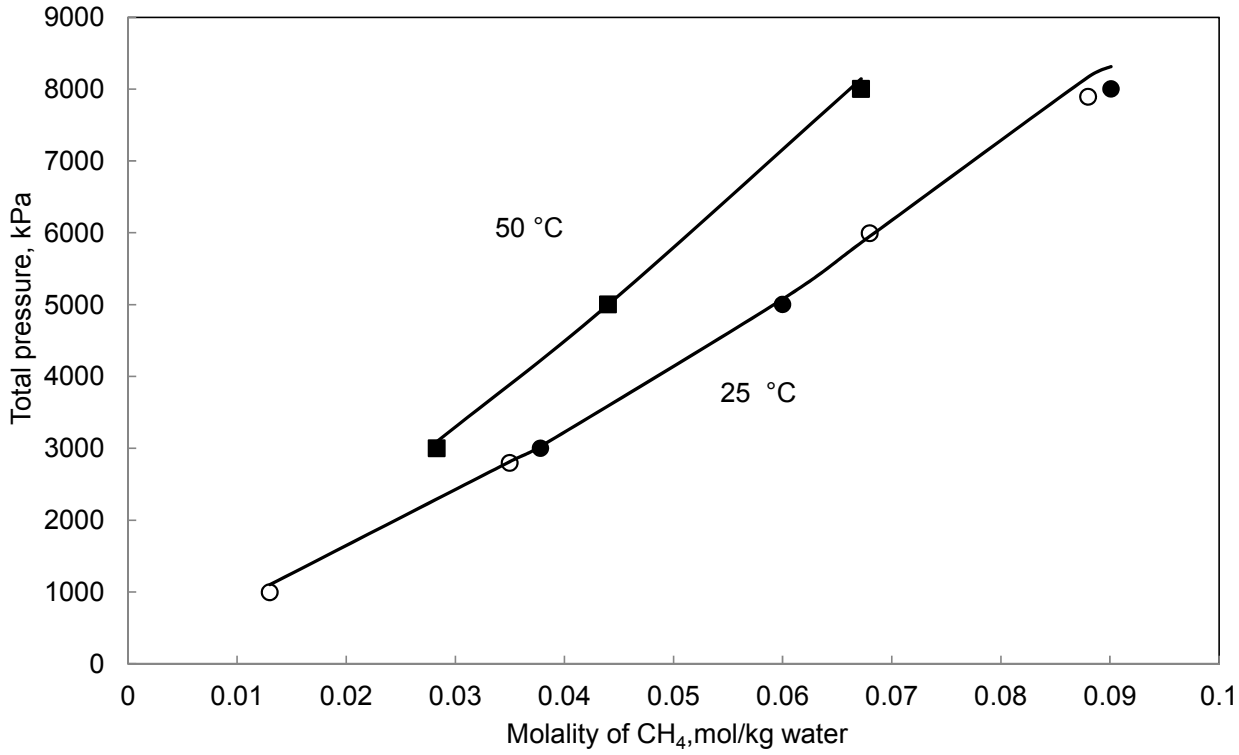

Figure 5-13. Comparison of measured total pressure of CH_4-H_2O solutions with the estimated values from model. Symbols stand for the experimental data and curves (lines) refer to the calculated values using the developed thermodynamic model.● (T = 25 °C), ■ (T = 50 °C), (Yokoyama et al. 1988)**; ○ (T = 25 °C),** (Awan et al. 2010)

All in all, the model calculates total pressure of binary CH_4-H_2O system within 4.84 AARD %.

5.5.2 H_2S-CH_4-MDEA-H_2O System and prediction Results

It is of high importance that the model adequately represents acid gas solubility at high pressures, where methane is present as an inert makeup gas. In natural gas treatment process, typical absorber pressure is around 70 bar (in the absorber, mixture of acid gas-hydrocarbons mainly methane-amine-water is present), whereas stripper pressure is between 1 to 2 bar (in the stripper mixture of acid gas-amine-water is present as methane is already separated). Therefore it is very important that the model describe influence of methane on acid gas solubility. This section will describe model calculation results for H_2S solubility in mixtures of CH_4-MDEA-H_2O. The results were obtained with model parameters determined for H_2S-MDEA-H_2O and CH_4-H_2O systems. As previously explained, in addition to ternary data, totally 17 quaternary (H_2S-CH_4-MDEA-H_2O) data points (at low total pressure) were utilized to adjust ternary model parameters, however the rest of high pressure quaternary data were used to check model validity (they were not used for regression).In what follows calculation results for the regressed data and model predictions for unregressed data will be discussed. Figure 5-14 shows results of fit for (Ter Maat et al. 2004) data for 50 wt % MDEA and at temperature of 40 °C and total pressure of 350 kPa.

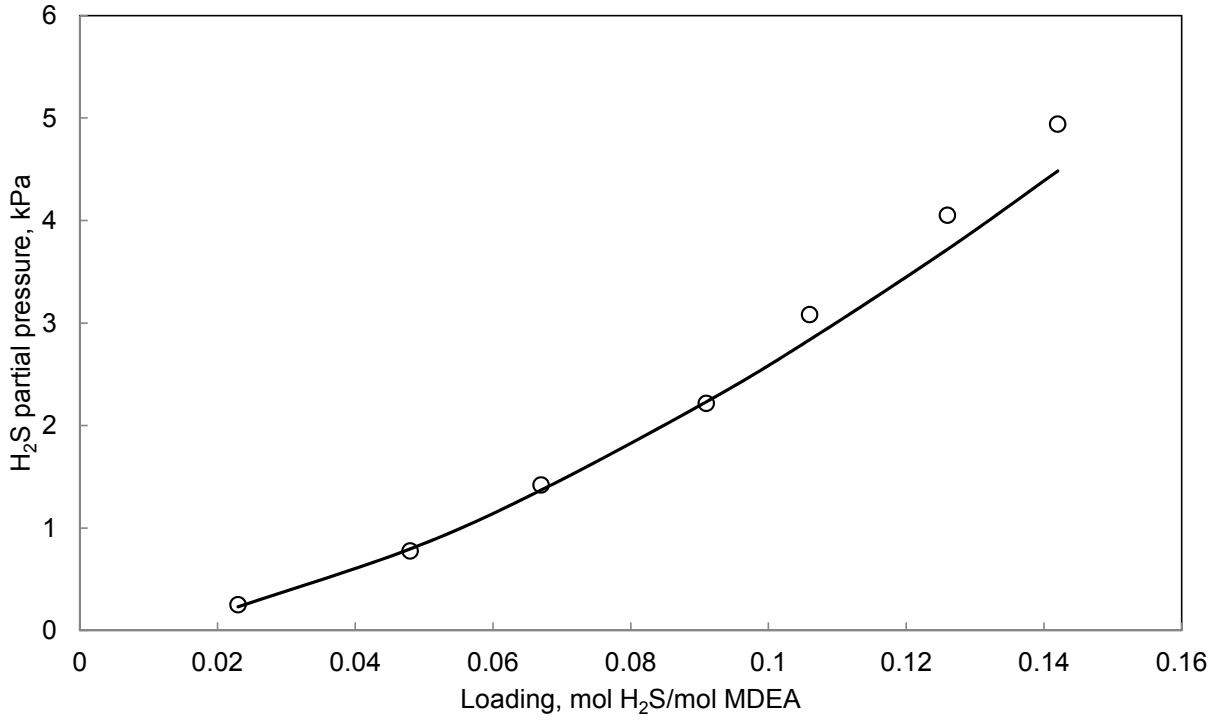

Figure 5-14. Comparison between experimental and regressed H_2S solubility for 50 wt % MDEA and at 40 °C and 350 kPa. Symbols stand for the experimental data and curve (line) refers to the calculated values using the developed thermodynamic model. ○**,** (Ter Maat et al. 2004)

Figure 5-15 and Figure 5-16 demonstrate model predictions at total pressures of 3450 and 6900 kPa. Figure 5-15 shows model predictions for unregressed data of (Huttenhuis et al. 2007) for 49.99 wt % MDEA, at temperature of 10 and 25 °C and at total pressure of 3450 kPa.

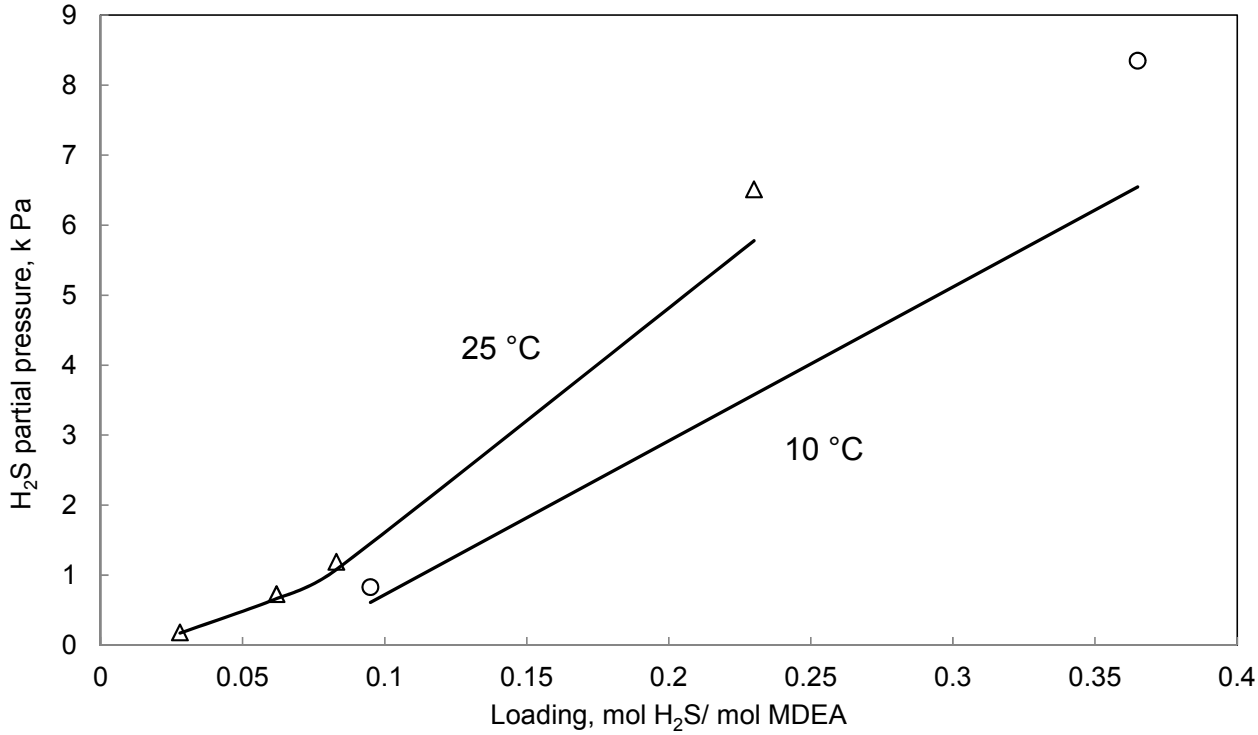

Figure 5-15. Prediction results for H_2S solubility at49.99 wt % MDEA and at 10 and 25°C and 3450 kPa. Symbols stand for the experimental data and curves (lines) refer to the calculated values using the developed thermodynamic model. ○, (T=10 °C), Δ, (T=25 °C),(Huttenhuis et al. 2007)

Figure 5-16 compares model predictions with unregressed data of (Huttenhuis et al. 2007) at total pressure of 6900 kPa which is a typical absorber pressure in natural gas treatment process.

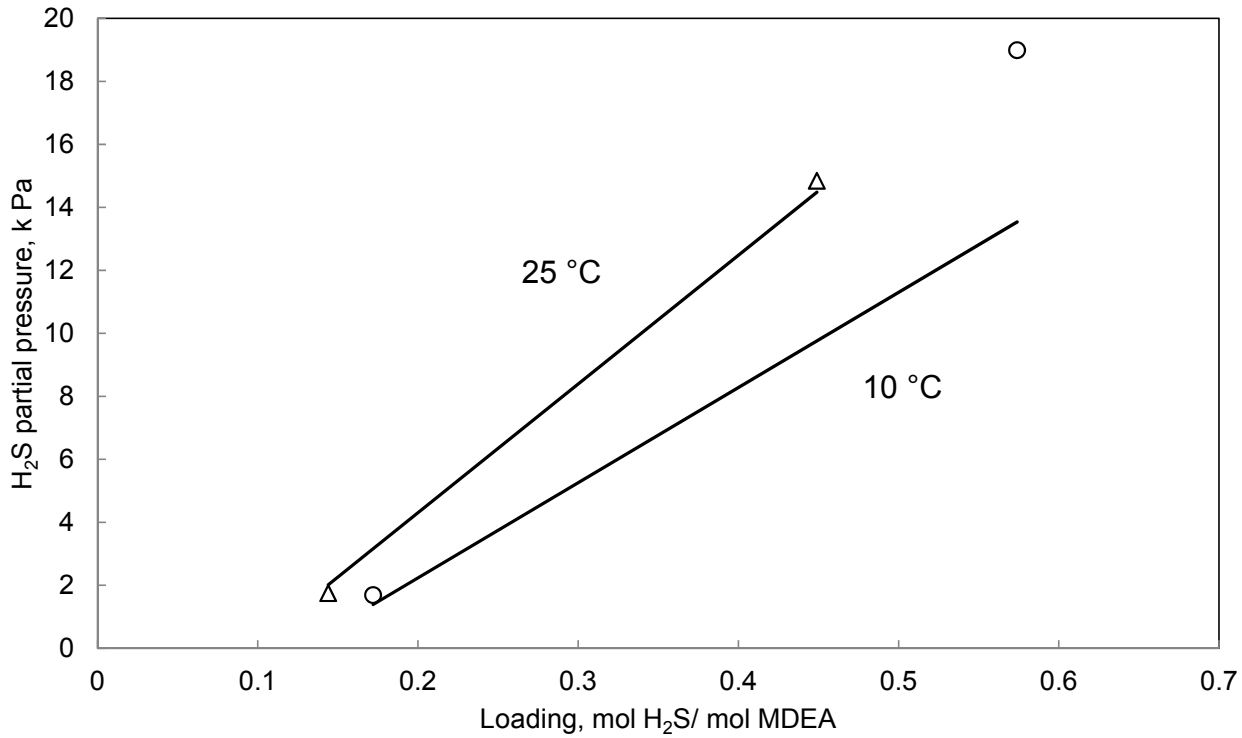

Figure 5-16. Prediction results for H_2S solubility at 34.99 wt % MDEA and at 10 and 25°C and 6900 kPa. Symbols stand for the experimental data and curves (lines) refer to the calculated values using the developed thermodynamic model. ○, (T=10 °C), Δ, (T=25 °C), (Huttenhuis et al. 2007)

Table 5-16 shows deviations between model predictions and unregressed data for quaternary system of H_2S-CH_4-MDEA-H_2O. All in all, in presence of methane, model predicts H_2S solubility in aqueous solutions within average absolute relative deviation of 15 %.

Table 5-16. Prediction results for H_2S-CH_4-MDEA-H_2O system

MDEA Concentration, Wt %	T ,°C	Total Pressure, kPa	Data Type	Reference	Number of Data Points	AARD %
50	50	499-700	VLE (H_2S Partial Pressure)	(Dicko et al. 2010)	5	15
34.99, 49.99	10, 25	690, 3450, 6900	VLE (H_2S Partial Pressure)	(Huttenhuis et al. 2007)	30	15

5.5.2.1 CO_2-CH_4-MDEA-H_2O System and prediction Results

Developed model for CO_2-MDEA-H_2O system (chapter 4) in combination with presented model for CH_4-H_2O system, was used to predict CO_2 solubility in aqueous MDEA mixtures at high pressures (where methane is present). Table 5-17 shows prediction results for CO_2 solubility in mixture of CH_4-MDEA-H_2O

Table 5-17. Prediction results for CO_2-CH_4-MDEA-H_2O systems

MDEA Concentration, wt %	T ,°C	Total Pressure, kPa	Data Type	Reference	Number of Data Points	AARD %
30, 50	40, 80	100000, 15000, 20000	VLE (CO_2 Partial Pressure)	(Addicks et al. 2002)	31	21
50	50	1268-1558	VLE (CO_2 Partial Pressure)	(Dicko et al. 2010)	5	31

Figure 5-17 plots predicted CO_2partial pressure against loading at total pressure of 100 bar.

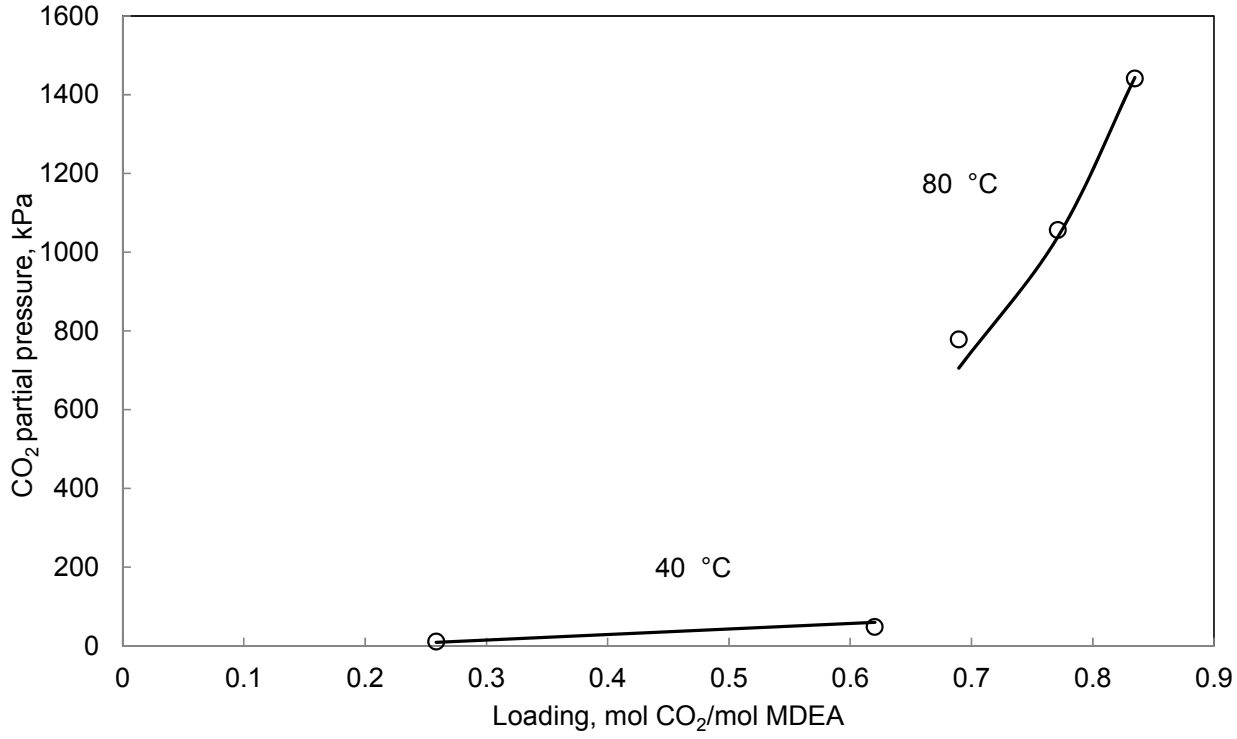

Figure 5-17. Prediction results for CO_2solubility at 30 wt % MDEA and at 40 and 80°C and 100000 kPa. Symbols stand for the experimental data and curves (lines) refer to the calculated values using the developed thermodynamic model. ○, (Addicks et al. 2002)

Overall, in presence of methane, the developed model predict CO_2 solubility within 26 AARD %.

5.6 Influence of methane on Acid Gas Solubility

In general acid gas solubility data are limited to low pressures, where there is no inert gas like nitrogen and hydrocarbons exist. Despite of this fact, in natural gas treatment industry typically hydrocarbons foremost methane is present in the absorber column. Therefore, it is crucial to investigate the effect of methane on acid gas solubility. The aim of this section is to examine the effect of methane on acid gas solubility quantitatively. To study the influence of presence of methane experimentally, literature data for H_2S-CH_4-MDEA-H_2O at different total pressures (methane partial pressure) were compared. Figure 5-18 and Figure 5-19 describe the effect of total pressure on H_2S solubility. Figure 5-18 shows H_2S partial pressure as a function of methane partial pressure for a definite loading, temperature and MDEA concentration, experimental data points are taken from (Dicko et al. 2010). Figure 5-19 plots H_2S partial pressure as a function of methane partial pressure at different loadings (mole H_2S/mole MDEA); data are from (Huttenhuis et al. 2007). As it can be observed from the figures, H_2S partial pressure increases when system total pressure (or methane partial pressure) is increased. Therefore it can be concluded that H_2S solubility decrease with increasing total pressure, in other words higher methane partial pressure cause lower H_2S solubility. This conclusion is in an agreement with literature studies, (Huttenhuis et al. 2007), (Addicks et al. 2002) and (Dicko et al. 2010). Measurements of (Dicko et al. 2010) show that at loading of 0.74 and at 50 °C and for 50 wt % MDEA solution, a variation of approximately 6 MPa in the CH_4 partial pressure leads to a variation of less than 30 % in H_2S partial pressure. From Figure 5-19 it can be concluded that at 25 °C and in 50 wt % MDEA aqueous solution, an increase of 6 MPa in CH_4 partial pressure, caused around 40 % increase in H_2S partial pressure. Comparing H_2S partial pressure does not allow determining which phase is mainly affected by methane presence, gas phase or liquid phase. Hence, further study is required to make clear that the decrease in H_2S solubility is the result of increasing system pressure in the gas phase or is due to dissolution of little amount of methane in the liquid phase.

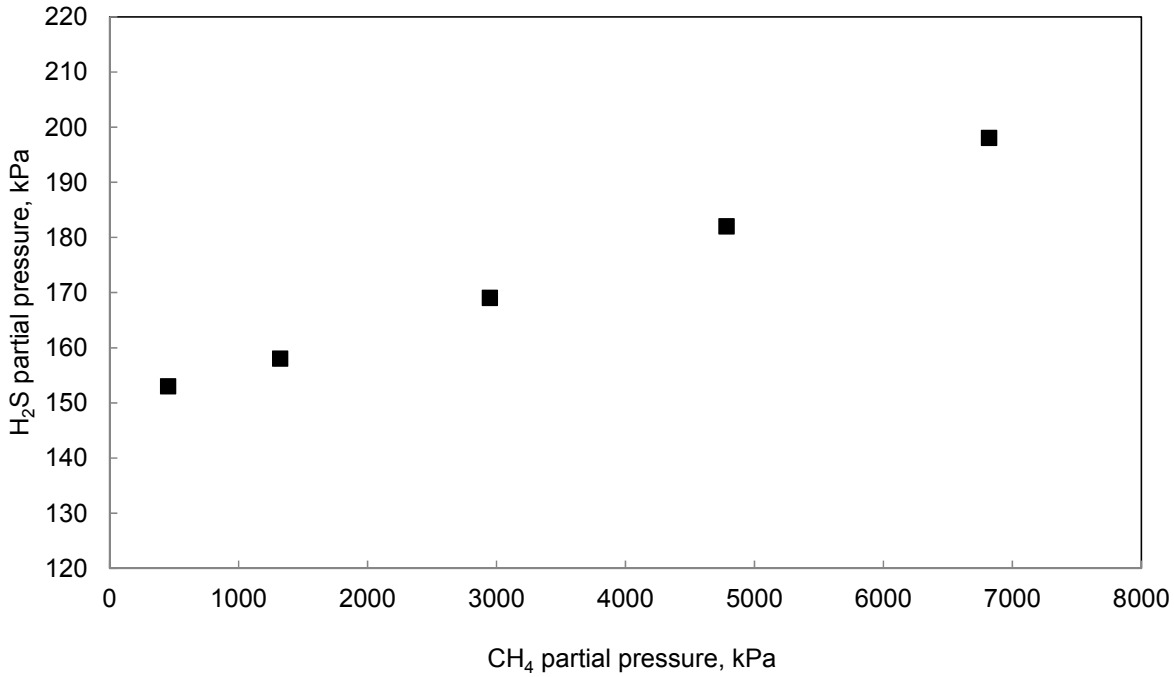

Figure 5-18. Experimental investigation on effect of methane presence on H_2S solubility into aqueous solution of 50 wt % MDEA at 50 °C and at loading (mole H_2S/mole MDEA) of 0.74. ■, (Dicko et al. 2010)**.**

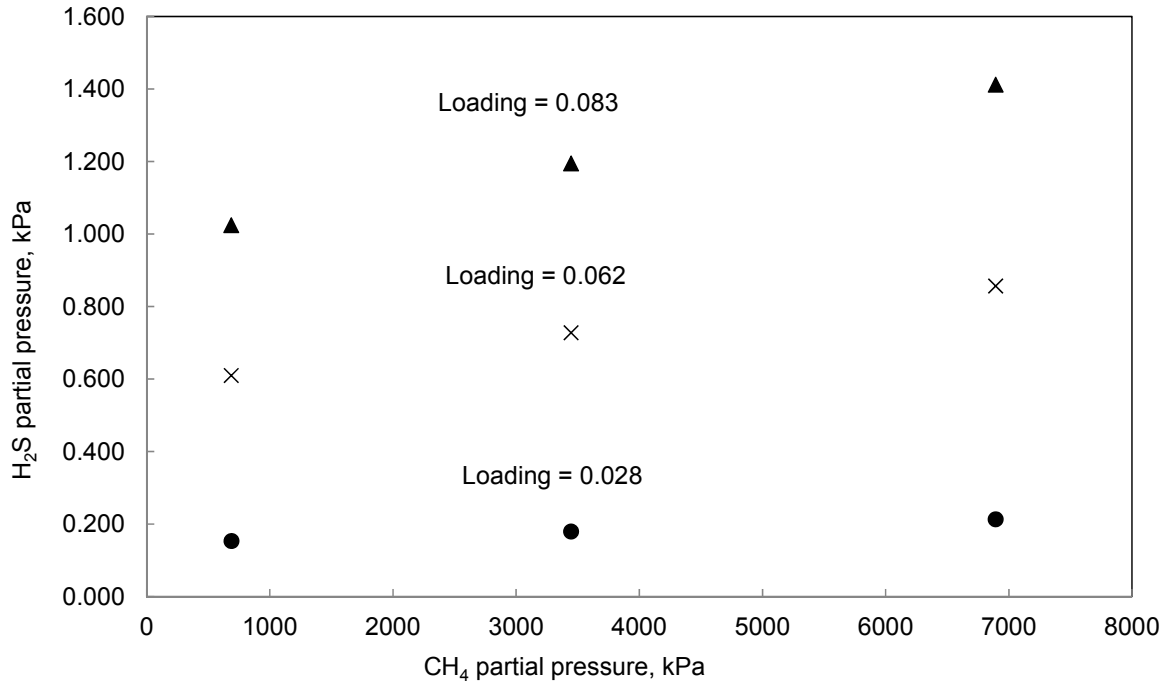

Figure 5-19. Experimental investigation on effect of methane presence on H_2S solubility in aqueous solution of 50 wt % MDEA at 25 °C and for three different loadings (mole H_2S/mole MDEA). ● (Loading = 0.028), × (Loading = 0.062), ▲ (Loading = 0.083), (Huttenhuis et al. 2007)

Figure 5-18 and Figure 5-19 show experimental investigations on methane influence on H_2S partial pressure, however as it mentioned partial pressure is not a good criterion for inspection as gas phase is not ideal. In order to assess the methane effect on acid gas equilibrium in liquid and gas phase, H_2S fugacity at low and high pressures should be compared. If the H_2S fugacity remains unchanged at low and high pressures, it can be concluded that methane does not have significant influence on the liquid phase and a decrease in acid gas solubility attributes to methane effect in the gas phase. To investigate the effect of methane on H_2S fugacity a gas mixture of H_2S and methane (MDEA and water presence in the gas phase is neglected) was considered. Note that at equilibrium H_2S fugacity in liquid and gas phase is the same. For this mixture, H_2S fugacity was calculated by SRK equation at the correspondence experimental conditions (temperature, total pressure, gas phase composition) to Dicko (Dicko et al. 2010) and Ter Maat (Ter Maat et al. 2004). Figure 5-20 shows H_2S fugacity calculations for mixture of CH_4 and H_2S at temperature, total pressure and vapor phase composition similar to what is reported in (Dicko et al. 2010).

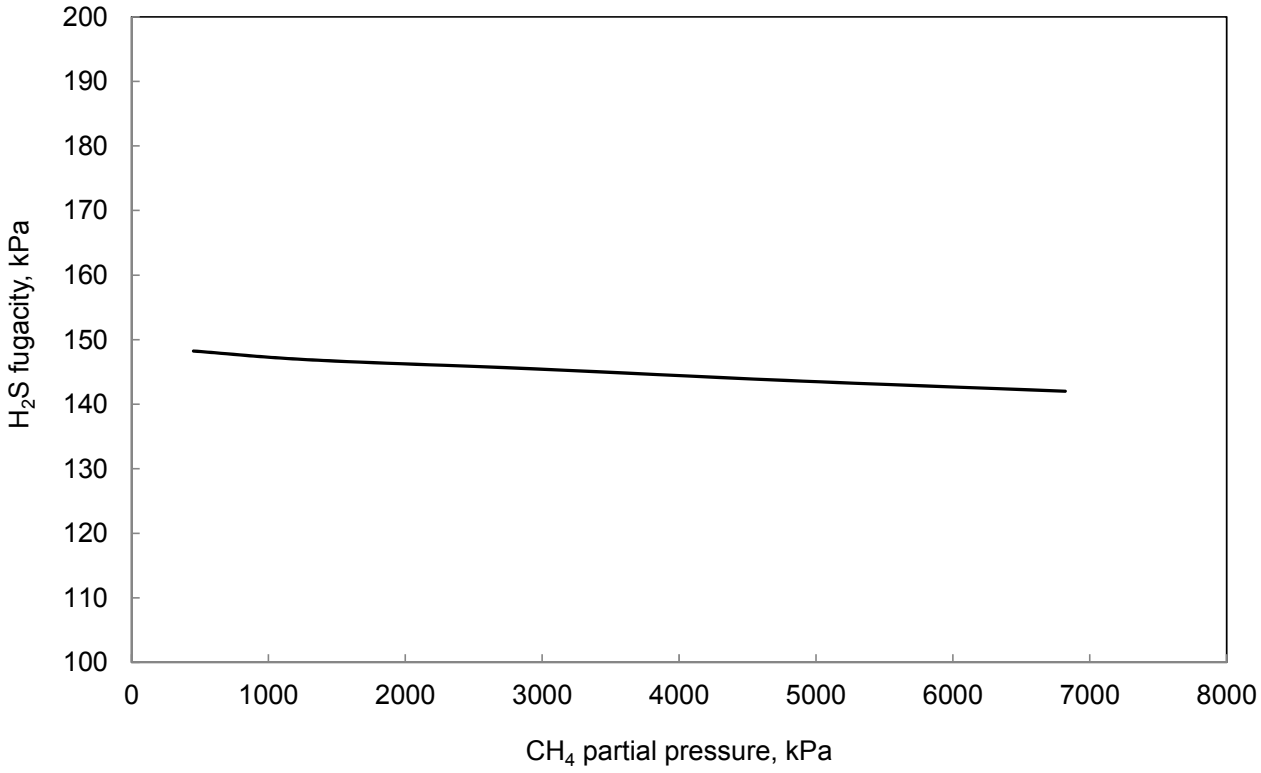

Figure 5-20. Modeling investigation on influence of methane partial pressure on H_2S fugacity for H_2S-CH_4 mixture at T, P_{Total}, y_i corresponds to Figure 5-18

As it can be seen from Figure 5-20, H_2S fugacity is constant and equal to 1.45 ± 0.03 bar in the pressure range of 6 MPa, this number is in agreement with the (Dicko et al. 2010) calculated results

with PR EoS, their calculations shows that H_2S fugacity is constant at 1.48 ± 0.01 bar at the studied pressure range. Figure 5-21 shows calculated results for H_2S fugacity in mixture of CH_4 and H_2S at Ter Maat (Ter Maat et al. 2004) reported experimental conditions (temperature, total pressure, and vapor phase composition).

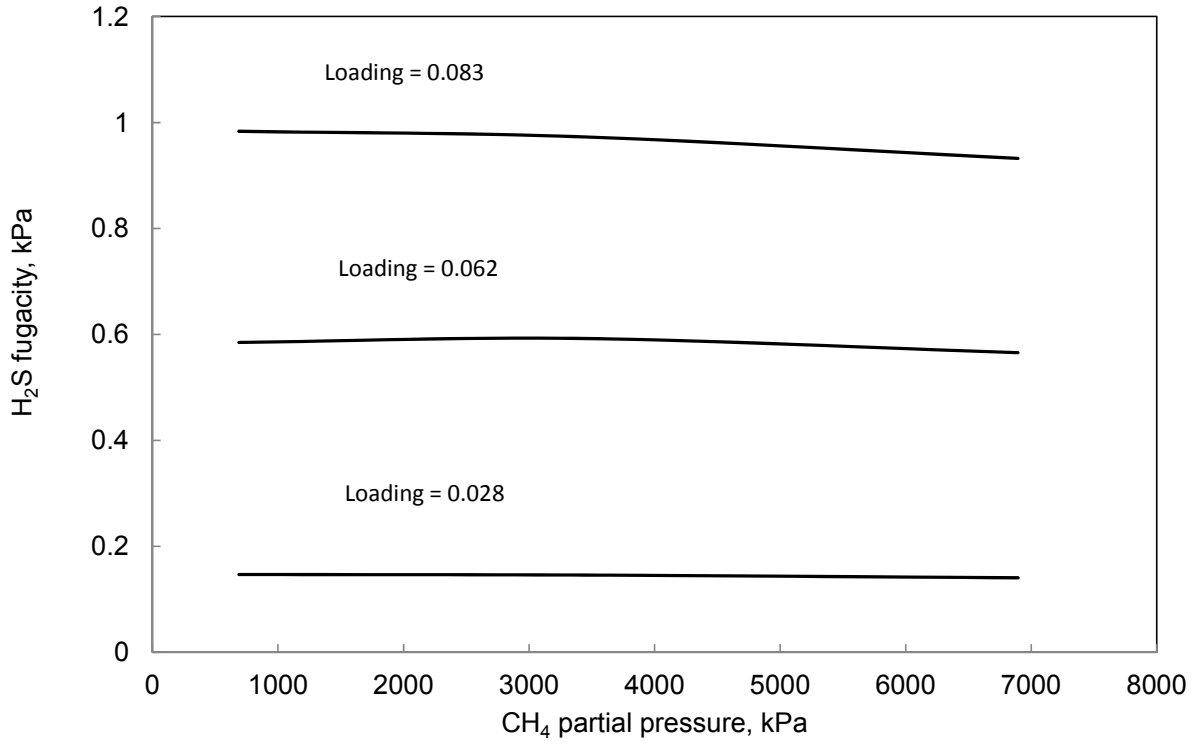

Figure 5-21. Modeling investigation on influence of methane partial pressure on H_2S fugacity for H_2S-CH_4 mixture at T, P_{Total}, y_i correspond to Figure 5-19

Figure 5-21 shows that H_2S fugacity at the same conditions as (Ter Maat et al. 2004) is independent of total pressure. From Figure 5-20 and Figure 5-21, it can be concluded that H_2S fugacity almost does not change with methane partial pressure in the studied pressure range. The following sections will discuss methane influence in liquid and gas phase separately.

Methane Influence on the liquid phase:

Calculations for H_2S fugacity in the gas phase show that H_2S fugacity is constant over the studied pressure range. Since at equilibrium H_2S fugacity is the same in gas and liquid phase, therefore it is concluded that at a given loading and temperature, increasing pressure over a liquid phase by inserting methane in the gas phase, does not change the H_2S fugacity in liquid phase. Depending on equilibrium calculations approach, non-ideality in the liquid phase is defined by fugacity

coefficients (when EoS is used for the liquid phase) or activity coefficients (when liquid phase is modeled by G^E models). Liquid phase is nearly incompressible, for this reason fugacity or activity coefficients in the liquid phase are assumed to be pressure independent. In the other hand the amount of methane dissolved in the liquid phase is very small and should not have significant influence on the liquid phase activity or fugacity coefficient. Therefore it can be concluded that high pressure over the liquid phase and presence of methane in the liquid phase do not significantly change H_2S activity or fugacity coefficients in the liquid phase.

Methane Influence on the gas phase:

Figure 5-22 plots the fugacity, partial pressure and fugacity coefficient of H_2S in a 50 wt % MDEA aqueous solution and a liquid loading of 0.74 and at 50 °C as a function of methane partial pressure. From this figure it can be seen that H_2S fugacity is independent of methane partial pressure. However, with increasing methane partial pressure, H_2S partial pressure is increasing (which is equivalent to decreasing H_2S solubility) while H_2S fugacity coefficient is decreasing. Therefore it can be concluded that a decrease in H_2S solubility with an increase in methane partial pressure can be attributed to a decrease in H_2S fugacity coefficient.

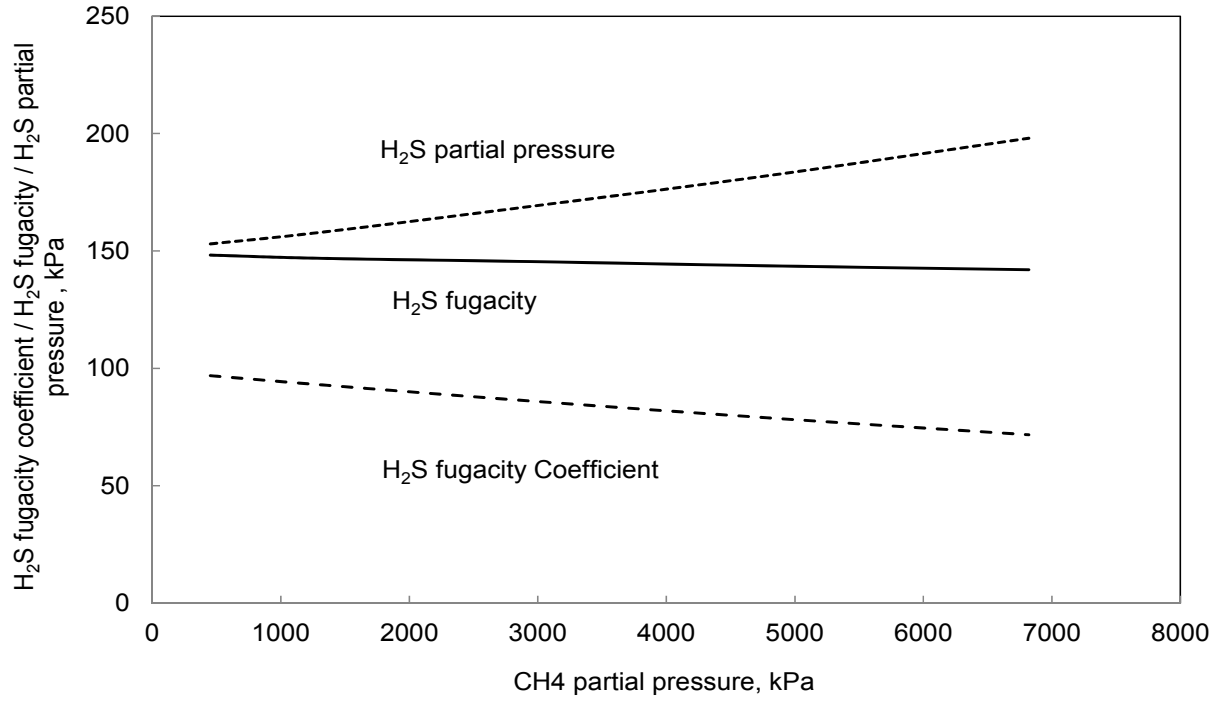

Figure 5-22. Fugacity, partial pressure and fugacity coefficient of H_2S in a 50 wt % MDEA aqueous solution and a liquid loading of 0.74 and at 50 °C. Solid line: H_2S fugacity, Dash line: H_2S fugacity coefficient, Dotted line: H_2S partial pressure

Eventually, it has been shown (experimentally and by the model) that H_2S solubility in aqueous MDEA solutions decrease with increasing total pressure or methane partial pressure. It was proven that H_2S fugacity is almost independent of the methane partial pressure (or system total pressure), however H_2S fugacity coefficient decrease with increasing methane partial pressure (or system total pressure). So, it was concluded that decreasing H_2S fugacity coefficient with methane partial pressure is responsible for decreasing H_2S solubility. It was also shown that decreasing H_2S solubility due to the increase in the gas phase pressure, so the methane affects the gas phase and not the liquid phase. It is worthwhile to mention that the same behavior was observed for CO_2 solubility in aqueous MDEA solutions (Huttenhuis et al. 2008). Experiments by (Huttenhuis et al. 2009) demonstrate that H_2S solubility (H_2Spartial pressure) is sensitive to the type of inert gas (nitrogen or methane). However, type of inert gas did not affect CO_2 solubility (CO_2 partial pressure) (Huttenhuis et al. 2009).

5.7 Conclusion

In this chapter models for H_2S-MDEA-H_2O and H_2S-CH_4-MDEA-H_2O systems have been developed, furthermore modeling results have been discussed. The models for H_2S-MDEA-H_2O and H_2S-CH_4-MDEA-H_2O systems begin with strong underlying models for H_2S-H_2O and CH_4-H_2O models systems. Binary interaction parameters for the H_2S-H_2O and CH_4-H_2O subsystems have been regressed to experimental data on pure H_2S vapor pressure, total pressure and H_2S solubility data of binary systems. The overall fit of the two subsystems are satisfactory and the developed models can fairly represent thermodynamic properties of the subsystems. Based on the developed model for H_2S-H_2O subsystem, a model for H_2S-MDEA-H_2O system were developed, model parameters were regressed to experimental total pressure, H_2S partial pressure and H_2S heat of absorption data. The developed model is valid over broad range of amine concentration, temperature, pressure and loading. Developed models for CH_4-H_2O and H_2S-MDEA-H_2O systems were combined to predict H_2S solubility at high pressures and in presence of methane, which is a typical absorber condition in natural gas treatment process. The same was done for CO_2 system, developed models for CH_4-H_2O and CO_2-MDEA-H_2O systems were used to predict CO_2 solubility at high pressures and in presence of methane. The predictions results prove that model adequately represent acid gas, CO_2 and H_2S, solubility in aqueous MDEA solutions at high pressures. Finally, methane influence on acid gas solubility was investigated and it was shown that methane has influence on acid gas fugacity coefficient, whereas acid gas fugacity is independent of methane

presence. Increasing methane partial pressure or system total pressure results in a decrease in acid gas solubility which is due to a decrease in acid gas fugacity coefficient. It was shown that this behavior is because of increasing gas phase pressure and methane dissolution in the liquid phase is not responsible for that.

Chapter 6

Vapor-Liquid Equilibrium and Density Measurements for CO_2-MDEA-H_2O and MDEA-H_2O Systems

6 Vapor-Liquid Equilibrium and Density Measurements for CO_2-MDEA-H_2O and MDEA-H_2O Systems

6.1 Chapter Overview

Alkanolamine processes is the dominant process in industry to remove acid gases, such as CO_2, H_2S and other sulfur compounds, from natural gas and industrial gas streams (Huttenhuis et al. 2007). The solvent composition is constantly changed in order to optimize the process (Huttenhuis et al. 2007). Solubility data of acid gases in aqueous alkanolamines are necessary to allow better design of acid gas removal processes. The solubility of a gas can be determined by measurement of the vapor-liquid equilibrium under known conditions of temperature and pressure. There is plenty of experimental CO_2 solubility data available in the open literature for aqueous solutions of MDEA. However, the reported data were measured for limited MDEA concentrations, to the best of our knowledge, so far 5 wt % and 75 wt % are the lowest and highest MDEA concentrations that CO_2 solubility data are reported for (Rho et al. 1997). The aim of this part of the study is to provide required experimental data and to fill the voids between the available experimental data for CO_2 solubility in aqueous MDEA solutions. Therefore, CO_2 solubility data were measured in aqueous MDEA solutions when MDEA wt % varies from 10 to 100. Most of the G^E thermodynamic models encounter problems in representing acid gas solubility at high amine concentrations because these models are not predictive and their parameters should adjust to proper experimental data. Inadequate data at high amine concentrations, results in unsuitable results of G^E models at these conditions. The data of this work that nearly cover the whole amine concentration range, could be used to validate available thermodynamic models and if necessary to refit model parameters.

These data could also serve as a validation tool for the developed thermodynamic model in the chapter 4 of this manuscript. This chapter details the experimental procedure used to measure CO_2 solubility and density measurements. Furthermore, it discusses developed model prediction results, together with prediction results from some commercial simulators against the measured experimental data.

6.2 Review on Experimental Techniques for Study of the Acid Gas Solubility

The methods involved in measuring acid gas solubility could be classified in three techniques, static, circulation and flow method (Anufrikov et al. 2007).

6.2.1 Static Method

In this measurement method, at constant temperature, amine aqueous solution with known composition is put into the cell, a required amount of the acid gas is introduced into the cell, the system is kept until equilibrium is attained. After equilibrium established (when temperature, pressure and composition become constant), equilibrium pressure and mole fractions of components in each of the coexisting phases are recorded (Anufrikov et al. 2007). This technique is widely used for measuring gas solubility data.

6.2.2 Circulation Method

In this method, a circulation pump is used to bubble the gas through the amine solution. The temperature is maintained constant with a thermostat during the experiments. The same as static method the amounts of each components of the system are fixed, the equilibrium pressure and phase compositions are recorded in the course of an experiment. The difference of this method with the static method is that in this method the vapor phase or the liquid phase or both phases are circulated and usually an inert gas is present in the system (Anufrikov et al. 2007).

6.2.3 Flow Method

Flow method is occasionally used to measure gas solubility. In this method, the partial pressure of the acid gas in the gas flow is set during the experiment and the liquid phase composition (the phase that gas passes through it) changes until equilibrium reached. In this method, temperature, numbers of moles of water and amine in the solution and partial pressure of the acid gas are the quantities which are set in the experiments (Anufrikov et al. 2007).

In summary, static method is sufficiently accurate, however the accuracy of the method decrease at low acid gas concentrations, that is due to the significant adsorption of gases to the apparatus wall. In contrast to static method, the flow method application is limited to low pressures. The circulation method is applicable at low and medium pressures. Unlike flow method it does not need a carrier gas. At elevated pressures, the circulation method is less accurate than the static method.

6.3 Experimental Design

The advantages of MDEA over the primary and secondary amines, like lower heat of reaction with acid gas, lower vapor pressure, lower corrosive tendency and capability of selective absorption of H_2S, make the process of natural gas treatment with MDEA more economically feasible. Solving problems associated with natural gas treatment process requires information on phase behavior of acid gas-alkanolamine-water systems mainly with MDEA as an alkanolamine. There are lots of data available for vapor-liquid equilibria of CO_2-MDEA-H_2O system. Table 6-1 summarized the available published experimental VLE data for CO_2-MDEA-H_2O system. Notice that collected data in Table 6-1 were gathered to the best of author knowledge and at the time of this work.

Table 6-1. Published VLE data for CO_2-MDEA-H_2O systems

MDEA Concentration, wt %	T, °C	P, kPa	Data Type	Reference
19, 32.11	40 to 140	139 to 5037 (P_{Total})	VLE	(Kuranov et al. 1996)
26, 47	25, 40, 75	3 to 4559 (P_{Total})	VLE	(Sidi-Boumedine et al. 2004)
19	40	791 to 4739 (P_{Total})	VLE	(Kamps et al. 2002)
32, 49	40, 80, 120	176.5 to 7565 (P_{Total})	VLE	(Kamps et al. 2001)
24	40	1155 to 3029 (P_{Total})	VLE	(Addicks et al. 2002)
24	40	12 to 3029 (P_{Total})	VLE	(Silkenbaumer et al. 1998)
19, 32, 48	40, 80, 120	0.12 to 69.3 (P_{CO_2})	VLE	(Ermatchkov et al. 2006a)
5, 20, 50, 75	50, 75, 100	0.775 to 268.3(P_{CO_2})	VLE	(Rho et al. 1997)
23, 47	40	0 to 93.6 (P_{CO_2})	VLE	(Austgen et al. 1991)
35	40, 100	0 to 262 (P_{CO_2})	VLE	(Jou et al. 1993)
50	25, 50, 75, 100	8.27 to 95.83(P_{CO_2})	VLE	(Park and Sandall 2001)
23, 50	40	0 to 0.55(P_{CO_2})	VLE	(Rogers et al. 1998)
23, 50	40, 70, 100, 120	0.002 to 5188 (P_{CO_2})	VLE	(Huang and Ng 1998)
11.8, 20, 23	25,38,50,65.5,115.5	11.1 to 6161.5(P_{CO_2})	VLE	(Maddox et al. 1987)
50	55, 70, 85	65.75 to 813.4(P_{CO_2})	VLE	(Ma'mun et al. 2005)
47	40, 55, 70, 80, 100	15.4 to 806.8(P_{CO_2})	VLE	(Xu et al. 1998a)
23, 28	25, 40, 70	101 to 2320(P_{CO_2})	VLE	(Jenab et al. 2005)
23	40, 60, 80	0.06 to 95.61(P_{CO_2})	VLE	(Ali and Aroua 2004)
23.8, 29.9	30, 40, 50	3.62 to 93(P_{CO_2})	VLE	(Kundu and Bandyopadhyay 2005)
22.98, 47.01	25, 40, 70, 100, 120	0.003 to 5260(P_{CO_2})	VLE	(JOU et al. 1982)
29.99	40	1.02 to 1169(P_{Total})	VLE	(Baek and Yoon 1998)
23.63	25	0.2 to 15.93(P_{CO_2})	VLE	(Lemoine et al. 2000b)

30	40, 80, 120	2000 to 10000 (P_{Total})	VLE	(Mathonat et al. 1997)
19.55, 47.01	100, 140, 160, 180, 200	103 to 4930(P_{CO_2})	VLE	(Chakma and Meisen 1987)
20, 30, 40	20, 40, 60	95.57 to 352.45(P_{CO_2})	VLE	(Kicrzkowska-Pawlak 2007)
18.96	40	1.17 to 3770(P_{CO_2})	VLE	(Macgregor and Mather 1991)

As expected majority of CO_2 solubility data in MDEA aqueous solutions are reported for 30 wt % to 50 wt % MDEA concentrations. Bibliographic study shows that (Rho et al. 1997)data contains the lowest and highest MDEA concentration for which CO_2 solubility is reported for. The main objective of this work is to fill the gaps in the available data and to provide the necessary data in order to make a reliable data base. As a result of this bibliographic study, it has been concluded that it is crucial to determine CO_2 solubility up to higher amine concentrations. As it mentioned earlier, CO_2 solubility in high concentrated amine solutions could be used to validate available G^E models since most of the G^E models do not show good results at high amine concentrations. It is worth to mention that nowadays industry starts to investigate higher MDEA concentrations. New data are reported herein for CO_2 solubility in aqueous MDEA solutions for MDEA wt % of 10 to 100, at constant pressure of 110 kPa (1.10 bar) and from 40 to 80 °C. The results of this study could serve as the basis for furthermore developing thermodynamic models for the acid gas removal process studies and the models can then be used for the design or optimization of acid gas treating plants.

6.4 Experimental Section

6.4.1 Chemicals

The chemicals used in this work include MDEA (Acros Organics, $\geq$ 99 % pure), CO_2 (Yara, $\geq$ 99 % pure) and Acetone (VWR (BDH PROLABO), $\geq$ 99 % pure). All chemicals were used without any further purification.

6.4.2 Experimental Apparatus

The apparatus used for measuring CO_2 solubility in aqueous MDEA solutions was called “low pressure cell”. The Low pressure cell was designed to give information on relative kinetics and phase equilibria. It could be used both for measuring rate of reaction and equilibrium CO_2 solubility in different solvents. It was designed to operate between 20° C and 80° C and between 100 and

7000 kPa (1 and 70bar).However the rig safety valve was set to 1800 kPa (18 bar). Figure 6-1 shows a schematic configuration of the Low pressure cell.

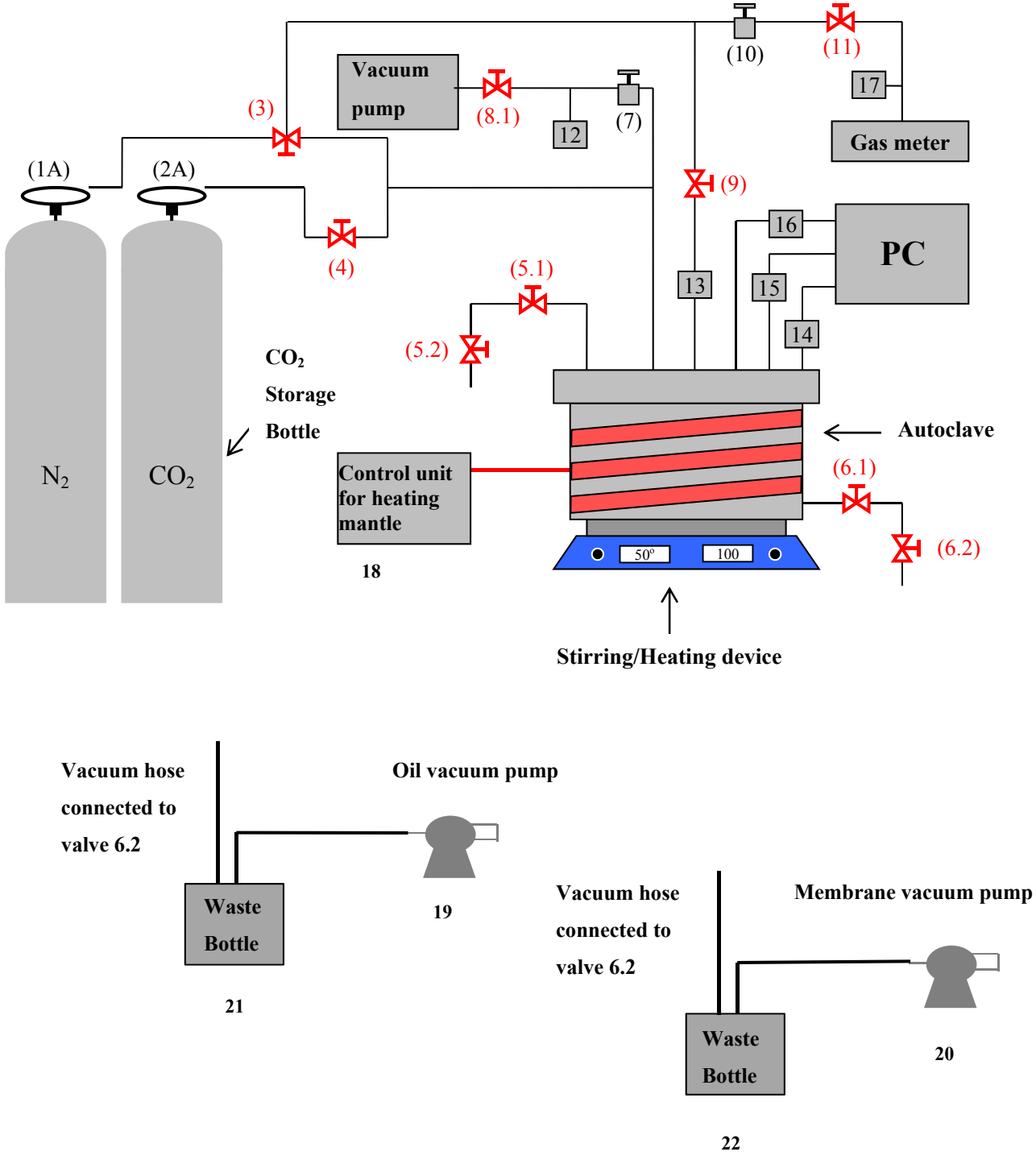

Figure 6-1. Sketch of the low pressure cell setup.

The main parts of the low pressure cell were a stainless steel autoclave, CO_2 gas storage bottle, a gas meter, a membrane vacuum pump, an oil vacuum pump, a stirring/heating device (combined hot plate and magnetic stirrer), autoclave heating mantle (there were heating cables surrounding the autoclave) and a PC with a control program for the rig, autoclave safety valve that was set to 1800 kPa (18 bar), a thermocouple in the gas phase inside the autoclave (T_1), a thermocouple in the liquid phase inside the autoclave (T_2), a temperature sensor in the Gas meter (T_{Gm}), a pressure sensor for measuring the pressure of the gas phase inside the autoclave (P_1), a pressure sensor for measuring gas pressure inside the gas meter (P_{Gm}) and the safety valve for the gas meter which operates at 130 kPa (1.3 bar). Different parts of the system are connected with several valves. Figure 6-1 is the sketch of the Low pressure cell set up; the corresponding numbers in Figure 6-1 refer to:

1. Nitrogen gas storage bottle
2. Carbon dioxide gas storage bottle
3. Ball valve to release nitrogen gas.
4. Ball valve to release carbon dioxide gas
5. Valves for filling the solvent. 5.1 is a needle valve and 5.2 is a ball valve.
6. Valves for the withdrawal of liquid samples, emptying, washing and vacuuming the autoclave. 6.1 is a ball valve and 6.2 is a needle valve.
7. Needle valve for withdrawal of gas sample and the suction of the vacuum.
8. Ball valve for withdrawal of gas samples. 8.1 and 8.2 are two different options for connecting a hose to a vacuum pump. Note that in this work, cell was vacuumed by connecting valve 6.2 with a hose to vacuum pumps.
9. Ball valve for connecting autoclave to the gas meter.
10. Needle valve for connecting autoclave to the gas meter.
11. Needle (Regulator) valve connected to the gas meters.
12. Pressure display
13. Safety valve set to 1800 kPa (18 bar). The release part of the safety valve was connected to the central exhaust system.
14. A thermocouple in the liquid phase inside the autoclave (T_2).
15. A thermocouple sensor in the gas phase inside the autoclave (T_1).
16. Pressure transducer for the autoclave (P_1).

17. Gas meter safety valve, set at 130 kPa (1.3 bar). The release part of the safety valve was connected to the central exhaust system.
18. Autoclave heating mantle, manufactured by Julabo (Julabo LC 3).
19. Oil vacuum pump.
20. Membrane vacuum pump.
21. Waste bottle connected to the oil vacuum pump.
22. Waste bottle connected to the membrane vacuum pump.

There were two vacuum pumps that were used for emptying and vacuuming the autoclave. A membrane vacuum pump which was made by GMBH+CO KG and it created the maximum vacuum of0.9 kPa (9 mbar). The oil vacuum pump was a rotary pump which created maximum 0.00004 kPa (0.0004 mbar) vacuum and was made by the same manufacture as the membrane pump. Pictures of the equipment are included in appendix 11.1.

6.4.2.1 Autoclave

As it mentioned autoclave was one of the main parts of the Low pressure cell (Figure 6-2) which was made of stainless steel. Figure 6-2 shows the autoclave more in detail. Figure 6-2 (a) shows the different parts of the autoclave and Figure 6-2 (b) presents the dimensions inside the autoclave. Autoclave was equipped with a stirring/heating device (which mixed the solution on a combined hotplate and magnetic stirrer device), surrounding electrical heat tracing, two K-type thermocouples and two pressure indicators. Autoclave and all linings connected to it were covered by insulated materials. Two thermometers were placed in the autoclave, one in the liquid phase and other one in the vapor phase. Both gas and liquid phase temperatures were measured with the two thermocouples within the accuracy of $\pm$0.1 °C. A pressure sensor was located outside the autoclave which measured the autoclave pressure within accuracy of $\pm$ 0.01 bar. The pressure in sampling port was read by a pressure indicator (0-4 bar, Keller, type: LE03/8104-0.2) within accuracy of $\pm$ 0.01 bar.

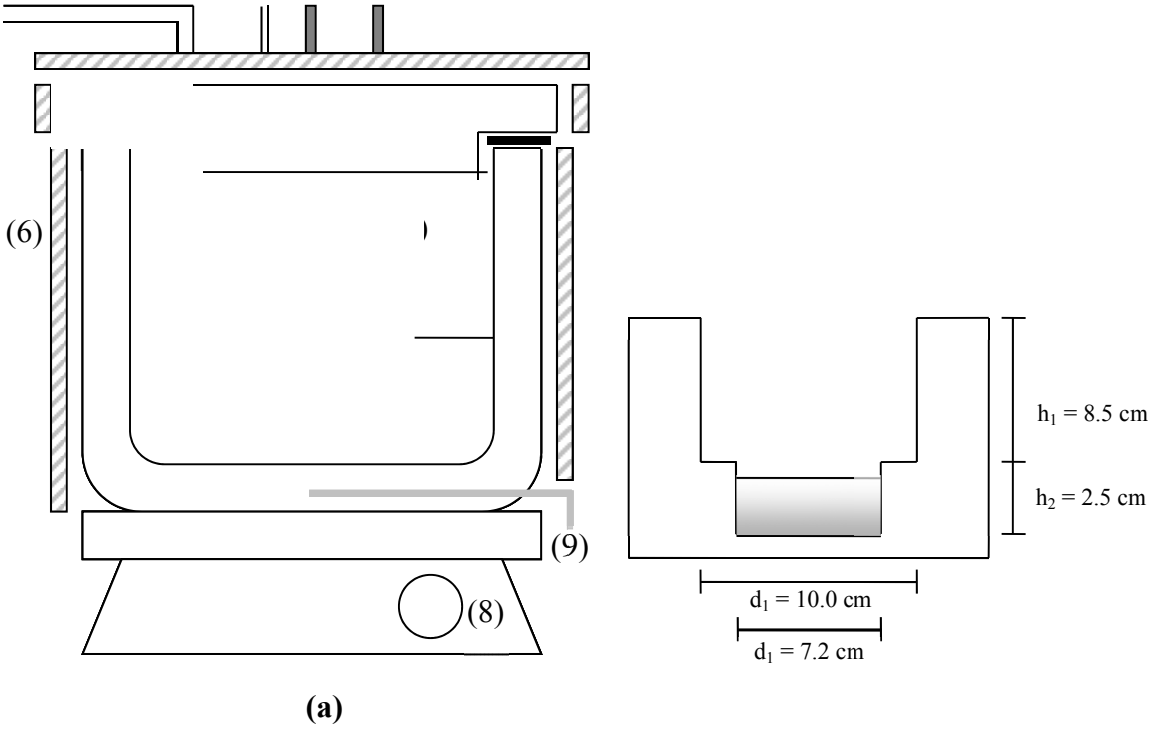

Figure 6-2. Sketch of the internal part of the autoclave: (1) thermocouple measuring temperature of gas phase inside autoclave, (2) thermocouple measuring temperature of liquid phase inside autoclave, (3) tube to insert solvent in the rig, (4) CO_2 gas inlet, (5) Washer, (6) insulation material, (7) stirring bar, (8) stirring and heating plate, (9) liquid withdrawal tube

The stir bar is manufactured by IKA RET, it monitors the temperature from 0 to 340 °C and the stirring rate could change from 0 to 1500 rpm[17].

6.4.2.2 Gas Meter

Gas meter is another main part of the rig which was manufactured by ROP France, temperature and pressure electronic devices (monitoring/reading) are from Eurotherm. The gas meter consists of a glass vessel with a piston to alter its volume, a volume meter, a temperature sensor, a pressure sensor, two vent valves and a safety valve set at 130 kPa (1.3 bar). The piston was driven by a motor. The volume of the gas was measured in a Pyrex tube with diameter of 100 ± 0.002 mm, in which the volume was measured within accuracy of ± 100 cm^3. The capacity of gas meter is 4000 cm^3. The gas meter is made of glass and therefore could not withstand high pressures; the maximum acceptable pressure in the gas meter was 130 kPa (1.3 bar). A safety valve set at 130 kPa (1.3 bar)

[17] rpm: Round per Minute

was connected to the gas meter to prevent it from breaking in case the pressure increases above 1.3 bar. During this study the gas meter pressure was set to be fixed at 110 kPa (1.1 bar). The temperature of the gas meter was measured with thermometer within the accuracy of ± 0.01°C. The pressure sensor has 0 to 4 bar pressure range and its accuracy was$\pm$ 0.01. Figure 6-3 shows the configuration of the gas meter. The gas meter can be operated in two modes: Manual and Automatic. In the manual mode the piston movement was done manually and in the automatic mode the piston movement was triggered automatically to keep the pressure constant. In this work, experiments were performed with the gas meter operated in the automatic mode. The gas meter allows for the automatic measurements of volumes of CO_2 at constant pressure.

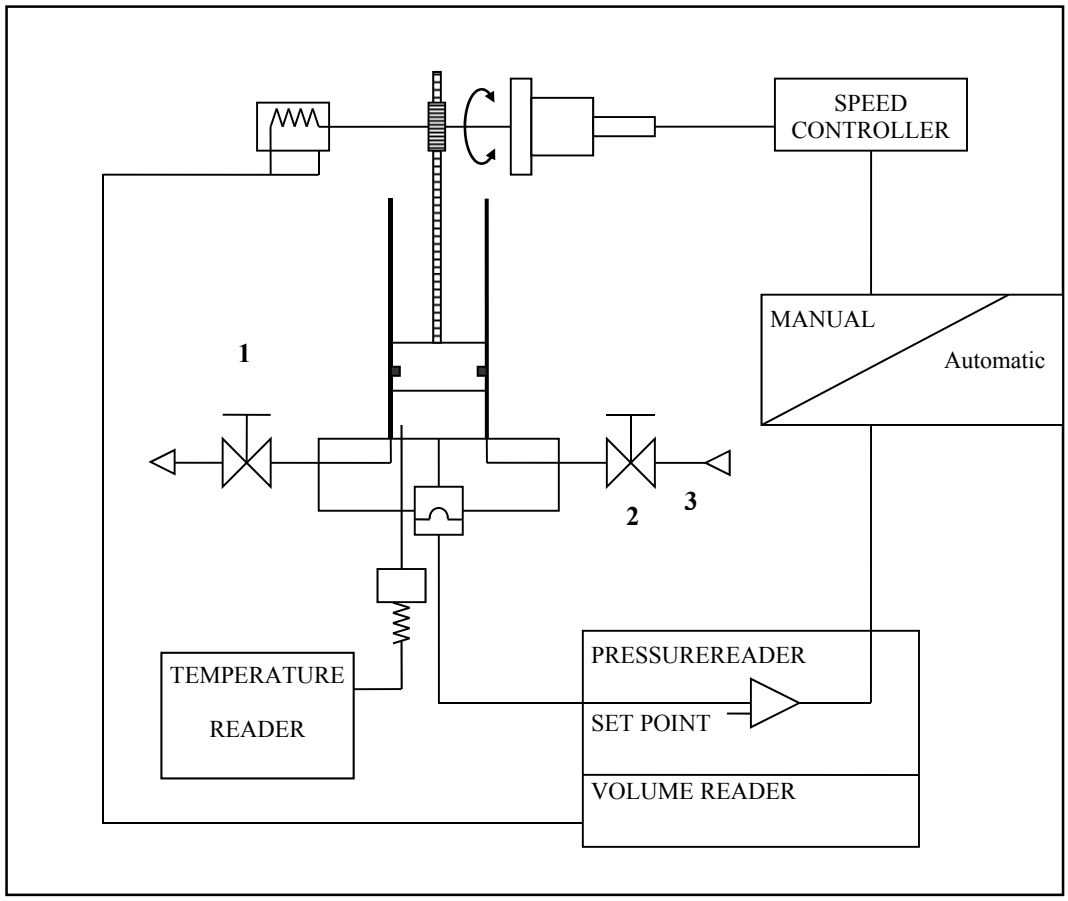

Figure 6-3. Sketch of the gas meter. (1) Valve connects the gas meter to the autoclave (corresponds number in Figure 6-1 is 11), (2) Vent valve, (3) Vent valve

6.4.3 Experimental Procedure

The experiments were performed using the static-synthetic method. Briefly, the rig was initially vacuumed and known amount of preloaded solvent (approximately 30g of the aqueous amine solution, note that for conditions where absorption capacity is low (low and high MDEA concentrations and high temperatures, the amount of solvent was increased to approximately 120 g in order to decrease the results inaccuracy (It will be discussed later in section 6.5.4)) was inserted through the valves 5.1 and 5.2. The solvent was continuously stirred during the experiment. The gas meter was filled with approximately 3.5 L pure CO_2. When the desired temperature was reached in the cell, the valves connecting the autoclave and the gas meter were opened, and the volume of the autoclave was filled with CO_2. The experiments were performed under constant pressure while volume of absorbed CO_2 per time was logged. Monitoring the temperature, the pressure and the cell volume ensured that the sample was withdrawn at equilibrium. Volume was always the last quantity that became constant. Stirring was very important to ensure while the system was approaching equilibrium. Due to slow mass transfer at the interface of gas and liquid, without stirring, pressure, temperature and volume could be unchanged without achieving equilibrium. A detailed procedure of performing experiments is as follows:

- Set the desired temperature: Both heaters (the hot plate and surrounded heater) were set to the target temperature.
- Clean the autoclave (Empty, Wash and Dry): Any remaining solvent from previous tests was removed by creating vacuum in the autoclave. The vacuum hose from the waste bottle (waste bottle which was connected to the membrane pump) was attached to the sampling port (valve 6.2). Membrane vacuum pump was turned on and the solvent was moved to the waste bottle. After emptying the autoclave, the cell was rinsed with approximately 600 cm^3 distilled water. Water was filled in a beaker and placed under the injection port (valve 5.2). The beaker was connected to the cell through the plastic hose attached to valve 5.2. At the same time the cell was vacuumed by attaching the vacuum hose from the waste bottle to the valve 6.2 and turning the membrane vacuum pump on. Water pulled in and was collected in a waste bottle. To dry water droplets remained in the cell, autoclave was rinsed with around 300 cm^3acetone. Afterwards the autoclave was vacuumed for a while with the oil vacuum pump in order to remove all the small droplets of the water or acetone remaining in the cell.

The cell was furthermore dried by CO_2. The cell was filled with CO_2 up to 250 kPa (2.5 bar) pressure, afterwards valves 5.1 and 5.2 were opened (or valves 6.2 and 6.1). Note that valve 5.2 (or 6.2) had been closed before the autoclave pressure went below atmospheric pressure to avoid the air entering the cell. Releasing CO_2 through valve 6.2 or valve 5.2 also flush the piping system.

- Fill the gas meter with CO_2: Gas meter was filled with CO_2 (approximately 3500 cm^3) through the autoclave. First autoclave was filled with CO_2. Notice that whenever there was CO_2 flow from storage bottle to autoclave, gas meter was isolated (all the valves between autoclave and gas meter were closed to avoid pressure build up inside the gas meter). Afterwards CO_2 was released to gas meter by opening valves 9, 10 and (slightly) valve 11. CO_2 flew from autoclave to gas meter until the pressure of the autoclave dropped to 1.1 bar. All the connection valves between CO_2 storage bottle and autoclave were closed during transferring CO_2 from autoclave to gas meter. As previously mentioned, gas meter was made of glass and was operated at constant pressure of 1.1 bar., it could not stand higher or lower pressures as the regulated one (1.1 bar).
- Injecting the solvent: Before injecting the solvent, cell was vacuumed through valve 6.2 while all valves except valve 5.2 and 11 were opened. A disposable syringe was filled with approximately 30cm^3 of the prepared solvent. The possible formed air bubbles inside the syringe were removed to avoid air bubbles entering the autoclave. The weight of filled syringe before injection was noted (w_1). Through valves 5.2 and 5.1 solvent was injected to the cell. After injection syringe was weighted again (w_2) in order to calculate exact amount of injected solvent.
- Start the experiments: A new log file was created and logging was started. The stirrer was turned on. After about 20 to 30 minutes when the solvent reached the stable temperature and thermal equilibrium between the gas phase and the solvent was attained (whenever P_1, T_1 and T_2 became constant with time) $CO_2$was introduced into the cell. Valves 10 and 11 were completely opened to let the CO_2 freely flow through the connecting pipes; gas meter volume and temperature were noted. Finally by opening valve 9, CO_2 was introduced to the cell and volume of the autoclave was filled with CO_2. The gas meter volume was continuously logged during the experiment and when this volume stopped changing with time, equilibrium was assumed. Logging was stopped and connecting valve between gas

meter and autoclave, valve 9, was closed. The final values of gas meter volume and temperature were noted down.

6.4.3.1 Solvent Preparation

All solvent solutions were prepared gravimetrically from distilled and degassed water. Water was degassed by vacuum. Based on the desired composition of the solution, required amounts of MDEA and degassed water were mixed to create a homogeneous solvent solution. Solvents were kept in a closed bottle and their exposure to air was minimized to avoid contamination with CO_2 from the air. According to (Huang and Ng 1998) the total residual amount of CO_2in a freshly prepared amine solution will increase to 0.0005 mole CO_2/mole MDEA if the solution is exposed to air for 6 hours in an Erlenmeyer. Therefore in this study the influence of residual CO_2 in the prepared amine solutions on experimental results were safely neglected since the exposure of the prepared solution to atmosphere was few minutes and the studied loading range was much greater than 0.0005. An analytical balance (Mettler Toledo) with resolution of 0.0001 g was used for the preparation of the solvent solutions

6.4.3.2 Set up Preparation

Calibration

The autoclave was connected to two temperature thermocouples and one pressure sensor. One thermocouple was used to measure the temperature of the gas phase, while the other was immersed in the liquid phase. The criterion to confirm that the system has reached thermal equilibrium was that these two K-type thermocouples probes show the same temperature within the correspondence experimental uncertainty. Both thermocouples were calibrated against a reference thermometer and the calibration parameters were entered into the calibration file used by the program that controls the rig and logs the results. The temperature calibrator is from Ametek (Type: ATC-650 B), the reference platinum probe (Type: STS-100 A 901) had a temperature range of -150 to 650 °C and an accuracy of $\pm$ 0.01 °C. The pressure transducer and the pressure indicator connected to the autoclave were calibrated using a reference pressure gauge. The DPI 610 pressure calibrator from GE Druck, with a pressure range of -1.01 to 413.68 bar and an accuracy of 0.025 % full scale range was used to calibrate the pressure sensor. The calibration of temperature, pressure and volume sensors in the gas meter was done by the supplier prior to these experiments. Two safety valves connected to the setup were also calibrated before starting the experiments.

Leak Test

Both gas meter and autoclave were tested against leakage. The test involves filling the autoclave with CO_2 and pressurization of the autoclave to the specified test pressure. Leak was tested by observing whether there is a pressure loss in the autoclave. In the same way, gas meter was filled with certain volume of CO_2andleak was tested by observing whether or not there is a volume loss. Autoclave, linings and gas meter were regularly checked for leakage.

Gas Meter Clean up

The gas meter was washed with $CO_2$to be certain that there is no other gas e.g. nitrogen or oxygen present in the gas meter. The gas meter was washed following two different methods. In the first method the gas meter was fully filled with CO_2 to the highest level and then emptied. The procedure was repeated for 5 times. This method allowed the gas diluted with respect to any possible impurities. In the Second method the piston was at its lowest level and CO_2 was purged through the gas meter.

6.4.3.3 Measuring Cell Volume

Volume refers to the volume of a cavity inside the autoclave and tubing. Volume of the autoclave was considered as the volume of cavity between valve 5.1 and 6.1. Volume of the autoclave (volume of cavity between valve 5.1 and 6.1) was measured by filling the autoclave with water. Volume of water that filled the autoclave was recorded as autoclave volume. This procedure was repeated for 5 times. Overall the average of repeat tests was considered as the cell volume. Cell volume was estimated to be 599.34 $cm^3 \pm 2.11$ cm^3. The reported expanded uncertainty is based on a standard uncertainty multiplied by a coverage factor k = 2, providing a level of confidence of approximately 95 %.

6.4.3.4 Measuring Cell Dead Volumes

Dead volume refers to the volume of a cavity inside the autoclave and tubing that does not have the possibility to meet acid gas or solvent. Low pressure cell total dead volume consists of two parts: **1)** Volume of the tube between valve 5.1 and 5.2 (sampling port) **2)** Volume of the tube that connects valve 9 to the autoclave (Notice that during the experiments volume of gas meter was recorded while valves 10 and 11 were opened and valve 9 was closed. Hence the volume of tube between valve 9 and gas meter was already included in gas meter volume).

- Volume of the tube between valve 5.1 and 5.2 (sampling port)

During the injection of solvent, some of the solvent may trapped in the tube connected valve 5.1 to 5.2. Therefore the mass of injected solvent should be corrected for the trapped amount. To measure the amount of solvent that may be trapped in the tubing, solvent with 50 wt % MDEA concentration (50 mass% was the average of injected solvent concentrations) was injected to the rig and mass of solvent that trapped in the tube was measured. The procedure was repeated in 4 parallels, average of the 4 measurements was considered as the amount of the solvent that during the injection trapped in tube connected valve 5.1 to valve 5.2. The trapped amount was estimated to be $0.50\ \mathrm{g} \pm 0.06\ \mathrm{g}$. Note that depending on the viscosity of the solvent and injection conditions, the trapped amount of solvent could be lower or higher than the estimated value. It was not possible to measure exact amount of trappedsolvent for each experiment, therefore the estimated amount of 0.5 g was considered as the trapped amount for all experiments. Bearing in mind that the amount of solvent that trapped in sampling tubing is one of the sources of the uncertainty of these measurements, however compare to the amount of injected solvent this amount is very little but not negligible (about 1.5 % of the injected solvent).

- Volume of the tube that connects valve 9 to the autoclave

The volume of tube volume that connects valve 9 to autoclave was neglected as it was very small compare to autoclave dead volume (The length of tube was approximated to be 20 cm with outer diameter of 1/8 inch). However it is recommended to measure this volume for future work.

6.5 Results

6.5.1 Validation

In order to test the experimental set up and procedure, some validation (introductory) experiments were performed and compared to Statoil data. Despite of this study, most of the data available in open literature were measured at constant volume while pressure varied. Therefore some previous Statoil measurements were chosen to validate this work experiments. The validation runs were conducted at 50 °C with 50 and 30 wt % MDEA. Comparison of the results showed that the new measurements were well in line with previous attempts. The uncertainty of the validation

measurements for loading (mole CO_2/mole MDEA) at 50 °C and 50 mass % MDEA was estimated to be $\pm$0.02 and at 50 °C and 30 wt % MDEA the inaccuracy was estimated to be $\pm$0.01.

6.5.2 Results Analysis

6.5.2.1 Volumetric Analysis

In these experiments generally liquid phase loading has been calculated from the volume of CO_2 absorbed in the liquid phase. Avoiding liquid phase analysis was one of the advantages of the used method. In this work the mentioned method is called volumetric analysis. This section demonstrates how loading was calculated from volumetric data. Loading indicates mole numbers of CO_2absorbed in the liquid phase per MDEA moles present in the liquid phase.

$$Loading = \frac{CO_2 \text{ mole numbers present in the liquid phase}}{MDEA \text{ mole numbers present in the liquid phase}} \quad (6\text{-}1)$$

The amount of CO_2 absorbed in the liquid phase was calculated from the total mole balance, CO_2 mole numbers in the liquid phase was calculated from the difference between total moles of CO_2 introduced to the system and number of moles present in the vapor phase.

$$n_{CO_2,\text{Introduced}} = n_{CO_2,Vapr\ phase} + n_{CO_2,Liquid\ phase} \quad (6\text{-}2)$$

Total mole numbers of CO_2 introduced to the system were calculated from the volume of CO_2transferred from gas meter to the autoclave and by considering the pure CO_2inside the gas meter as an ideal gas. This assumption seems realistic as the pressure of gas meter is low (1.1 bar), therefore:

$$n_{CO_2,\text{Introduced}} = \frac{P_{G\_m} V_{CO_2}}{R T_{G\_m}} \quad (6\text{-}3)$$

Where P_{G_m} is the pressure of gas meter which is equal to 1.1 bar, V_{CO_2} is the volume of CO_2 absorbed in the liquid phase, R is the gas constant and T_{G_m} is the temperature of gas meter. Volume of CO_2 absorbed in the liquid phase was obtained from the recorded values of initial and final volume of CO_2 inside the gas meter.

$$V_{CO_2} = V_{G_m,Final} - V_{G_m,Initial} \quad (6\text{-}4)$$

Number of moles of CO_2 present in the vapor phase was calculated based on the ideal gas assumption for the vapor phase which is in equilibrium with the liquid phase inside the autoclave. Hence:

$$n_{CO_2,Vaporphase} = \frac{P_{CO_2} V_{Vaporphase}}{RT_{Autoclave}} \quad (6\text{-}5)$$

Where R is the gas constant, $T_{Autoclave}$ is the temperature of autoclave, P_{CO_2} is the partial pressure of CO_2 and $V_{Vapor\ phase}$ is the volume of the vapor phase. $V_{Vapor\ phase}$ was calculated through equation (6-6):

$$V_{Vapor\ phase} = V_{Cell\ total\ volume} - V_{Solvent} \quad (6\text{-}6)$$

$V_{Cell\ total\ volume}$ is the cell volume and as already illustrated was measured equal to 599.34 $cm^3 \pm 2.11\ cm^3$. $V_{Solvent}$ is the solvent volume calculated by the following equation.

$$V_{Solvent} = m_{Solvent} . d_{Solvent} \quad (6\text{-}7)$$

Where $m_{Solvent}$ is mass of solvent inside the autoclave and was calculated from equation (6-8):

$$m_{Solvent} = m_{Injected\ solvent} - m_{Stuck\ solvent} \quad (6\text{-}8)$$

Where $m_{Injected\ solvent}$ is the mass of injected solvent and $m_{Stuck\ solvent}$ is the mass of solvent that trapped in the tube between valve 5.1 and valve 5.2 and as already illustrated equal to 0.5 g. $d_{Solvent}$ is the solvent density, note that instead of density of loaded solution, density of unloaded solvent was measured by Anton-Paar density meter and was considered as density of solvent. This is a reasonable assumption as density of unloaded solution at the conditions of this work was almost similar to the density of loaded solution. Density of liquid sample withdrawn from the cell at 70 °C and MDEA mass % of 50 and 60 and at 80 °C and MDEA mass % of 20 was measured by Anton-Paar method and compared to density of unloaded solution at the same conditions. Comparison between densities of unloaded and loaded solutions demonstrated that densities of loaded solutions were in average 2.1170 % (0.0210 g/cm^3) higher than densities of unloaded solutions. Therefore because density of unloaded solvent was very close to the density of loaded solution and since loading calculations was not sensitive to density of solvent density of unloaded solutions were measured and utilized in loading calculations.

Partial pressure of CO_2 was calculated through the following equation. MDEA presence in the vapor phase was neglected because the studied temperature range was far below MDEA boiling point.

$$P_{CO_2} = P_{Total} - P_{H_2O} \quad (6\text{-}9)$$

Where P_{Total} is the total pressure (1.1 bar) and P_{H_2O} is the partial pressure of water. Partial pressure of water was calculated form the Rault law and by considering both liquid and vapor as ideal phases, hence:

$$P_{H_2O} = P_{Total} \cdot y_{H_2O} = x_{H_2O} \cdot P_{H_2O}^{Sat} \quad (6\text{-}10)$$

Where y_{H_2O} is the mole fraction of water in the vapor phase, x_{H_2O} is the mole fraction of water in the liquid phase and $P_{H_2O}^{Sat}$ is the vapor pressure of water at the interested temperature. x_{H_2O} was calculated from the following equations.

$$x_{H_2O} = \frac{n_{H_2O}}{n_{H_2O} + n_{MDEA}} \quad (6\text{-}11)$$

MDEA mole numbers, n_{MDEA} , was calculated from :

$$n_{MDEA} = \frac{m_{MDEA}}{Mw_{MDEA}} \quad (6\text{-}12)$$

Mw_{MDEA} is MDEA molecular weight and equal to 119.1628 g/mole and m_{MDEA} is the mass of MDEA in the solution and calculated by:

$$m_{MDEA} = \left(\frac{MDEA\ wt\%}{100}\right) . m_{Solvent} \quad (6\text{-}13)$$

Water mole numbers, n_{H_2O} , was calculated from :

$$n_{H_2O} = \frac{m_{H_2O}}{Mw_{H_2O}} \quad (6\text{-}14)$$

Mw_{H_2O} is water molecular weight and equal to 18.01532 g/mole and m_{H_2O} is the mass of water in the solution and calculated from the total mass balance:

$$m_{H_2O} = m_{Solvent} - m_{MDEA} \quad (6\text{-}15)$$

Applying above procedure results in calculation of loading (equation (6-1)) from volumetric data obtained from set up. Note that after CO_2 absorption, solvent composition and MDEA mass % was

calculated again and subsequent loading was obtained. However calculation results showed that solvent composition and consequently loading almost remained unchanged, therefore to avoid further calculations, loading was obtained as illustrated above, based on the initial solvent composition.

6.5.2.2 Titration Analysis

Loading results presented here were calculated based on the volumetric data obtained from the set up and calculations were done according to the procedure presented in section 6.5.2. However in order to validate the method used to calculate CO_2 solubility from volumetric data, liquid phase was also analyzed by precipitation titration method, note that this method is very time consuming thus only few measurements were done with this method. In precipitation titration method liquid phase sample withdrawn from the cell was mixed with NaOH. Therefore CO_2 and HCO_3^- present in the liquid phase react with NaOH and create CO_3^{2-}. Then $BaCl_2$ was added to the mixture, which made CO_3^{2-} precipitate as $BaCO_3$. The created solution was heated in order to agglomerate the $BaCO_3$ particles. Then the solution was cooled to ambient temperature and filtered. The filter and filtrate were placed in distilled water and $BaCO_3$ was dissolved by the addition of HCl. Then the solution was boiled in order to remove CO_2. Afterwards the solution was cooled to ambient temperature and titrated with NaOH to find the amount of HCl that was not used for dissolving $BaCO_3$. From the amount of HCl found by titration and the amount used for dissolving $BaCO_3$, the amount of CO_2 present in the solution was calculated. The titration was performed with automate titrator (Metrohm 809 Titrando). As it will be shown in Table 6-9 toTable 6-12 later on, the titration results confirmed volumetric results except for 10 mass % MDEA in which suspected results were obtained. The reason behind the inaccuracy of results at 10 mass % MDEA is unknown.

6.5.3 Measured Values

The VLE experiments for CO_2-MDEA-H_2O system as defined in section 6.3 were executed at constant total pressure 110 kPa (1.1 bar), for 10 to 100 wt % MDEA concentrations and from 40 to 80 °C.As illustrated in section 6.5.2 information on density of solution is required for converting volume based data to mass based data, density experiments were carried out for MDEA-H_2O solutions for 10 to 100 wt % MDEA and at 40 to 80 °C. The remainder of this section will demonstrate results of density and VLE experiments in figures and tables.

6.5.3.1 Density Experiments

Before starting VLE experiments, density of prepared aqueous MDEA solutions were measured using Anton-Paar (DMA 4500 M) density meter. To test the accuracy of the procedure and equipment some validation experiments were performed and compared to literature data. The validation runs were carried out for 20 and 30 wt % MDEA and at 40, 50 and 60 °C. Table 6-2 presented comparison between introductory experiments with data of (Li and Lie 1994).

Table 6-2. Comparison between this study and literature densities of aqueous MDEA solutions

T (°C)	ρ ($g.cm^{-3}$)			
	20 mass% MDEA		**30 mass% MDEA**	
	Li et al.[18](Li and Lie 1994)	**This study**	**Li et al.** (Li and Lie 1994)	**This study**
40	1.0089	1.0087	1.0171	1.0172
50	1.0040	1.0037	1.0116	1.0116
60	0.9983	0.9984	1.0057	1.0057
AAD%		**0.0200**		**0.0082**

AAD% refers to absolute relative deviation between two sources data and calculated by the following formula:

$$AAD\% = \sum_{i=1}^{n} \frac{abs\,(x_{i,source\,1} - x_{i,source\,2})}{n} \quad (6\text{-}16)$$

Where $x_{i,source}$ refers to the value from the specified source and n represents the number of data. The accuracy of the measured densities was estimated to be $\pm 0.0001 g.cm^{-3}m$, on the basis of comparison with literature data. Densities of 10 to 50 mass % MDEA aqueous solutions at temperature of 15 to 60 °C have been studied by (Alghawas et al. 1989), (Rinker et al. 1994) studied densities at the same concentration range but from 20 to 100 °C. (Li and Lie 1994) measured densities of 20 to 30 mass % MDEA aqueous solutions from 30 to 60 °C. (Bernal-García et al. 2003) measured densities of MDEA aqueous solutions over whole amine concentration range from 10 to 90 °C. In this work density measurements were done for 10 to 90 mass % MDEA aqueous solutions from 40 to 80 °C. Measurement results are tabulated in Table 6-3 to Table 6-7. As previously mentioned the accuracy of the density measurements in this work was estimated to be ± 0.0001 $g.cm^{-3}$(± 0.01 %) on the basis of comparison with literature data.

[18](Li and Lie 1994) data were in good agreement with Alghawas et al.(Alghawas et al. 1989).

Table 6-3. Density measurements at 40 °C

MDEA mass %	$\rho\ (g.cm^{-3})$			
	Test 1	**Test 2**	**Test 3**	**Average of tests (Reported value)**
10.00	1.0001	1.0002	1.0002	1.0002
20.00	1.0087	1.0089	1.0087	1.0088
29.88	1.0172	1.0173	1.0172	1.0172
39.99	1.0256	1.0257	1.0260	1.0258
49.96	1.0330	1.0331		1.0330
60.00	1.0384	1.0387		1.0385
64.27	1.0400	1.0403		1.0401
69.87	1.0416	1.0417		1.0417
79.88	1.0394	1.0396		1.0395
90.00	1.0352	1.0342		1.0347
100.00	1.0251		1.0002	1.0251

Table 6-4. Density measurements at 50 °C

MDEA mass %	$\rho\ (g.cm^{-3})$		
	Test1	**Test 2**	**Average of tests (Reported value)**
10.00	0.9956	0.9958	0.9957
20.00	1.0038		1.0038
29.88	1.0117		1.0117
39.99	1.0195		1.0195
49.96	1.0265		1.0265
60.00	1.0313		1.0313
64.27	1.0325		1.0325
69.87	1.0338		1.0338
79.88	1.0326		1.0326
90.00	1.0275	1.0218	1.0275
100.00	1.0176		1.0176

Table 6-5. Density measurements at 60 °C

MDEA mass %	$\rho\ (g.cm^{-3})$		
	Test 1	**Test 2**	**Average of tests (Reported value)**
10.00	0.9901	0.99071	0.9904
20.00	0.9984		0.99843
29.88	1.0058		1.00576
39.99	1.0129		1.01293
49.96	1.0195		1.0195
60.00	1.0234		1.0234
69.87	1.0259		1.02587
79.88	1.0245		1.0245
90.00	1.0194		1.0194
100.00	1.0098		1.00975

Table 6-6. Density measurements at 70 °C

MDEA mass %	$\rho\ (g.cm^{-3})$
10.00	0.9848
20.00	0.9920
29.88	0.9989
39.99	1.0057
49.96	1.0112
60.00	1.0154
69.87	1.0177
79.88	1.0163
90.00	1.0114
100.00	1.0018

Table 6-7. Density measurements at 80 °C

MDEA mass %	$\rho\ (g.cm^{-3})$
10.00	0.9784
20.00	0.9855
29.88	0.9922
39.99	0.9984
49.96	1.0035
60.00	1.0071
69.87	1.0092
79.88	1.0079
90.00	1.0032
100.00	0.9946

Figure 6-4 presents measured densities against MDEA mass % at four different temperatures. As expected, densities of aqueous MDEA solutions decrease with increasing temperature.

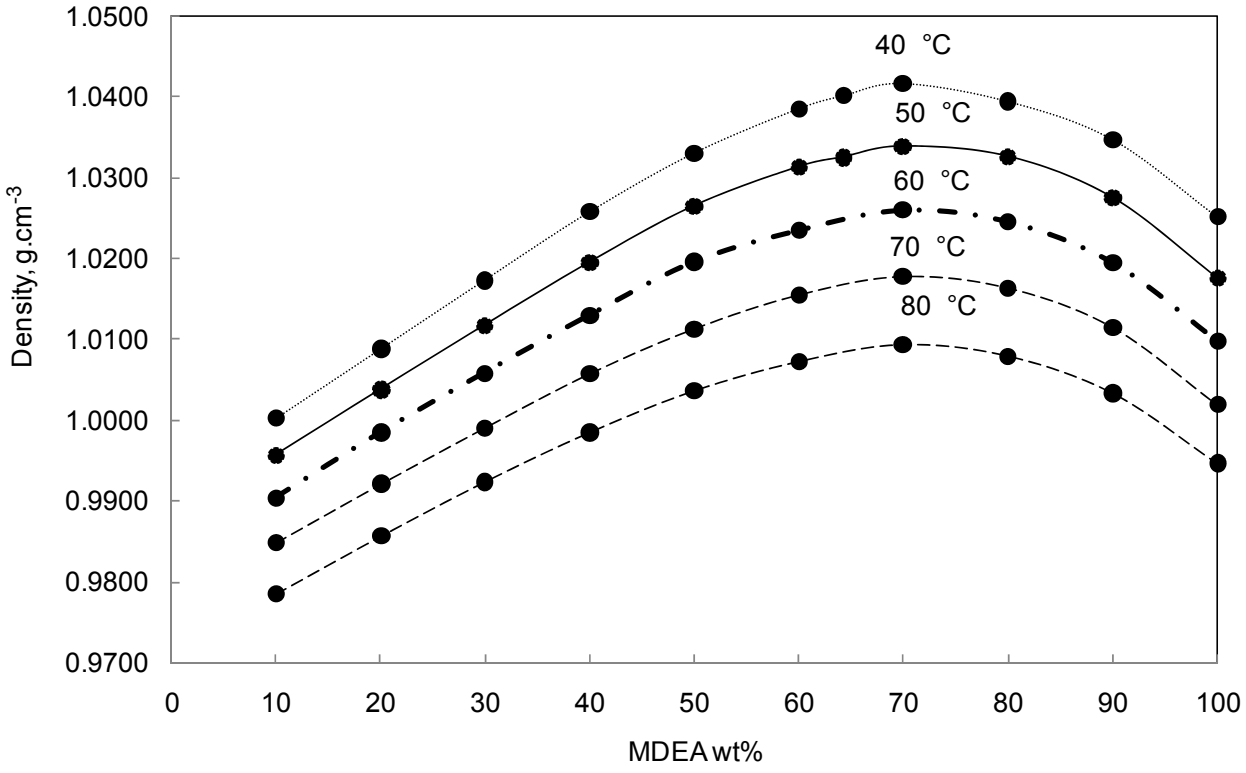

Figure 6-4. Measured densities of aqueous MDEA solutions at 40, 50, 60, 70 and 80 °C. Lines are added to show trend of measured data.

6.5.3.2 VLE Experiments

This section illustrates CO_2 solubility data obtained for 10 different amine solutions with concentration of MDEA from 10 mass % to pure at five different temperatures, 40 to 80 °C and at constant total pressure of 110 kPa (1.1 bar). The experimental data are reported in tables and plotted in figures. Tables and figures contain the results obtained from volumetric and titration analyses. It is worth to note both volumetric and titration values presented in tables and figures are the average between tests. Generally most of the measurements were repeated two or three times (repeatability tests), and the average between tests was considered as the final reported value.

Table 6-8. Experimental solubility data of CO_2 in an aqueous solution of MDEA at 40.00 °C and 110.00kPa (1.10bar)

MDEA mass %	$\alpha(\frac{\text{mol } CO_2}{\text{mol MDEA}})$[19]	
	Volumetric Analyses	Titration Analysis
10.06	0.91	1.13*
20.00	0.78	
29.88	0.76	
39.99	0.70	
49.96	0.62	
64.27	0.45	
69.87	0.38	
79.88	0.24	
90.00	0.12	
100.00	0.04	

**As mentioned, this value does not validate the volumetric method.*

Figure 6-5 shows the obtained experimental CO_2 solubility data at 40.00 °C and 110.00 kPa (1.1 bar). Results are plotted as loading against MDEA mass %.

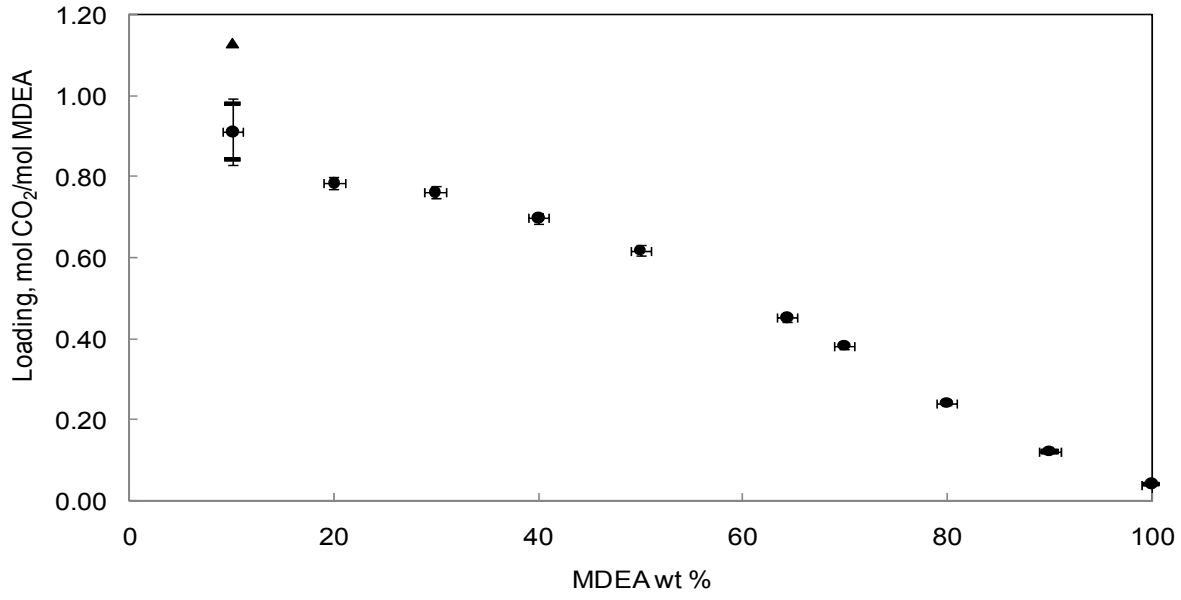

Figure 6-5. Solubility data of CO_2 at 40.00 °C and 110.00 kPa.●, Volumetric Analyses; ▲, Titration analysis; ═, Repeatability Tests

[19] α represents loading, mole CO_2 per mole MDEA

Table 6-9. Experimental solubility data of CO_2 in an aqueous solution of MDEA at 50.00 °C and 110.00 kPa (1.10bar)

MDEA mass %	$\alpha(\frac{\text{mol } CO_2}{\text{mol MDEA}})$	
	Volumetric Analyses	Titration Analysis
10.06	0.80	
20.00	0.67	
29.88	0.59	
39.99	0.52	0.54
49.96	0.42	
64.27	0.30	
69.87	0.24	
79.88	0.16	
90.00	0.07	
100.00	0.02	

Figure 6-6 presents the obtained experimental CO_2 solubility data at 50.00 °C and 110.00 kPa (1.1 bar).

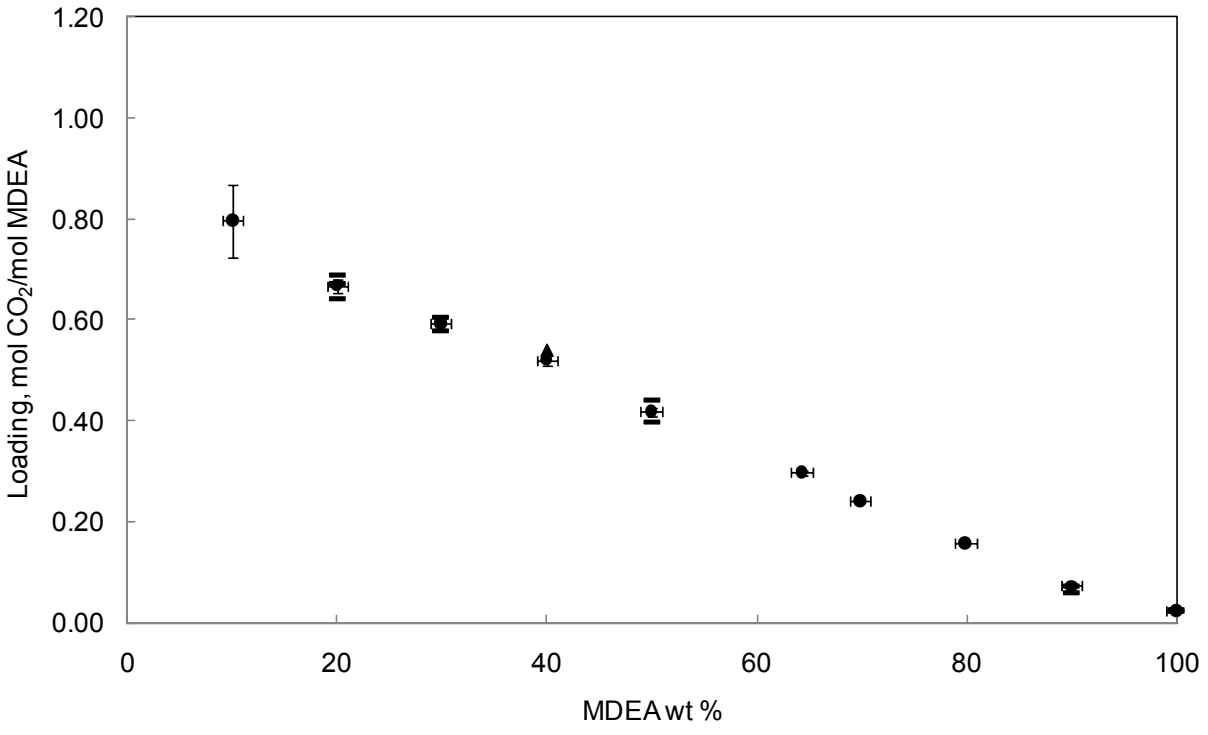

Figure 6-6. Solubility data of CO_2 at 50.00 °C and 110.00kPa.●, Volumetric Analyses; ▲, Titration analysis; —, Repeatability Tests

Table 6-10. Experimental solubility data of CO_2 in an aqueous solution of MDEA at 60.00 °C and 110.00 kPa (1.10bar)

MDEA mass %	$\alpha(\frac{\text{mol } CO_2}{\text{mol MDEA}})$	
	Volumetric Analyses	Titration Analysis
10.00	0.72	0.98*
20.00	0.58	
29.88	0.47	
39.99	0.39	
49.96	0.31	
60.00	0.23	0.25
69.87	0.15	
79.88	0.08	
90.00	0.04	
100.00	0.01	

**As mentioned, this value does not validate the volumetric method.*

Figure 6-7 represents the experimental loading against MDEA concentration data at 60.00 °C and 110.00 kPa (1.10bar).

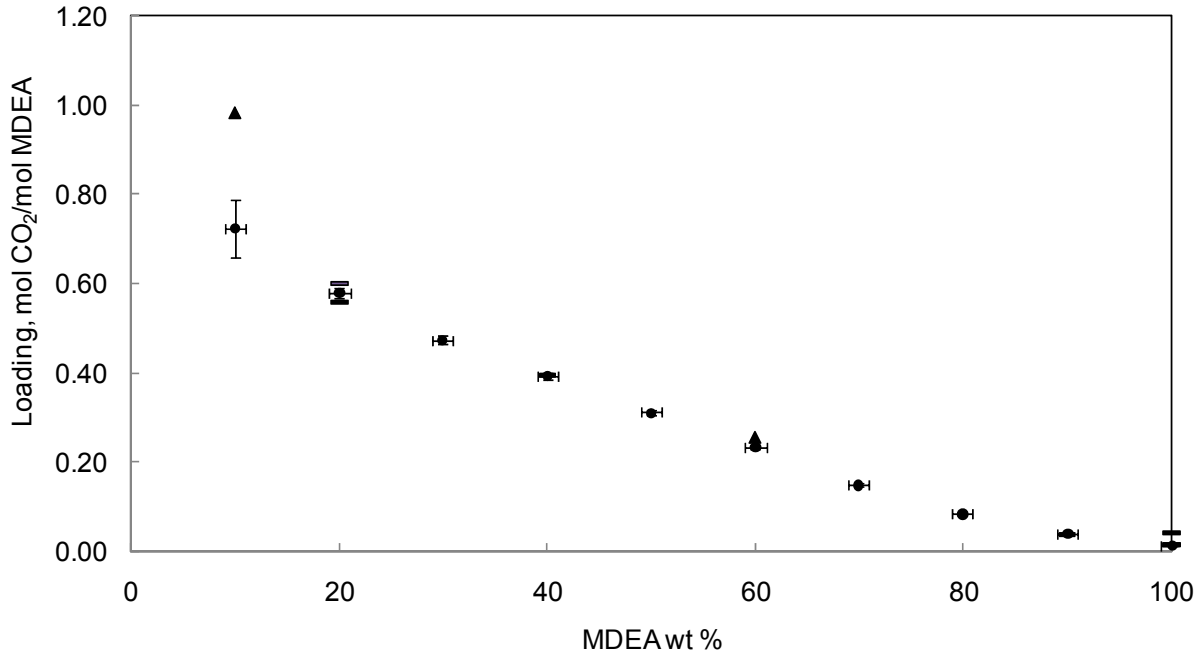

Figure 6-7. Solubility data of CO_2 at 60.00 °C and 110.00kPa.●, Volumetric Analyses; ▲, Titration analyses; —, Repeatability Tests

Table 6-11. Experimental solubility data of CO_2 in an aqueous solution of MDEA at 70.00 °C and 110.00 kPa (1.10bar)

MDEA mass %	$\alpha(\frac{\text{mol } CO_2}{\text{mol MDEA}})$	
	Volumetric Analyses	Titration Analyses
10.00	0.53	0.93*
20.00	0.39	
29.88	0.34	
39.99	0.28	0.27
49.96	0.20	
60.00	0.14	
69.87	0.09	
79.88	0.05	
90.00	0.02	
100.00	0.01	0.01

**As mentioned, this value does not validate the volumetric method.*

Figure 6-8 shows the measured CO_2 solubility at 70.00 °C and 110.00 kPa (1.10bar).

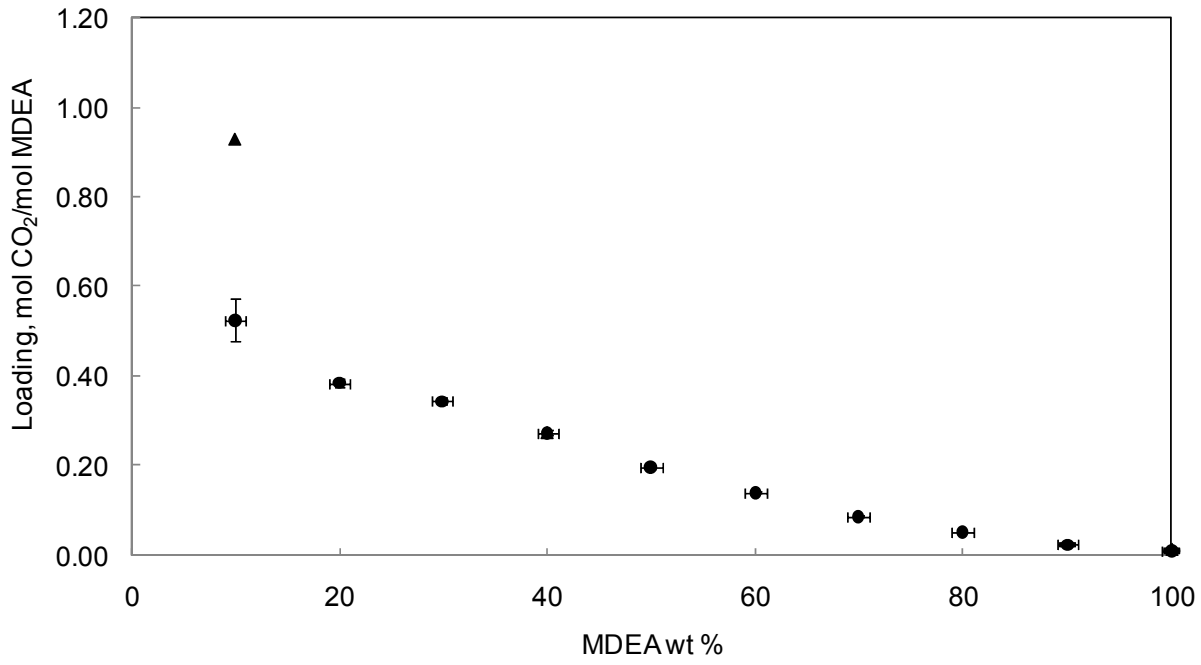

Figure 6-8. Solubility data of CO_2 at 70.00 °C and 110.00kPa.●, Volumetric Analyses; ▲, Titration analyses; —, Repeatability Tests

Table 6-12. Experimental solubility data of CO_2 in an aqueous solution of MDEA at 80.00 °C and 110.00 kPa (1.10bar)

MDEA mass %	$\alpha(\frac{\text{mol } CO_2}{\text{mol MDEA}})$	
	Volumetric Analyses	Titration Analyses
10.00	0.45	
20.00	0.28	
29.88	0.20	
39.99	0.15	0.21
49.96	0.11	0.10
60.00	0.07	0.05
69.87	0.05	
79.88	0.03	
90.00	0.01	0.01
100.00	0.01	0.008

Figure 6-9 represents measured values at 80.00 °C and 110.00 kPa (1.10bar).

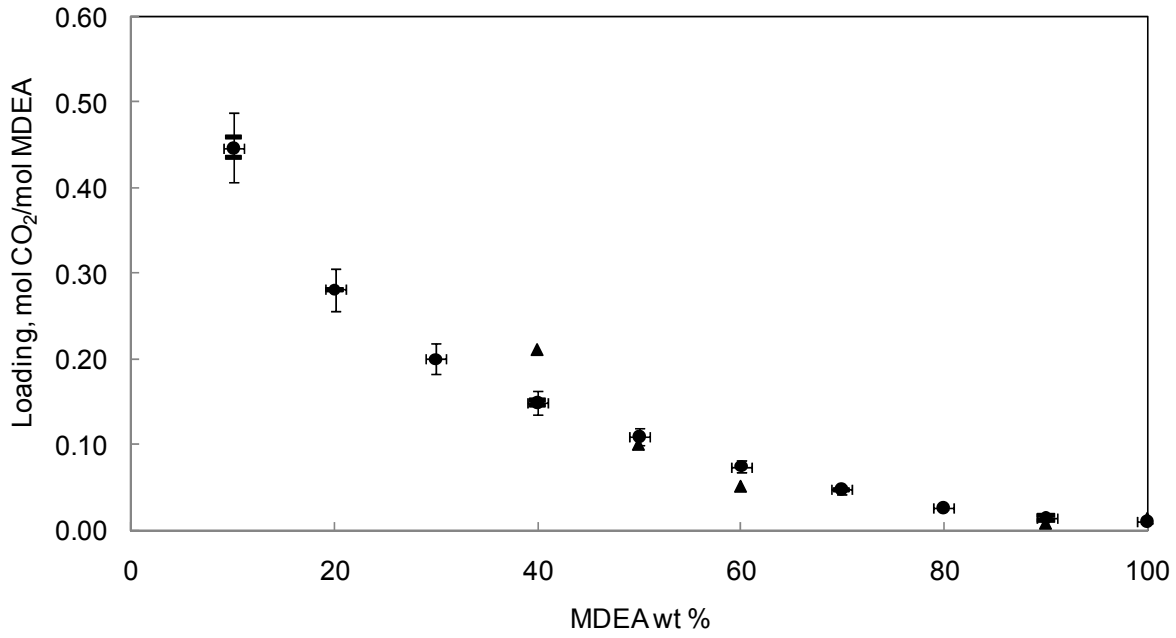

Figure 6-9. Solubility data of CO_2 at 80.00 °C and 110.00kPa.●, Volumetric Analyses; ▲, Titration analyses; ═, Repeatability Tests

As mentioned earlier due to some unknown reasons titration analysis results for 10 wt % MDEA were not accurate. Therefore titration results for 10 wt % MDEA were disregarded, however they were presented in the tables and figures.

6.5.4 Uncertainty Analysis

6.5.4.1 Equipment Uncertainties

The aqueous MDEA solutions were prepared in a flask by dissolving known amounts of amines in distilled degassed water. 500 cm^3 of solvent was prepared and kept in a sealed bottle, for each experiment the required amount of solvent was taken from the bottle. The amine concentration in the aqueous solution was determined gravimetrically with an uncertainty of $\pm$ 0.0001 g.

The gas meter pressure was measured within $\pm$ 0.01 bar, gas meter temperature was measured with uncertainty of $\pm$ 0.01°C and volume of gas meter was determined within accuracy of $\pm$100 cm^3.

The temperature in the autoclave were measured with two thermocouples within $\pm$ 0.1 ℃, the autoclave pressure was measured with calibrated pressure sensor within $\pm$ 0.01 bar.

6.5.4.2 Overall Uncertainties

The amount of CO_2 absorbed in the liquid phase was calculated based on volumetric method.

Volumetric Method

As it mentioned earlier, liquid phase was mainly determined through the volumetric method. The main sources of uncertainty are listed below:

- Cell total volume: Cell total volume is one of the main sources of uncertainty of the solubility data obtained from the volumetric method. At conditions where absorption capacity is low, uncertainty in cell total volume is more pronounced. At high temperatures, low and high amine concentrations, the absorption capacity is thus the volume of CO_2 that entered the autoclave is small and comparable to the cell total volume. Therefore the amount of CO_2that entered the autoclave becomes almost similar to the amount of remainedCO_2 in the vapor and consequently the amount of CO_2 in the liquid phase will be very small which leads to increase the inaccuracy of solubility data. In conclusion, at these conditions the uncertainty in the total volume played significant role in the overall uncertainty of loading. Notice that this uncertainty could be reduced by using more solvent.

- Volume measurements in the gas meter.
- Pressure measurements in the gas meter.
- Temperature measurements in the gas meter.
- Temperature measurements in the gas and liquid phase inside the autoclave.
- Mass of the solvent.
- Dead volume in the injection tube (tubing between valve 5.1 and 5.2).
- Dead volume of the tube between valve 9 and autoclave
- Isobaric condition of the measurements (autoclave and gas meter should had the same pressure).

Analysis over the mentioned sources of uncertainty showed that cell total volume and gas meter volume measurements are the main effective sources on overall loading uncertainty. However uncertainty in the gas meter volume were taken into account both in initial and final CO_2 volume and the difference between these values was used for loading calculations. The overall of uncertainty of results is estimated to be between 7 % and 10 % for 10 mass % MDEA and for 20 to 100 mass % MDEA the uncertainty is estimated to be 2%. However the error for the loading results at 80 °C is estimated to increase to 8 to 10 %.

6.6 Model Validation

The results of CO_2 solubility experiments of this work were compared to the developed thermodynamic model and four thermodynamic models available in commercial simulators. Developed thermodynamic model in chapter4and thermodynamic packages of four simulators have been used to predict CO_2 solubility in aqueous solutions of 10 to 90 mass % MDEA at temperatures of 40, 50, 60, 70 and 80 °C and total pressure of 110.00 kPa (1.10 bar). Notice that parameters of the developed model have not been fitted to the new data; data of this work were utilized to validate the developed model as a predictive tool. It is recommended to retune the model parameters to the new data of this work. Table 6-13 to

Table 6-17 summarized predicted and measured values at each studied temperature. Deviations between models and measured values are shown in bold in tables. Calculated and measured results are also depicted graphically in Figure 6-10 to Figure 6-16. At the end of the section a comparison between different models proficiency and the reason for the difference between developed model predictions and experimental values will be discussed.

Table 6-13. Comparison between experimental CO_2 solubility and models predictions at T = 40.00 °C and P = 110.00kPa

MDEA mass %	Experimental Loading* Values	Predicted Loading Values									
		Developed Model, Extended UNIQUAC		Simulator 1		Simulator 2		Simulator 3		Simulator 4	
		Calculated Values	*Bias Dev.***	Calculated Values	Bias Dev.	Calculated Values	Bias Dev.	Calculated Values	Bias Dev.	Calculated Values	Bias Dev.
10.06	0.91	0.93	*-0.02*	0.93	*-0.02*	0.92	*0.00*	0.87	*0.04*	0.93	*-0.02*
20.003	0.78	0.87	*-0.08*	0.87	*-0.08*	0.85	*-0.07*	0.78	*0.01*	0.86	*-0.08*
29.88	0.76	0.81	*-0.05*	0.83	*-0.07*	0.81	*-0.05*	0.72	*0.04*	0.81	*-0.05*
39.99	0.70	0.74	*-0.04*	0.80	*-0.10*	0.78	*-0.08*	0.68	*0.02*	0.77	*-0.07*
49.96	0.62	0.63	*-0.01*	0.79	*-0.17*	0.75	*-0.13*	0.65	*-0.03*	0.75	*-0.13*
64.27	0.45	0.43	*0.02*	0.79	*-0.34*	0.71	*-0.26*	0.64	*-0.19*	0.70	*-0.25*
69.87	0.38	0.35	*0.04*	0.83	*-0.45*	0.67	*-0.28*	0.61	*-0.23*	0.68	*-0.30*
79.88	0.24	0.20	*0.04*	0.83	*-0.59*	0.00	*0.24*	0.56	*-0.32*	0.68	*-0.44*
90	0.12	0.03	*0.09*	0.84	*-0.71*	0.00	*0.12*	0.10	*0.02*	0.70	*-0.58*
AARD*%**		**15**		**120**		**42**		**29**		**93**	

**Loading = mole CO_2/mole Amine*

**Bias Dev.: Bias Deviation = loading $_{Exp}$- loading $_{Calc}$*

$^{***}AARD = \frac{1}{n}\sum_{i=1}^{n}\frac{|P_{CO_2S,exp}-P_{CO_2,calc}|}{P_{CO_2,exp}}$

Figure 6-10 plotted model predictions and measured values at 40 °C.

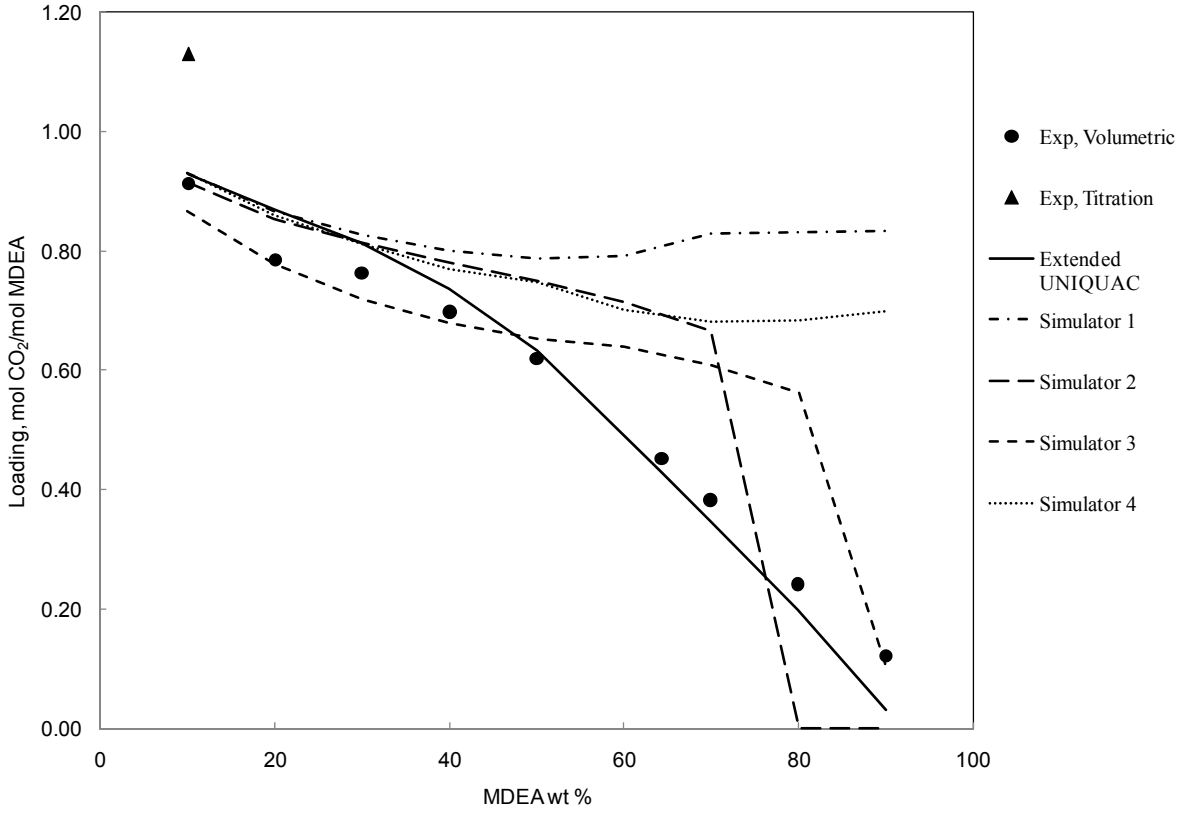

Figure 6-10. Comparison between model predictions and measured values at 40.00 °C and 110.00kPa. ●, Experimental (Volumetric Analysis);▲, Experimental (Titration analysis); Solid Line, Extended UNIQUAC; Dash-Dot Line, Simulator 1; Long Dash Line, Simulator 2; Dash Line, Simulator 3; Dot Line, Simulator 4

Table 6-14. Comparison between experimental CO_2 solubility and models predictions at T = 50.00 °C and P = 110.00kPa

MDEA mass %	Experimental Values	Predicted Loading Values									
		Developed Model, Extended UNIQUAC		Simulator 1		Simulator 2		Simulator 3		Simulator 4	
		Calculated Values	Bias Dev.	Calculated Values	Bias Dev.	Calculated Values	Bias Dev.	Calculated Values	Bias Dev.	Calculated Values	Bias Dev.
10.06	0.80	0.86	*-0.06*	0.85	*-0.05*	0.84	*-0.04*	0.77	*0.02*	0.85	*-0.05*
20.003	0.67	0.78	*-0.11*	0.76	*-0.09*	0.76	*-0.09*	0.67	*0.00*	0.76	*-0.09*
29.88	0.59	0.70	*-0.11*	0.71	*-0.11*	0.70	*-0.11*	0.61	*-0.01*	0.70	*-0.10*
39.99	0.52	0.61	*-0.09*	0.67	*-0.15*	0.65	*-0.13*	0.56	*-0.04*	0.64	*-0.12*
49.96	0.42	0.50	*-0.08*	0.65	*-0.23*	0.59	*-0.17*	0.53	*-0.11*	0.60	*-0.18*
64.27	0.30	0.32	*-0.02*	0.64	*-0.35*	0.49	*-0.20*	0.55	*-0.26*	0.57	*-0.27*
69.87	0.24	0.25	*-0.01*	0.68	*-0.44*	0.32	*-0.08*	0.58	*-0.34*	0.55	*-0.30*
79.88	0.16	0.13	*0.02*	0.68	*-0.52*	0.00	*0.16*	0.20	*-0.04*	0.55	*-0.39*
90	0.07	0.01	*0.06*	0.69	*-0.61*	0.00	*0.07*	0.06	*0.02*	0.56	*-0.49*
AARD%		**21**		**184**		**28**		**34**		**144**	

Figure 6-11 shows model predictions in comparison with the measured values at 50 °C.

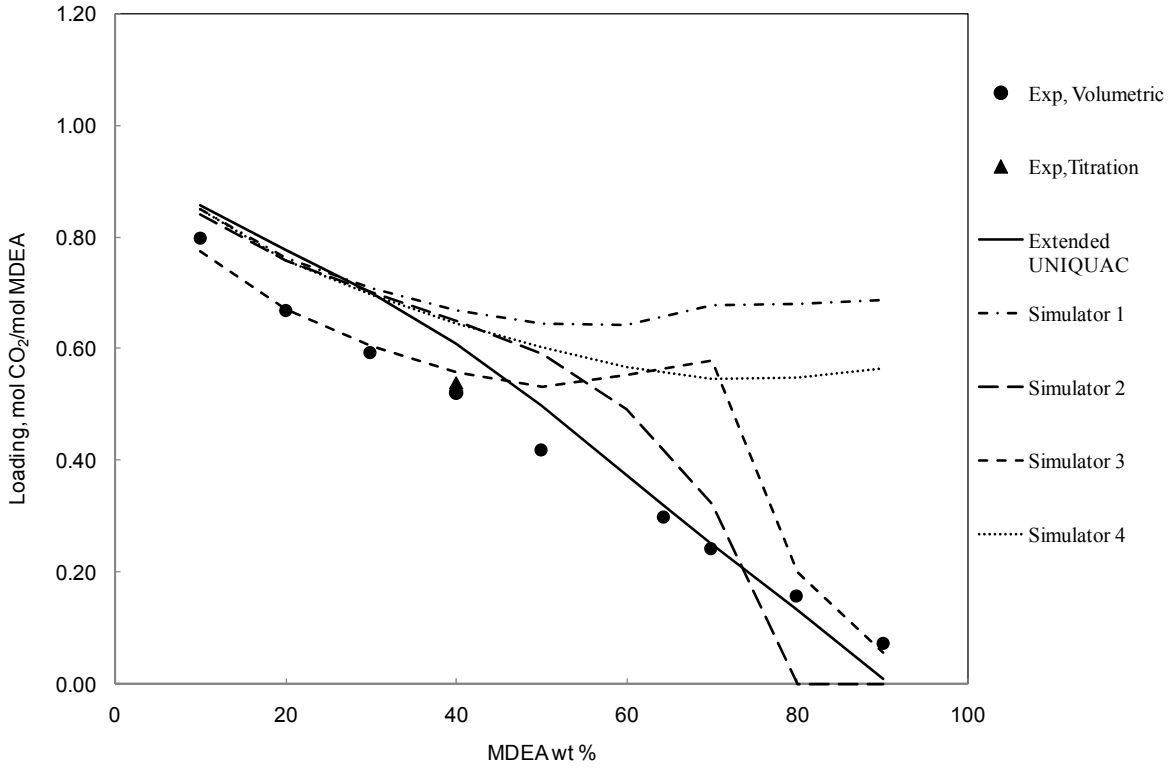

Figure 6-11. Comparison between model predictions and measured values at 50.00 °C and 110.00 kPa. ●, Experimental (Volumetric Analysis);▲, Experimental (Titration analysis); Solid Line, Extended UNIQUAC; Dash-Dot Line, Simulator 1; Long Dash Line, Simulator 2;Dash Line, Simulator 3;Dot Line, Simulator 4

Table 6-15. Comparison between experimental CO_2 solubility and models predictions at T = 60.00 °C and P = 110.00 kPa

MDEA mass %	Experimental Values	Predicted Loading Values									
		Developed Model, Extended UNIQUAC		Simulator 1		Simulator 2		Simulator 3		Simulator 4	
		Calculated Values	Bias Dev.	Calculated Values	Bias Dev.	Calculated Values	Bias Dev.	Calculated Values	Bias Dev.	Calculated Values	Bias Dev.
10	0.72	0.75	*-0.03*	0.74	*-0.01*	0.74	*-0.01*	0.66	*0.07*	0.74	*-0.01*
20.003	0.58	0.65	*-0.07*	0.63	*-0.05*	0.63	*-0.05*	0.54	*0.04*	0.63	*-0.05*
29.88	0.47	0.56	*-0.09*	0.57	*-0.09*	0.55	*-0.08*	0.47	*0.00*	0.56	*-0.09*
39.99	0.39	0.47	*-0.08*	0.52	*-0.13*	0.47	*-0.08*	0.41	*-0.02*	0.51	*-0.12*
49.96	0.31	0.37	*-0.06*	0.49	*-0.18*	0.38	*-0.07*	0.36	*-0.05*	0.47	*-0.16*
60	0.23	0.27	*-0.03*	0.47	*-0.24*	0.28	*-0.05*	0.29	*-0.06*	0.44	*-0.20*
69.87	0.15	0.17	*-0.02*	0.48	*-0.33*	0.19	*-0.04*	0.19	*-0.04*	0.42	*-0.27*
79.88	0.08	0.08	*0.00*	0.49	*-0.41*	0.00	*0.08*	0.10	*-0.02*	0.42	*-0.34*
90	0.04	0.01	*0.03*	0.50	*-0.46*	0.00	*0.04*	0.03	*0.00*	0.43	*-0.39*
AARD%		**29**		**232**		**34**		**13**		**198**	

Figure 6-12 compares developed model and mentioned simulators prediction results with the measured values obtained in this study at 60 °C.

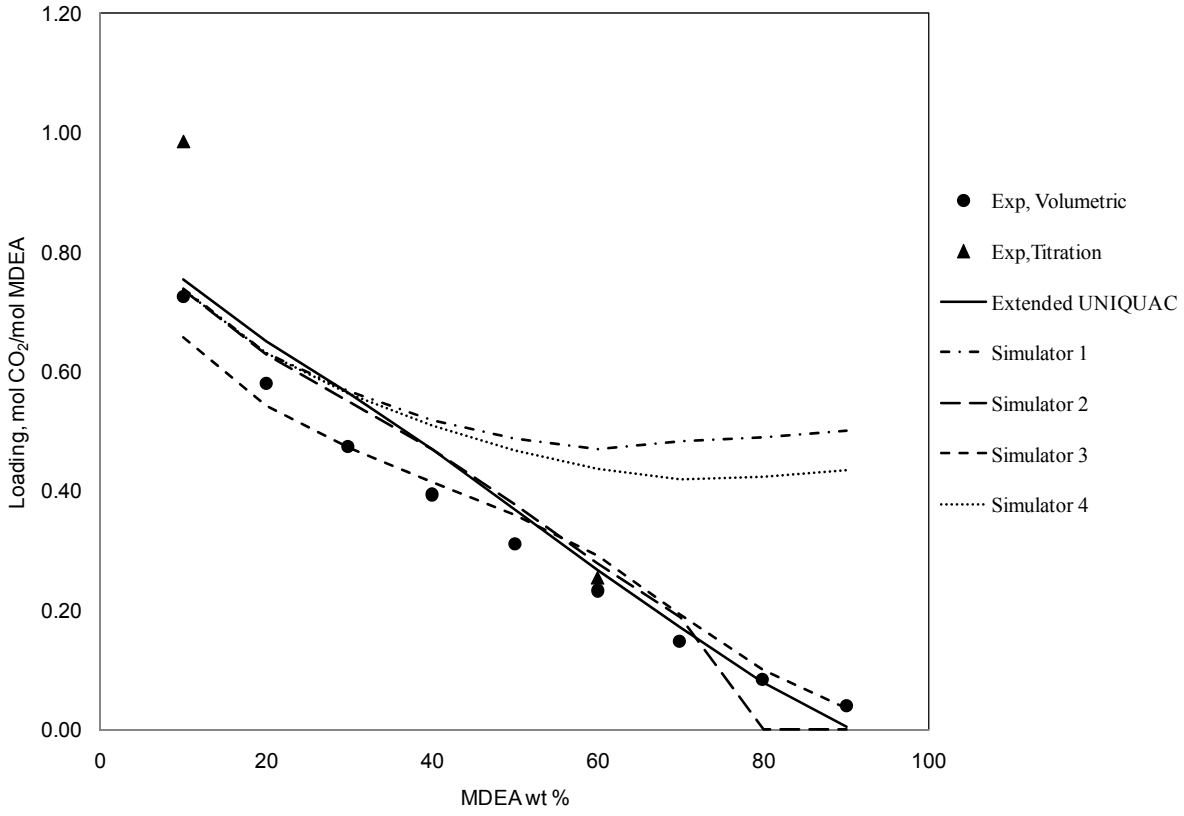

Figure 6-12. Comparison between model predictions and measured values at 60.00 °C and 110.00 kPa. ●, Experimental (Volumetric Analysis);▲, Experimental (Titration analysis); Solid Line, Extended UNIQUAC; Dash-Dot Line, Simulator 1; Long Dash Line, Simulator 2;Dash Line, Simulator 3; Dot Line, Simulator 4

Table 6-16. Comparison between experimental CO_2 solubility and models predictions at T = 70.00 °C and P = 110.00 kPa

MDEA mass %	Experimental Values	Predicted Loading Values									
		Developed Model, Extended UNIQUAC		Simulator 1		Simulator 2		Simulator 3		Simulator 4	
		Calculated Values	Bias Dev.	Calculated Values	Bias Dev.	Calculated Values	Bias Dev.	Calculated Values	Bias Dev.	Calculated Values	Bias Dev.
10	0.53	0.61	*-0.09*	0.60	*-0.07*	0.60	*-0.08*	0.52	*0.01*	0.59	*-0.07*
20.003	0.39	0.50	*-0.11*	0.48	*-0.10*	0.48	*-0.09*	0.41	*-0.02*	0.49	*-0.10*
29.88	0.34	0.41	*-0.07*	0.42	*-0.07*	0.39	*-0.04*	0.34	*0.01*	0.42	*-0.08*
39.99	0.28	0.33	*-0.05*	0.37	*-0.09*	0.31	*-0.03*	0.28	*0.00*	0.38	*-0.10*
49.96	0.20	0.25	*-0.05*	0.33	*-0.14*	0.23	*-0.03*	0.22	*-0.03*	0.34	*-0.15*
60	0.14	0.17	*-0.03*	0.31	*-0.16*	0.17	*-0.03*	0.16	*-0.02*	0.32	*-0.18*
69.87	0.09	0.11	*-0.02*	0.29	*-0.20*	0.12	*-0.03*	0.11	*-0.02*	0.30	*-0.22*
79.88	0.05	0.04	*0.01*	0.30	*-0.25*	0.00	*0.05*	0.06	*-0.01*	0.31	*-0.26*
90	0.02	0.00	*0.02*	0.31	*-0.29*	0.00	*0.02*	0.02	*0.00*	0.31	*-0.29*
AARD%		**29**		**237**		**35**		**9**		**245**	

Figure 6-13 represents predicted and measured CO_2 solubility at 70 °C.

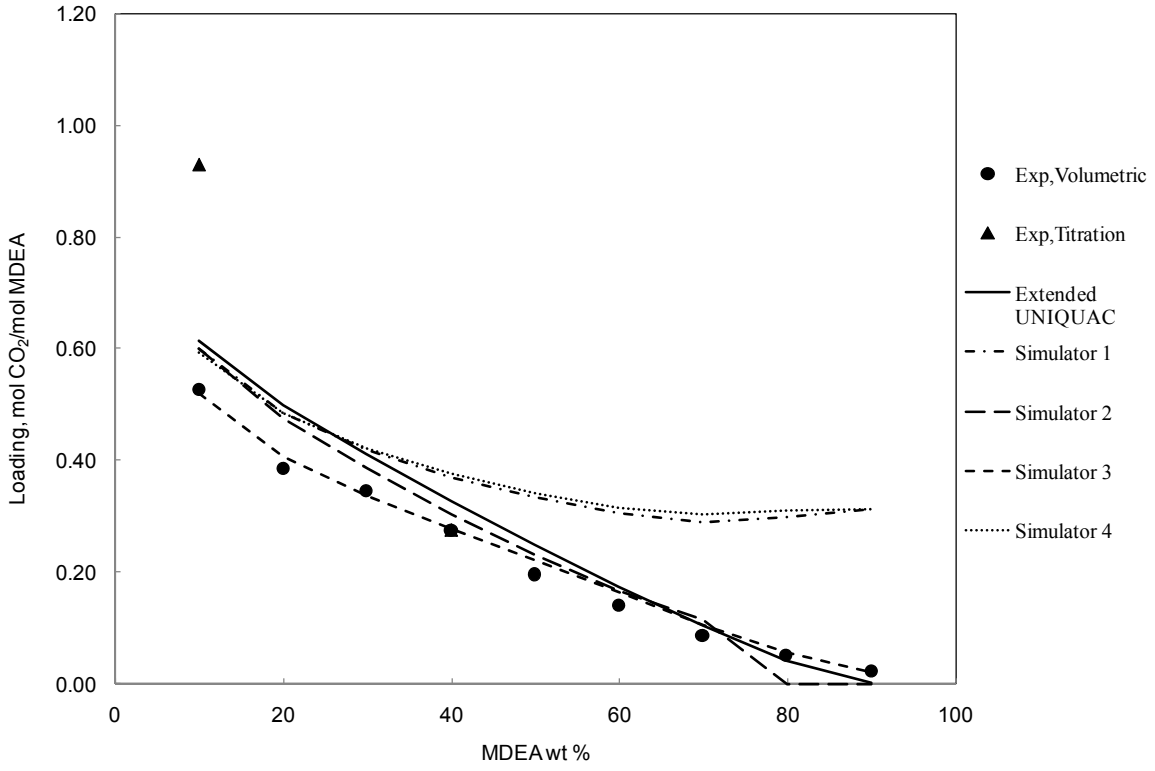

Figure 6-13. Comparison between model predictions and measured values at 70.00 °C and 110.00 kPa. ●, Experimental (Volumetric Analysis);▲, Experimental (Titration analysis); Solid Line, Extended UNIQUAC; Dash-Dot Line, Simulator 1; Long Dash Line, Simulator 2; Dash Line, Simulator 3; Dot Line, Simulator 4

Table 6-17. Comparison between experimental CO_2 solubility and models predictions at T = 80.00 °C and P = 110.00 kPa

MDEA mass %	Experimental Values	Predicted Loading Values									
		Developed Model, Extended UNIQUAC		Simulator 1		Simulator 2		Simulator 3		Simulator 4	
		Calculated Values	Bias Dev.	Calculated Values	Bias Dev.	Calculated Values	Bias Dev.	Calculated Values	Bias Dev.	Calculated Values	Bias Dev.
10	0.45	0.45	*0.00*	0.44	*0.01*	0.45	*0.00*	0.38	*0.07*	0.43	*0.02*
20.003	0.28	0.34	*-0.06*	0.34	*-0.06*	0.33	*-0.04*	0.28	*0.00*	0.34	*-0.06*
29.88	0.20	0.27	*-0.07*	0.28	*-0.08*	0.25	*-0.05*	0.22	*-0.02*	0.29	*-0.09*
39.99	0.15	0.20	*-0.06*	0.24	*-0.09*	0.19	*-0.04*	0.17	*-0.02*	0.25	*-0.10*
49.96	0.11	0.15	*-0.04*	0.21	*-0.10*	0.14	*-0.03*	0.13	*-0.02*	0.23	*-0.12*
60	0.07	0.10	*-0.03*	0.18	*-0.11*	0.10	*-0.03*	0.10	*-0.02*	0.21	*-0.13*
69.87	0.05	0.06	*-0.01*	0.15	*-0.11*	0.07	*-0.03*	0.06	*-0.02*	0.20	*-0.15*
79.88	0.03	0.02	*0.00*	0.16	*-0.14*	0.00	*0.03*	0.04	*-0.01*	0.21	*-0.18*
90	0.01	0.00	*0.01*	0.18	*-0.16*	0.00	*0.01*	0.01	*0.00*	0.21	*-0.19*
AARD%		**39**		**251**		**26**		**10**		**312**	

Figure 6-14 presents comparison between predicted values and measured points at 80 °C.

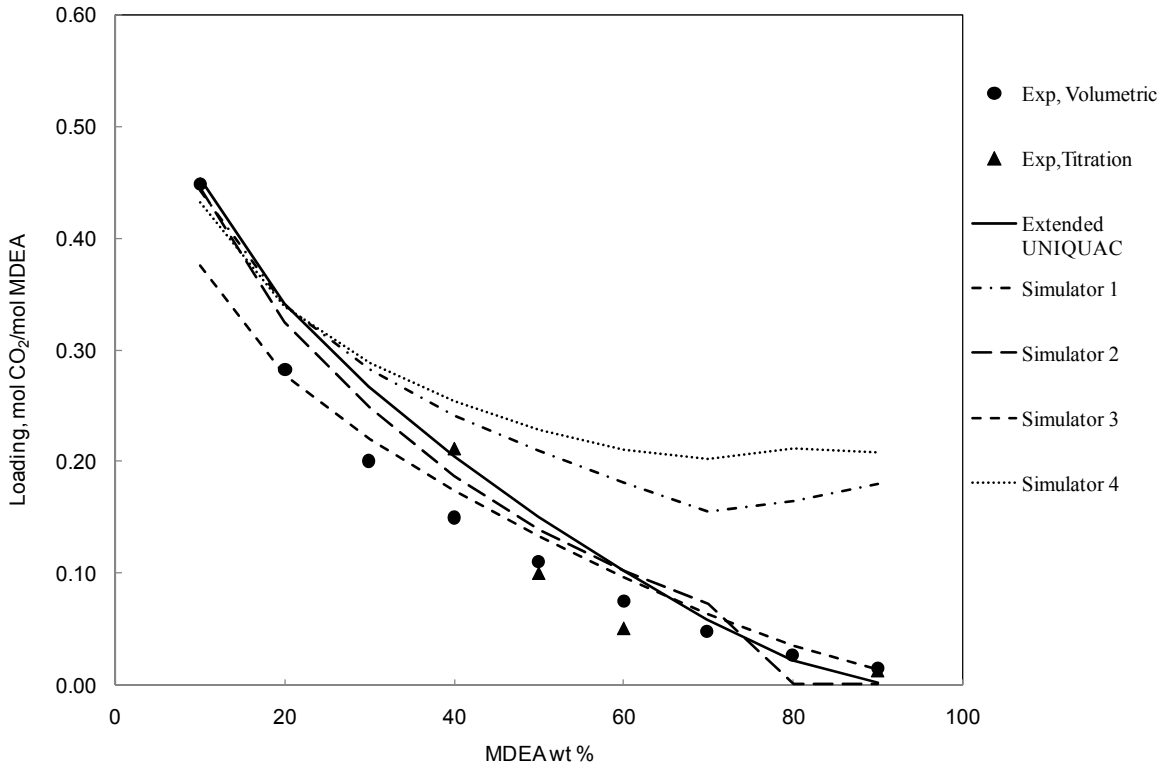

Figure 6-14. Comparison between model predictions and measured values at 80.00 °C and 110.00 kPa. ●, Experimental (Volumetric Analysis);▲, Experimental (Titration analysis); Solid Line, Extended UNIQUAC; Dash-Dot Line, Simulator 1; Long Dash Line, Simulator 2;Dash Line, Simulator 3; Dot Line, Simulator 4

Comparison between developed model and measured values demonstrated that Extended UNIQUAC appropriately predict CO_2 solubility over whole amine concentration range. Note that this section showed prediction results for 10 to 90 mass % MDEA, model calculations for 5 mass % MDEA (data of (Rho et al. 1997)) were already shown in chapter 4. Despite Extended UNIQUAC, studied simulators show good results in a limited amine concentration range. That is expected as most probably parameters of the models of commercial simulators were regressed to the data limited to the industrial application range. In addition commercial simulators need computationally robust models with very low calculation time, so that simplified models describing a smaller range of concentration is usually preferred. However simulator 3 showed good results at 60, 70 and 80 °C. Comparison between Extended UNIQUAC prediction values and experimental data revealed that with rising temperature the deviation between model and experimental data increased. As it can be seen from Figure 6-14 at 80 °C there is a systematic error in the experiments that pulls all the

measured points down. The probable reason behind this error is that with increasing temperature the volume of consumed CO_2 decreased to values comparable to cell dead volume. Therefore the accuracy of experimental data obtained from the cell decline with increasing temperature. Hence the uncertainties of experiments at higher temperatures may explain the deviation between developed model and experimental data at elevated temperatures. The observations revealed that the developed Extended UNIQUAC model overestimate the CO_2 solubility up to MDEA concentration of 70 mass % and from 70 wt % MDEA the model underestimate experimental CO_2 solubility data.

6.7 Results and Discussion

In this section above mentioned CO_2 solubility data are compared graphically in Figure 6-15 and Figure 6-16. Figure 6-15 shows the loading as mole of absorbed CO_2 per mole of MDEA as a function of MDEA mass % at the different studied temperatures. Figure 6-16 also depicts the measurements graphically however in Figure 6-16 loading is defined as mole of absorbed CO_2 per kg of rich solvent[20]. Because the experiments were performed for different concentrations of MDEA solution, defining loading as mole of CO_2 per kg of rich solvent gives a more consistent basis for comparison between the results.

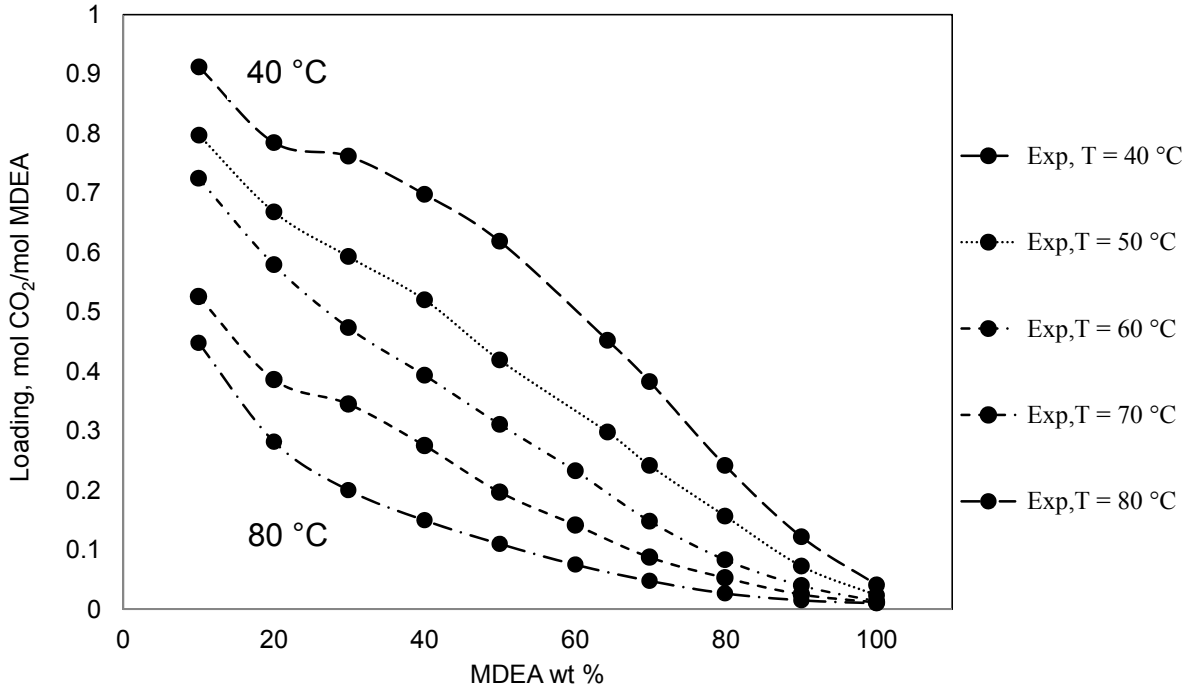

Figure 6-15. Comparison between obtained experimental data. ●, Experimental data obtained from volumetric analysis

[20] Rich solvent is defined as the solvent which is loaded by CO_2.

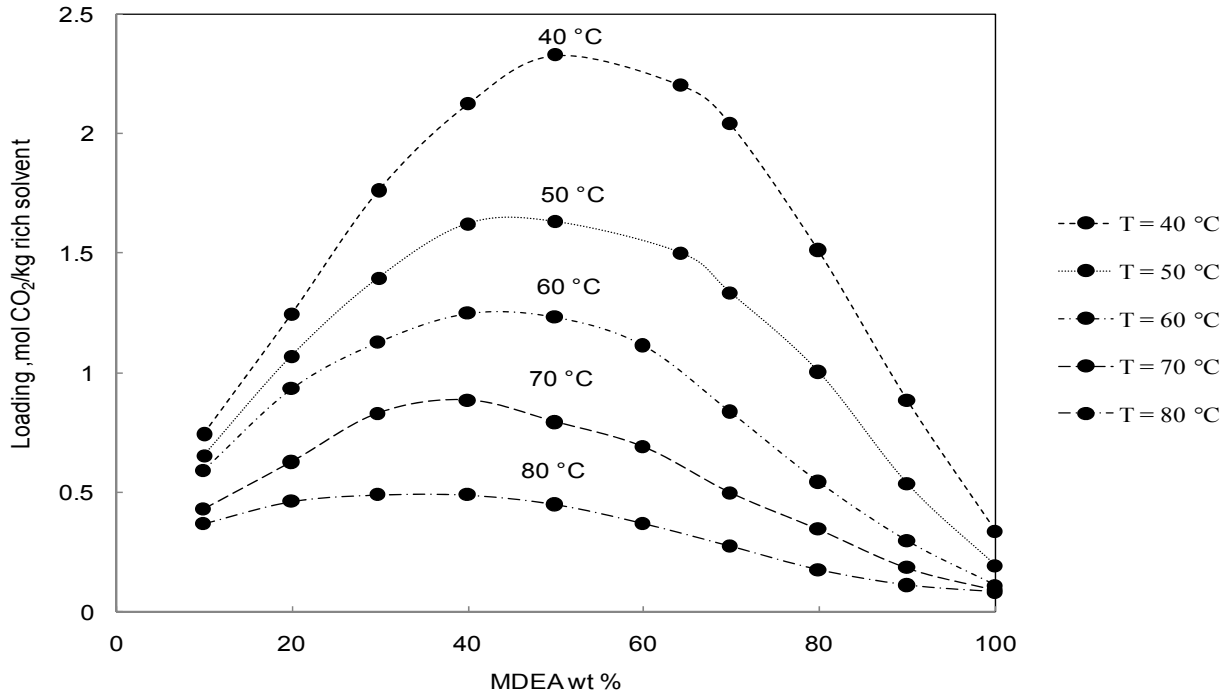

Figure 6-16. Comparison between obtained experimental data.●, Experimental data obtained from volumetric analysis

From the above figures, following observations can be made.

- For a given MDEA concentration and total pressure, the amount of CO_2 that is absorbed in the liquid phase (CO_2 gas solubility in the liquid phase) increase with decreasing the temperature. The behavior is expected since the reaction between CO_2 and MDEA is exothermic, thus at a temperature drop the reaction proceeds to the product side, which makes more molecular forms of CO_2 react with MDEA and convert to soluble ionic species so that the amount of absorbed CO_2will increase. As it can be seen from the figures the highest CO_2 is absorbed at the temperature of 40 °C. This observation is in accordance with industrial absorber condition, in industrial installation the most part of CO_2 is absorbed in the temperature range of 40 to 60 °C (Anufrikov et al. 2007). Absorption at lower temperatures of 40 °C is unfeasible because the very slow rate of reaction.
- For a given temperature and total pressure, the highest absorption capacity was observed for MDEA mass % of 40 to 60.
- At higher temperatures CO_2 is more absorbed physically than chemically, thus loading is less sensitive to MDEA concentration.

6.8 Conclusions

To sum up, in this section density data for MDEA-H_2O solutions and new vapor-liquid equilibrium data for CO_2-MDEA-H_2O systems were presented. Density experiments were performed for aqueous MDEA solutions with MDEA concentration of 10 to 100 wt % and at 40 to 80°C. VLE experiments were carried out in a cell named Low pressure cell for aqueous solutions of 10 to 100 mass % MDEA at constant pressure of 110 kPa (1.10 bar) and temperatures of 40 to 80 °C. In VLE experiments analysis of the liquid phase was avoided and loading was calculated from the volumetric data obtained from the cell. From these experiments it was concluded that the highest absorption capacity occurs at 40 °C and for MDEA concentration of 40 to 60 mass %. The results of VLE experiments were used to validate the developed thermodynamic model in chapter 4. Four thermodynamic packages of commercial simulators were also used to calculate CO_2 solubility in the studied conditions. Unlike studied commercial simulators, the developed Extended UNIQUAC model showed very promising results. It is recommended to measure the cell dead volume more accurately (measuring the cavity of tubing). Overall, the new vapor-liquid equilibrium data over whole MDEA concentration range provide an opportunity for future work on validation of G^E thermodynamic models.

Chapter 7

Vapor-Liquid Equilibrium and Density Measurements for CO_2-MDEA-PZ-H_2O and MDEA-PZ-H_2O Systems

7 Vapor-Liquid Equilibrium and Density Measurements for CO_2-MDEA-PZ-H_2O and MDEA-PZ-H_2O Systems

7.1 Chapter Overview

As mentioned in previous chapters, MDEA which is a tertiary amine is the most useful amine in natural gas processing. The main advantages of MDEA over other kind of amines can be addressed as lower heat of reaction with acid gas, lower vapor pressure, lower corrosive tendency and capability of selective absorption of H_2S. Despite these benefits, MDEA has a slow rate of reaction with CO_2. To overcome this problem, piperazine (PZ) which is a cyclic amine is added to MDEA. The PZ activated MDEA is widely applied in CO_2 removal from natural gas processes. This blended solvent, which is called "activated MDEA solvent", has advantage of high rate of reaction of cyclic amine with CO_2 combined with lower heat of reaction and other benefits of MDEA which makes it a successful solvent for natural gas processing. Recently activated MDEA solvent has found widespread application in bulk removal of CO_2 (Derks et al. 2008). Accurate estimation of thermodynamic equilibrium between CO_2 and aqueous blend of MDEA-PZ is crucial for obtaining a good design of amine based acid gas removal process. This chapter presents new CO_2solubility data in aqueous blend of MDEA-PZ at temperatures from 40 to 70 °C. In addition to VLE data, density data for mixtures of MDEA-PZ-H_2O at temperatures between 40 to 80 °C will be presented in this chapter. Moreover, prediction results from some commercial simulators against the measured experimental data will be discussed in the remainder of this chapter.

7.1 The reason for Use of Piperazine

Piperazine is so called modifying additive which is used to improve efficiency of absorption of acid gases.

As mentioned earlier, even though the use of MDEA is beneficial compared to other amines, its slow rate of reaction with CO_2 makes it with limited usage of CO_2 absorption. Therefore in order to raise the absorption rate with CO_2, it was aimed to mix aqueous solution of MDEA with other kinds of amine. In 1985 it was suggested to add primary or secondary amine to aqueous solution of MDEA in order to simultaneously take advantage of the benefits of each kind of amine. However addition of primary and secondary amines increased the rate of reaction, but introduced negative factor of rising solvent corrosive power (Bishnoi 2000). In 1982 BASF introduced adding piperazine to aqueous solution of MDEA. The success of the so called"activated MDEA solvent" is based on the high reaction rate of CO_2 with MDEA (Derks et al. 2008). Piperazine is a cyclic amine which has high capacity of protonation (each molecule of piperazine can add two protons) and it can form three different carbonate ions with CO_2. Due to the mentioned features, adding piperazine to aqueous solutions of MDEA highly improve the rate of CO_2 absorption. Addition of piperazine also increases the selectivity of absorption of hydrogen sulfide in a mixture of carbon dioxide and hydrogen sulfide. Note that piperazine increases the heat required for regeneration, but not as much as other common activators. It is worthwhile to mention that addition of piperazine almost does not introduce any negative factor. These advantages made piperazine as a frequent additive to aqueous solutions of MDEA in natural gas treatment process.

7.2 Experimental Design

Table 7-1 summarizes the available published experimental VLE data for CO_2-PZ-MDEA-H_2O system. Notice that collected data in Table 7-1 are gathered according to the best of author knowledge and at the time of this work.

Table 7-1. Published VLE data for CO_2-MDEA-PZ-H_2O systems

MDEA Concentration, wt %	PZ Concentration, wt %	T, °C	P_{CO_2}, kPa	Reference
18, 33, 37, 43, 54.5	1.5, 3, 5, 6, 13	30 to 90	13.16 to 935.3	(Liu et al. 1999) (Liu et al. 1999)
46	5	40, 80	0.03 to 7.48	(Bishnoi and Rochelle 2002)
16.8	12.1	80	200 to 6400	(Kamps et al. 2003)
21, 22, 23	0.1, 0.4	40, 60, 80	0.1 to 95.78	(Ali and Aroua 2004)
24, 29, 35	3.1, 7.4, 11.7	40,55,70	27.79 to 3938.43	(Jenab et al. 2005)
18.5, 30, 44.2	8.5, 10.3, 11.8	40, 60, 80, 120	200 to 11900	(Böttger et al. 2009)

17 to 47.9	4.1 to 18.8	26.1 to 46.8	0.31 to 146.8	(Speyer et al. 2010)
50	0.9, 2.2, 2.4	101.05 to 104.95	3.83 to 76.77	(Xu et al. 1998b)
6, 25, 46	5, 6, 13	25, 30, 40, 50	0.25 to 10.2	(Derks et al. 2010)

As it can be observed from Table 7-1, compared to CO_2-MDEA-H_2O system, there are limited equilibrium data available for CO_2-MDEA-PZ-H_2O mixture. Available VLE data for CO_2-MDEA-PZ-H_2O systems are limited to MDEA concentrations less than 55 mass %. The aim of the present study is to extend the experimental data base available in open literature for the solubility of CO_2 in aqueous mixtures of MDEA and piperazine at wider range of MDEA concentrations. New data are reported herein for CO_2 solubility in aqueous mixtures of MDEA and piperazine with MDEA mass % of 25 to 75, piperazine mass % of 5 and 10, at constant pressure of 110 kPa (1.10 bar) and at temperatures between 40 to 70 °C. The results of this study could be also used to evaluate formerly published thermodynamic models.

7.3 Experimental Section

The chemicals used in this work include MDEA (Acros Organics, ≥ 99 % pure) ,Piperazine Hexahydrate (Fisher Scientific, ≥ 98 % pure), Piperazine Anhydrous (MERCK, ≥ 99 % pure), CO_2 (Yara, ≥ 99 % pure) and Acetone (VWR (BDH PROLABO), ≥ 99 % pure). All chemicals were used without any further purification. Experiments were performed using the same apparatus as in chapter 6. The experimental procedure is similar to what is described in chapter 6. Blended solvents with 40 mass % MDEA-10 mass % PZ, 45 mass % MDEA-5 mass % PZ and 35 mass % MDEA-5 mass % PZ were prepared using piperazine hexahydrate chemical and the rest were made with piperazine anhydrous. Note that in these experiments 250 $cm^3$of solvent was prepared and kept in a sealed closed bottle, for each experiment the required amount of solvent was taken from the bottle. Recall from chapter 6, due to set up restrictions (the absorption capacity decrease with increasing temperature, and at 80 °C the amount of CO_2 interred in the cell is small and comparable to cell total volume), data obtained from the Low pressure cell equipment at 80 °C were not accurate enough, therefore in this chapter the maximum temperature that data are measured for is 70 °C.

7.4 Results

7.4.1 Measured Values

The VLE experiments for CO_2-MDEA-PZ-H_2O system as described in section 7.2 were performed at 110 kPa (1.1 bar), constant total pressure, temperatures from 40 to 70 °C and for 25, 35, 45, 55, 65, 75 mass % MDEA concentrations mixed with 5 and 10 mass% PZ.As illustrated in section 6.5.2 information on density of solutions is required for converting volume based data to mass based data, therefore density experiments were carried out for MDEA-PZ-H_2O solutions for 25 to 75 wt % MDEA mixed with 5 and 10 wt % PZ, at temperatures between 40 to 80 °C. The remainder of this section explains results of density and VLE measurements in figures and tables. Note that all the VLE data reported in this chapter are obtained from the volumetric method as already explained in chapter 6.

7.4.1.1 Density Experiments

Prior to VLE experiments, density of prepared aqueous activated MDEA solutions were measured using Anton-Paar (DMA 4500 M) density meter. The procedure and equipment was already validated for density measurements of aqueous MDEA solutions. To the best of author knowledge and at the time of this work only two articles reported density of aqueous blend of MDEA-PZ.(Paul and Mandal 2006) measured density of aqueous MDEA-PZ mixtures between 14.85 to 59.85 °C and for mass percent ratio (mass percent of PZ/mass percent of MDEA) of 3/27, 6/24, 9/21 and 12/18. (Derks et al. 2008)determined density of aqueous blends of MDEA-PZ at temperatures from 20to 50 °C and with concentration of MDEA at 1, 2, 3, 4 $mol.dm^{-3}$ while concentration of PZ vary between 0 to 1 $mol.dm^{-3}$.In this work density measurements were performed for aqueous solutions of 25 to 75 mass % MDEA mixed with 5 and 10 mass % PZ and at temperatures between 40 to 80 °C. Measurement results are reported in Table 7-2 toTable 7-6 and plotted in Figure 7-1 and Figure 7-2.

Table 7-2. Density measurements at 40 °C

MDEA mass %	PZ mass	$\rho\ (g.cm^{-3})$			
		Test 1	**Test 2**	**Test 3**	**Average of tests (Reported value)**
25.05	5.00	1.0161	1.0160		1.0160
24.97	9.93	1.0191	1.0194		1.0192
35.33	5.34	1.0250	1.0256		1.0253
35.02	9.96	1.0275	1.0281		1.0278
45.00	4.99	1.0302	1.0325		1.0314
44.90	9.96	1.0341			1.0341
64.94	4.99	1.0401	1.0404		1.0403
64.99	9.98	1.0391	1.0391		1.0391
74.94	4.99	1.0391	1.0390	1.0391	1.0391
74.90	9.99	1.0354	1.0358		1.0356

Table 7-3. Density measurements at 50 °C

MDEA mass %	PZ mass	$\rho\ (g.cm^{-3})$		
		Test 1	Test 2	Average of tests (Reported value)
25.05	5.00	1.0103	1.0105	1.0104
24.97	9.93	1.0132		1.0132
35.33	5.34	1.0187		1.0187
35.02	9.96	1.0208	1.0215	1.0211
45.00	4.99	1.0251		1.0251
44.90	9.96	1.0270	1.0276	1.0273
64.94	4.99	1.0324		1.0324
64.99	9.98	1.0311	1.0312	1.0311
74.94	4.99	1.0312		1.0312
74.90	9.99	1.0275		1.0275

Table 7-4. Density measurements at 60 °C

MDEA mass %	PZ mass	ρ ($g.cm^{-3}$)			
		Test 1	Test 2	Test 3	Average of tests (Reported value)
25.05	5.00	1.0042	1.0044		1.0043
24.97	9.93	1.0067			1.0067
35.33	5.34	1.0120			1.0120
35.02	9.96	1.0138			1.0138
45.00	4.99	1.0179			1.0179
44.90	9.96	1.0193			1.0193
64.94	4.99	1.0243			1.0243
64.99	9.98	1.0231			1.0231
74.94	4.99	1.0231	1.0230	1.0230	1.0230
74.90	9.99	1.0195			1.0195

Table 7-5. Density measurements at 70 °C

MDEA mass %	PZ mass	ρ ($g.cm^{-3}$)			
		Test 1	Test 2	Test 3	Average of tests (Reported value)
25.05	5.00	0.9976			0.9976
24.97	9.93	0.9998			0.9998
35.33	5.34	1.0048			1.0048
35.02	9.96	1.0064			1.0064
45.00	4.99	1.0102			1.0102
44.90	9.96	1.0115			1.0115
64.94	4.99	1.0161	1.0163		1.0162
64.99	9.98	1.0149			1.0149
74.94	4.99	1.0150			1.0150
74.90	9.99	1.0113	1.0114		1.0113

Table 7-6. Density measurements at 80 °C

MDEA mass %	PZ mass	$\rho\ (g.cm^{-3})$		
		Test 1	Test 2	Average of tests (Reported value)
25.05	5.00	0.9908		0.9908
24.97	9.93	0.9927		0.9927
35.33	5.34	0.9973	0.9977	0.9975
35.02	9.96	0.9987		0.9987
45.00	4.99	1.0024		1.0024
44.90	9.96	1.0034		1.0034
64.94	4.99	1.0078		1.0078
64.99	9.98	1.0064		1.0064
74.94	4.99	1.0064	1.0063	1.0064
74.90	9.99	1.0031	1.0030	1.0031

Figure 7-1 presents measured densities for aqueous blended mixtures of MDEA and 5 wt % PZ. Results are plotted against MDEA mass % at five different temperatures. As expected, densities of aqueous blended MDEA-PZ solutions decrease with increasing temperature.

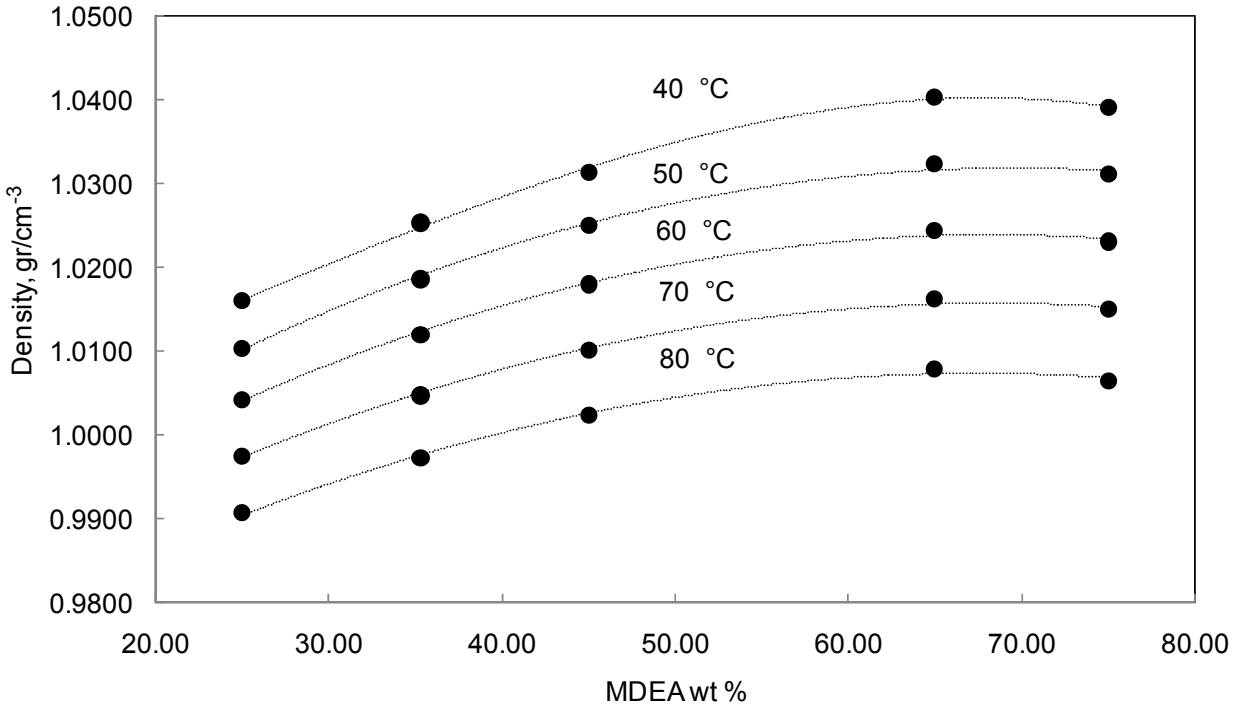

Figure 7-1. Measured densities of aqueous MDEA-PZ (5 mass % PZ) solutions at various temperatures. Lines are added to show trend of measured data.

Figure 7-2 presents measured densities for aqueous blended mixtures of MDEA and 10 wt % PZ. Results are plotted against MDEA mass % at five different temperatures. The same behavior is seen in density as a function of temperature.

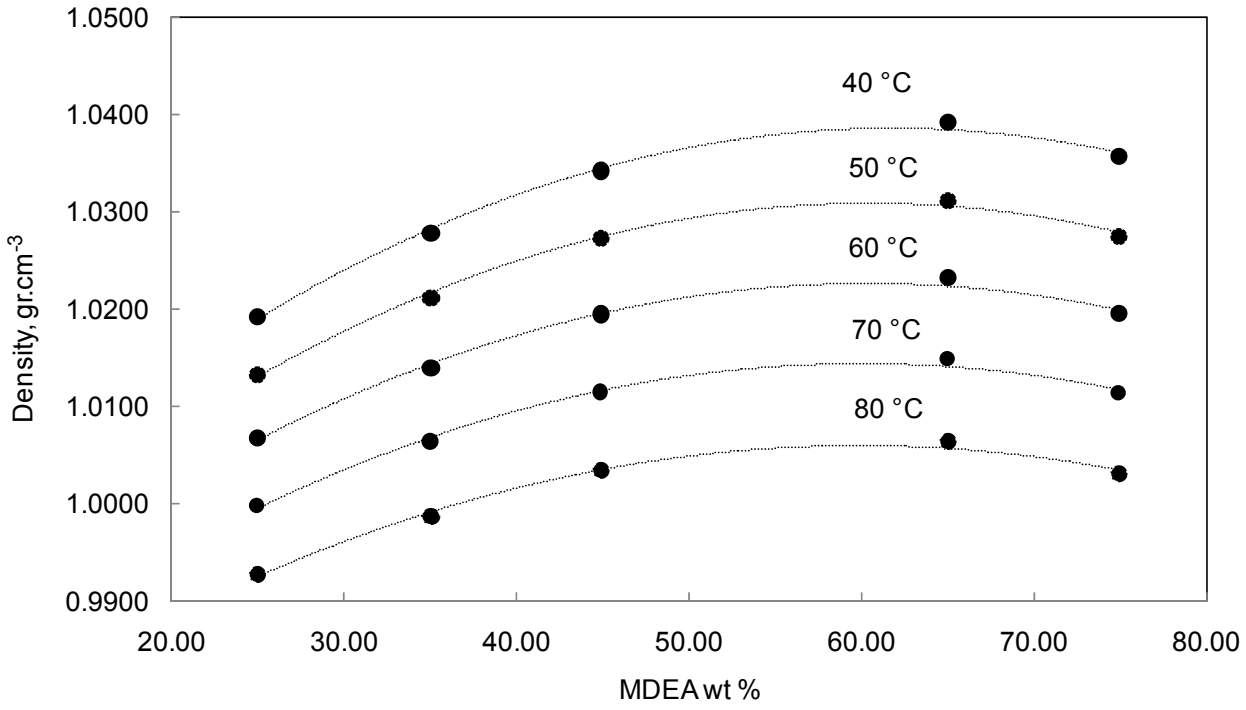

Figure 7-2. Measured densities of aqueous MDEA-PZ (10 mass % PZ) solutions at various temperatures. Lines are added to show trend of measured data.

7.4.1.2 VLE Experiments

This section illustrates CO_2 solubility data obtained for blend mixtures of MDEA and PZ with concentration of MDEA varying from 25 to 75 mass % while concentration of PZ is kept constant at 5 and 10 mass %, at four different temperatures, 40 to 70 °C and at constant total pressure of 110 kPa (1.10 bar). The experimental data are reported in tables and plotted in figures. Keep in mind that values presented in tables and figures are average values between tests. Notice that equipment and experimental procedure (volumetric analysis) were already validated (explained in chapter 6).

Table 7-7. Experimental solubility data of CO_2 in an aqueous blended mixtures of MDEA and PZat 40.00 °C and 110.00kPa (1.1000 bar)

MDEA mass %	PZ mass %	$\alpha(\frac{\text{mol } CO_2}{\text{mol amine}})$[21]	$\acute{\alpha}\ (\frac{\text{mol } CO_2}{\text{kg rich solvent}})$[22]
25.05	5.00	0.76	1.86
24.97	9.93	0.77	2.25
35.33	5.34	0.71	2.29
35.02	9.96	0.73	2.63
45.00	4.99	0.66	2.55
44.90	9.96	0.68	2.92
64.94	4.99	0.42	2.30
64.99	9.98	0.43	2.55
74.94	4.99	0.33	2.04
74.90	9.99	0.34	2.29

Figure 7-3 shows the obtained experimental CO_2 solubility data at 40.00 °C and 110.00 kPa (1.100 bar). Results are plotted as loading against MDEA mass %, while loading is defined as mole CO_2 per kg of rich solvent.

[21] α represents loading, mole CO_2 per mole amine (where mole amine is the sum of MDEA mole numbers and PZ mole numbers)

[22] $\acute{\alpha}$ represents loading, mole CO_2 per kg rich solvent (where rich solvent indicates the loaded solvent (mixture of CO_2-MDEA-PZ-H_2O))

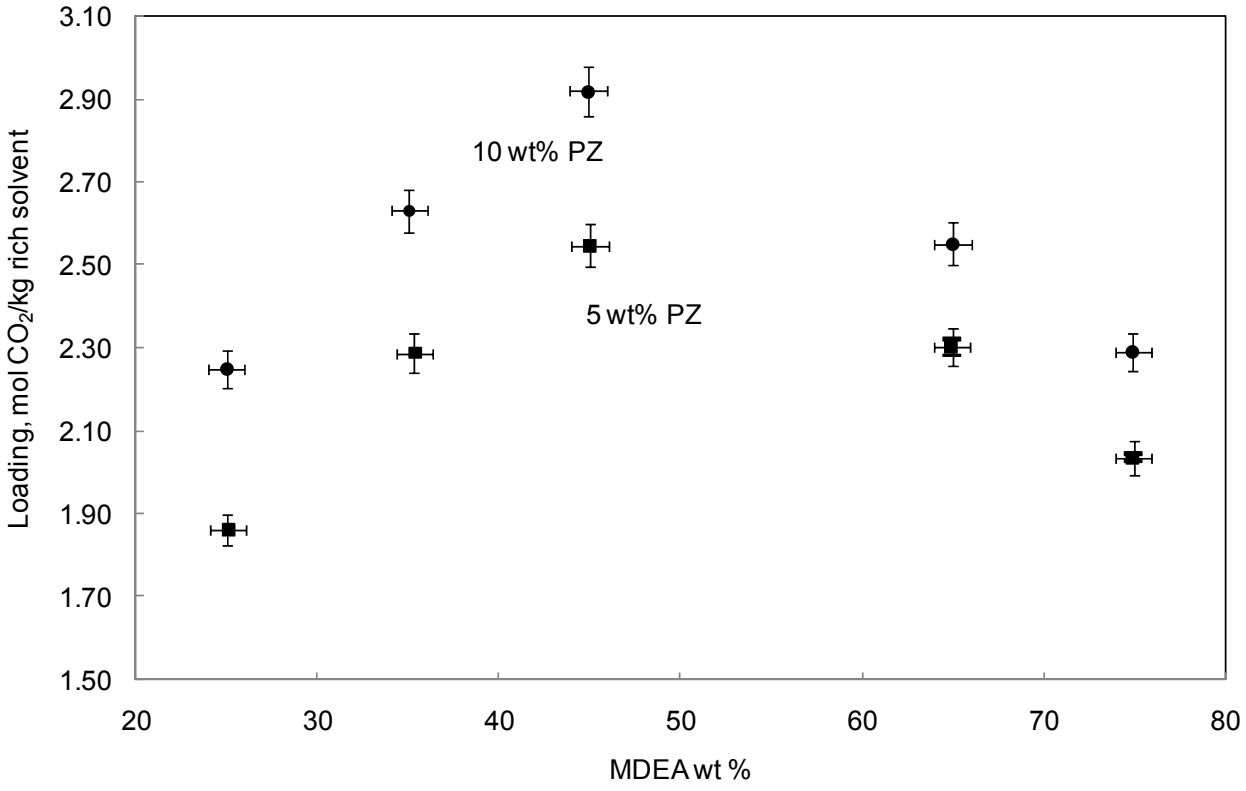

Figure 7-3. Solubility data of CO_2in blended mixtures of MDEA-PZat 40.00 °C and 110.00 kPa.■, 5 mass % PZ; ●, 10 mass % PZ; ―, Repeatability Tests. Error bars are added to the measured points.

Table 7-8.Experimental solubility data of CO_2in an aqueous blended mixtures of MDEA and PZ at 50.00 °C and 110.00 kPa (1.1000 bar)

MDEA mass %	PZ mass %	$\alpha(\frac{\text{mol } CO_2}{\text{mol amine}})$	$\acute{\alpha}\ (\frac{\text{mol } CO_2}{\text{kg rich solvent}})$
25.05	5.00	0.68	1.69
24.97	9.93	0.69	2.05
35.33	5.34	0.59	1.94
35.02	9.96	0.61	2.26
45.00	4.99	0.52	2.05
44.90	9.96	0.55	2.41
64.94	4.99	0.34	1.88
64.99	9.98	0.36	2.15
74.94	4.99	0.27	1.69
74.90	9.99	0.29	1.96

Figure 7-4 presents the obtained experimental CO_2 solubility data at 50.00 °C and 110.00 kPa (1.10 bar).

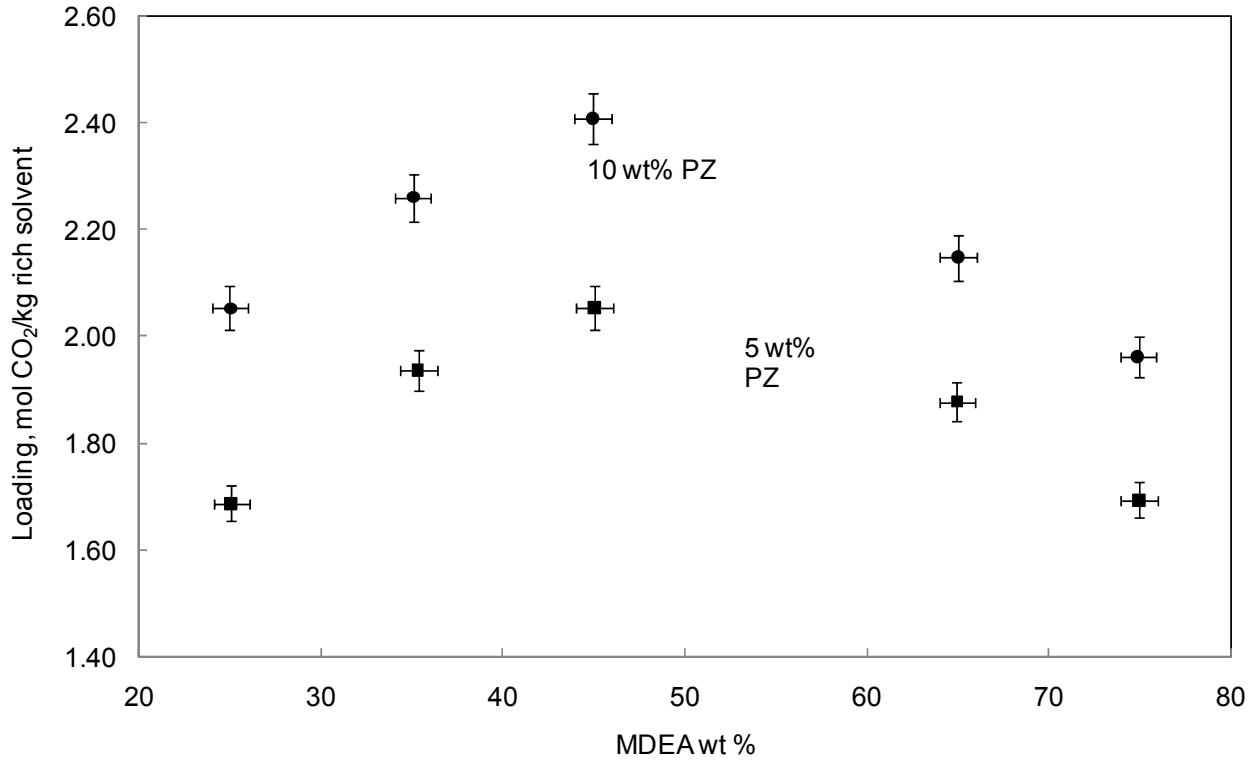

Figure 7-4. Solubility data of CO_2in blended mixtures of MDEA-PZ at 50.00 °C and 110.00 kPa.■, 5 mass % PZ; ●, 10 mass % PZ; ═, Repeatability Tests. Error bars are added to the measured points.

Table 7-9. Experimental solubility data of CO_2in an aqueous blended mixtures of MDEA and PZ at 60.00 °C and 110.00 kPa (1.1000 bar)

MDEA mass %	PZ mass %	$\alpha(\frac{\text{mol } CO_2}{\text{mol amine}})$	$\acute{\alpha}\ (\frac{\text{mol } CO_2}{\text{kg rich solvent}})$
25.05	5.00	0.60	1.51
24.97	9.93	0.61	1.82
35.33	5.34	0.53	1.75
35.02	9.96	0.53	1.99
45.00	4.99	0.46	1.84
44.90	9.96	0.47	2.10
64.94	4.99	0.26	1.48
64.99	9.98	0.31	1.88
74.94	4.99	0.20	1.28
74.90	9.99	0.24	1.64

Figure 7-5 represents the experimental loading against MDEA concentration data at 60.00 °C and 110.00 kPa (1.10bar).

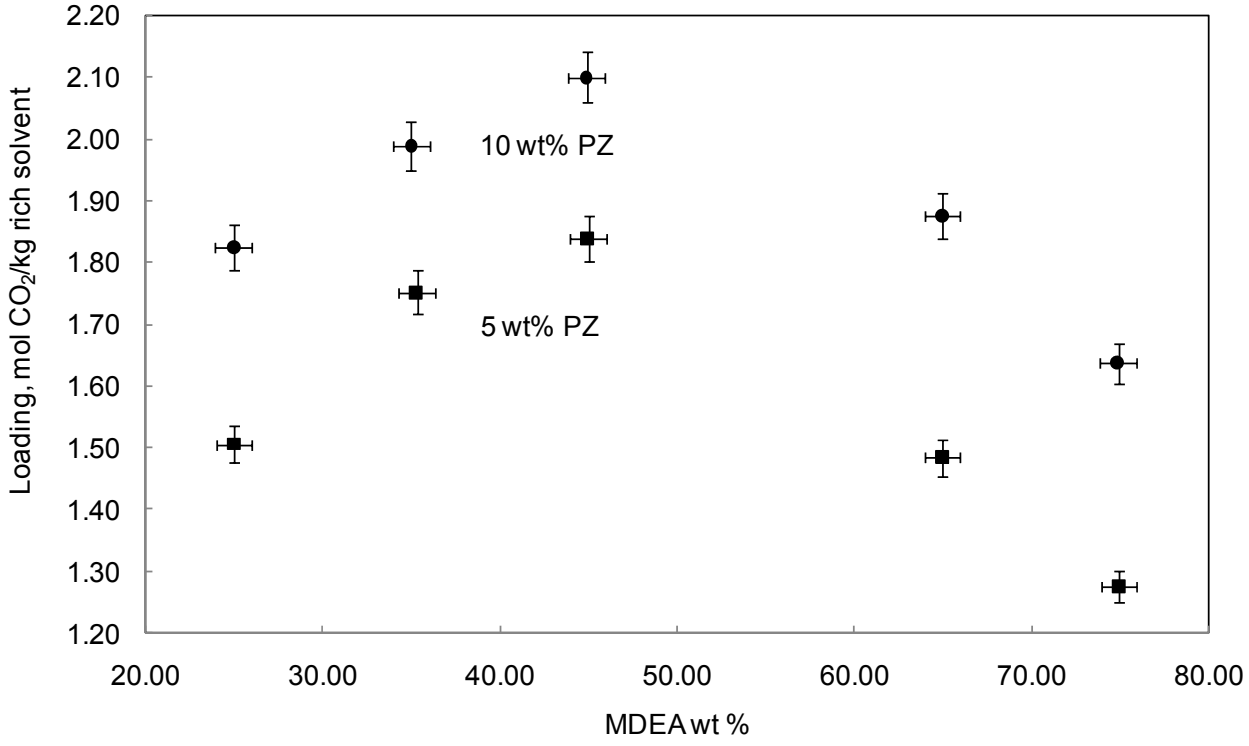

Figure 7-5. Solubility data of CO_2in blended mixtures of MDEA-PZ at 60.00 °C and 110.00 kPa.■, 5 mass % PZ; ●, 10 mass % PZ; ═, Repeatability Tests. Error bars are added to the measured points.

Table 7-10. Experimental solubility data of CO_2 in an aqueous blended mixtures of MDEA and PZ at 70.00 °C and 110.00 kPa(1.1000 bar)

MDEA mass %	PZ mass %	$\alpha(\frac{\text{mol } CO_2}{\text{mol amine}})$	$\acute{\alpha}\,(\frac{\text{mol } CO_2}{\text{kg rich solvent}})$
25.05	5.00	0.45	1.14
24.97	9.93	0.49	1.50
35.33	5.34	0.37	1.26
35.02	9.96	0.43	1.62
45.00	4.99	0.32	1.31
44.90	9.96	0.35	1.62

64.94	4.99	0.20	1.15
64.99	9.98	0.24	1.49
74.94	4.99	0.15	0.99
74.90	9.99	0.19	1.36

Figure 7-6 shows the measured CO_2 solubility at 70.00 °C and 110.00 kPa (1.10bar).

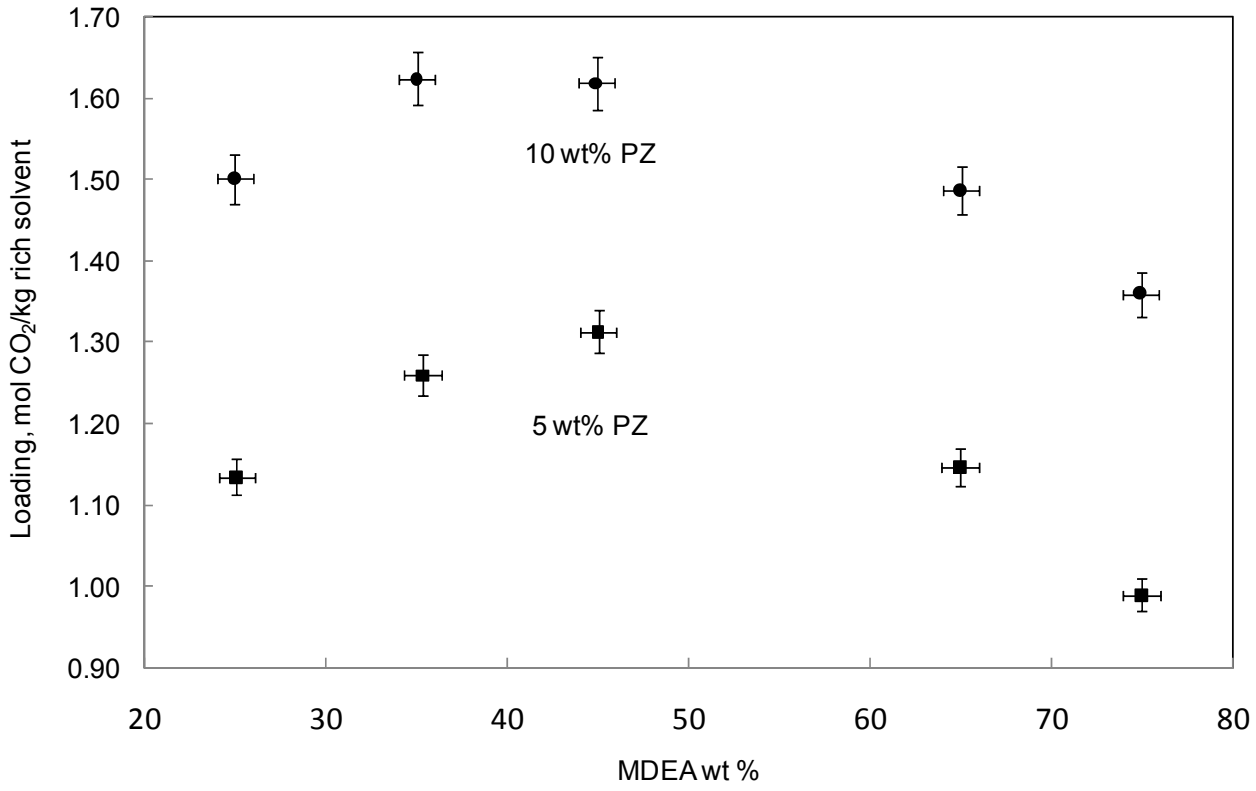

Figure 7-6. Solubility data of CO_2in blended mixtures of MDEA-PZ at 70.00 °C and 110.00 kPa.■, 5 mass % PZ; ●, 10 mass % PZ; —, Repeatability Tests. Error bars are added to the measured points.

The main sources of uncertainty of the results are as discussed in section 6.5.4. However, it is worthwhile to mention that the CO_2 absorption capacity in aqueous blend of MDEA-PZ is higher compared to aqueous MDEA. Therefore the volume of CO_2 that entered the autoclave is much bigger than the cell total volume and consequently the amount of CO_2 in the liquid phase become greater than the amount of CO_2 in the vapor phase. Hence in case of CO_2 solubility measurements in aqueous activated MDEA, total volume inaccuracy has smaller effect in overall uncertainty

compared to CO_2 solubility measurements in aqueous MDEA. The overall of uncertainty of results is estimated to be about 2 %.

7.5 Model Validation

The results of CO_2 solubility experiments in aqueous blends of MDEA and PZ were compared to the thermodynamic models available in two commercial simulators. Simulators have been used to predict CO_2 solubility in aqueous solutions of 25 to 75 mass % MDEA mixed with 5 and 10 mass% PZ at 40, 50, 60, 70 °C and total pressure of 110 kPa (1.10 bar). Table 7-11 to Table 7-14 summarize simulators calculation results at each studied temperature. Calculated and measured results for CO_2 solubility in aqueous blended mixtures of 25 to 75 mass % MDEA with 0, 5 and 10 mass % PZ at constant pressure of 110 kPa (1.10 bar) and temperatures between 40 to 70 °C are compared graphically through Figure 7-7 to Figure 7-10.

Table 7-11. Simulation Results forCO_2 solubility in aqueous blends of MDEA-PZ at T = 40.00 °C and P = 110.00kPa

MDEA mass %	PZ mass%	Predicted Values			
		Simulator 2		Simulator 3	
		∝(mole CO_2/mole amine*)	∝́ (mole CO_2/kg rich solvent	∝(mole CO_2/mole amine*)	∝́ (mole CO_2/kg rich solvent
20.00	5.00	0.85	1.77	0.78	1.63
30.00	5.00	0.79	2.21	0.72	2.04
40.00	5.00	0.72	2.53	0.69	2.41
50.00	5.00	0.66	2.77	0.66	2.77
60.00	5.00	0.59	2.89	0.65	3.14
70.00	5.00	0.45	2.60	0.63	3.43
80.00	5.00			0.58	3.58
20.00	10.00	0.84	2.15	0.79	2.05
30.00	10.00	0.76	2.47	0.74	2.43
40.00	10.00	0.67	2.68	0.70	2.79
50.00	10.00	0.59	2.79	0.68	3.14
60.00	10.00	0.51	2.77	0.86	4.32
70.00	10.00			0.84	4.68
80.00	10.00			0.60	3.90

**mole amine = mole MDEA + mole PZ*

Figure 7-7 plotted simulators prediction results compared to the measured values at 40 °C.

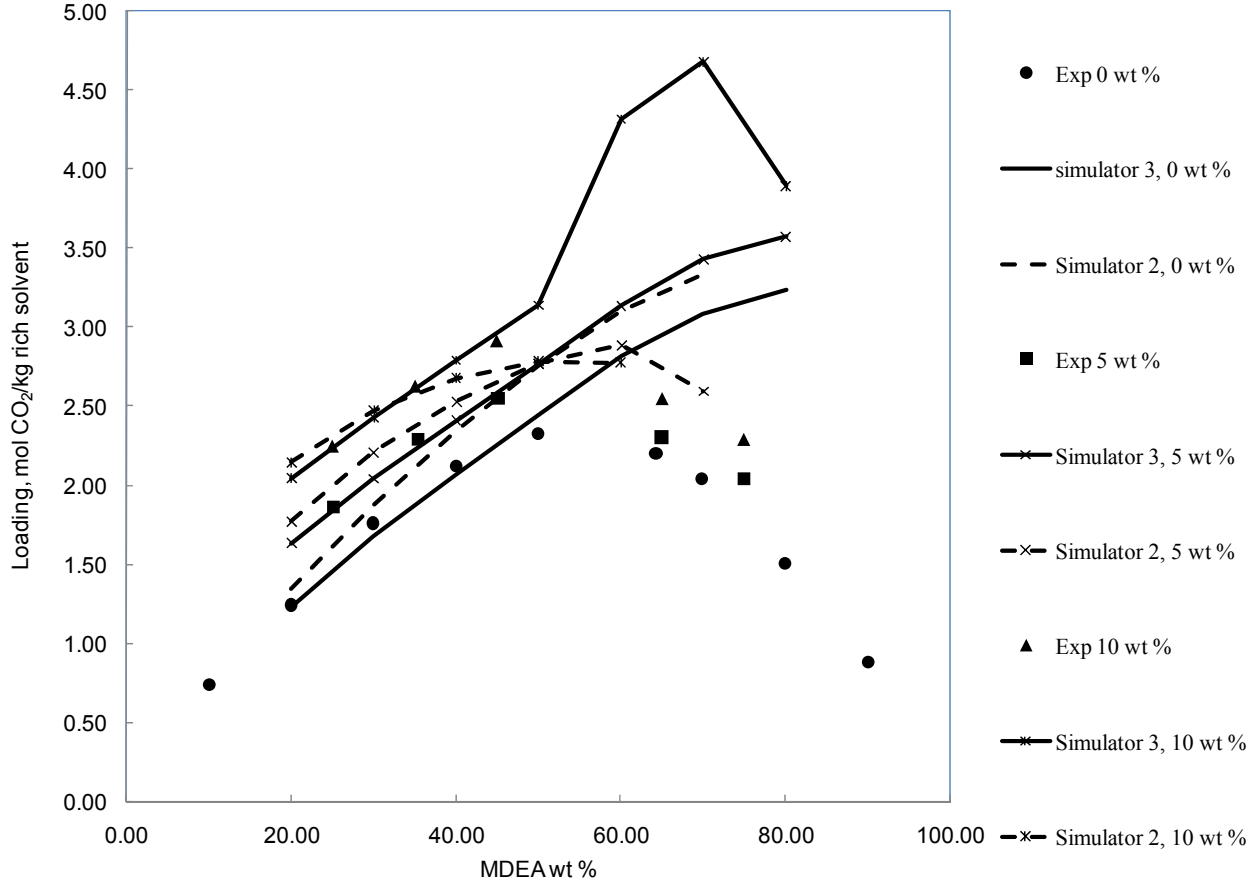

Figure 7-7. Comparison between simulators predictions and measured CO_2solubility datain aqueous blend mixtures of MDEA-PZ at 40.00 °C and 110.00kPa. ●, Experimental (PZ = 0 wt %); ■, Experimental (PZ = 5 wt %); ▲, Experimental (PZ = 10 wt %); Solid Line, Simulator 3; Dash Line, Simulator 2

Table 7-12. Simulation Results forCO_2 solubility in aqueous blends of MDEA-PZ at T = 50.00 °C and P = 110.00kPa

MDEA mass %	PZ mass%	Predicted Values			
		Simulator 2		Simulator 3	
		∝(mole CO_2/mole amine)	∝́ (mole CO_2/kg rich solvent	∝(mole CO_2/mole amine)	∝́ (mole CO_2/kg rich solvent
20.00	5.00	0.77	1.62	0.71	1.49
30.00	5.00	0.69	1.95	0.65	1.84
40.00	5.00	0.60	2.14	0.60	2.15

50.00	5.00	0.51	2.20	0.57	2.44
60.00	5.00	0.41	2.09	0.58	2.83
70.00	5.00	0.31	1.83	0.60	3.30
80.00	5.00			0.57	3.52
20.00	10.00	0.76	1.97	0.74	1.92
30.00	10.00	0.66	2.19	0.68	2.26
40.00	10.00	0.56	2.28	0.64	2.57
50.00	10.00	0.47	2.28	0.61	2.86
60.00	10.00	0.40	2.22	0.61	3.22
70.00	10.00			0.63	3.70
80.00	10.00			0.59	3.85

Figure 7-8 depicts graphically simulators prediction results in comparison with the measured values at 50 °C.

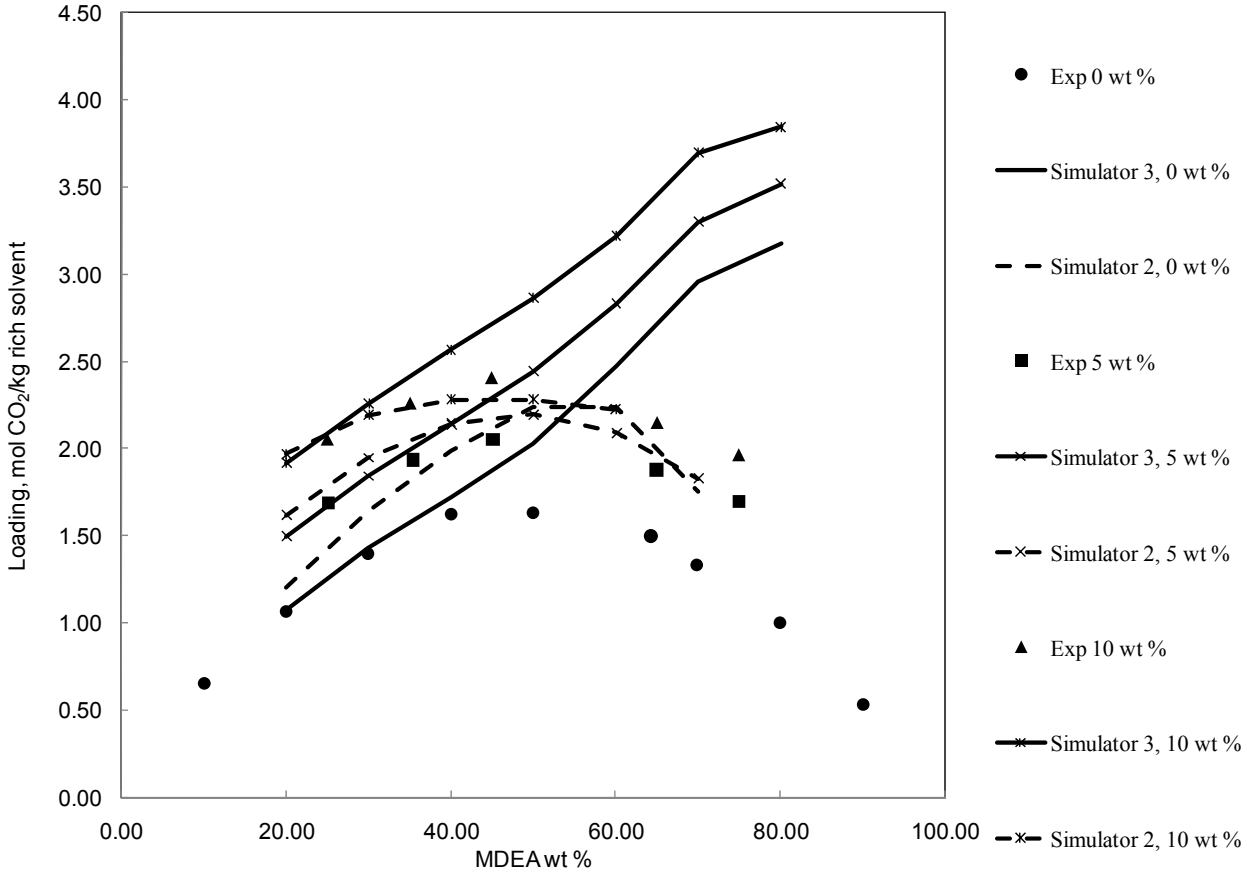

Figure 7-8. Comparison between simulators predictions and measured CO_2solubility datain aqueous blend mixtures of MDEA-PZ at 50.00 °C and 110.00kPa. ●, Experimental (PZ = 0 wt %); ■, Experimental (PZ = 5 wt %);▲, Experimental (PZ = 10 wt %); Solid Line, Simulator 3; Dash Line, Simulator 2

Table 7-13. Simulation Results forCO_2 solubility in aqueous blends of MDEA-PZ at T = 60.00 °C and P = 110.00kPa

MDEA mass %	PZ mass%	Predicted Values			
		Simulator 2		Simulator 3	
		∝(mole CO_2/mole amine)	∝ (mole CO_2/kg rich solvent	∝(mle CO_2/mole amine)	∝ (mole CO_2/kg rich solvent
20.00	5.00	0.66	1.40	0.62	1.33
30.00	5.00	0.55	1.59	0.56	1.60
40.00	5.00	0.45	1.64	0.50	1.82
50.00	5.00	0.36	1.61	0.46	1.99
60.00	5.00	0.29	1.52	0.41	2.10
70.00	5.00	0.23	1.39	0.34	1.99
80.00	5.00			0.23	1.57
20.00	10.00	0.66	1.73	0.67	1.76
30.00	10.00	0.54	1.83	0.61	2.05
40.00	10.00	0.44	1.83	0.57	2.30
50.00	10.00	0.37	1.82	0.53	2.52
60.00	10.00	0.32	1.80	0.50	2.73
70.00	10.00			0.58	3.48
80.00	10.00			0.58	3.80

Figure 7-9 compares simulators prediction results with the measured values obtained in this study at 60 °C.

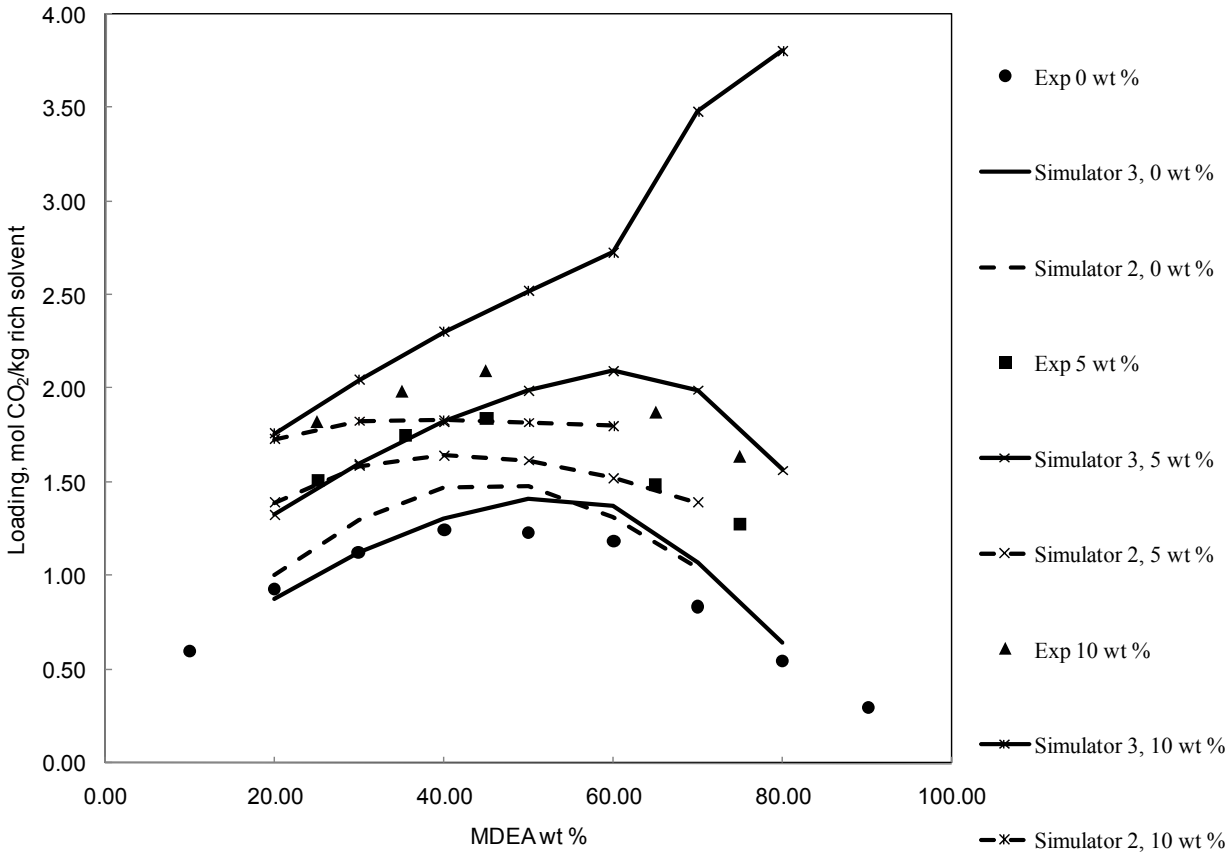

Figure 7-9. Comparison between simulators predictions and measured CO_2 solubility data in aqueous blend mixtures of MDEA-PZ at 60.00 °C and 110.00kPa. ●, Experimental (PZ = 0 wt %); ■, Experimental (PZ = 5 wt %); ▲, Experimental (PZ = 10 wt %); Solid Line, Simulator 3; Dash Line, Simulator 2

Table 7-14. Simulation Results forCO_2 solubility in aqueous blends of MDEA-PZ at T = 70.00 °C and P = 110.00kPa

MDEA mass %	PZ mass%	Predicted Values			
		Simulator 2		Simulator 3	
		∝(mole CO_2/mole amine)	∝ (mole CO_2/kg rich solvent	∝(mole CO_2/mole amine)	∝ (mole CO_2/kg rich solvent
20.00	5.00	0.53	1.13	0.53	1.13
30.00	5.00	0.41	1.21	0.46	1.33
40.00	5.00	0.32	1.20	0.40	1.48
50.00	5.00	0.26	1.18	0.35	1.56
60.00	5.00	0.21	1.14	0.30	1.56
70.00	5.00	0.18	1.09	0.24	1.46

80.00	5.00			0.19	1.28
20.00	10.00	0.54	1.44	0.59	1.57
30.00	10.00	0.42	1.45	0.53	1.80
40.00	10.00	0.34	1.44	0.48	2.00
50.00	10.00	0.29	1.45	0.44	2.15
60.00	10.00	0.25	1.47	0.40	2.25
70.00	10.00			0.36	2.27
80.00	10.00			0.31	2.18

Figure 7-10 exhibits predicted and measured CO_2 solubility at 70 °C.

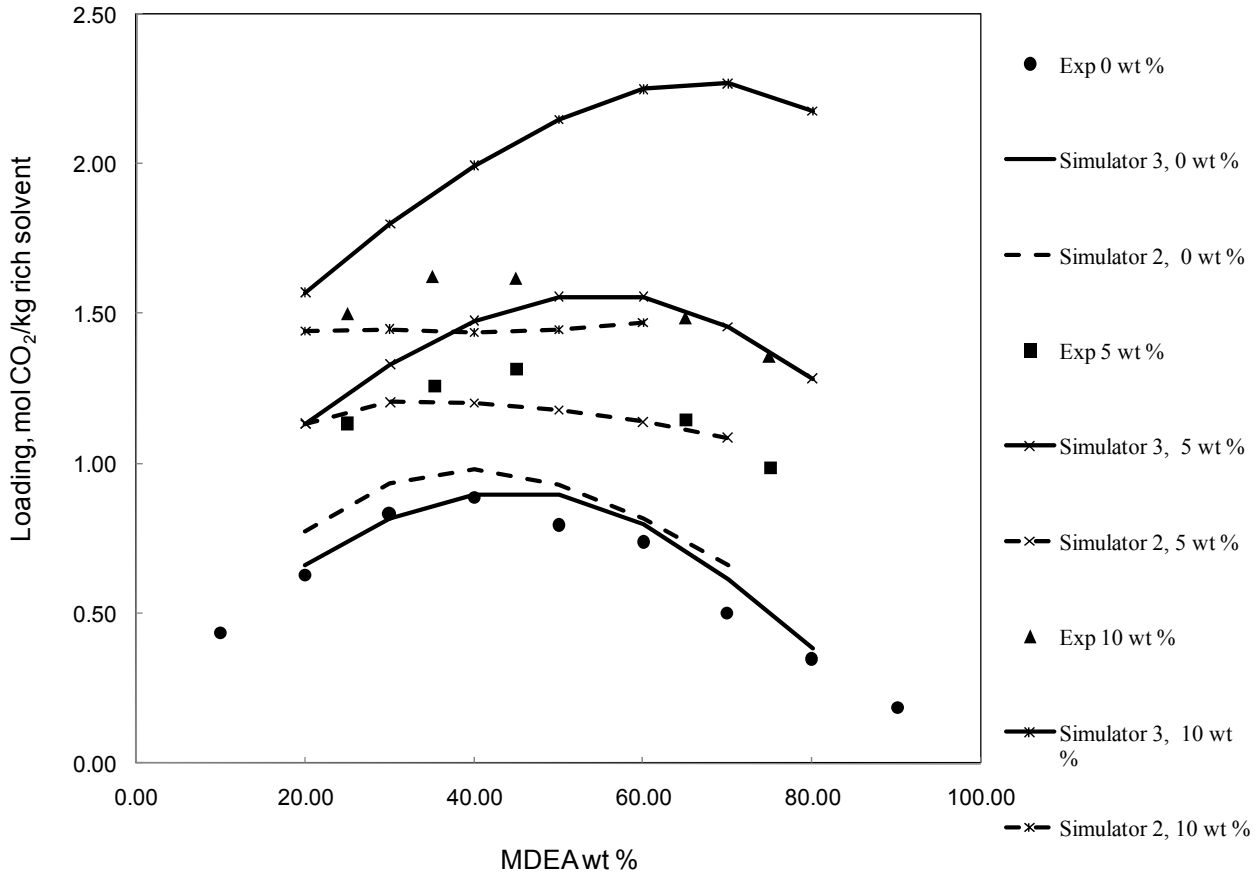

Figure 7-10. Comparison between simulators predictions and measured CO_2 solubility data in aqueous blend mixtures of MDEA-PZ at 70.00 °C and 110.00kPa. ●, Experimental (PZ = 0 wt %); ■, Experimental (PZ = 5 wt %);▲, Experimental (PZ = 10 wt %); Solid Line, Simulator 3; Dash Line, Simulator 2

Following Figure 7-7 to Figure 7-10, it is obvious that the studied simulators cannot provide even the trend of the changes of loading versus MDEA concentration. It is notable that at 40 °C and 50

°C, simulator 2 outperforms simulator 3 and at 60 °C and 70°C simulator 3 provides better estimation of the loading compare to Simulator 2.

7.6 Results and Discussion

In order to study the effect of PZ concentration on the solubility of CO_2 in aqueous MDEA, mole of absorbed CO_2per kg of rich solvent, at each studied temperature in presence of 0, 5 and 10 wt % of PZ is graphically shown in Figure 7-11 to Figure 7-14. It is notable that these measured data were provided in chapter 6 and previous sections of this chapter.

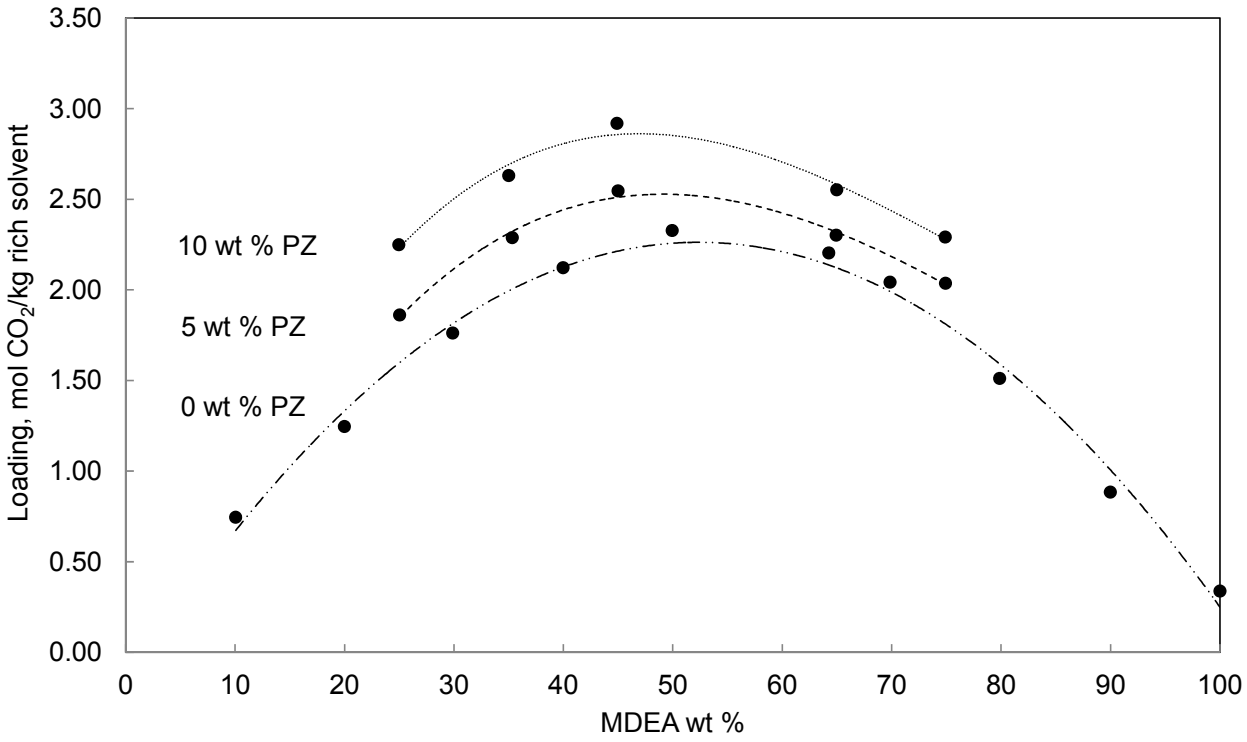

Figure 7-11. Comparison between measured CO_2 solubility data in aqueous MDEA and in presence of 0, 5 and 10 mass% PZ at 40.00 °C and 110.00 kPa (1.10 bar).Lines show the trend of each data set. ●, Experimental data.

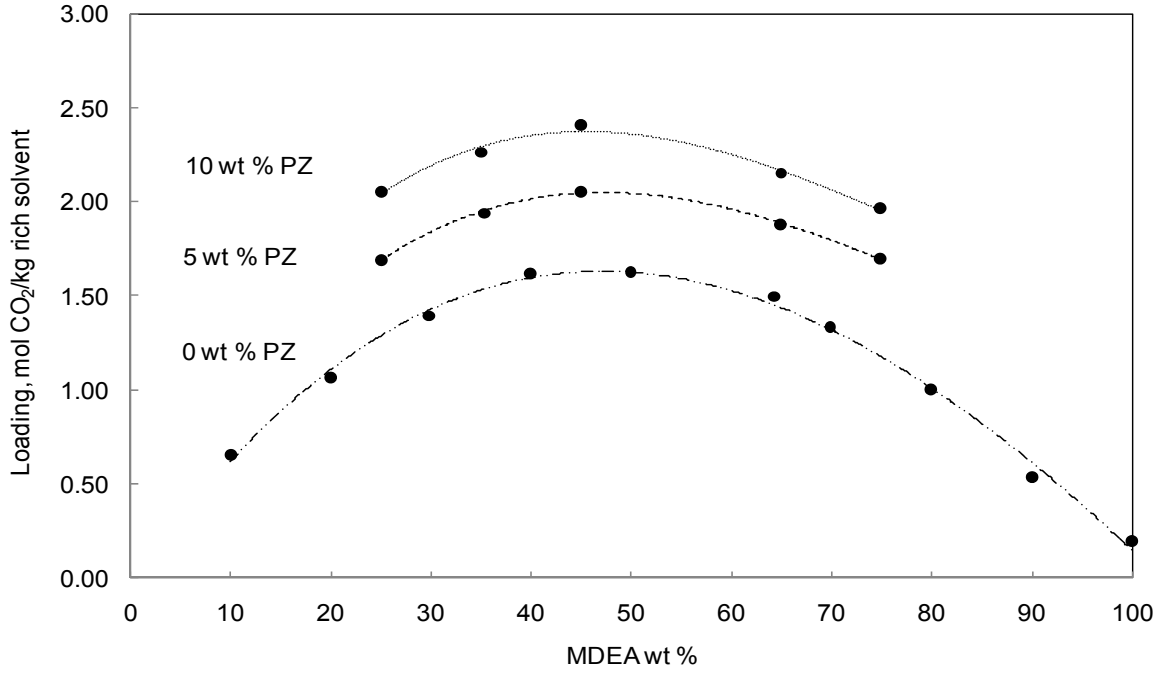

Figure 7-12. Comparison between measured CO_2 solubility data in aqueous MDEA and in presence of 0, 5 and 10 mass% PZ at 50.00 °C and 110.00 kPa (1.10 bar).Lines show the trend of each data set. ●, Experimental data.

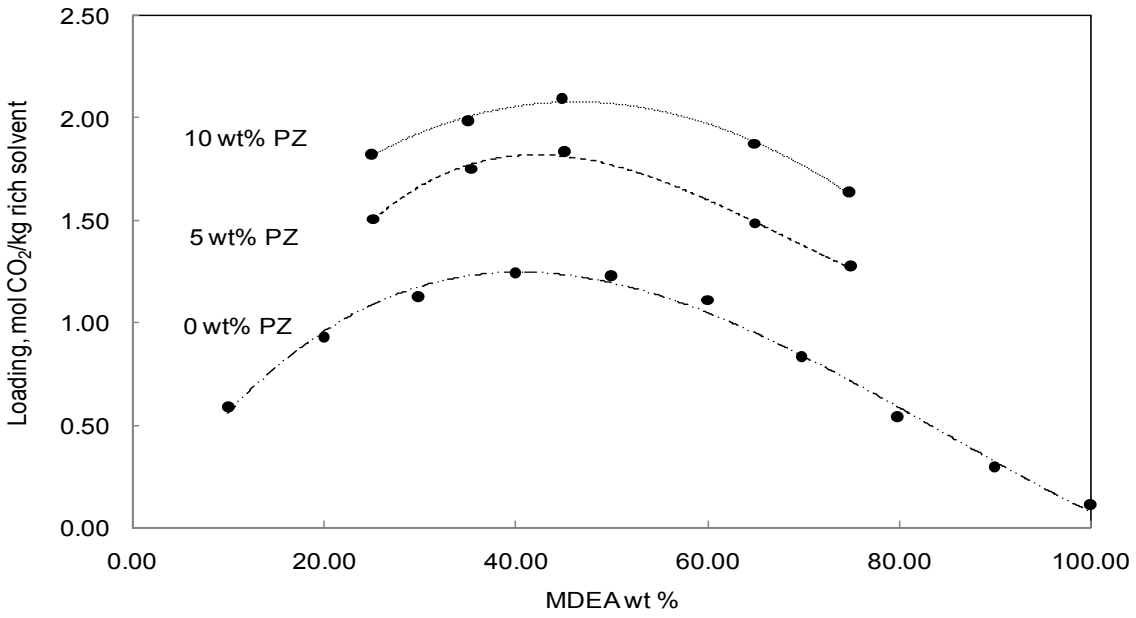

Figure 7-13. Comparison between measured CO_2 solubility data in aqueous MDEA and in presence of 0, 5 and 10 mass% PZ at 60.00 °C and 110.00 kPa (1.10 bar).Lines show the trend of each data set. ●, Experimental data.

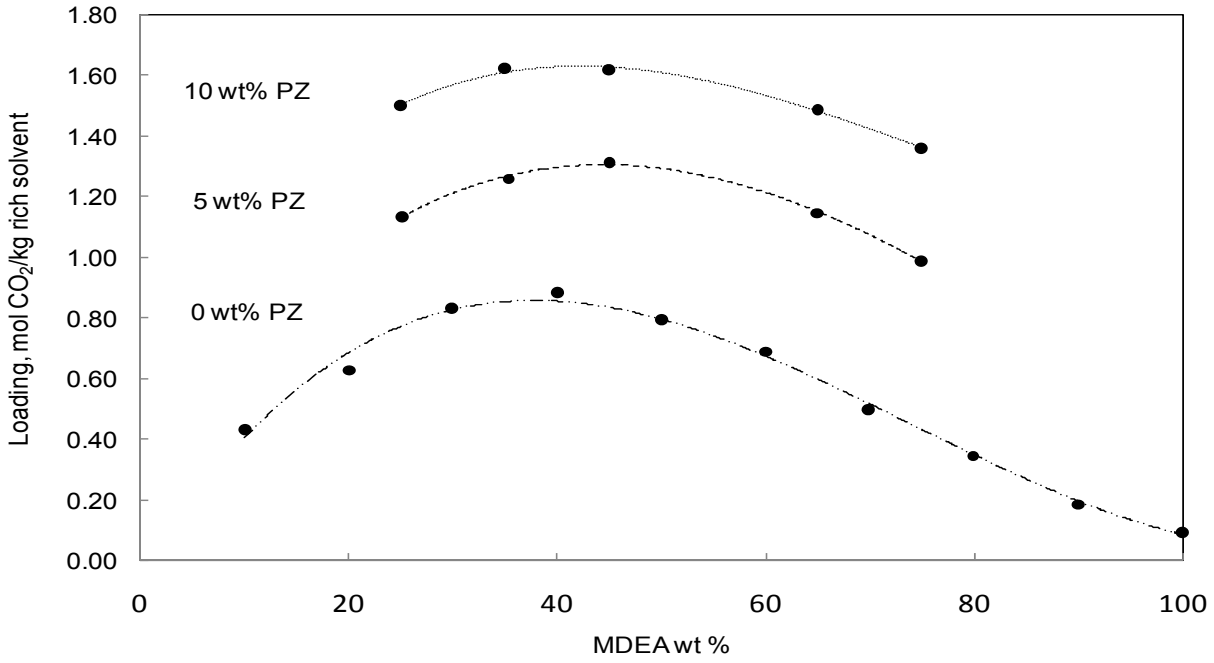

Figure 7-14. Comparison between measured CO_2 solubility data in aqueous MDEA and in presence of 0, 5 and 10 mass% PZ at 70.00 °C and 110.00 kPa (1.1 bar).Lines show the trend of each data set. ●, Experimental data.

Figure 7-15 compares CO_2 absorption capacity for this work studied conditions.

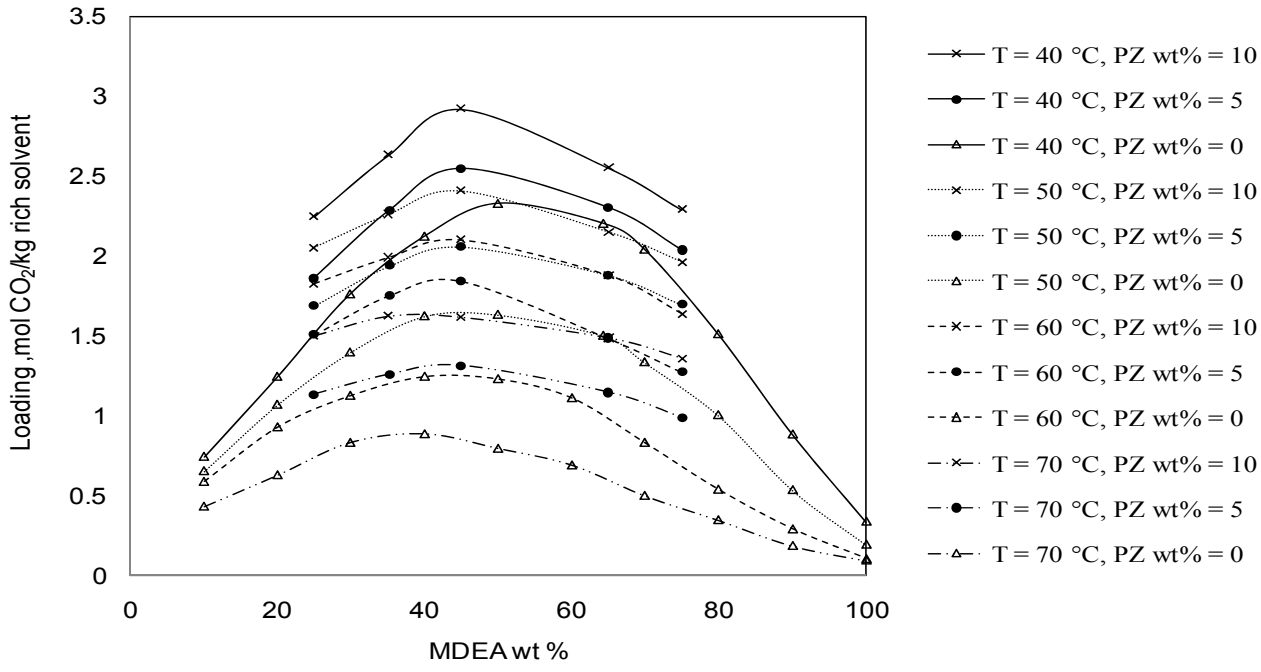

Figure 7-15. Comparison between measured CO_2 solubility in aqueous MDEA and aqueous blends of MDEA-PZ (with 5 and 10 mass% PZ) at 40, 50, 60 and 70.00 °C and 110.00 kPa (1.10 bar).

From Figure 7-11 to Figure 7-14 it is obvious that for a given MDEA concentration, temperature and total pressure, adding certain amount of piperazine increase CO_2 absorption capacity in the aqueous MDEA. In addition, the enhancing effect of PZ on CO_2 absorption capacity is more pronounced at higher temperatures. This owes to the influence of PZ on the kinetic reaction.

For the sake of easy comparison, the information provided in Figure 7-11 to Figure 7-14 are overlapped in Figure 7-15. It can easily be seen that in the studied conditions, the highest absorption capacity is achieved at the temperature of 40 C and for blend of 40 mass% MDEA with 10 mass % PZ.

7.7 Conclusions

To sum up, this section presented measured density data for MDEA-PZ-H_2O solutions and new vapor-liquid equilibrium data for CO_2-MDEA-PZ-H_2O systems. Density experiments were carried out for aqueous blends of MDEA-PZ with MDEA concentration of 25 to 75 wt % and PZ mass % of 5 and 10, at temperatures between 40 to 80 °C. VLE experiments were performed for aqueous blends of MDEA-PZ with MDEA concentration of 25 to 75 wt % and PZ mass % of 5 and 10, at constant pressure of 1.1 bar and temperatures range of 40 to 70 °C. In VLE experiments loading were calculated from the volumetric data obtained from the cell without any requirement for liquid phase analysis. From these experiments it was concluded that adding certain amounts of PZ to MDEA significantly increase the solvent absorption capacity occurs. Investigations over the effect of PZ concentration demonstrates that the highest absorption capacity happens in the solutions with 10 mass % PZ. Tow thermodynamic packages of commercial simulators, were used to calculate CO_2 solubility in the studied conditions. None of them were successful to predict CO_2 solubility in blend mixtures of MDEA-PZ. Since PZ is a widely used additive in natural gas treatment process, it is vital to improve available thermodynamic models to characterize the behavior the systems.

Chapter 8

Measurement and Modeling of High Pressure Phase Equilibrium of Methane, H_2S and Aqueous Solutions of MDEA

8 Measurement and Modeling of High Pressure Phase Equilibrium of Methane, H_2S and Aqueous Solutions of MDEA

8.1 Chapter Overview

As already mentioned aqueous solutions containing alkanolamines are widely used for the removal of acid gases from natural gas. MDEA has many advantages over other amines; so that MDEA is becoming the most common solvent in natural gas industry (Jou et al. 1998), (Anufrikov et al. 2007). One of the most specific advantages of MDEA is its capability for selective separation of H_2S from a stream containing CO_2. In natural gas treatment process the absorber is operated at high total pressures (about 70 to 100 bar), but the regenerator operating pressure is low (around 1 to 3 bar) (Huttenhuis et al. 2007). Therefore, it is important to investigate the effect of pressure on the acid gas solubility. So if the total pressure affects the acid gas solubility, the low pressure experimental solubility data could not be used directly (without any correction) in the conditions of high pressure absorber (Huttenhuis et al. 2007). The effect of system pressure on acid gas solubility data was already discussed in section 5.6 of chapter 5, in this section the effect of total pressure will be examined experimentally through the determined measured data. To design gas cleaning process, equilibrium, mass transfer, and chemical reaction data at industrial conditions are required. The aim of this chapter is to provide experimental data on solubility of H_2S in aqueous MDEA at conditions encountered in natural gas treatment process, 70 bara[23] total pressure. In order to investigate the effect of pressure, H_2S solubility data were also determined at 15 bara.

[23]bara: The last a refers to absolute pressure.

In this chapter, vapor-liquid equilibrium (VLE) data for the systems composed of CH_4 (methane), H_2S, MDEA, and water will be presented at two different total pressures, 15 and 70 bara. Determined data at 70 bara will be presented for partial pressures of H_2S from 0.3 to 9.7 bar, and at 50 and 70 °C. Measured data at 15 bara will be presented at 50 °C for H_2S partial pressures from 0.5 to 3.9 bar. The concentration of the aqueous MDEA solution is 50 mass % for all the experiments. Moreover, the obtained data are used to validate the developed Extended UNIQUAC model in chapter 5. Results of model predictions are compared to the measured data in the remainder of this chapter.

8.2 Experimental Design

Most of the data available in open literature are presented as acid gas partial pressure without specifying the total pressure, because normally data were measured at low total pressures (Huttenhuis et al. 2007). This section contains bibliographic study over the experimental vapor-liquid equilibrium data available in open literature, for H_2S-MDEA-H_2O and H_2S-CH_4-MDEA-H_2O systems. Bibliographic results are summarized in Table 8-1. Table 8-1 represent literature data for ternary mixtures of H_2S-MDEA-H_2O and quaternary mixtures of H_2S-CH_4-MDEA-H_2O, it includes temperature, pressure, amine concentration and number of data points for each source. Note that collected data in Table 8-1 were gathered to the best of author knowledge and at the time of this work.

Table 8-1. VLE data for H_2S-MDEA-H_2O and H_2S-Methane-MDEA-H_2O

MDEA Concentration, wt %	T, °C	P_{H_2S}, kPa	Loading, mole H_2S/mole MDEA	Reference	Number of experiments
12, 23, 50	25, 40, 70, 100, 120	0.0012 to 5890	0.001 to 3.220	(JOU et al. 1982)	153
12 , 20	25, 37.8, 65.6, 115.6	13.23 to 1536.60	0.180 to 2.1700	(Maddox et al. 1987)	49
23	40	52 to 1600	0.130 to 1.725	(Macgregor and Mather 1991)	27
35, 50	40, 100	0.0018 to 313	0.0040 to 1.077	(Jou et al. 1993)	50
30	40, 60, 80, 100	1.498 to 445.7	0.082 to 0.902	(LI and SHEN 1993)	43
18.7, 32.2	40, 60, 100, 120, 140	165.2 to 4895.9*	0.480 to1.934	(Kuranov et al. 1996)	71

23, 50	40, 70, 100, 120	0.0033 3673	to	0.0020 1.74	to	(Huang and Ng 1998)	42
11.83, 23.63	25, 40	0.023 1.611	to	0.0100 0.261	to	(Lemoine et al. 2000b)	29
48.8	40, 80	351.5 2783*	to	0.727 1.428	to	(Lemoine et al. 2000b)	13
35, 50	10, 25, 40	141 to18.98		0.023 0.575	to	(Ter Maat et al. 2004), (Huttenhuis et al. 2007)**	37
50	50	3 to 278		0.096 0.889	to	(Dicko et al. 2010)**	10

* *Bubble pressure is measured (P_{H_2S}+ solvent vapor pressure)*

** *Methane is present*

As it can be seen, there are only a few measured points at high total pressure, however there is a requirement for more data points at high pressures, the typical absorber pressure in amine based gas sweetening units. To execute H_2S measurements at high pressures, it is required to have methane or nitrogen as a makeup gas. Existing literature data reveals a gap in high pressure VLE data for H_2S-Methane/Nitrogen-MDEA-H_2O systems. One objective of this study is to obtain complementary points where there is a lack of data. In chapter 5 the effect of total pressure on H_2S solubility in aqueous MDEA was discussed through both modeling and experimental investigations. Notice that it is not very feasible to quantify the effect of total pressure accurately by comparing low pressure data from one source and high pressure data from another source. Experience tells that the deviations between different sources are related to other reasons as well (apparatus, analysis methods, chemicals used, etc.). Therefore another aim of this work was set to study the effect of total pressure on H_2S solubility in the same equilibrium cell, with the same chemicals, the same analysis techniques, etc. Hence the effect of pressure on H_2S solubility could be quantified more accurately. In this work new VLE data points are measured for H_2S-CH_4-MDEA-H_2O system at 70 and 15 bara, 50 and 70 °C and loading range of 0.28 to 1. To the best of our knowledge there is no measured data at 70 °C and at loadings higher than 1.

8.3 Experimental Section

8.3.1 Chemicals

The chemicals used in this work include MDEA (Merck, ≥ 98 % pure), H_2S (Yara, ≥ 99 % pure) and CH_4 (Yara, ≥ 99 % pure). All chemicals were used without any further purification.

8.3.2 Experimental Apparatus

The experiments were done in the apparatus shown in Figure 8-1. The cell is constructed for a "static-analytic" method with liquid and vapor samplings at constant temperature and pressure. The apparatus is a modified version of the one used by (Addicks 2002) for high pressure VLE measurements for the system CO_2-CH_4-MDEA-H_2O.

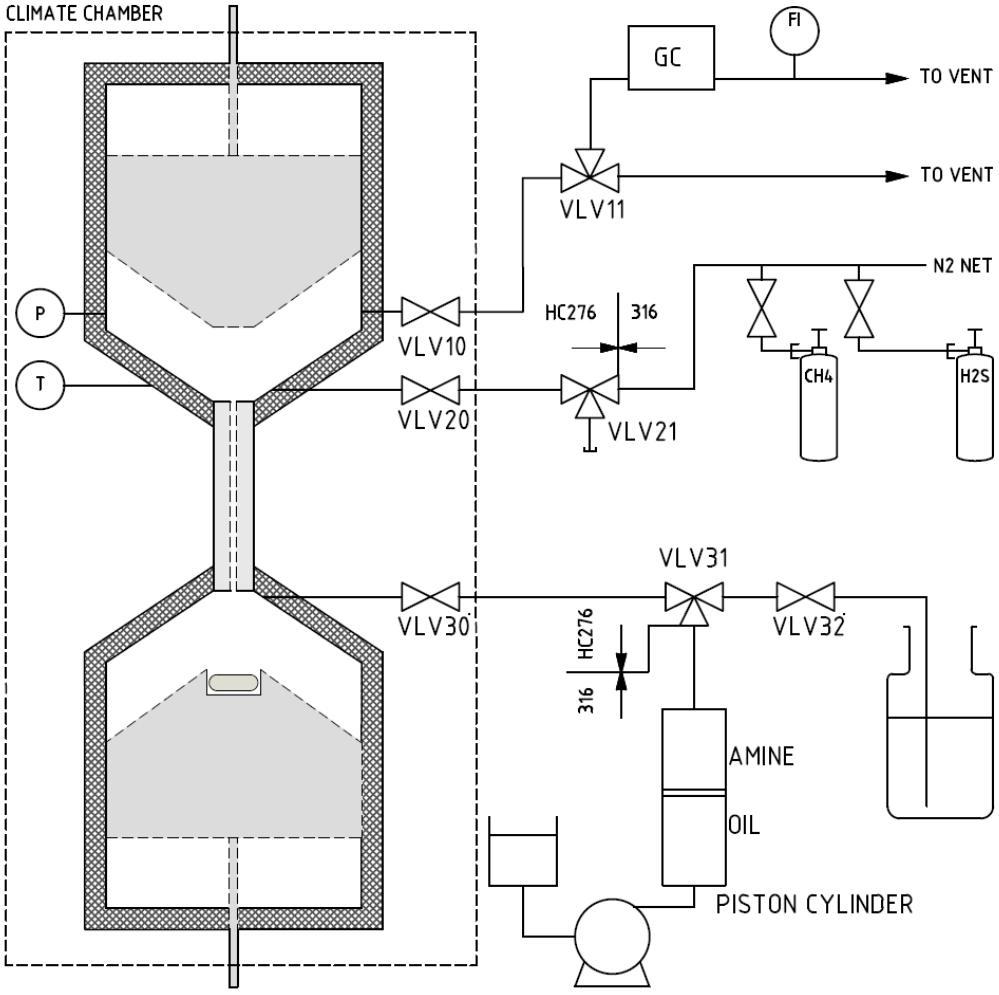

Figure 8-1. Sketch of the equilibrium cell.

The central part of the apparatus is a variable volume cell consisting of two cylindrical compartments connected through a cylindrical sapphire window. Both compartments are equipped with pistons which make it possible to vary the cell volume. A stirrer is fitted inside the lower piston to ensure mixing in the liquid phase. There is hydraulic oil on the back side of the pistons. The maximum volume is 450 cm^3, and the cell can be operated up to 700 bar (70000 kPa) and in the temperature range -50 to 200°C. The cell is placed inside an air bath to keep the temperature inside the cell constant. The air bath temperature fluctuated with $\pm$ 0.5 °C. The temperature in the cell is measured with a platinum resistance thermometer with an accuracy of $\pm$ 0.1°C, which is placed within the wall the cell. Each piston is driven by the pressure difference between the hydraulic oil and the "process". The pressure in the hydraulic oil is controlled during an experiment. The pressure on the process side is slightly lower than the pressure in the hydraulic oil due to the friction between the piston and the cell wall. The pressure is measured with a high-pressure sensor up to 1000 bar (100000kPa), and its accuracy is $\pm$ 0.1 % of full scale. All the measuring devices are connected to a PC to store measurements and to control the operation of the cell. In order to avoid leaking between the hydraulic oil and the process side, there are two sets of O-rings on each piston. During operation, the O-rings and the bearings for the stirrer are affected by the harsh environment inside the cell. The cell is therefore emptied and taken apart for cleaning and maintenance every so often. The O-rings and bearings of the stirrer are then changed. Figure 8-1 shows that there are three inlet/outlet valves from the cell. The upper valve was used for gas sampling to a gas chromatograph and for depressurizing of the apparatus. The H_2S in the waste gas was removed with solid adsorbents before the gas was vented. The middle inlet/outlet valve was used for filling of methane and H_2S, and for purging with nitrogen during cleaning. The lower inlet/outlet valve was used for loading of the solvent into the cell, and for taking liquid samples. The liquid sample was taken directly into 1 M NaOH in order to stabilize H_2S in the liquid phase. Methane which had been dissolved in the solvent inside the cell escaped to the atmosphere and was vented. The solvent was pumped into the cell from a separate storage vessel. Valves, tubing and fittings in contact with the H_2S-loaded solvent or in contact with wet gas containing H_2S are made of Hastelloy C276. Some parts of the gas and solvent loading system are made of 316 stainless steel as shown Figure 8-1. Equipment in more details was explained in Addicks PhD thesis (Addicks et al. 2002). Pictures of the equilibrium cell are shown in appendix 11.2.

8.3.3 Experimental procedure

The cell was cleaned and vacuumed before the initial filling of gas and solvent. The initial filling procedure was: First, the cell was filled completely full (450 cm^3) with H_2S gas at the pressure in the H_2S-bottle. Then, around 150 cm^3 of solvent was pumped into the cell from the storage vessel. After waiting for some hours, more H_2S gas was filled into the cell in order to reach high H_2S loadings in the solvent. This was sometimes repeated several times to reach H_2S loadings in the order of 1 mole/mole MDEA. Finally, methane was filled. The solvent was an aqueous solution with 50 wt % MDEA made from degassed ion exchanged water. The system was left to equilibrate at specified pressure and temperature. Equilibrium was most often reached over night, but the system was always left for at least two whole days to make sure equilibrium had been reached. Gas samples (5-10 tests) were routed directly to a gas chromatograph for analysis. One liquid sample was taken for each experiment. The liquid sampling line was first flushed with some sample, before 15 to 20 cm^3 of solvent was taken directly into a glass bottle which was preloaded with 150 to 200 cm^3 1M[24] NaOH. Accurate weights of caustic and stabilized sample (caustic plus sample) were noted in order to know the degree of dilution of the sample. The sampling line is 1/16 inch Hastelloy C276 tubing with no heat tracing, so the sample was cooled through the sampling line. The outlet of the sampling line was at the bottom of the sampling bottle. During sampling, methane escaped out of the bottle, and some H_2S followed the methane. In order to ensure that loss of H_2S was negligible, the sampling was done very slowly. The pistons inside the cell ensured that the pressure did not decrease during this operation. The stabilized sample was stored in a closed bottle. After sampling, more solvent was pumped into the cell and the system was left for another equilibration. In this way, a series of experiments was done for each initial filling of the cell. The H_2Sloading in the solvent and partial pressure of H_2S decreased through the series since only solvent was added between each experiment. The length of a series was limited either by low liquid level inside the cell, or the need to do maintenance on the stirrer. At the end of each series, the cell was emptied, cleaned, opened for maintenance and vacuumed before the next initial filling.

[24] M: Molar is defined as mole numbers of the constituent per one liter of the solution.

8.3.4 Analytical Details

Gas samples were analyzed thanks to a gas chromatograph[25] equipped with a poraplot column and a thermal conductivity detector (TCD). The sampling lines and valves are made of Hastelloy C276. Some adsorption of H_2S in the sampling lines was observed, but calibration with external standards showed that the calibration curve was linear in the H_2S concentration range of interest (0.5-20 mole %) and in the volume range of calibration. For each experiment between 5 and 10 tests were done and the GC results stabilized after 2-4 injections on the GC. The liquid sample was analyzed by titration on anautotitrator (Metrohm 809 Titrando). Two titration methods were used. The total concentration of dissolved H_2S was determined by titration with 0.1 M AgNO3 using a sulfide selective titrode. Silver and sulfide ions will not coexist in a solution because silver sulfide is sparingly soluble and will precipitate. The sulfide selective titrode has Ag/Ag_2S coated electrode which detects the shift from a finite sulfide concentration (up to the equivalence point) to the extremely low concentration present when there is a surplus of silver ions in the solution (beyond the equivalence point). The sum of the MDEA and the H_2S concentrations was determined by pH-titration with 0.1 M HCl. For both analyses, 1-2 gram of stabilized sample was used, and it was diluted to approximately 100 cm^3 with water. Two estimates of the H_2S loading were obtained from the titration data. The first value was calculated from the total H_2S concentration, the MDEA-concentration of the makeup solvent and the degree of dilution when liquid sample was stabilized in 1M NaOH. The other value was calculated from the titration results directly.

8.4 Results

The H_2S solubility in aqueous MDEA in presence of methane as a makeup gas was measured attotal pressures of 15 (1500 kPa) and 70 bar (7000kPa). VLE experiments for H_2S-CH_4-MDEA-H_2O system were carried out for aqueous solutions of 50 mass % MDEA at total pressure of 70 bara and temperatures of 50 and 70 °C and at total pressure of 15 bara and temperature of 50 °C. This section describes results of VLE measurements. Table 8-2 reports H_2S solubility measurements at 70 bara total pressure.

[25]GC Details: SRI 8610C. Column: 6 feet Haysep D. Detector: TCD, temp=156 °C. Carrier gas: He, 10psi. Injector: 10 port gas sampling valve, 250µl loop, temp = 100 °C. Oven temp.=100°C.

Table 8-2. Experimental VLE data for H_2S-CH_4-MDEA-H_2O system at total pressure =70 bara and MDEA mass% = 50

T, °C	Loading, moleH_2S/mole MDEA	P_{H_2S} , kPa	P, kPa
49.8	0.29	31.03	69.7
49.8	0.35	42.10	69.8
49.8	0.38	50.36	69.9
49.8	0.54	94.77	69.6
49.8	0.64	136.38	69.9
49.8	0.71	192.19	69.8
49.8	0.80	269.00	69.9
49.8	0.86	383.39	70.6
49.8	0.88	398.39	69.7
49.8	0.89	431.30	69.1
49.8	0.97	626.75	69.3
49.7	0.97	683.65	70.9
49.8	1.01	790.34	69.3
49.7	1.03	973.84	70.7
49.8	1.04	911.24	69.9
49.8	1.04	880.41	70.2
69.9	0.27	65.76	69.9
69.9	0.39	114.66	69.7
69.9	0.51	175.86	69.4
69.9	0.65	302.97	69.5
69.9	0.70	365.02	69.9
69.9	0.78	506.91	69.5
69.9	0.85	711.61	70.2
69.9	0.86	717.87	70.5
69.9	0.92	890.68	69.7

Table 8-3 presented measured values at total pressures of 15 bara.

Table 8-3. VLE data for H_2S-CH_4-MDEA-H_2O system at total pressure = 15 bara and MDEA mass % = 50

T, °C	Loading, mole H_2S/mole MDEA	P_{H_2S} , kPa	P, kPa
49.8	0.44	52.67	15.2
49.8	0.45	54.42	15.5
49.8	0.52	70.90	15.7
49.8	0.52	72.28	15.3
49.8	0.55	82.54	15.2
49.8	0.60	95.36	15.4
49.8	0.69	141.44	15.3

49.8	0.70	132.69	15.0
49.8	0.73	161.34	16.1
49.8	0.73	163.98	14.8
49.8	0.76	182.48	15.2
49.8	0.79	210.73	15.3
49.8	0.83	244.78	15.3
49.8	0.92	386.37	15.7

Figure 8-2 plotted H_2S partial pressure as a function of loading at total pressure of 70 bara. Error bars are added to each measured point on the figure. Figure 8-3 depicts the measured data graphically at total pressure of 15 bara, the same as Figure 8-2, error bars are shown on the figure, however they are not visible for all points because the markers hide them.

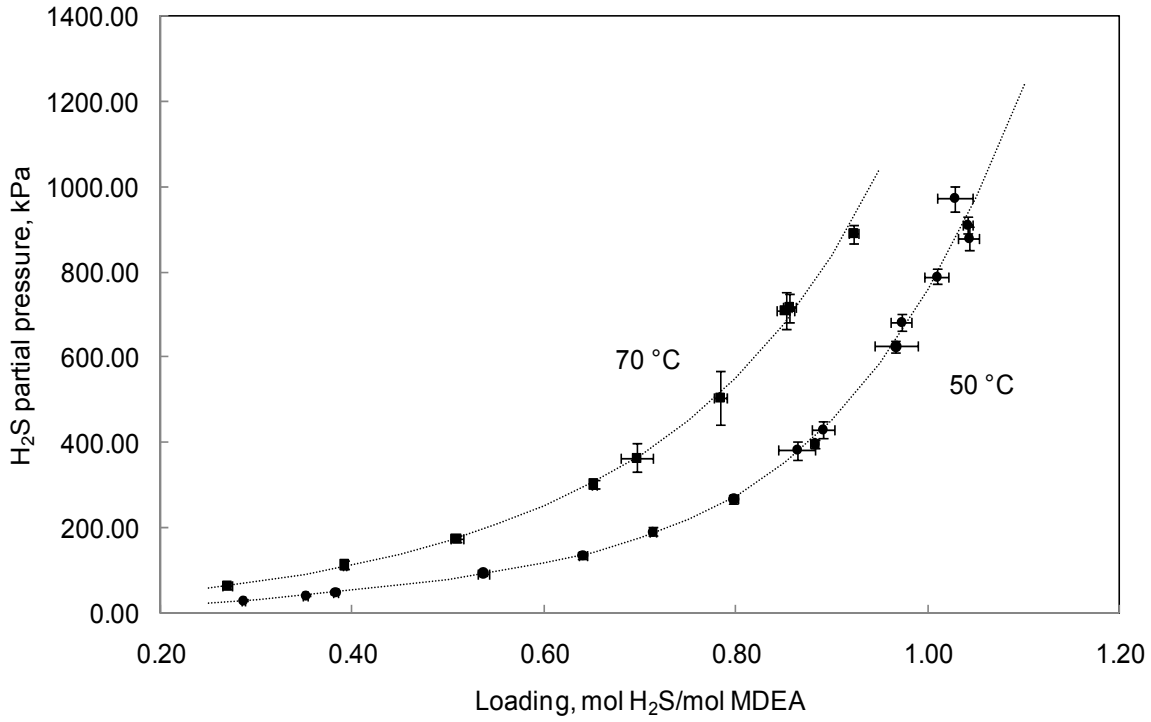

Figure 8-2. Solubility data of H_2S in 50 mass % MDEA aqueous solutions and at 70 bara total pressure. ●, experimental data at 50 °C; ■, experimental data at 70 °C. Error bars are shown in the figure. Lines are added to show trends of data.

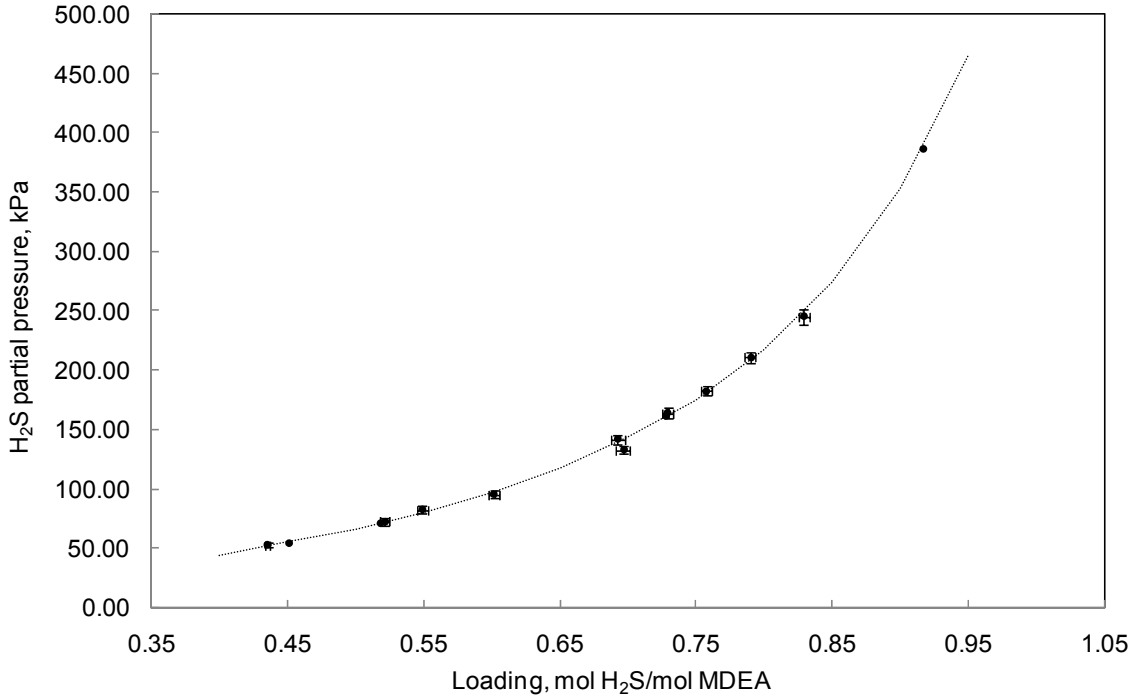

Figure 8-3. Solubility data of H_2S in 50 mass % MDEA aqueous solutions and at 15 bara total pressure and at 50°C. ●, experimental data. Error bars are shown in the figure. Lines are added to show trends of data.

As it can be seen from Figure 8-2 and Figure 8-3, the uncertainty goes down with a decrease in loading and partial pressure. Unlike absolute uncertainty, the relative uncertainty increase when loading and partial pressure decrease.

8.5 Results and Discussion

This section explains the effect of the total pressure on H_2S solubility. Figure 8-4 compares the measured data of this work at 50 °C and for 50 mass % MDEA aqueous solutions at two different total pressures of 15 and 70 bara.

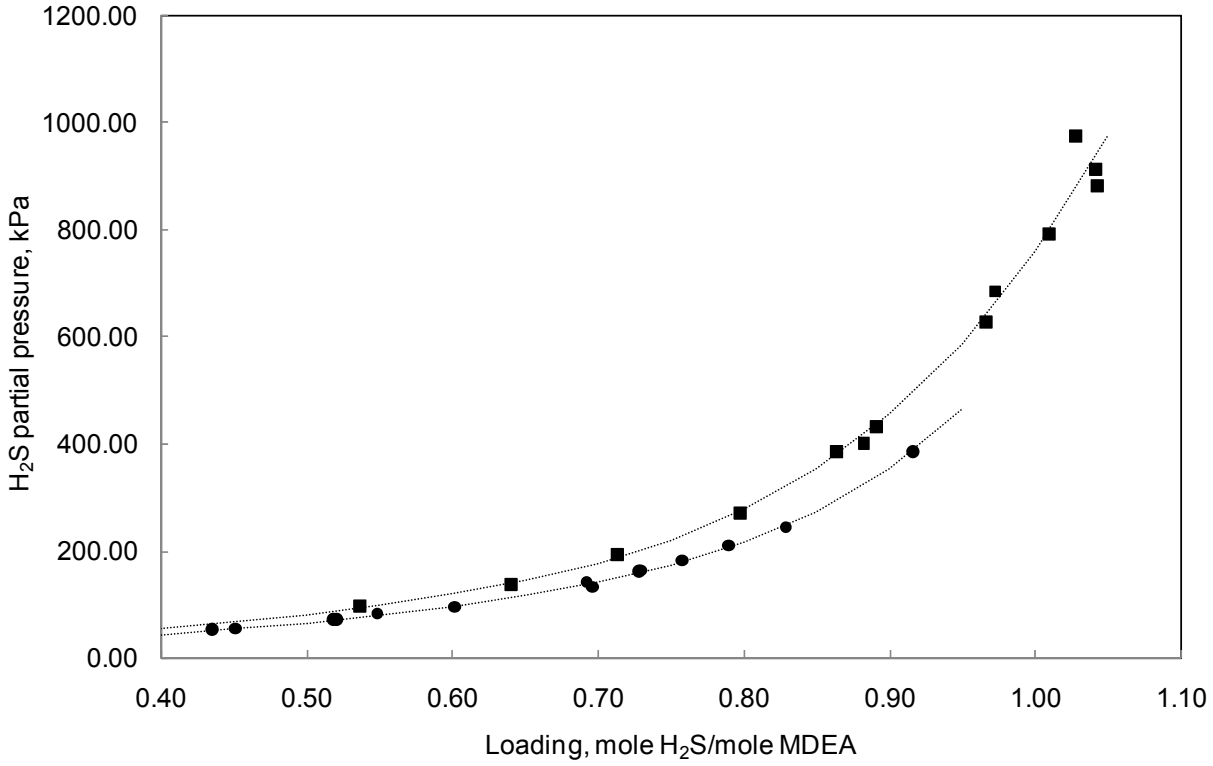

Figure 8-4. H_2S solubility in 50 mass % MDEA aqueous solutions in presence of methane at 50 °C and total pressure of 15 and 70 bara.

As it can be observed from the Figure 8-4, increasing total pressure leads to decrease in H_2S solubility (increase in H_2S partial pressure). Quantitative analysis over the measured data shows that, in the studied conditions (50 °C and 50 mass % MDEA) an increase of 55 bar (5.5 MPa) in total pressure leads to about 28 % decrease in H_2S solubility in aqueous MDEA. This conclusion is in accordance to the observations explained in section 5.6 of chapter 5.

8.6 Model Validation

The results of H_2S solubility experiments of this work were compared to the developed thermodynamic model in chapter 5. Note that parameters of the developed model have not been fitted to the new data; data of this work were utilized to validate the developed model as a predictive tool.

Table 8-4 and Table 8-5 summarized predicted and measured values at each studied temperature. Deviations between models and measured values are shown in bold in tables. Calculated and

measured results are also depicted graphically in Figure 8-5 and Figure 8-6. Error bars are shown for the points; however they are not visible for all points because the markers hide them. At the end of the section a comparison between different models proficiency and the reason for the difference between developed model predictions and experimental values will be discussed.

Table 8-4. Experimental and calculated H_2S partial pressure for mixtures of H_2S-CH_4-MDEA-H_2O at total pressure = 70 bara and MDEA mass % = 50

T, °C	Loading, mole H_2S/mole MDEA	ExpP_{H_2S} , kPa	CalcP_{H_2S} , kPa	Bias Deviation*, kPa
49.8	0.29	31.03	28.34	2.69
49.8	0.35	42.10	40.34	1.76
49.8	0.38	50.36	47.31	3.05
49.8	0.54	94.77	95.68	-0.92
49.8	0.64	136.38	151.08	-14.70
49.8	0.71	192.19	209.15	-16.96
49.8	0.80	269.00	311.20	-42.20
49.8	0.86	383.39	432.01	-48.61
49.8	0.88	398.39	475.06	-76.67
49.8	0.89	431.30	494.18	-62.88
49.8	0.97	626.75	729.16	-102.41
49.8	0.97	683.65	753.04	-69.40
49.8	1.01	790.34	899.41	-109.07
49.8	1.03	973.84	985.95	-12.11
49.8	1.04	911.24	1049.74	-138.51
49.8	1.04	880.41	1056.22	-175.82
70.0	0.27	65.76	53.21	12.55
70.0	0.39	114.66	99.76	14.91
70.0	0.51	175.86	168.33	7.54
70.0	0.65	302.97	310.83	-7.86
69.9	0.70	365.02	374.88	-9.86
69.9	0.78	506.91	542.73	-35.81
69.9	0.85	711.61	726.24	-14.63
69.9	0.86	717.87	739.35	-21.48
69.9	0.92	890.68	973.73	-83.04
AARD%**	**9.6**			

*$AARD = \frac{1}{n}\sum_{i=1}^{n}\frac{|P_{H_2S,exp}-P_{H_2S,calc}|}{P_{H_2S,exp}}$

*$Bias\ Deviation = P_{H_2S,exp} - P_{H_2S,calc}$

Table 8-5. Experimental and calculated H_2S partial pressure for mixtures of H_2S-CH_4-MDEA-H_2O at total pressure = 15 bara and MDEA mass % = 50

T, °C	Loading, mole H_2S/mole MDEA	ExpP_{H_2S} , kPa	CalcP_{H_2S} , kPa	Bias Deviation, kPa
49.8	0.44	52.67	47.18	5.49
49.8	0.45	54.42	50.74	3.68
49.8	0.52	70.90	68.70	2.20
49.8	0.52	72.28	69.37	2.91

49.8	0.55	82.54	78.18	4.37
49.8	0.60	95.36	98.65	-3.29
49.8	0.69	141.44	146.68	-5.24
49.8	0.70	132.69	149.29	-16.60
49.8	0.73	161.34	172.90	-11.56
49.8	0.73	163.98	172.87	-8.88
49.8	0.76	182.48	197.44	-14.97
49.8	0.79	210.73	230.26	-19.53
49.8	0.83	244.78	278.35	-33.57
49.8	0.92	386.37	431.94	-45.58
AARD%	**7.4**			

As it can be seen in the above tables the developed model could very well predict high pressure H_2S solubility data which is highly requested by industry. Figure 8-5 compares model predictions with experimental data graphically.

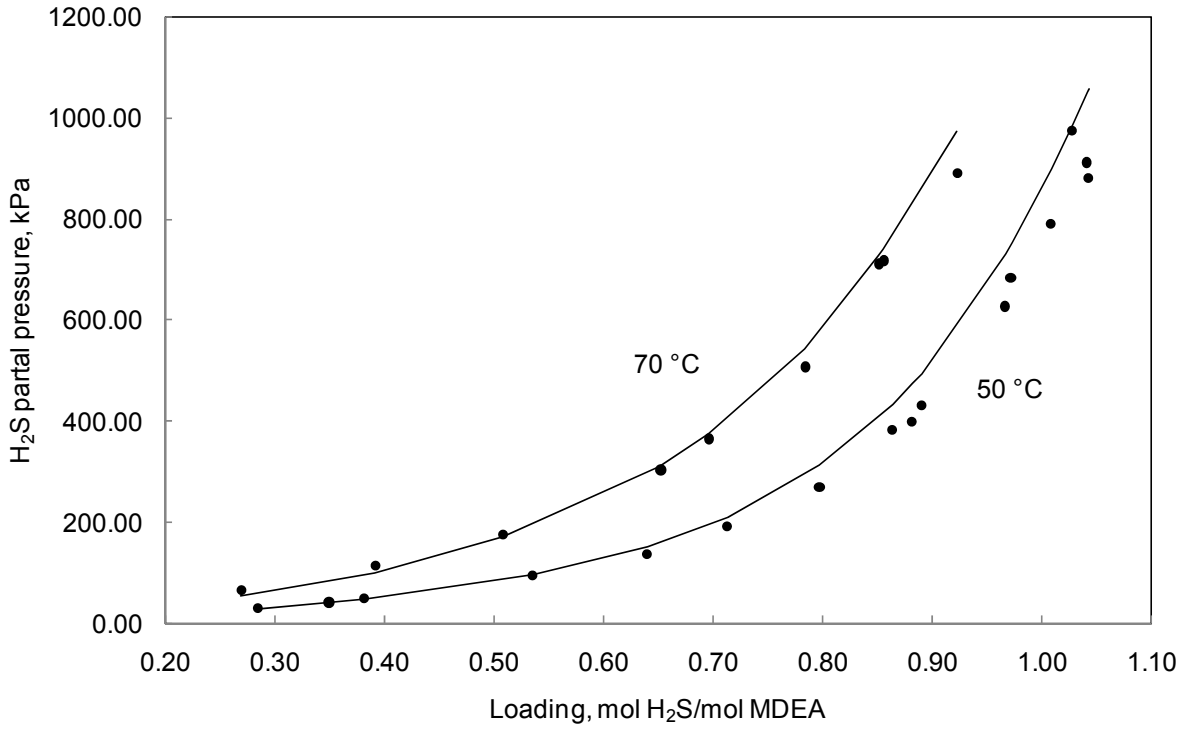

Figure 8-5. H_2S partial pressure for of H_2S-CH_4-MDEA-H_2O at total pressure = 70 bara and MDEA mass % = 50. ●, Experimental data; Solid line, Developed Extended UNIQUAC

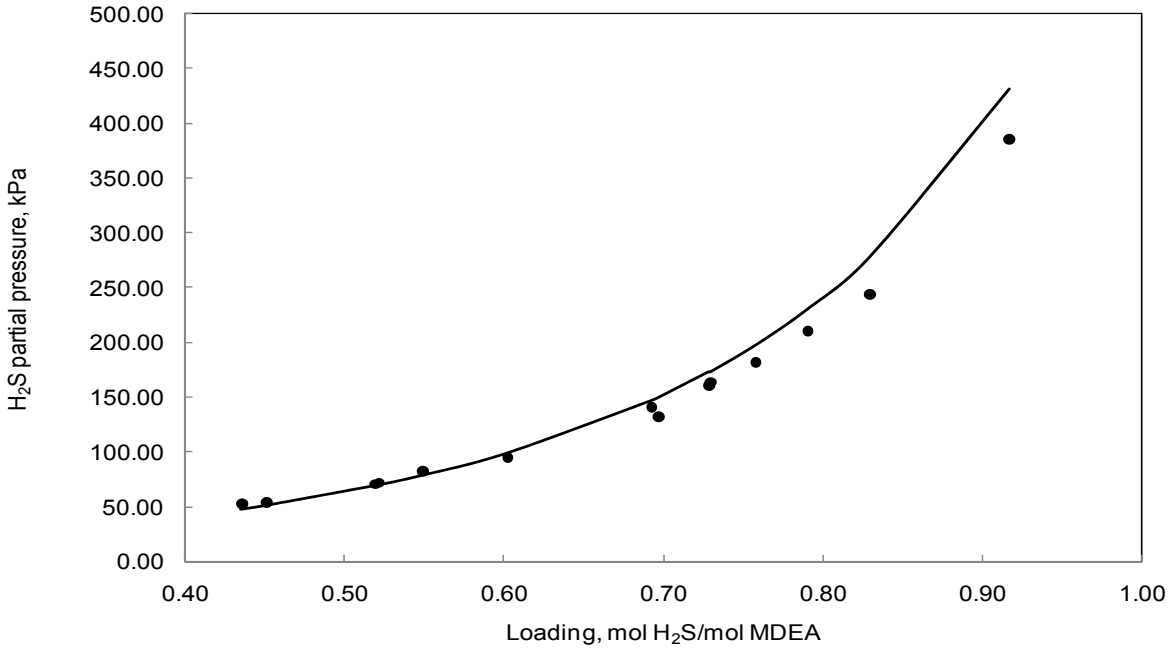

Figure 8-6. H_2S partial pressure for of H_2S-CH_4-MDEA-H_2O at total pressure = 15 bara and MDEA mass % = 50. ●, Experimental data; Solid line, Developed Extended UNIQUAC

8.7 Conclusions

This chapter presents new vapor-liquid equilibrium data for mixtures of H_2S-CH_4-MDEA-H_2O. H_2S solubility in aqueous MDEA was measured in presence of methane as a make up gas and at conditions encountered in industrial conditions. Data were presented for 50 mass % MDEA, at 50 and 70 °C and at total pressures of 15 and 70 bara. The influence of high pressure on H_2S solubility was examined by utilizing the obtained data and it was concluded that in the studied conditions an increase of 5.5 MPa in total pressure results in decrease of 28 % in H_2S solubility. The developed thermodynamic model in chapter 5 was compared against this work measured data. Model prediction results were very promising specifically at 70 °C and approved model capability for predicting high pressure solubility data. However comparison between experimental and modeling results at 50 °C and at loadings greater than 0.80 shows that adjusting model parameters to the new obtained data can improve model performance at these conditions.

Chapter 9

Conclusions and Recommendations

9 Conclusions and Recommendations

9.1 Chapter Overview

At the end of each chapter detailed conclusions on each covered topic were presented. This chapter provides a summary based on previous chapters and suggests recommendations for the future work.

9.2 Summary

In order to better design of acid gas removal systems that are based on aqueous alkanolamine solutions, mass transfer, kinetic and solubility data are required. Concentrations of amines in the applied solvents are often changed in order to obtain the optimized process. In natural gas treating process, the absorber pressure is high around 70 bar, however regenerator operates at low pressures about 1 to 2 bar. Since there is a substantial difference between absorber and regenerator pressure in natural gas sweetening process, it is of high importance to investigate the effect of pressure on solubility of acid gases in aqueous alkanolamines. Therefore, the aim of this work was to model thermodynamic behavior of these systems, to measure required acid gas solubility data and to examine the effect of pressure on acid gas solubility. In the modeling part of this work, consistent thermodynamic models have been developed for the acid gas-alkanolamine systems. In the experimental part of the project, the goal was to provide required solubility data for the conditions where data in open literature was non-existent. Some preliminary results for solubility of piperazine in aqueous MDEA were also obtained in this study.

9.3 Conclusions

In modeling part of the project, thermodynamic models were developed for CO_2-MDEA-H_2O, CO_2-MEA-H_2O, CO_2-MDEA-MEA-H_2O, H_2S-MDEA-H_2O, H_2S-CH_4-MDEA-H_2O systems and the constituent binary subsystems of the mentioned mixtures.

Solubility, speciation and thermal properties (heat of reaction, excess enthalpy and heat capacity) data are shown to be accurately predicted by the developed models. The obtained results revealed that the developed thermodynamic models can effectively predict both thermodynamic and thermal properties of acid gas-alkanolamine systems over an extensive range of pressure, temperature and amine concentration. The developed models confidently predict the conditions encountered in industrial natural gas treating plants. The effect of high pressure on acid gas solubility was quantitatively investigated both through experimental and modeling approaches. In the experimental part of the project a unique set of data for CO_2 solubility in aqueous MDEA at constant total pressure of 110 kPa (1.10 bar), temperatures between 40 to 80 °C and for MDEA concentration vary in the range of 10 to 100 mass % were obtained. Density data of MDEA-H_2O solutions at temperatures between 40 to 80 °C were also acquired. Furthermore, CO_2 solubility were measured in blends of MDEA-PZ at total pressure of 110 kPa (1.10 bar), temperatures between 40 to 70 °C and for MDEA concentration vary from 25 to 75 mass % while PZ concentration was kept constant at 5 and 10 mass%. The effect of PZ additive was investigated on increasing absorption capacity of aqueous MDEA. Density data of MDEA-PZ-H_2O solutions at temperatures between 40 to 80 °C were also measured. Another part of the experimental study related to the high VLE pressure measurements. In this part of the study H_2S solubility in aqueous MDEA and in presence of methane as a make up gas at temperatures of 50 and 70 °C, for MDEA concentration of 50 mass % and at two different total pressures, 15 and 70 bara was measured. The effect of increasing pressure on acid gas solubility was also investigated through the obtained measured data. The developed thermodynamic models in previous chapters of this work were used to validate against the experimental data obtained in this study. Results show that the devolved models promisingly predict the measured solubility data. Some commercial simulators were also used to predict this work measured data for CO_2-MDEA-H_2O and CO_2-MDEA-PZ-H_2O systems. During this study, out of the scope of preliminary plan, an effort was made to measure the solubility of piperazine in aqueous MDEA, however due to time limitation the measurements remained incomplete. The obtained results provide an approximate estimate of the solubility of piperazine in aqueous MDEA, however more investigations are required in order to obtain the exact limit of solubility.

9.4 Recommendations

9.4.1 Modeling

In the modeling part it is recommended to:

- Further developed the thermodynamic model for aqueous MDEA blended with PZ or other additives like Sulfolane
- More developed the thermodynamic model for mixtures of CO_2-H_2S
- Retune parameters of the developed model to the new obtained data of this work.

9.4.2 Experimental

- In the VLE experiments performed with the low pressure cell set up (CO_2solubility in aqueous MDEA and CO_2solubility in aqueous blends of MDEA-PZ) in order to obtain more accurate data it is suggested to:
    - Measure the dead volume between valve 9 and autoclave.
    - Use degassed MDEA.
    - At conditions that absorption capacity is low (low and high amine concentrations) it is recommended to minimize the volume of vapor phase by maximizing the volume of liquid phase, to reduce the inaccuracy of the results. Therefore at these conditions it is advised to use about 300 cm^3 solvent.
- To investigate the effect of adding higher concentrations of PZ to MDEA, on acid gas solubility
- Perform high pressure H_2S solubility measurement in blends of MDEA-PZ
- Measure heat capacity of aqueous blends of MDEA-PZ
- Measure PZ solubility in aqueous MDEA more accurately
- In case of density measurements for the loaded solutions, in order to avoid creating bubbles at high temperatures (CO_2 bubbles may release as bubble), measurements should be performed under pressure.

References

10 References

References

ABRAMS D, PRAUSNITZ J (1975) Statistical Thermodynamics of Liquid-Mixtures - New Expression for Excess Gibbs Energy of Partly Or Completely Miscible Systems. AIChE J 21:116-128.

Addicks J (2002) Solubility f Carbon Dioxide and Methane in Aqueous N-Methyldiethanolamine Solutions at Pressures between 100 and 200 bar.

Addicks J, Owren GA, Fredheim AO, Tangvik K (2002) Solubility of carbon dioxide and methane in aqueous methyldiethanolamine solutions. J Chem Eng Data 47:855-860.

Alghawas HA, Hagewiesche DP, Ruizibanez G, Sandall OC (1989) Physicochemical Properties Important for Carbon-Dioxide Absorption in Aqueous Methyldiethanolamine. J Chem Eng Data 34:385-391.

Ali B, Aroua M (2004) Effect of piperazine on CO2 loading in aqueous solutions of MDEA at low pressure. Int J Thermophys 25:1863-1870.

Anufrikov YA, Kuranov GL, Smirnova NA (2007) Solubility of CO2 and H2S in alkanolamine-containing aqueous solutions 80:515-527.

Arcis H, Rodier L, Ballerat-Busserolles K, Coxam J (2009) Enthalpy of solution of CO2 in aqueous solutions of methyldiethanolamine at T=372.9 K and pressures up to 5 MPa 41:836-841.

Arcis H, Rodier L, Ballerat-Busserolles K, Coxam J (2008) Enthalpy of solution of CO2 in aqueous solutions of methyldiethanolamine at T=322.5 K and pressure up to 5 MPa 40:1022-1029.

Austgen DM, Rochelle GT, Chen CC (1991) Model of Vapor-Liquid-Equilibria for Aqueous Acid Gas-Alkanolamine Systems .2. Representation of H2s and Co2 Solubility in Aqueous Mdea and Co2 Solubility in Aqueous Mixtures of Mdea with Mea Or Dea. Ind Eng Chem Res 30:543-555.

Austgen DM (1989) A modelof vapor-liquid equilibria for acid gas-alkanolamine-water systems.

Awan JA, Thomsen K, Coquelet C, Fosbol PL, Richon D (2010) Vapor-Liquid Equilibrium Measurements and Modeling of the Propyl Mercaptan plus Methane plus Water System. J Chem Eng Data 55:842-846.

Baek JI, Yoon JH (1998) Solubility of carbon dioxide in aqueous solutions of 2-amino-2-methyl-1,3-propanediol. J Chem Eng Data 43:635-637.

BARKER J (1953) Determination of Activity Coefficients from Total Pressure Measurements. Aust J Chem 6:207-210.

Bernal-García JM, Ramos-Estrada M, Iglesias-Silva G, Hall KR (2003) Densities and Excess Molar Volumes of Aqueous Solutions of n-Methyldiethanolamine (MDEA) at Temperatures from (283.15 to 363.15) K 48:1442-1445.

Bishnoi S, Rochelle G (2002) Absorption of carbon dioxide in aqueous piperazine/methyldiethanolamine. AIChE J 48:2788-2799.

Bishnoi S (2000) Carbon Dioxide Absorption and Solution Equilibrium in Piperazine Activated Methyldiethanolamine.

Boettinger W, Maiwald M, Hasse H (2008) Online NMR spectroscopic study of species distribution in MEA-H2O-CO2 and DEA-H2O-CO2. Fluid Phase Equilib 263:131-143.

Böttger A, Ermatchkov V, Maurer G (2009) Solubility of carbon dioxide in aqueous solutions of N-methyldiethanolamine and piperazine in the high gas loading region. J Chem Eng Data 54:1905-1909.

Button JK, Gubbins KE (1999) SAFT prediction of vapour-liquid equilibria of mixtures containing carbon dioxide and aqueous monoethanolamine or diethanolamine. Fluid Phase Equilib 158:175-181.

Cai ZY, Xie RJ, Wu ZL (1996) Binary isobaric vapor-liquid equilibria of ethanolamines plus water. J Chem Eng Data 41:1101-1103.

Cardoso E (1921) The vapor tension of hydrogen sulfide 51:153-164.

Carson JK, Marsh KN, Mather AE (2000) Enthalpy of solution of carbon dioxide in (water plus monoethanolamine, or diethanolamine, or N-methyldiethanolamine) and (water plus monoethanolamine plus N-methyldiethanolamine) at T=298.15 K 32:1285-1296.

Chakma A, Meisen A (1987) Solubility of Co2 in Aqueous Methyldiethanolamine and N,n-Bis(hydroxyethyl)piperazine Solutions. Ind Eng Chem Res 26:2461-2466.

Chang HT, Posey M, Rochelle GT (1993) Thermodynamics of Alkanolamine Water Solutions from Freezing-Point Measurements. Ind Eng Chem Res 32:2324-2335.

Chapoy A, Mohammadi A, Tohidi B, Valtz A, Richon D (2005) Experimental measurement and phase behavior modeling of hydrogen sulfide-water binary system. Ind Eng Chem Res 44:7567-7574.

Chen CC, Britt HI, Boston JF, Evans LB (1982) Local Composition Model for Excess Gibbs Energy of Electrolyte Systems .1. Single Solvent, Single Completely Dissociated Electrolyte Systems. AIChE J 28:588-596.

Chen Y, Shih T, Li M (2001) Heat Capacity of Aqueous Mixtures of Monoethanolamine with N-Methyldiethanolamine 46:51-55.

Chiu L, Li M (1999) Heat Capacity of Alkanolamine Aqueous Solutions 44:1396-1401.

Clarke ECW, Glew DN (1971) Aqueous Nonelectrolyte Solutions .8. Deuterium and Hydrogen Sulfides Solubilities in Deuterium Oxide and Water 49:691-&.

Clarke ECW, Glew DN (1970) Deuterium and Hydrogen Sulfides - Vapor Pressures, Molar Volumes, and Thermodynamic Properties 48:764-&.

Crovetto R, Fernández-Prini R, Japas ML (1982) Solubilities of inert gases and methane in H2O and in D 2O in the temperature range of 300 to 600 K. J Chem Phys 76:1077-1086.

DANCKWER.PV, MCNEIL K (1967) Absorption of Carbon Dioxide into Aqueous Amine Solutions and Effects of Catalysis 45:T32-&.

Daneshvar N, Moattar MTZ, Abdi MA, Aber S (2004) Carbon dioxide equilibrium absorption in the multi-component systems Of CO2+TIPA+MEA+H2O, CO2+TIPA+Pz+H2O and CO2+TIPA+H2O at low CO2 partial pressures: experimental solubility data, corrosion study and modeling with artificial neural network 37:135-147.

DAWODU O, MEISEN A (1994) Solubility of Carbon-Dioxide in Aqueous Mixtures of Alkanolamines. J Chem Eng Data 39:548-552.

Derks PWJ, Hogendoorn JA, Versteeg GF (2010) Experimental and theoretical study of the solubility of carbon dioxide in aqueous blends of piperazine and N-methyldiethanolamine 42:151-163.

Derks PWJ, Hamborg ES, Hogendoorn JA, Niederer JPM, Versteeg GF (2008) Densities, viscosities, and liquid diffusivities in aqueous piperazine and aqueous (piperazine plus N-methyldiethanolamine) solutions. J Chem Eng Data 53:1179-1185.

Deshmukh RD, Mather AE (1981) A Mathematical-Model for Equilibrium Solubility of Hydrogen-Sulfide and Carbon-Dioxide in Aqueous Alkanolamine Solutions 36:355-362.

Dicko M, Coquelet C, Jarne C, Northrop S, Richon D (2010) Acid gases partial pressures above a 50 wt% aqueous methyldiethanolamine solution: Experimental work and modeling. Fluid Phase Equilib 289:99-109.

DIPPR (Design Inistitute for Physical Property Research), 2011, Predicted by Project Staff at the Pennsylvania State University using either published or internal methods.

Edwards TJ, Maurer G, Newman J, Prausnitz JM (1978) Vapor-Liquid-Equilibria in Multicomponent Aqueous-Solutions of Volatile Weak Electrolytes. AIChE J 24:966-976.

Edwards TJ, Newman J, Prausnitz JM (1975) Thermodynamics of Aqueous-Solutions Containing Volatile Weak Electrolytes. AIChE J 21:248-259.

Ermatchkov V, Maurer G (2011) Solubility of carbon dioxide in aqueous solutions of N-methyldiethanolamine and piperazine: Prediction and correlation. Fluid Phase Equilib 302:338-346.

Ermatchkov V, Perez-Salado Kamps A, Maurer G (2006a) Solubility of carbon dioxide in aqueous solutions of N-methyldiethanolamine in the low gas loading region. Ind Eng Chem Res 45:6081-6091.

Ermatchkov V, Perez-Salado Kamps A, Maurer G (2006b) Solubility of carbon dioxide in aqueous solutions of N-methyldiethanolamine in the low gas loading region. Ind Eng Chem Res 45:6081-6091.

Faramarzi L, Kontogeorgis GM, Thomsen K, Stenby EH (2009) Extended UNIQUAC model for thermodynamic modeling of CO(2) absorption in aqueous alkanolamine solutions. Fluid Phase Equilib 282:121-132.

Fletcher R (1971) A modified Marquardt subroutine for non-linear least squares, Harwell report (1971).
http://www.hsl.rl.ac.uk/ Accessed March 2010.

Fosbol PL, Pedersen MG, Thomsen K (2011) Freezing Point Depressions of Aqueous MEA, MDEA, and MEA-MDEA Measured with a New Apparatus. J Chem Eng Data 56:995-1000.

FURST W, RENON H (1993) Representation of Excess Properties of Electrolyte-Solutions using a New Equation of State. AIChE J 39:335-343.

Gabrielsen J, Michelsen ML, Stenby EH, Kontogeorgis GM (2005) A model for estimating CO2 solubility in aqueous alkanolamines. Ind Eng Chem Res 44:3348-3354.

Garcia AV, Thomsen K, Stenby EH (2006) Prediction of mineral scale formation in geothermal and oilfield operations using the Extended UNIQUAC model - Part II. Carbonate-scaling minerals. Geothermics 35:239-284.

Garcia A, Thomsen K, Stenby E (2005) Prediction of mineral scale formation in geothermal and oilfield operations using the extended UNIQUAC model Part I. Sulfate scaling minerals. Geothermics 34:61-97.

Gillespie PC, Wilson GM (1982) GPA,RR-48, Vapor·Uquid and Uquid·Uquid Equilibria:Water-Methane, Water-Carbon Dioxide, water·Hydrolen Sulfide, Water·nPentane, Water-Methane-nPentane RR 48.

Goppert U, Maurer G (1988) Vapor Liquid Equilibria in Aqueous-Solutions of Ammonia and Carbon-Dioxide at Temperatures between 333-K and 393-K and Pressures Up to 7 Mpa. Fluid Phase Equilib 41:153-185.

Guggenheim EA, Turgeon JC (1955) Specific interaction of ions 51:747-761.

Hawrylak B, Palepu R, Tremaine PR (2006) Thermodynamics of aqueous methyldiethanolamine (MDEA) and methyldiethanolammonium chloride (MDEAH(+)Cl(-)) over a wide range of

temperature and pressure: Apparent molar volumes, heat capacities, and isothermal compressibilities 38:988-1007.

Hawrylak B, Burke SE, Palepu R (2000) Partial Molar and Excess Volumes and Adiabatic Compressibilities of Binary Mixtures of Ethanolamines with Water 29:575-594.

Hayden TA, Smith TGA, Mather AE (1983) Heat-Capacity of Aqueous Methyldiethanolamine Solutions. J Chem Eng Data 28:196-197.

Hessen ET, Haug-Warberg T, Svendsen HF (2010) The refined e-NRTL model applied to CO(2)-H(2)O-alkanolamine systems 65:3638-3648.

Hilliard MD (2008) Predictive Thermodynamic Model for an Aqueous Blend of Potassium Carbonate, Piperazine, and Monoethanolamine for Carbon Dioxide Capture from Flue Gas .

Huang SH, Ng HJ (1998) Solubility of H2S and CO 2 in Alkanolamines GPA Research Report-RR-155.

Huttenhuis PJG, Agrawal NJ, Versteeg GF (2009) Solubility of Carbon Dioxide and Hydrogen Sulfide in Aqueous N-Methyldiethanolamine Solutions. Ind Eng Chem Res 48:4051-4059.

Huttenhuis PJG, Agrawal NJ, Solbraa E, Versteeg GF (2008) The solubility of carbon dioxide in aqueous N-methyldiethanolamine solutions. Fluid Phase Equilib 264:99-112.

Huttenhuis PJG, Agrawal NJ, Hogendoorn JA, Versteeg GF (2007) Gas solubility of H2S and CO2 in aqueous solutions of N-methyldiethanolamine 55:122-134.

Iliuta MC, Larachi F (2007) Solubility of total reduced sulfurs (hydrogen sulfide, methyl mercaptan, dimethyl sulfide, and dimethyl disulfide) in liquids. J Chem Eng Data 52:2-19.

ISAACS E, OTTO F, MATHER A (1980) Solubility of Mixtures of H2s and Co2 in a Monoethanolamine Solution at Low Partial Pressures. J Chem Eng Data 25:118-120.

Jakobsen JP, Krane J, Svendsen HF (2005) Liquid-phase composition determination in CO2-H 2O-alkanolamine systems: An NMR study 44:9894-9903.

Jenab MH, Abdi MA, Najibi SH, Vahidi M, Matin NS (2005) Solubility of carbon dioxide in aqueous mixtures of N-methyldiethanolamine plus piperazine plus sulfolane. J Chem Eng Data 50:583-586.

Jones JH, Froning HR, Claytor Jr. EE (1959) Solubility of acidic gases in aqueous monoethanolamine. J Chem Eng Data 4:85-92.

Jou FY, Carroll JJ, Mather AE, Otto FD (1993) The Solubility of Carbon-Dioxide and Hydrogen-Sulfide in a 35 Wt-Percent Aqueous-Solution of Methyldiethanolamine. Can J Chem Eng 71:264-268.

Jou F, Carroll J, Mather A, Otto F (1998) Solubility of methane and ethane in aqueous solutions of methyldiethanolamine. J Chem Eng Data 43:781-784.

JOU F, MATHER A, OTTO F (1995) The Solubility of Co2 in a 30-Mass-Percent Monoethanolamine Solution. Can J Chem Eng 73:140-147.

JOU F, MATHER A, OTTO F (1982) Solubility of H2s and Co2 in Aqueous Methyldiethanolamine Solutions 21:539-544.

Kamps APS, Xia JZ, Maurer G (2003) Solubility of CO2 in (H2O+piperazine) and in (H2O+MDEA+piperazine). AICHE J 49:2662-2670.

Kamps APS, Rumpf B, Maurer G, Anoufrikov Y, Kuranov G, Smirnova NA (2002) Solubility of CO2 in H2O plus N-methyldiethanolamine plus (H2SO4 or Na2SO4). AIChE J 48:168-177.

Kamps APS, Balaban A, Jodecke M, Kuranov G, Smirnova NA, Maurer G (2001) Solubility of single gases carbon dioxide and hydrogen sulfide in aqueous solutions of N-methyldiethanolamine at temperatures from 313 to 393 K and pressures up to 7.6 MPa: New experimental data and model extension. Ind Eng Chem Res 40:696-706.

Kamps A, Maurer G (1996) Dissociation constant of N-methyldiethanolamine in aqueous solution at temperatures from 278 K to 368 K. J Chem Eng Data 41:1505-1513.

Kent RL, Eisenberg B (1976) Better Data for Amine Treating. Hydrocarbon Process 55:87-90.

Kicrzkowska-Pawlak H (2007) Enthalpies of Absorption and Solubility of CO2 in Aqueous Solutions of Methyldiethanolamine 42:2723-2737.

Kim I, Svendsen HF, Borresen E (2008) Ebulliometric Determination of Vapor-Liquid Equilibria for Pure Water, Monoethanolamine, N-Methyldiethanolamine, 3-(Methylamino)-propylamine, and Their Binary and Ternary Solutions. J Chem Eng Data 53:2521-2531.

Kim I, Svendsen HF (2007) Heat of absorption of carbon dioxide (CO2) in monoethanolamine (MEA) and 2-(Aminoethyl)ethanolamine (AEEA) solutions. Ind Eng Chem Res 46:5803-5809.

Kling G, Maurer G (1991) Solubility of Hydrogen in Aqueous Ethanolamine Solutions at Temperatures between 323-K and 423-K. J Chem Eng Data 36:390-394.

Koschel D, Coxam J, Majer V (2007) Enthalpy and solubility data of H2S in water at conditions of interest for geological sequestration. Ind Eng Chem Res 46:1421-1430.

Kritchevsky I, Iliinskaya A (1945) Partial molal volumes of gases dissolved in liquids (a contribution to the thermodynamics of dilute solutions of non-electrolytes) 20:327-348.

Kundu M, Bandyopadhyay SS (2005) Modelling vapour - Liquid equilibrium of CO2 in aqueous N-methyldiethanolamine through the simulate annealing algorithm. Can J Chem Eng 83:344-353.

Kuranov G, Rumpf B, Smirnova N, Maurer G (1996) Solubility of single gases carbon dioxide and hydrogen sulfide in aqueous solutions of N-methyldiethanolamine in the temperature range 313-413 K at pressures up to 5 MPa. Ind Eng Chem Res 35:1959-1966.

Lawson JD, Garst AW (1976) Gas Sweetening Data - Equilibrium Solubility of Hydrogen-Sulfide and Carbon-Dioxide in Aqueous Monoethanolamine and Aqueous Diethanolamine Solutions. J Chem Eng Data 21:20-30.

le Bouhelec EB, Mougin P, Barreau A, Solimando R (2007) Rigorous modeling of the acid gas heat of absorption in alkanolamine solutions. Energy Fuels 21:2044-2055.

Lee JI, Mather AE (1977) Solubility of Hydrogen-Sulfide in Water 81:1020-1023.

Lee JI, Otto FD, Mather AE (1974) Solubility of H2s and Co2 in Aqueous Monoethanolamine Solutions. Can J Chem Eng 52:803-805.

LEE J, OTTO F, MATHER A (1976) Equilibrium between Carbon-Dioxide and Aqueous Monoethanolamine Solutions 26:541-549.

LEE J, OTTO F, MATHER A (1975) Solubility of Mixtures of Carbon-Dioxide and Hydrogen-Sulfide in 5.0n Monoethanolamine Solution. J Chem Eng Data 20:161-163.

Lemoine B, Li YG, Cadours R, Bouallou C, Richon D (2000a) Partial vapor pressure of CO2 and H2S over aqueous methyldiethanolamine solutions. Fluid Phase Equilib 172:261-277.

Lemoine B, Li YG, Cadours R, Bouallou C, Richon D (2000b) Partial vapor pressure of CO2 and H2S over aqueous methyldiethanolamine solutions. Fluid Phase Equilib 172:261-277.

Li CX, Furst W (2000) Representation of CO2 and H2S solubility in aqueous MDEA solutions using an electrolyte equation of state 55:2975-2988.

Li MH, Lie YC (1994) Densities and Viscosities of Solutions of Monoethanolamine Plus N-Methyldiethanolamine Plus Water and Monoethanolamine Plus 2-Amino-2-Methyl-1-Propanol Plus Water. J Chem Eng Data 39:444-447.

Li MH, Shen KP (1992) Densities and Solubilities of Solutions of Carbon-Dioxide in Water Plus Monoethanolamine Plus N-Methyldiethanolamine. J Chem Eng Data 37:288-290.

LI M, SHEN K (1993) Solubility of Hydrogen-Sulfide in Aqueous Mixtures of Monoethanolamine with N-Methyldiethanolamine. J Chem Eng Data 38:105-108.

Li YG, Mather AE (1994) Correlation and Prediction of the Solubility of Carbon-Dioxide in a Mixed Alkanolamine Solution. Ind Eng Chem Res 33:2006-2015.

Liu H, Zhang C, Xu G (1999) A study on equilibrium solubility for carbon dioxide in methyldiethanolamine-piperazine-water solution. Ind Eng Chem Res 38:4032-4036.

Macgregor RJ, Mather AE (1991) Equilibrium Solubility of H2s and Co2 and their Mixtures in a Mixed-Solvent. Can J Chem Eng 69:1357-1366.

Maddox RN, Bhairi AH, Diers JR (1987) Equilibrium Solubility of Carbon Dioxide or Hydrogen Sulfide in Aqueous Solutions of Monoethanolamine, Diglycolamine, Diethanoiamine and Methyldiethanolamine GPA Research Report, PR-104.

Maham Y, Mather AE, Mathonat C (2000) Excess properties of (alkyldiethanolamine plus H2O) mixtures at temperatures from (298.15 to 338.15) K 32:229-236.

Maham Y, Mather AE, Hepler LG (1997) Excess molar enthalpies of (water plus alkanolamine) systems and some thermodynamic calculations. J Chem Eng Data 42:988-992.

Ma'mun S, Nilsen R, Svendsen HF, Juliussen O (2005) Solubility of carbon dioxide in 30 mass % monoethanolamine and 50 mass % methyldiethanolamine solutions. J Chem Eng Data 50:630-634.

Mandal BP, Kundu M, Bandyopadhyay SS (2003) Density and Viscosity of Aqueous Solutions of (N-Methyldiethanolamine + Monoethanolamine), (N-Methyldiethanolamine + Diethanolamine), (2-Amino-2-methyl-1-propanol + Monoethanolamine), and (2-Amino-2-methyl-1-propanol + Diethanolamine) 48:703-707.

Marcus Y (1997) Ion Properties. MARCEL DEKKER, INC., U.S.A.

Mason J, Dodge B (1936) Equilibrium absorption of carbon dioxide by solutions of the ethanolamines 32:27-48.

Mathonat C, Majer V, Mather A, Grolier J (1997) Enthalpies of absorption and solubility of CO2 in aqueous solutions of methyldiethanolamine. Fluid Phase Equilib 140:171-182.

Murrietaguevara F, Rebolledolibreros E, Trejo A (1993) Gas Solubility of Carbon-Dioxide and Hydrogen-Sulfide in Mixtures of Sulfolane with Monoethanolamine. Fluid Phase Equilib 86:225-231.

Nath A, Bender E (1983) Isothermal Vapor Liquid Equilibria of Binary and Ternary Mixtures Containing Alcohol, Alkanolamine, and Water with a New Static Device. J Chem Eng Data 28:370-375.

NIST Chemical Thermodynamics Database Vesion 1.1, 1990. U.S. Department of Commerce, National Inistitute of Standards and Technology. Gaithesburg Maryland 20899.

NREL L (2009) Survey and Down-Selection of Acid Gas Removal Systems for the Thermochemical Conversion of Biomass to Ethanol with a Detailed Analysis of an MDEA System, Task 1: Acid Gas Removal Technology Survey and Screening for Thermochemical Ethanol Synthesis.

Oscarson JL, lzatt RM (1990) GPA-RR-127, Enthalpies of Solution of H2S in Aqueous Methyldiethanolamine Solutions RR-127.

Oscarson JL, Chen X, Izatt RM (August, 1995) A Thermodynamically Consistent Model for the Prediction of Solubilities and Enthalpies of Solution of Acid Gases in Aqueous Alkanolamine Solutions GPA-PR-130, Gas Processors Association Research Report.

Park MK, Sandall OC (2001) Solubility of carbon dioxide and nitrous oxide in 50 mass % methyldiethanolamine. J Chem Eng Data 46:166-168.

Paul S, Mandal B (2006) Density and viscosity of aqueous solutions of (N-methyldiethanolamine plus piperazine) and (2-amino-2-methyl-1-propanol plus piperazine) from (288 to 333) K. J Chem Eng Data 51:1808-1810.

Pitzer KS, Simonson JM (1986) Thermodynamics of Multicomponent, Miscible, Ionic Systems - Theory and Equations. J Phys Chem 90:3005-3009.

Posey M, L. (1997)
Thermodynamic Model for Acid Gas Loaded Aqueous Alkanolamine Solutions PhD Disseration.

Posey M, Rochelle G (1997) A thermodynamic model of methyldiethanolamine-CO2-H2S-water. Ind Eng Chem Res 36:3944-3953.

Prausnitz JM, Lichtenthaler RN, Azevedo EG (1999) Molecular thermodynamics of fluid-phase equilibria. Prentice Hall, Upper Saddle River.

Reamer HH, Sage BH, Lacey WN (1950) Volumetric Behavior of Hydrogen Sulfide 42:140-143.

Rho S, Yoo K, Lee J, Nam S, Son J, Min B (1997) Solubility of CO2 in aqueous methyldiethanolamine solutions. J Chem Eng Data 42:1161-1164.

Rinker EB, Oelschlager DW, Colussi AT, Henry KR, Sandall OC (1994) Viscosity, density, and surface tension of binary mixtures of water and N-methyldiethanolamine and water and diethanolamine and tertiary mixtures of these amines with water over the temperature range 20-100 Â°C. J Chem Eng Data 39:392-395.

Rochelle GT (1991) Research needs for acid gas kinetics and equilibria in alkanolamine systems:66-82.

Rogers WJ, Bullin JA, Davison RR (1998) FTIR measurements of acid-gas-methyldiethanolamine systems. AICHE J 44:2423-2430.

RUMPF B, NICOLAISEN H, OCAL C, MAURER G (1994) Solubility of Carbon-Dioxide in Aqueous-Solutions of Sodium-Chloride - Experimental Results and Correlation 23:431-448.

RUMPF B, MAURER G (1993) An Experimental and Theoretical Investigation on the Solubility of Carbon-Dioxide in Aqueous-Solutions of Strong Electrolytes 97:85-97.

Selleck FT, Carmichael LT, Sage BH (1952) Phase Behavior in the Hydrogen Sulfide Water System 44:2219-2226.

Shen KP, Li MH (1992) Solubility of Carbon-Dioxide in Aqueous Mixtures of Monoethanolamine with Methyldiethanolamine. J Chem Eng Data 37:96-100.

Sidi-Boumedine R, Horstmann S, Fischer K, Provost E, Furst W, Gmehling J (2004) Experimental determination of carbon dioxide solubility data in aqueous alkanolamine solutions. Fluid Phase Equilib 218:85-94.

Silkenbaumer D, Rumpf B, Lichtenthaler RN (1998) Solubility of carbon dioxide in aqueous solutions of 2-amino-2-methyl-1-propanol and N-methyldiethanolamine and their mixtures in the temperature range from 313 to 353 K and pressures up to 2.7 MPa. Ind Eng Chem Res 37:3133-3141.

Solbraa E (2002) PhD Thesis, Measurement and Modelling of Absorption of Carbon Dioxide into Methyldiethanolamine Solutions at High Pressures.

Song H, Lee S, Maken S, Park J, Park J (2006) Solubilities of carbon dioxide in aqueous solutions of sodium glycinate. Fluid Phase Equilib 246:1-5.

Source1 C Unpublished Data.

Source2 C Unpublished Data.

Speyer D, Ermatchkov V, Maurer G (2010) Solubility of Carbon Dioxide in Aqueous Solutions of N-Methyldiethanolamine and Piperazine in the Low Gas Loading Region. J Chem Eng Data 55:283-290.

StatLib N Applied Statistics Algorithms, Nelder-Mead routine. http://lib.stat.cmu.edu/apstat/.

Ter Maat H, Praveen S, IJben P, Arslan D, Wouters HF, Huttenhuis JG, Hogendoorn JA, Versteeg GF (2004) GPA-RR-186, The Determination of VLE Data on CO2 and H2S in MDEA and its Blends with other Amines RR 186.

Thomsen K, Rasmussen P (1999) Modeling of vapor-liquid-solid equilibrium in gas-aqueous electrolyte systems 54:1787-1802.

Thomsen K, Rasmussen P, Gani R (1996) Correlation and prediction of thermal properties and phase behaviour for a class of aqueous electrolyte systems RID A-4865-2011 51:3675-3683.

Tochigi K, Akimoto K, Ochi K, Liu F, Kawase Y (1999) Isothermal vapor-liquid equilibria for water+2-aminoethanol plus dimethyl sulfoxide and its constituent three binary systems. J Chem Eng Data 44:588-590.

Vallee G, Mougin P, Jullian S, Furst W (1999) Representation of CO2 and H2S absorption by aqueous solutions of diethanolamine using an electrolyte equation of state. Ind Eng Chem Res 38:3473-3480.

Van Krevelen DW, Hoftijzer PJ, Huntjens FJ (1949) Composition and vapour pressures of aqueous solutions ... 68:191-216.

von Kiss A, Lajtai I, Thury G (1937) Solubility of gases in water nickel non electrolyte compounds 233:346-352.

VonNiederhausern DM, Wilson GM, Giles NF (2006a) Critical point and vapor pressure measurements for seven compounds by a low residence time flow method. J Chem Eng Data 51:1982-1985.

VonNiederhausern DM, Wilson GM, Giles NF (2006b) Critical point and vapor pressure measurements for seven compounds by a low residence time flow method. J Chem Eng Data 51:1982-1985.

Voutsas E, Vrachnos A, Magoulas K (2004) Measurement and thermodynamic modeling of the phase equilibrium of aqueous N-methyldiethanolamine solutions. Fluid Phase Equilib 224:193-197.

Wang LK, Chen GJ, Han GH, Guo XQ, Guo TM (2003) Experimental study on the solubility of natural gas components in water with or without hydrate inhibitor. Fluid Phase Equilib 207:143-154.

Weiland RH, Chakravarty T, Mather AE (1993) Solubility of Carbon-Dioxide and Hydrogen-Sulfide in Aqueous Alkanolamines. Ind Eng Chem Res 32:1419-1430.

Weiland RH, Dingman JC, Cronin DB (1997) Heat Capacity of Aqueous Monoethanolamine, Diethanolamine, N-Methyldiethanolamine, and N-Methyldiethanolamine-Based Blends with Carbon Dioxide 42:1004-1006.

West JR (1948) Thermodynamic Properties of Hydrogen Sulfide. Chem Eng Prog 44:287-292.

Wright. RH, Maass O (1932) The Solubility of Hydrogen Sulphide in Water from the Vapor Pressures of the Solutions 6:94-101.

Xu GW, Zhang CF, Qin SJ, Gao WH, Liu HB (1998a) Gas-liquid equilibrium in a CO2-MDEA-H2O system and the effect of piperazine on it. Ind Eng Chem Res 37:1473-1477.

Xu GW, Zhang CF, Qin SJ, Gao WH, Liu HB (1998b) Gas-liquid equilibrium in a CO2-MDEA-H2O system and the effect of piperazine on it. Ind Eng Chem Res 37:1473-1477.

Xu S, Qing S, Zhen Z, Zhang C, Carroll JJ (1991) Vapor pressure measurements of aqueous N-methyldiethanolamine solutions. Fluid Phase Equilib 67:197-201.

Yokoyama C, Wakana S, Kaminishi G, Takahashi S (1988) Vapor Liquid Equilibria in the Methane Diethylene Glycol Water-System at 298.15 and 323.15-K. J Chem Eng Data 33:274-276.

Zhang K, Hawrylak B, Palepu R, Tremaine PR (2002) Thermodynamics of aqueous amines: Excess molar heat capacities, volumes, and expansibilities of {water + methyldiethanolamine (MDEA)} and {water + 2-amino-2-methyl-1-propanol (AMP)} 34:679-710.

Zhang Y, Chen C (2011) Thermodynamic Modeling for CO(2) Absorption in Aqueous MDEA Solution with Electrolyte NRTL Model RID C-3054-2008. Ind Eng Chem Res 50:163-175.

11 Appendixes

11.1 Low pressure cell Pictures

This section shows the pictures from the set up called “low pressure cell” and the chemicals used in low pressure experiments. This set up was used to perform CO_2 solubility experiments in aqueous MDEA and aqueous activated MDEA (MDEA-PZ) solutions.

Figure 11-1. Picture of the low pressure cell set up.

Figure 11-2. MDEA and PZ used in low pressure experiments.

11.2 Equilibrium Cell Set up

This set up shows the pictures from the equilibrium cell set up. The set up was used to measure H_2S solubility in aqueous MDEA solutions at high pressures and in presence of methane.

Figure 11-3. Picture from the equilibrium cell set up

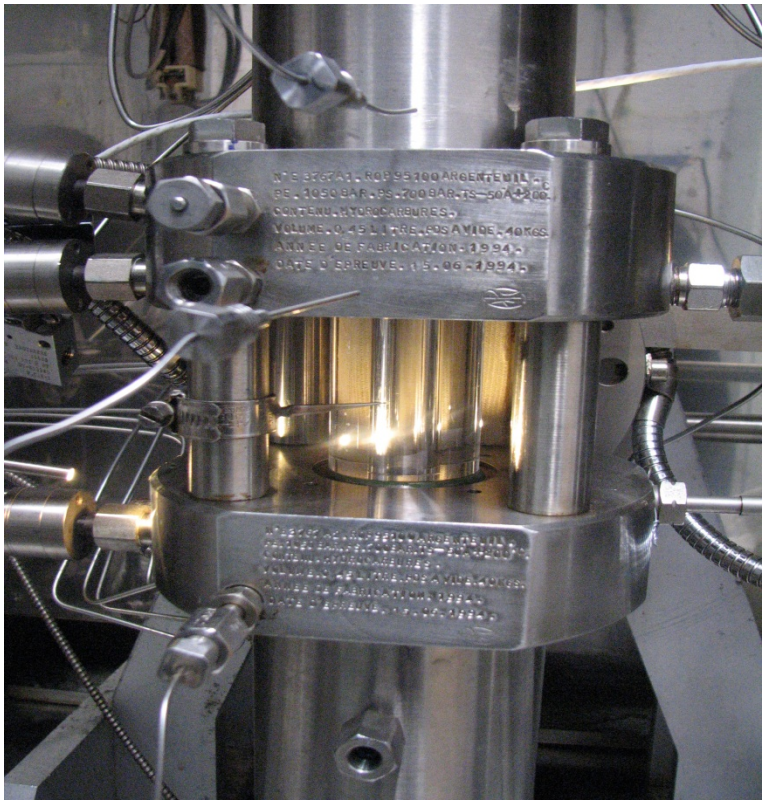

Figure 11-4. Picture of the cylinder where gas and liquid phase are contacted to reach equilibrium.

Figure 11-5. Picture of the stirrer.

11.3 Piperazine Solubility Measurements

This section shows the preliminary results that obtained in this study for measuring piperazine solubility in aqueous MDEA. Note that these measurements were not in the preliminary plan of the project, however because of the industrial demand they were considered in this work. Measurements were performed in Statoil laboratories. The lack of time did not allow repeating the measurements and performing them more accurately.

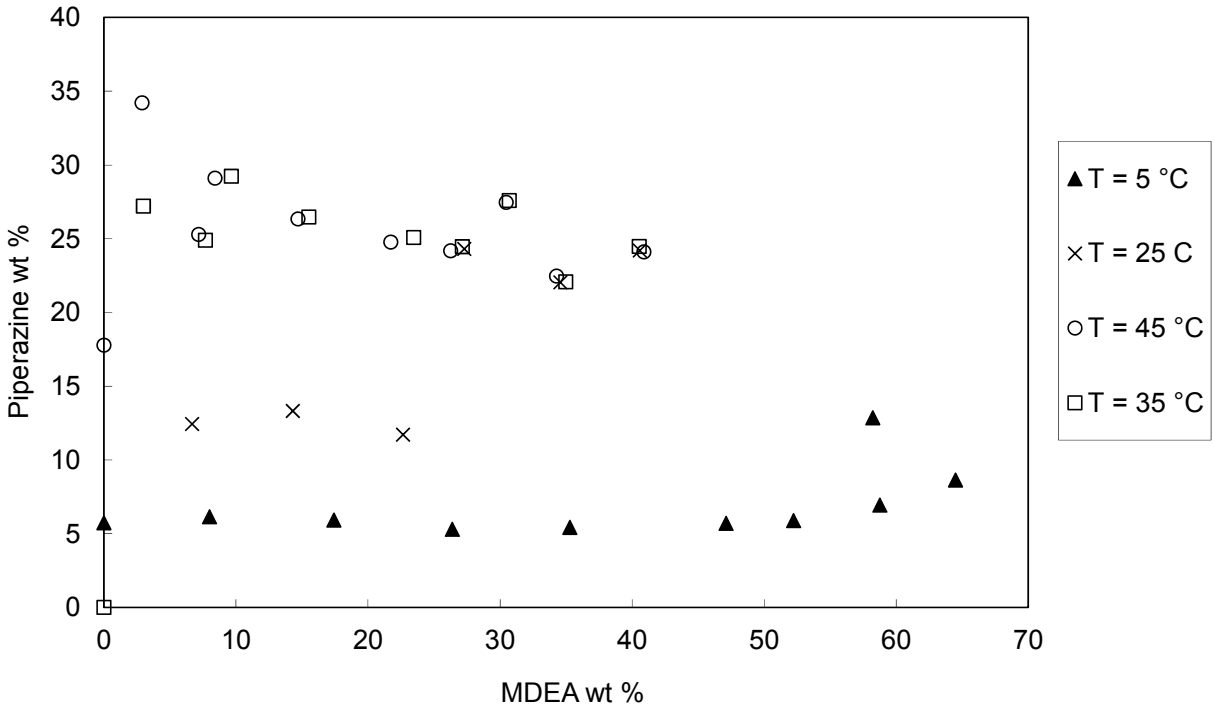

Figure 11-6. PZ solubility measurements in aqueous MDEA.

11.4 List of Publications

This section shows the list of publications derived from this Ph.D. study.

11.4.1 List of Presentations at International Conferences

- Full conference paper and oral presentation, Proceedings of 9th AIChE Annual Meeting, Nashville, USA, November 2009.
- Oral presentation at ICCT-2010, Ibaraki, Japan, August 2010.
- Invited speaker at STC-2010 (Student SPE conference), Germany, October 2010.
- Oral presentation at ESAT-2011, Russia, June 2011.

11.4.2 List of Upcoming Journal Publications

- Sadegh, N., Thomsen, K., Kontogeorgis, G., Stenby, E. H., "Thermodynamic Modeling of CO_2-MDEA/MEA/Blend-H_2O with Extended UNIQUAC Model", will submit to a journal.
- Sadegh, N.,Thomsen, Stenby, E. H., "Thermodynamic Modeling of H_2S+MDEA+H_2O at Low and High pressures (in Presence of Methane and Nitrogen as Make up Gas)", will submit to a journal.
- Sadegh, N., Thomsen, K., Solbraa, E., Johannessen, E., Rudolfsen, G.I., Berg, O.J, "Measurements and Modeling of High Pressure Phase Equilibrium of Methane, H_2S and Aqueous Solutions of MDEA", will submit to a journal.
- Sadegh, N., Thomsen, K., Solbraa, E., Johannessen, E., "Measurements and modeling of Atmospheric Phase Equilibrium of CO_2 and Aqueous Solutions of MDEA, Covering whole MDEA Concentration Range (10-100 wt %) - Part I", will submit to a journal.
- Sadegh, N., Thomsen, K., Solbraa, E., Johannessen, E., "Measurements and Modeling of Atmospheric Phase Equilibrium of CO_2 and Aqueous Solutions of Activated MDEA - Part II", will submit to a journal.